



**Sara Patrícia
Magalhães da Silva**

**Cork - Polymer Composites - A sustainable solution
in Injection Molding and Additive Manufacturing**



Universidade de Aveiro

2021

**Sara Patrícia
Magalhães da Silva**

**Compósitos de Cortiça – Uma solução sustentável em
Moldação por Injeção e Manufatura Aditiva**

**Cork-Polymer Composites – A sustainable solution in
Injection Moulding and Additive Manufacturing**



Universidade de Aveiro

2021

**Sara Patrícia
Magalhães da Silva**

**Compósitos de Cortiça – Uma solução sustentável
em Moldação por Injeção e Manufatura Aditiva**

**Cork-Polymer Composites – A sustainable solution
in Injection Moulding and Additive Manufacturing**

Tese apresentada à Universidade de Aveiro para cumprimento dos requisitos necessários à obtenção do grau de Doutor em Ciência e Engenharia dos Materiais, realizada sob a orientação científica do Doutor José Martinho Marques de Oliveira, Professor Coordenador sem Agregação da Escola Superior Aveiro Norte da Universidade de Aveiro.

Thesis submitted to the University of Aveiro for fulfilment of the necessary requirements leading to the Doctoral degree in Science and Materials Engineering, carried out under the scientific supervision of Doctor José Martinho Marques de Oliveira, Coordinator Professor without Aggregation of the School of Design, Management and Production Technologies, Aveiro North from the University of Aveiro.

Dedico este trabalho aos meus pais, ao meu irmão e às minhas tias.

o júri

presidente

Prof. Doutor Carlos Fernandes da Silva

Professor Catedrático da Universidade de Aveiro

Prof. Doutor Fernando Jorge Lino Alves

Professor Associado da Faculdade de Engenharia da Universidade do Porto

Prof. Doutor José Martinho Marques de Oliveira

Professor Coordenador da Escola Superior Aveiro Norte da Universidade de Aveiro (Orientador)

Prof. Doutor Ricardo José Alves de Sousa

Professor Auxiliar com Agregação da Universidade de Aveiro

Prof. Doutora Ofélia Maria Serralha dos Anjos

Professora Adjunta da Escola Superior Agrária do Instituto Politécnico de Castelo Branco

Doutor Emanuel Mouta Fernandes

Investigador Auxiliar do I3Bs – Instituto de Investigação em Biomateriais, Biodegradáveis e Biomiméticos da Universidade do Minho

agradecimentos

É com enorme gratidão que expresso os meus agradecimentos a todas as pessoas que, de certa forma, estiveram envolvidas na execução desta tese.

Ao meu orientador, José Martinho Oliveira, agradeço todos os desafios, todas as oportunidades e todos os ensinamentos que me foram dados ao longo destes anos. Agradeço também toda a amizade que foi demonstrada ao longo deste percurso.

A todos os colegas da ESAN e da UA, o meu obrigada pelo vosso apoio e companheirismo. Um agradecimento muito especial ao Jorge Luís e à Liliana Pires por terem estado sempre ao meu lado ao longo de todo este percurso.

Aos meus amigos, agradeço a vossa amizade e dedicação e, acima de tudo, todos os momentos que vivemos e partilhamos juntos.

Ao Diogo, agradeço todo o amor, compreensão e apoio incansáveis.

Aos meus pais, irmão e tias, um agradecimento muito especial, pelo contínuo amor e apoio que sempre me proporcionaram.
É a vós que devo tudo o que sou hoje e é a vós que dedico esta tese.

Sou-vos eternamente grata. Obrigada!

palavras-chave

Cortiça; Compósitos Poliméricos de Cortiça; Agentes compatibilizante; Moldação por Injeção; Manufatura Aditiva; Fabricação por Filamento Fundido; Impressão 3D

resumo

Hoje, vivemos num mundo que caminha rapidamente para o Digital, o que provoca profundas mutações tecnológicas. A Manufatura Aditiva (MA), comumente denominada de Impressão 3D (3DP) é um dos símbolos desta efervescência digital e tecnológica. Inicialmente, as tecnologias de MA eram vistas como ferramentas de prototipagem rápida. Atualmente, esse estigma foi alterado e o mercado começou a olhar para as tecnologias de MA como uma alternativa eficaz e competitiva no fabrico de produtos para além das tecnologias de fabrico convencionais.

A cortiça é o embaixador português no mundo dos materiais! É um material 100% natural e apresenta uma combinação única de propriedades, dada a sua composição e estrutura celular. Baixa densidade, carácter hidrofóbico, elasticidade e resistência ao impacto são exemplo de algumas das suas propriedades. Esta combinação única torna a cortiça num material com um elevado potencial em diversas aplicações. A produção de rolhas é a principal aplicação da cortiça. Desta produção são gerados resíduos com diferentes granulometrias, onde os resíduos com calibres superiores a 0.5-1.0 mm são já aplicados no fabrico de compósitos, nomeadamente para aplicações de revestimento e isolamento. A valorização destes resíduos de cortiça através do desenvolvimento de novos materiais compósitos sustentáveis foi uma das principais motivações que desencadeou o presente trabalho.

A presente tese reporta o desenvolvimento de compósitos poliméricos de cortiça (CPC) e de formulações à base de cortiça adaptadas a tecnologias convencionais e de MA. O estudo envolve uma tecnologia convencional, a moldação por injeção (MI), e duas tecnologias de MA, nomeadamente as tecnologias de Fabricação por Filamento Fundido (FFF) e de 3DP. Após o processamento por estas tecnologias, procurar-se-á manter intacta a estrutura alveolar da cortiça.

A tese é composta por um conjunto de artigos publicados em revistas científicas e em conferências. Os artigos encontram-se integrados em dois capítulos (Capítulo II e III). No início de cada capítulo é apresentada uma introdução ao tópico em questão.

O Capítulo II apresenta um estudo reológico e um estudo de cristalização não-isotérmica de CPC. Estes estudos demonstraram que a adição de cortiça não comprometeu a fluidez do CPC e o seu processamento por MI. Além disso, a superfície das partículas do pó de cortiça atuaram como agentes nucleantes durante a cristalização não-isotérmica. A presença de um agente compatibilizante à base de anidrido maleico (AM) contribuiu para o desenvolvimento de CPC com maior fluidez, grau de cristalinidade e adesão interfacial entre a matriz polimérica e a cortiça.

Um estudo de caso foi conduzido para avaliar o efeito das pressões elevadas aplicadas, durante o processo de MI, na integridade da estrutura alveolar da cortiça. O efeito da injeção a baixas pressões, a remoção da pressão de compactação e de contrapressão e o uso de bicos obturadores foram analisados como uma solução adaptada ao processo de MI. Nesta solução adaptada de MI, os alvéolos da cortiça foram capazes de recuperar da deformação, em especial quando estavam próximos de defeitos da matriz (vazios). Um resultado promissor, pois indica que as partículas de cortiça podem recuperar a sua estrutura e tamanho após um processo de MI.

Por outro lado, o Capítulo III relata o (i) desenvolvimento de um filamento de cortiça com uma incorporação de pó de cortiça igual a 15 % (p/p), o que representa 55% em volume e (ii) o desenvolvimento de formulações à base de cortiça adaptadas ao processo de 3DP. Focando na tecnologia de FFF, foi realizado um caso de estudo para avaliar a usabilidade e a capacidade de impressão do filamento de CPC desenvolvido. As peças impressas por FFF exibiram características únicas, nomeadamente um toque não plástico e quente, uma cor natural e a libertação de odor agradável durante a impressão. Foi efetuado, por 3DP, um estudo de caso para avaliar a capacidade de impressão das formulações desenvolvidas. Previamente, a aplicabilidade do método de Washburn foi estudada para avaliar a molhabilidade de pós de cortiça por um ligante comercial (água $\geq 95\%$ (p/p)). Os pós de cortiça são ligeiramente molhados pelo ligante comercial (ângulo de contacto (θ) de $\approx 86 - 87^\circ$). Foram impressas peças com geometrias complexas por 3DP. As peças exibiram leveza e um toque quente e macio. Do conhecimento disponível julga-se ter sido esta a primeira vez que se processaram pós de cortiça por 3DP. Além disso, foi também estudada e validada a técnica de autoclave como fase de pós-processamento no processo de 3DP.

As principais conclusões e as perspetivas de trabalhos futuros estão descritas no Capítulo IV. A presente tese constitui uma abordagem original na valorização de resíduos de pó de cortiça. A combinação de um material natural e tradicional, como a cortiça, com tecnologias de ponta, irá contribuir para o desenvolvimento de produtos de cortiça nunca antes processados ou, até mesmo, para novas aplicações de produtos de cortiça nunca antes pensadas.

keywords

Cork; Cork-Polymer Composites; Coupling agent; Injection Moulding; Additive Manufacturing; Fused Filament Fabrication; 3D Printing

abstract

Today, the world that we live in is moving fast towards the Digital, which is causing profound technological mutations. Additive Manufacturing (AM), commonly called “3D printing”, is one of the symbols of these digital and technological effervescence. Initially, AM technologies were only seen as rapid prototyping tools. Nowadays, this stigma has changed and the market began to look at AM technologies as an effective and competitive alternative to the manufacture of products besides the conventional techniques.

Cork is the world’s ambassador Portuguese material! A 100% natural material and it presents a unique combination of properties, given its composition and alveolar structure. Low density, hydrophobic character, elasticity and impact resistance are some its properties. This feature makes cork a material high potential in several applications. Wine stoppers is the major application of cork. From this production is generated a large amount of cork residues with different granulometries, where residues with calibres superior than 0.5-1.0 mm are already used in the development of cork-based composites for flooring and insulation applications. The valorisation of these cork residues through the development of new sustainable composite materials was one of the main motivations that triggered the present work.

This thesis reports the development of cork-polymer composites (CPC) and cork-based formulations adapted to conventional and AM technologies. It will involve a conventional technology, the injection moulding (IM) technique, and two AM technologies, namely Fused Filament Fabrication (FFF) and 3D Printing (3DP). The preservation of cork alveolar structure after processing by these technologies was always sought.

The present thesis is composed by a set of published papers in scientific journals and in conferences. Papers are integrated into two chapters (Chapter II and Chapter III). At the beginning of each chapter, it is presented an introduction to the topic. Chapter II concerns the development of CPC solutions adapted for IM, while Chapter III focus on the development of CPC and cork-based formulations solutions adapted to FFF and 3DP, respectively.

Chapter II presents the study of the rheological and the non-isothermal crystallization behaviours of CPC. These studies have shown that the addition of cork did not compromise the flowability of CPC and its processability by IM. In addition, cork powder surface acted as a nucleating agent during non-isothermal crystallization. The presence of a coupling agent based on maleic anhydride (MA) contributed to the development of CPC with enhanced flowability, crystallinity degree and interfacial adhesion between the polymeric matrix and cork particles. A case study related to the effect of the high pressures applied during a standard IM process on the integrity of cork alveoli was performed.

The application of low pressures, the removal of holding and back pressures and the use of shut-off nozzles were analysed as an adapted IM solution. Cork alveoli were able to recover from the deformation caused by the IM process, especially when cork granules were near to matrix defects (voids). A promising result which indicates that after an IM process the cork particles can recover its initial shape and size.

On the other hand, Chapter III reports (i) the development of a cork-like filament with an incorporation of cork powder equal to 15 % (w/w), which represents 55 % in volume and (ii) the development of cork-based formulations adapted to 3DP. Focusing on the FFF technology, a case study was conducted to evaluate the usefulness and printability of the developed CPC filament. The printed parts exhibited unique characteristics, such as a non-plastic and warm touch, a natural colour and the release of a pleasant odour during the printing process. A case study, based on the 3DP technology, was conducted to evaluate the printability of the developed cork-based formulations. Previously, the applicability of the Washburn Capillary Rise (WCR) method was studied to determine the wettability of cork powders by a commercial binder ($\geq 95\%$ (w/w) of water). Cork powders are slightly wetted by the commercial binder (contact angles of $(\theta) \approx 86 - 87^\circ$). 3DP cork parts with complex geometry were successfully printed. Parts exhibited lightweight and, warmth and softness to the touch. From the available knowledge, it is believed that this was the first time that cork powders were processed by 3DP. In addition, the autoclave technique was also studied and validated as a post-processing phase in the 3DP process.

The main conclusions and perspectives of future work are presented in Chapter IV. The present thesis constitutes an original approach for the valorisation of cork powder residues. The combination of a natural and traditional product, such as cork, with high-tech technologies, can lead to the development of cork products never processed before, or to new applications of cork products never thought before.

Table of Contents

Nomenclature	xv
Chapter I - Introduction	1
1.1 Motivation	3
1.2 The context.....	5
1.3 Cork	6
1.3.1 Characteristics and Properties.....	6
1.3.2 From Montados to Industry.....	9
1.4 Thermoplastic matrices and composites	11
1.5 Cork-based products	12
References	13
Chapter II - Cork-Polymer Composites for Injection Moulding	15
2.1 Introduction.....	17
2.1.1 Cork-Polymer Composites.....	17
2.1.2 Coupling agents.....	19
2.1.3 Injection Moulding.....	20
References	22
2.2 Rheological behaviour of cork-polymer composites for injection moulding	25
2.3 Non-isothermal crystallization kinetics of cork-polymer composites for injection moulding	39
2.4 Nucleating ability of cork in polypropylene-based composites	57
2.5 Cork-Polymer Composites for Injection Moulding	63
Chapter III - Cork-Polymer Composites and cork-based formulations for Additive Manufacturing ..	73
3.1 Introduction.....	75
3.1.1 Biopolymers	75
3.1.2 Additive Manufacturing	80
3.1.2.1 Fused Filament Fabrication.....	83
3.1.2.2 3D Printing.....	85
3.2 Non-isothermal Cold Crystallization Kinetics of Cork-Polymer Biocomposites based on Polylactic Acid for Fused Filament Fabrication	91
3.3 Cork-Polylactide Composites reinforced with polyhydroxyalkanoates for Additive Manufacturing	110
3.4 Cork-like Filaments for Additive Manufacturing.....	119
3.5 Cork powders wettability by the Washburn capillary rise method.....	137
3.6 Cork powders as material for 3D Printing: A case-study	149
Chapter IV - Concluding remarks and future perspectives	165
4.1 IM.....	167
4.2 AM	167
4.3 Future work perspectives	168

Nomenclature

<i>3DP</i>	3D Printing
<i>AM</i>	Additive Manufacturing
<i>CA</i>	Coupling agent
<i>CLIP</i>	Continuous Liquid Interface Production
<i>CO₂</i>	Carbon dioxide
<i>CPC</i>	Cork-Polymer Composite
<i>DLP</i>	Digital Light Processing
<i>E</i>	Young Modulus
<i>ECSO</i>	Epoxidized Cottonseed Oil
<i>FFF</i>	Fused Filament Fabrication
<i>FTIR</i>	Fourier Transform Infra-Red
<i>HDPE</i>	High Density Polyethylene
<i>IM</i>	Injection Moulding
<i>MA</i>	Maleic Anhydride
<i>MAgPLA</i>	Poly(lactic Acid grafted Maleic Anhydride
<i>MCSO</i>	Maleinized Cottonseed Oil
<i>MFI</i>	Melt Flow Index
<i>M_n</i>	Molar mass
<i>MVO</i>	Modified Vegetable Oil
\overline{M}_w	Average Molecular Weight
<i>MWD</i>	Molecular Weight Distribution
<i>NaOH</i>	Sodium hydroxide
<i>P3HB</i>	Poly(3- hydroxyalkanoate)
<i>P4HB</i>	Poly(4- hydroxybutyrate)
<i>PBS</i>	Polybutylene succinate
<i>PE</i>	Polyethylene
<i>PHA</i>	Polyhydroxyalkanoate
<i>PHBV</i>	Poly(3- hydroxybutyrate-co-3-hydroxyvalerate)
<i>PLA</i>	Poly(lactic Acid
<i>POM</i>	Polarized Optical Microscopy
<i>PP</i>	Polypropylene
<i>PPgMA</i>	Polypropylene grafted Maleic Anhydride
<i>PVA</i>	Polyvinyl Alcohol
<i>SEM</i>	Scanning Electron Microscopy
<i>SLA</i>	Stereolithography
<i>SLS</i>	Selective Laser Sintering

T_c	Crystallization temperature
T_{cc}	Cold crystallization temperature
T_g	Glass transition temperature
T_m	Melting temperature
<i>TPS</i>	Thermoplastic Starch
<i>UV</i>	Ultraviolet
<i>WCR</i>	Washburn capillary rise
<i>WPC</i>	Wood-plastic composites
X_c	Degree of crystallinity
<i>XRD</i>	X-Ray diffraction
ρ	Density
ϵ_{max}	Maximum elongation
σ_{max}	Tensile strength
θ	Contact angle

Volume 133 | Issues 41-42 | 2016
Included in This Print Edition:
Issue 41 (November 5, 2016)
Issue 42 (November 10, 2016)

JOURNAL OF
Applied Polymer
SCIENCE

WILEY

WILEYONLINELIBRARY.COM/JAPP

Chapter I

Introduction

1.1 Motivation.....	3
1.2 The context.....	5
1.3 Cork.....	6
1.3.1 Characteristics and Properties.....	6
1.3.2 From Montados to Industry.....	9
1.4 Thermoplastic matrices and composites.....	11
1.5 Cork-based products.....	12
References.....	13

1.1 Motivation

Cork is the world's ambassador Portuguese material! A 100% natural material, it presents a unique combination of properties, given its composition and alveolar structure. Low density, hydrophobicity, high elasticity and impact resistance are some of its properties. Cork applications have been known since antiquity, especially as a floating artefact and as a seal. Nowadays, wine stoppers are the major application of cork. From this production cork residues are generated with different granulometries. Residues with calibres superior than 0.5-1.0 mm are already used in the development of cork-based composites for flooring and insulation applications. Low granulometric residues (<0.5mm), obtained during the rectification phase of stoppers' top- and downs, represents annually 50000 tons of cork powder residues (equivalent to 30% in residues)¹. Owing to the low granulometry of these residues, they are not suitable for typical cork applications and, usually they are burned or disposed in landfills².

The incorporation of these residues into polymeric matrices can be a solution for the development of new materials tailoring the needs of different and innovative applications. CPC are a viable and a possible strategy for up-grading cork industrial residues under circular economy principles. The advantages of applying natural materials as fillers to reinforce thermoplastic composites are based on their low density and cost, good relation between strength/weight, good insulation properties and high levels of filling. They are, also, renewable and readily available materials, recyclable and non-toxic^{2,3}.

Extrusion, compression, rotational moulding and IM processes can be used for CPC production. IM processes are relevant when it comes to large-scale production and complexity of the parts. Studies focused on the CPC industrialization processes by IM technology are scarce. Regarding this process, the major drawback is the high pressure applied which deeply damage the cork structure and so, the cork structure is not kept and the main cork properties are lost.

AM offers a set of techniques that opens a possibility of creating new products with a high level of design freedom. It is a disruptive set of techniques on a constantly growing market demanding for innovation in the materials area. The restricted availability of AM materials is a strongly constrain for a more widespread use of these techniques.

Figure 1.1 displays the scientific impact of IM and AM technologies by tracing the number of publications (research and review articles) from 1998 and 2019. The interest in AM has been increasing exponentially, mainly from 2010. Whereas interest in IM has been constant, where a slight increase is noticed over the past years. Lately, the combination of AM with thermoplastic and composites materials revealed a growing scientific interest. However, the combination of AM with cork and IM with cork has shown a reduced interest and for some years it is not existing. These trends urge the development of cork-based solutions for IM and AM by taking advantage of cork unicity.

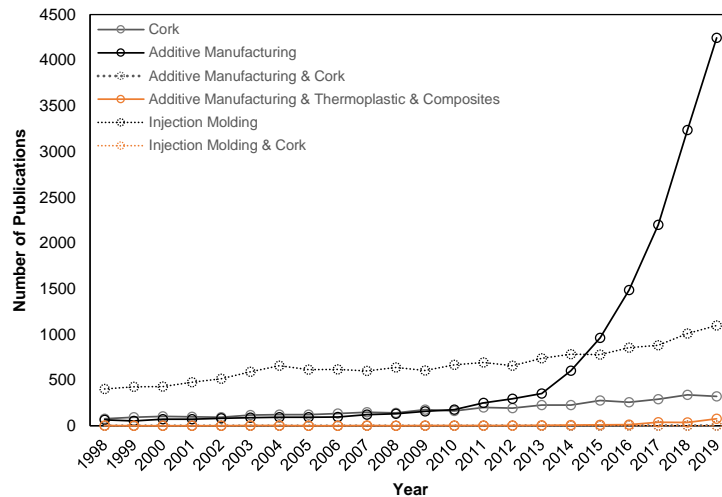


Figure 1.1| Number of scientific documents (research and review articles) retrieved from the Web of Science™ Core Collection between 1998 and 2019, using the terms “additive manufacturing”, “cork”, “injection moulding”, “thermoplastic” and “composites”.

According to National Geographic⁴ “For a material which has been used since antiquity, the chameleon-like versatility of cork is astonishing (...) thanks to its capacity for renewal and for adapting to new technological demands”. Now we have new technological demands and cork should be used to open new horizons in IM and AM.

The present thesis proposes to contribute for the development of CPC and cork-based formulations, adapted to manufacturing solutions that should preserve the cork structure. It will involve manufacturing techniques such as a modified IM technology and two AM techniques, namely 3DP and FFF. Figure 1.2 shows the effect of high pressure applied during IM process. Cork structure is compressed and its intrinsic properties are compromised. A comparative study of product properties obtained by both technologies will be performed.

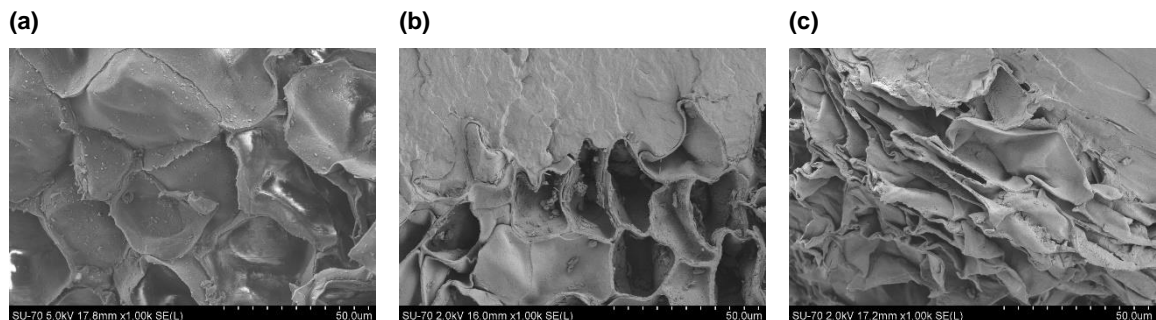


Figure 1.2| Scanning Electron Microscopy (SEM) images of (a) cork, (b) CPC before IM and (c) after IM.^a

^a All details are presented in Chapter II.

1.2 The context

At the very beginnings of humankind, humans had only access to materials naturally available from nature, as wood, stones, skins, fibres, etc.. In XVIII-XIX centuries, with the first industrial revolution, an important mark in Human Evolution was achieved, characterized by the transition from natural to synthetic products. From this moment, chemical compounds from fossil resources start being used to develop new materials. This moment was the beginning of the current age that we are living, the “plastic age” (Figure 1.3)⁵.

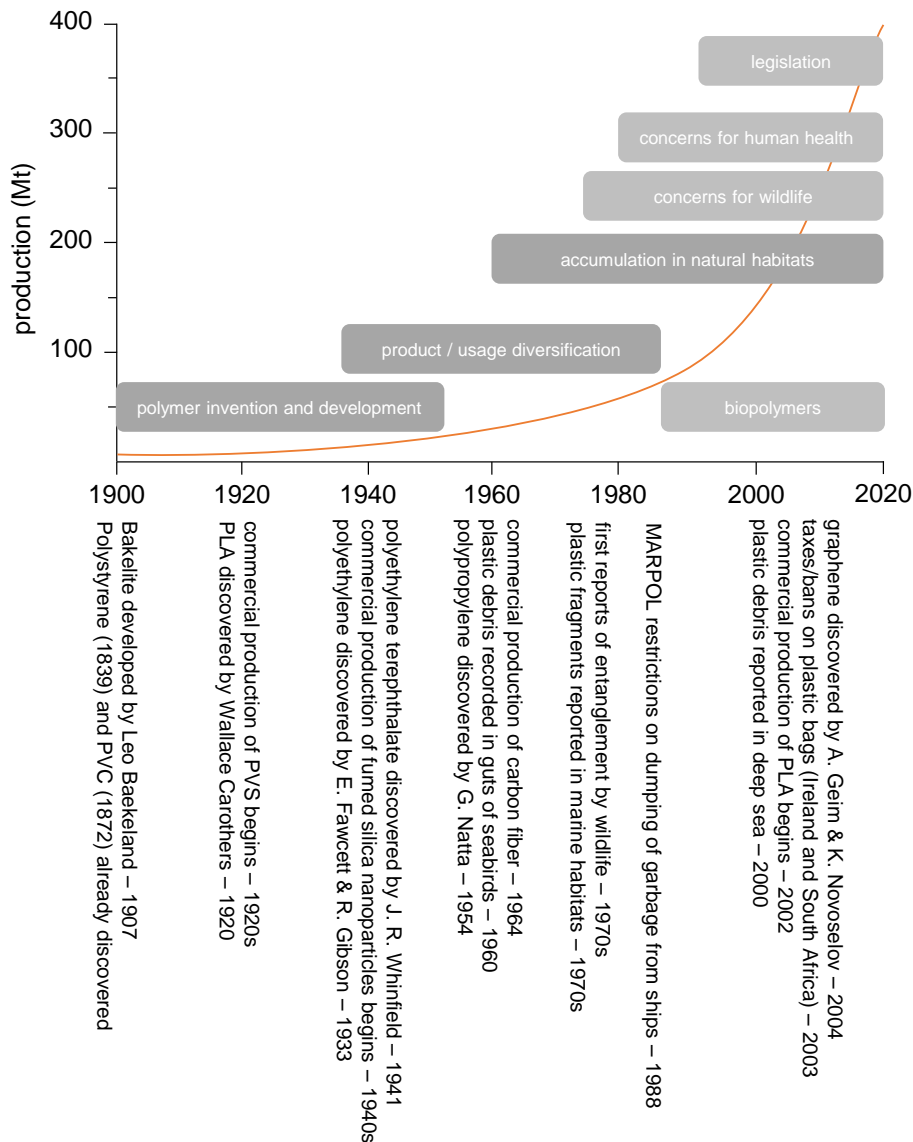


Figure 1.3| Illustration of historical marks on the development, production and concerns about the use of plastics. Solid line represents the worldwide production of plastic in millions of tonnes. PVC, polyvinyl chloride; PLA, polylactic acid. (Adapted from Thompson, R. *et al.*⁵ and Gibb, B. C.⁶)

Examples of synthetic materials that arose at this point were Bakelite and Nylon. In 1907, Leo Baekeland developed Bakelite, the first polymer being synthesized⁵. A few years later, in the late

1930s, Nylon was produced from a renewable resource, furfural, by Carothers at DuPont^{5,7}. Over time, it was discovered new chemical synthetic routes for producing materials that had properties superior to those of the natural ones. As an example, the vulcanization of natural rubber suitable for application in tires industry. A higher number of chemicals from fossil resources suitable for the production macromolecular materials were available at lower prices⁷. As a consequence, a variety of materials were developed, namely plastics, inks, textiles and soaps. Materials which still play an important role in our daily basis.

The over-exploitation of fossil resources over time led to the awareness that these are non-renewable sources. As a result, geopolitical tensions created by the increasing fuel prices and the environmental problems generated by the greenhouse emissions urged the need to find sustainable alternatives. Such alternatives to overcome our high demand and dependency of fossil resources. With this, several alternatives are being studied to provide solutions to such global challenges as climate change, sustainable agriculture, energy, toxics in the environment, and the depletion of natural resources⁸.

The Brundtland Commission (1987)⁹ defined sustainable development as “*development that meets the needs of the present without compromising the ability of future generations to meet their own needs*”. In 2015 it was set the “Transforming our World: the 2030 Agenda for Sustainable Development” with 17 sustainable development goals and it was adopted by all United Nations Member States¹⁰. The present work lines up with the following goals: 9 – Industry, innovation and infrastructure; 12 – Responsible production and consumption; 13 – Climate action; and, 15 – Life on land. A renewed interest in using renewable resources to produce chemicals has aroused through the implementation of the biorefinery concept. Agricultural and forestry residues are used as feedstock to produce valuable chemicals^{11,12}. From lignocellulosic materials, a source of biopolymers, such as cellulose, hemicelluloses, lignin and starch are readily available.

The present work aims to contribute for the development of new cork-based materials through the valorisation of low granulometric cork powder residues from the cork industry.

1.3 Cork

1.3.1 Characteristics and Properties

Cork is a product obtained directly from the outer bark of an oak species tree. Its growth is dependent of a Mediterranean climate, in which is natural distribution is limited to the western part of the Mediterranean basin and the adjacent Atlantic coasts¹³. *Quercus suber L.* is the most abundant cork oak subspecies in Portugal and have a long lifetime of around 250-350 years. The cork industry is one of the most important Portuguese economic sectors accounting for 49% of the world's total cork production. On a daily basis around 40 million cork stoppers are produced in Portugal¹⁴.

Cork presents layers of tiny hollow cells of hexagonal shape in closed-cell foam (Figure 1.4). These cells are surrounded with cellular membranes and filled with gas, similar to air. There are 40 million cells for each cubic centimeter¹⁵. This characteristic closed-foam feature allows the restriction

of the loss water, the control of gas transfer and unable the passage of large molecules and microorganisms.

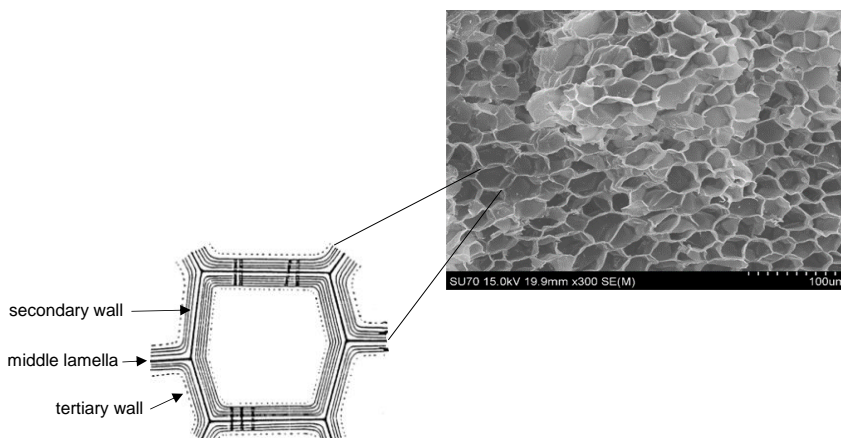


Figure 1.4| SEM image of cork structure. (Adapted from Gil, L. (2007)¹⁶)

In terms of volume, cellular walls represents ca. 10-15% of the total volume, which results an empty volume of ca. 85-95%¹⁷. Cork low density, insulation and resilience properties are determined by this high percentage of empty volume. The cellular walls of cork cells are constituted by five layers (Figure 1.4): two layers having a cellulosic nature which line the cells cavities; two layers having a suberinic nature which confer impermeability; and, a lignified middle lamella which gives rigidity and structure¹⁷.

The cork cells dimensions vary according the seasonal growth rate, being usually distinguished as early-cork and late-cork cells¹³. Early-cork cells are bigger, and have thinner cell walls, whereas late-cork cells are smaller and have thicker cell walls (Table 1.1).

Table 1.1| Typical cork cells dimensions. (Adapted from Pereira, H. (2007)¹³)

	Early-cork	Late-cork
Height (μm)	30-40	10-15
Cell thickness (μm)	1-1.5	2-3
Number of cells per cm³	4x10 ⁷ to 7x10 ⁷	10x10 ⁷ to 20x10 ⁷

Cork possesses a unique chemical composition when compared to other plant tissues. This is due to the presence of suberin, the major compound located at the cork cells periderm, accounting for ca. 50% of the total material¹³. The monomeric composition of suberin is constituted by fatty acids, fatty alcohols and glycerol. These aliphatic moieties give the characteristic hydrophobic behaviour of cork and it is also responsible for its elastic behaviour. Today is still unknown the real macromolecular structure of suberin. A complete description of suberin monomers composition can be found in a study published by Graça, J. & Pereira, H. (2000)¹⁸.

The second major compound present in cork cell wall is lignin (20-25 % wt), followed by polysaccharides (12-20 % wt), extractives (14-18% wt) and inorganic compounds (1-2% wt)¹³. All

these compounds are dispersed in the cell wall providing mainly structural features. A schematic representation of on how these components are placed in cork cell wall is shown in Figure 1.5.

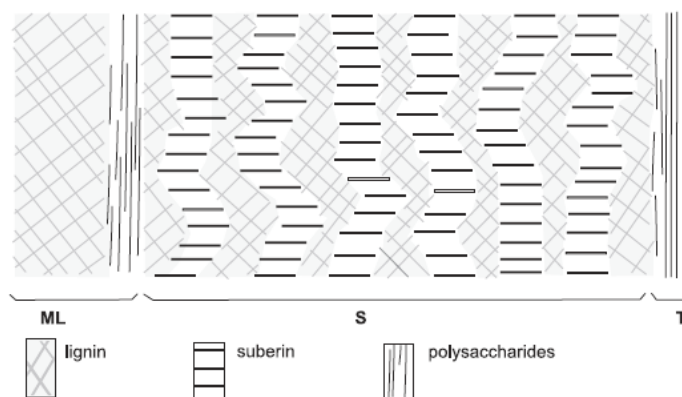











Figure 1.5] Schematic representation of *Quercus suber* L. cell wall: ML, middle lamella; S, secondary wall; T, tertiary wall. (Reprinted from Pereira, H. (2007)¹³).

Lignin is an amorphous three-dimensional polymer of phenylpropane units, which has an important role in the cell's endurance and development. Thus, it affects the transport of water, nutrients and metabolites in the plant cell. More specifically these phenylpropane units are three monolignol precursors, coniferyl alcohol, sinapyl alcohol and *p*-coumaryl alcohol with various degrees of oxygenation/substitution on the aromatic ring. The aromatic rings of *Quercus suber* L. are usually guaiacyl (G) type, which is composed mainly by coniferyl alcohol monomers. In addition, these precursors are covalently linked to hemicelluloses and suberin¹³. Polysaccharides comprise the cellulose and hemicellulose fraction, where they play a small role on cork properties. Contrarily to other wood materials, suberin and lignin fractions are the ones that play the leading role. Regarding cork extractives fraction, they include non-polar and polar compounds, mainly phenolic compounds (example, tannins and ceroids). When it comes to the inorganic components, calcium is the most abundant, where phosphorous, sodium, potassium and magnesium can also be found¹³.

Cork structure allied with its chemical composition turns cork into a material with a characteristic set of properties. This is the essence and uniqueness of cork. In Table 1.2 it is described all the properties that allows cork to be considered a unique natural material.

As presented in Table 1.2, cork has a hydrophobic behaviour. However, the lenticular channels in its structure can act as water reservoirs. Nevertheless, the water absorption of cork is a slow process involving in a first phase the diffusion of water through the external layers of cork and then, into the lenticular channels. The boiling of cork in water is a necessary procedure on cork processing¹³. Several changes occur on cork, as a consequence of the swelling of cork cells (commonly in radial direction), namely (i) on the mechanical behaviour, (ii) on the chemical composition and (iii) on the migration of some chemical compounds. More specifically, the dissolution of 2, 4, 6-trichloroanisole is of great interest on cork stoppers industry, since its presence is associated with a musty smell.

Table 1.2| Cork properties.

Symbol	Property
	<u>Acoustic Insulation</u> due to closed-cell foam structure, where each cell is filled with a gas and isolated from other cells. Sound absorption coefficient (500-1500 c/s) is around 0.33-0.8 ($\leq 100 \text{ kg/m}^3$) ¹⁶ .
	<u>Thermal Insulation</u> owing to a poor heat transfer caused by the low solid fraction and small cell size which eliminate gas convection and reduce radiation. Cork heat conductivity (λ) varies from 0.040-0.045 W/m·K and has a heat diffusivity (α) ranging from 10^{-7} - $1.5 \times 10^{-7} \text{ m}^2/\text{s}$ (these values consider a cork density of 140-170 kg/m^3) ¹³ .
	<u>Fire Resistance</u> ability, in which cork burns without a flame maintaining its shape and does not emit toxic gases during combustion ¹⁶ .
	<u>Lightweight</u> material due to the closed-cell foam structure and thin cell walls without intercellular communication channels. Cork density values can vary from 120-200 kg/m^3 . ¹³
	<u>Compressibility and Elasticity</u> : cork is an elastic material and compress without lateral expansion by the fact that cell walls are able to buckle without fracture ($v_{R/NR} = v_{NR/R} \approx 0$; $v_{NR/NR} = 0.2$) ¹³ .
	<u>Impermeability</u> to liquids and gases, once again, due to the closed-cell foam structure and thin cell walls without intercellular communication channels, allied with a cell wall composed mainly by suberin ($\theta_{\text{water}} = 84^\circ$) ¹³ .
	<u>Hypoallergenic</u> by the fact that does not absorb dust and microorganism associated with allergies.
	<u>Comfortable</u> and a warm material related to cork texture and the fact that cork has a very low heat transfer coefficient.
	<u>Friction Resistance</u> due to closed-cell foam structure which have a greater resistance to impact and friction when compared to hard surfaces.

(v , Poisson coefficient; R , radial; NR , Non-radial; θ_{water} , contact angle of water on cork)

1.3.2 From Montados to Industry

Cork oak forests occupy an estimated area of around 736000 hectares¹⁹ in Portugal, concentrated in the south of the country. *Montado* constitutes the Portuguese cork oak forests where a multifunctional system, combining forest, agriculture and cattle.

The extraction of cork is made periodically, usually every 9-12 years according to conditions growth. Climatic factors are the ones which have a stronger impact on cork oak tree growth, mainly high temperatures in early Spring and precipitation during Summer time.¹³ For industrial cork stoppers requirements' production, cork planks should present a thickness over 27 mm and no deep fractures. This limits the use of extracted virgin and second cork for stoppers production¹³. Only the cork extracted from the third extraction – reproduction cork – is suitable. There is a Portuguese saying: “*Quem se preocupa com os seus netos, planta um sobreiro*” which reflects this inability of

using virgin cork planks for stoppers production and the fact that, at least, 43 years will be necessary to wait.

After cork extraction, there are a series of stages until reaching the final product and vary according to the type of product. These stages can be categorized as: i) storage in stainless steel structures in order to prevent microbial contamination; ii) selection of cork planks according to its thickness and quality; iii) in the case of the cork selected for stoppers production, they will be subjected to a boiling process, already discussed above. In Figure 1.6, it is represented a scheme of the possible cork products obtained from the different types of cork.

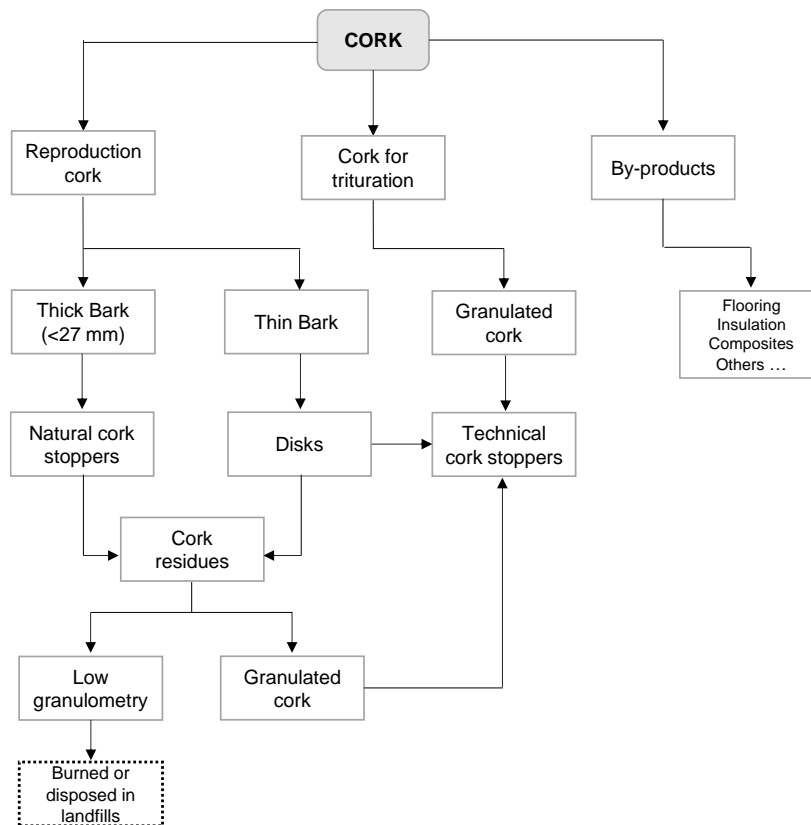


Figure 1.6] Schematic representation of cork products production. (Adapted from Pereira, H. (2007)¹³)

As it can be seen from Figure 1.6, all cork types are considered for stoppers production, for cork-based products development and, in the case of the low granulometric cork powder residues, as “fuel” for the boilers, where the excess is usually disposed in landfills². This work proposes to contribute to the valorisation of these residues, leading to the sustainable development of new cork-based products. Another important feature about cork production is its contribution for sequestration of carbon dioxide (CO₂), maintenance of biodiversity, soil protection, regulation of hydrological cycle and so on²⁰. Besides the economic contribution, an environmental and social commitment is found when it comes for cork production.

1.4 Thermoplastic matrices and composites

Nowadays, there has been an effort to produce sustainable plastic products made from recycled or bio-based plastics to compete with petroleum-based polymers^b. Sustainable plastic products can be considered the ones having lower carbon footprint, waste and pollution generation than traditional plastics, and also have minimum levels of regulated heavy metals²¹. Feedstock resources for bioplastic production are mainly agro-based materials consisting on carbohydrate-rich plants (first generation feedstock). The use of feedstock based on materials, which are not eligible for food, or feed production is also present. Namely, the use of lignocellulosic-based materials or organic-waste materials (second-generation feedstock) and algae biomass or methane (third-generation feedstock). The use of first-generation feedstock results on a cheaper bioplastic production compared to the other feedstock generations that requires the use of biotechnological processes. However, the use of food crops for industrial bioplastic production is seen to have a negative impact by interfering with the food and feed chain. Nevertheless, it is estimated that 2% of land is used to grow biomass for material use and only 0.01% is attributed to bioplastics²². Three main categories divide bioplastics according to their feedstock origin and biodegradability. Polymers from bio-derived resources, but are not biodegradable, which includes bio-based polyamides (PA), polyethylene (PE) and polyethylene terephthalate; polymers from petrochemical resources but are biodegradable, such as polybutylene terephthalate and polybutylene succinate (PBS); or, polymers from renewable resources and biodegradable, such as polylactic acid (PLA), polyhydroxyalkanoates (PHA) and thermoplastic starch (TPS).

Biopolymers with biodegradable and compostable abilities are being designed to produce sustainable bioplastics. Biodegradation occurs slowly in natural environments open to oxygen and water, in the presence of microorganisms, such as bacteria and fungi (yeasts and moulds). The landfill sites are usually anaerobic places which inhibits bio-activity and biodegradation ability. It is needed to fully characterize the biodegradability of these materials in external conditions, such as in soil under ambient outdoor conditions, and to comprehend the impacts on the surrounded medium^{23,24}. NatureWorks® is the world-leading biopolymers supplier and developer of materials made from renewable sources with performance and economics that compete with oil-based intermediates, plastics, and fibers²⁵. In 2016, their investment on the development of new strategies to produce biopolymers on an industrial level resulted on the commercialization of a fermentation process based on the transformation of methane, a greenhouse gas, into lactic acid.

Natural fibres have been replacing traditional reinforcing materials (glass fibres, aramid, nylon, calcium carbonate) in polymeric matrices for several application areas²⁶. Low density, hardness and cost, good relation between strength/weight, good insulation properties, and high levels of filling are some of the advantages of applying natural materials as fillers in composites. They are, also,

^b Polypropylene (PP), a synthetic polymer, was also used in the present thesis. However, the State of Art will focus on biodegradable matrices.

renewable, readily available materials, recyclable and non-toxic²⁷. Jute, hemp, kenaf and sisal are some of the natural fibers that can be found in several areas varying from furniture manufacturing, interior parts in automotive industry, barrier applications, non-structural building applications, etc.²⁷. Several challenges can be found when compounding natural fibers with polymeric matrices, namely (i) different densities, (ii) fibers hygroscopicity, (iii) fibers thermal degradation, (iv) fibers shape, size and weight fraction, (v) different polarities, among others²⁸. A proper fibre distribution within the polymeric matrices as well as enhanced physical properties will depend on a successful surpassing of such challenges.

1.5 Cork-based products

Cork harvested from the two first extractions, as well as cork removed from the bottom of the cork tree, is inadequate for cork stoppers production. These industrial cork residues are then converted into granules (usually, with particle sizes varying from 0.5 – 7.0 mm) and used to prepare agglomerates for a variety of applications. Cork agglomerates are divided into black and white agglomerates³¹. Black agglomerates, also known as expanded agglomerates, were discovered accidentally in 1891 by John Smith, an American lifeguard vests producer. They are obtained solely by volumetric expansion of cork alveoli and exudation of cork natural waxes, when subjected to autoclave treatments¹³. Nowadays, these types of agglomerates are mainly used in flooring (anti-vibrational) and insulation (thermal and sound) applications. On the other hand, the white agglomerates, are all cork composite-based materials obtained in the presence of resins (natural or synthetic), rubbers (natural or synthetic), polymeric matrices (thermoplastic or thermoset), fibres, laminates, etc.. This variety of agents that can be added or mixed with cork leads to the production of a diversity of products for multiple applications. Manufacturing technologies commonly used are Computerized Numerical Control, compression and IM (e. g. Lifocork, Hexpol[®])³². A wide range of applications can be found for these composite cork-based materials, from conventional to high-tech applications, such as construction and aerospace industries^{33,34}, medicine³⁵ and cosmetics (e.g. Uplift Skincare[®]), fashion and footwear, architecture and design³⁶, bioenergy production³⁷, ecoceramics³⁸ and activated carbons production³⁹, water/oil separation⁴⁰ and others³⁵. Such distinct applications are settled on the unique set of cork properties (Table 1.2).

Recently, it can be found some developments on exploring cork as material for AM world, more specifically on the preparation of CPC filaments for FFF^{41–43}. In the market, there are two filaments^{44,45} commercially available with the reference ‘cork’ on its trade name^c.

The uniqueness of cork creates potential for endless applications allying natural with technological. The present thesis proposes to valorise cork powder residues through the development of cork-based products by IM, and by FFF and 3DP, two AM technologies. The

^c Given the easiness on detecting the presence of cork in this type of material, filament⁴⁴ was subjected to morphological analyses. The presence of cork was not detected, which it was assumed that the reference to cork assumes only a commercial value.

development of such cork-based solutions will be always settled in the premise of maintaining cork's unique structure and chemical composition. So, which are the next challenges for cork?

References

1. APCOR - Associação Portuguesa da Cortiça. Cork. (2012). Available at: <https://www.apcor.pt/wp-content/uploads/2015/07/AnuarioAPCOR2012.pdf>. (Accessed: 28th May 2020)
2. Fernandes, E. M., Aroso, I. M., Mano, J. F., Covas, J. A. & Reis, R. L. Functionalized cork-polymer composites (CPC) by reactive extrusion using suberin and lignin from cork as coupling agents. *Compos. Part B Eng.* **67**, 371–380 (2014).
3. Thakur, V. K. *Lignocellulosic Polymer Composites: Processing, Characterization and Properties*. (Scrivener Publishing, Wiley, 2015).
4. The Chemistry of Cork. *National Geographic* 162 (2009).
5. Thompson, R. C., Swan, S. H., Moore, C. J. & vom Saal, F. S. Our plastic age. *Philos. Trans. R. Soc. London B Biol. Sci.* **364**, 1973–1976 (2009).
6. Gibb, B. C. Plastics are forever. *Nat. Chem.* **11**, 394–395 (2019).
7. Gandini, A. & Belgacem, M. N. The State of the Art. in *Monomers, Polymers and Composites from Renewable Resources* 1–16 (Elsevier, 2008).
8. Manley J.B., Anastas, P. T. & Cue, B. W. Frontiers in Green Chemistry: meeting the grand challenges for sustainability in R&D and manufacturing. *J. Clean. Prod.* **16**, 743–750 (2008).
9. Brundtland, G. *Our common future: the world commission on environment and development*. (Oxford University Press, 1987).
10. Nations, U. Transforming our World: The 2030 Agenda for Sustainable Development. 41 (2015). Available at: <https://sustainabledevelopment.un.org/post2015/transformingourworld/publication>.
11. Magalhães da Silva, S. P., Da Costa Lopes, A. M., Roseiro, L. B. & Bogel-Lukasik, R. Novel pre-treatment and fractionation method for lignocellulosic biomass using ionic liquids. *RSC Adv.* **3**, 16040–16050 (2013).
12. Magalhães da Silva, S. P., Morais, A. R. C. & Bogel-Lukasik, R. The CO₂-assisted autohydrolysis of wheat straw. *Green Chem.* **16**, 238–246 (2014).
13. Pereira, H. *Cork: Biology, Production and Uses*. (Elsevier, 2007).
14. APCOR - Associação Portuguesa da Cortiça. (2015). Available at: <https://www.apcor.pt/media-center/estatisticas/>. (Accessed: 11th September 2017)
15. APCOR - Associação Portuguesa da Cortiça. Cork - What is it? (2015). Available at: <https://www.apcor.pt/en/cork/what-is-it/>. (Accessed: 11th September 2017)
16. Gil, L. *A cortiça como material de construção - Manual técnico*. (APCOR - Associação Portuguesa de Cortiça, 2007).
17. Gil, L. *Cortiça: Produção, Tecnologia e Aplicação*. (I.N.E.T.I., 1998).
18. Graça, J. & Pereira, H. Methanolysis of bark suberins: analysis of glycerol and acid monomers. *Phytochem. Anal.* **11**, 45–51 (2000).
19. APCOR-Associação Portuguesa da Cortiça. Available at: <http://www.apcor.pt/montado/#Montado>. (Accessed: 15th September 2017)
20. Gil, L. Cork: a strategic material. *Front. Chem.* **2**, 16 (2014).
21. Greene, J. P. *Sustainable Plastics: Environmental Assessments of Biobased, Biodegradable, and Recycled Plastics*. (John Wiley & Sons, Inc., 2014).
22. European Bioplastics. *Biobased plastics – fostering a resource efficient circular economy*. (2016).
23. Cinelli, P. *et al.* Processability and Degradability of PHA-Based Composites in Terrestrial Environments. *Int. J. Mol. Sci.* **20**, 284–298 (2019).
24. Chan, C. M. *et al.* Insights into the biodegradation of PHA / wood composites: Micro- and macroscopic changes. *Sustain. Mater. Technol.* **21**, 1–12 (2019).
25. NatureWorks LLC. NatureWorks. Available at: <https://www.natureworksllc.com/>. (Accessed: 16th May 2018)

26. Jawaid, M. & Abdul Khalil, H. P. S. Cellulosic/synthetic fibre reinforced polymer hybrid composites: A review. *Carbohydr. Polym.* **86**, 1–18 (2011).
27. Pandey, J. K., Ahn, S. H., Lee, C. S., Mohanty, A. K. & Misra, M. Recent Advances in the Application of Natural Fiber Based Composites. *Macromol. Mater. Eng.* **295**, 975–989 (2010).
28. Stokke, D. D., Wu, Q. & Han, G. *Introduction to Wood and Natural Fibers Composites*. (John Wiley & Sons, Ltd., 2014).
29. Redwood, B., Schöffner, F. & Garret, B. *The 3D Printing Handbook - Technologies, design and applications*. (3D Hubs B.V., 2017).
30. Ligon, S. C., Liska, R., Stampfl, J., Gurr, M. & Mülhaupt, R. Polymers for 3D Printing and Customized Additive Manufacturing. *Chem. Rev.* **117**, 10212–10290 (2017).
31. Mestre, A. & Gil, L. Cork for Sustainable Product design. *Ciência Tecnol. dos Mater.* **234**, 52–63 (2011).
32. ACC. Cork Solutions & Manufacturing Processes. (2017). Available at: https://amorimcorkcomposites.com/media/3948/171124_acc_book_cork_solutions_and_processes_short_digital_web.pdf. (Accessed: 13th December 2019)
33. ACC. Thermal Protection System. Available at: <https://amorimcorkcomposites.com/en/materials-applications/aerospace/>. (Accessed: 13th December 2019)
34. ACC. Cork on mission to Mars. Available at: <https://amorimcorkcomposites.com/en/about-us/news/cork-on-mission-to-mars/>. (Accessed: 13th December 2019)
35. Pereira, H. & Pereira, H. Cork. in *Cork: Biology, Production and Uses* 243–261 (Elsevier, 2007).
36. ACC. Campana brothers create furniture made of cork. Available at: <https://amorimcorkcomposites.com/en/innovation/case-studies/campana-brothers-create-furniture-made-of-cork/>. (Accessed: 13th December 2019)
37. Costa Oliveira, F. A. *et al.* High performance cork-templated ceria for solar thermochemical hydrogen production via two-step water-splitting cycles. *Sustain. Energy Fuels* **4**, 3077–3089 (2020).
38. Pullar, R. C. & Novais, R. M. Ecoceramics. *Mater. Today* **20**, 45–46 (2017).
39. Novais, R. M., Caetano, A. P. F., Seabra, M. P., Labrincha, J. A. & Pullar, R. C. Extremely fast and efficient methylene blue adsorption using eco-friendly cork and paper waste-based activated carbon adsorbents. *J. Clean. Prod.* **197**, 1137–1147 (2018).
40. Zhou, Y., Qu, K., Zhang, L., Luo, X. & Liao, B. Green fabrication of biodegradable cork membrane for switchable separation of oil/water mixtures. *J. Dispers. Sci. Technol.* **0**, 1–12 (2019).
41. Gama, N., Ferreira, A. & Barros-Timmons, A. 3D printed cork/polyurethane composite foams. *Mater. Des.* **179**, 107905–107914 (2019).
42. F.Brites, C. Malça, F.Gaspar, J.F.Horta, M.C. Franco, S. Biscaia, A. M. Cork Plastic Composite Optimization for 3D Printing Applications. *Procedia Manuf.* **12**, 156–165 (2017).
43. Daver, F., Lee, K. P. M., Brandt, M. & Shanks, R. Cork–PLA composite filaments for fused deposition modelling. *Compos. Sci. Technol.* **168**, 230–237 (2018).
44. ColorFabb. CorkFill. Available at: <https://colorfabb.com/corkfill>. (Accessed: 13th December 2019)
45. FormFutura, 3D Printing Materials. EasyCork. Available at: <https://www.formfutura.com/shop/product/easycork-light-167?category=167>. (Accessed: 13th December 2019)

Cork-Polymer Composites for Injection Moulding

2.1 Introduction.....	17
2.1.1 Cork-Polymer Composites.....	17
2.1.2 Coupling agents.....	19
2.1.3 Injection Moulding.....	20
References.....	22
2.2 Rheological behaviour of cork polymer composites for injection moulding.....	25
2.3 Non-isothermal crystallization kinetics of cork-polymer composites for injection moulding.....	39
2.4 Nucleating ability of cork in polypropylene-based composites.....	57
2.5 Cork-Polymer Composites for Injection Moulding.....	63

2.1 Introduction

2.1.1 Cork-Polymer Composites

In the last decade there has been an increasing interest in developing and using cork-based composites¹. As presented earlier, several challenges can be found when compounding natural fibres with polymeric matrices, namely (i) different densities, (ii) fibres hygroscopicity, (iii) fibres thermal degradation, (iv) fibres shape, size and weight fraction, (v) different polarities, among others². Natural fibres have lower densities which tend to bundle and producing a non-continuous dispersion of fibres within the polymeric matrix. The moisture of natural fibres also plays an important role. Prior compounding, it is necessary to remove the moisture content to prevent the releasement of water vapour and guarantee polymer wetting of fibres. Cork absorbs moisture at ambient conditions, despite of its intrinsic impermeability feature (Table 1.2)³. The production of composites with natural materials are also limited by the thermal degradation of natural components and longer processing times. It is known that cork structure and composition do not suffer significant changes up to 250°C⁴. Fibbers size, shape and weight fraction have influence on the miscibility of fibre-matrix composites and, consequently, on melt rheological properties. The effect of difference on polarities will be explained in the following topic. A proper fibre distribution within the polymeric matrices as well as enhanced physical properties will depend on a successful surpassing of such challenges.

In Table 2.1, it is exemplified published studies regarding the development of cork-based thermoplastic composite materials, defined as CPC. Extrusion-based techniques and melt mixing are the main selected processes to prepare CPC. It is seen that the addition of cork particles to polymeric matrices affected the mechanical behaviour.

It is detected an accentuated decrease on the tensile properties as the amount of cork increases in the matrix. Cork is a soft, porous material, where cork cell walls are pulled in the direction of tensile stress and fracture at the vicinity of a pore. In addition, cork is anisotropic, and for axial and tangential directions, cork fractures for tensile strength (σ_{\max}) equal to 1.0 and 0.6 MPa, after an elongation (ε_{\max}) of about 5 – 6%, respectively; and, for radial direction, fracture occurs at σ_{\max} of 1.1 MPa for an ε_{\max} of 8%. The tensile modulus (E) values for cork are 31.7, 23.9 and 31.2 MPa for axial, tangential and radial directions, respectively⁵. The number and size of cork pores and the undulations amplitude of cell walls influence tensile properties of cork. The addition of acetylated cork had a negative impact on the tensile properties, caused by the degradation of cork particles. Contrarily, the addition of coupling agent (CA) resulted in an increase of the tensile properties. The presence of natural fibres, such as coco fibres and wood flour, act as reinforcing agents having a positive effect on the mechanical behaviour of the developed CPC.

Table 2.1 | Published studies regarding the development of CPC (Adapted from ^{3,6-11}).
PSD, Particle Size Distribution; CA, Coupling Agent; ρ , density; T_m , melting temperature

CPC	Cork (% wt)	PSD (mm)	CA (% wt)	Natural Fibres (%wt)	Process	Neat Polymer		CPC					
						σ_{max} (MPa)	E (MPa)	ρ (Kg/m ³)	σ_{max} (MPa)	E (MPa)	T_m (°C)		
PP-Cork ⁷	50	0.5 – 1	NA	NA	Pultrusion	36±1	645±75	660	16±2	600±50	155.0 ^b		
	49		2 ^a					675	19±1	650±50	155.2 ^b		
PE-Cork ⁷	50	<0.25	NA	NA	Pultrusion	32±3	600±30	580	14±1	360±30	NA		
	49		2 ^a					590	16±1	400±10			
PE-Cork ⁸	45	<0.5	NA	NA	Counter-rotating twin-screw extrusion	26.8±0.4	630±40	1066±4	14.2±0.5	573±45	NA		
	44		2 ^a	10 ^c				1062±2	20.4±0.3	599±20			
PLA-Cork ⁹	30	0.25 – 0.5	NA	NA	Melt mixing (Brabender type)	68±2	11900±1000	580	35±1	2000±500	170 ^b		
PLA-ACork ⁹								310	8±2	2100±200	164 ^b		
PCL-Cork ⁹	30	0.25 – 0.5	NA	NA		22.5±2.0	1650±250	580	8±1	400±50	60 ^b		
PCL-HCork ⁹								720	11±2	420±60	59 ^b		
PP-Cork ³	15	<0.5	NA	NA	Co-rotating twin-screw extrusion	34.9±0.5	623.6±14.3	945±0.8	28.1±0.8	655±15	156.5 ^b		
			4 ^a					937±1.9	33.6±0.4	588 ±48	156.5 ^b		
PE-Cork ¹⁰	20	<0.5	2 ^a	NA	Co-rotating twin-screw extrusion	25.1±0.5	407.2±19.9	NA	18.5±0.5	445±30	126.2 ^b		
			2 ^d						17.9±0.8	370±29	124.5 ^b		
			2 ^e						20.2±0.5	475±30	125.5 ^b		
PLLA-Cork ⁶	30	0.5 – 1	NA	NA	Co-rotating twin-screw extrusion	52.2±5.9	1257±123	1196±4	25.7±3.3	851±93	154.2 ^f		
PHBV-Cork ⁶								30.3±2.4	1490±126	1210±3	21.6±1.7	1012±69	153.7 ^f
SPCL-Cork ⁶								18.5±0.7	362±46	1229±5	16.0±0.5	368±46	50.3 ^f
PP-Cork ¹¹	30	0.2 – 0.5	NA	NA	Twin-screw extrusion	32	1495	955	16	1260	NA		
	15			15 ^g				970	17	1510			
PLA-Cork ¹¹	30	15 ^g	NA	69	3250	1170	27.5	2100					
	15		15 ^g			1240	32	3100					

^a CA based on MA; ^b 10°C/min; ^c Coco fibres; ^d Suberin as CA; ^e Lignin as CA; ^f 20°C/min; ^g wood fibres
PP, Polypropylene; PCL, Polycaprolactone; ACork, Acetylated cork; HCork, Hexanoylated cork; PLLA, Poly-L-Lactic Acid; PHBV, Polyhydroxybutyrate-co-hydroxyvalerate; SPCL, starch-poly-ε-caprolactone

2.1.2 Coupling agents

The two major mechanisms of bond failure in composite materials are the poor chemical and physical interfacial adhesion between the polymeric matrix and the natural fibres. Both components only mix together without creating interactions between them, which simply result on a mechanical adhesion¹². This lack of interactions is a result of polarities incompatibility, in which the majority of thermoplastics are nonpolar and natural fibres are polar materials. Fibre–matrix interaction can be improved either via the fibre, usually by modifying its surface, or via the matrix, usually by employing additives called CA. Chemical treatments via the fibre aim to reduce the hydroxyl groups and impurities present on the surface of the fibre. Alkali treatments with sodium hydroxide (NaOH) are the most used^{12–14}. Chemical modification via the matrix, by the addition of CA, is the most common method to improve chemical affinity. CA act as bridges, creating linkages between the chemical groups on the fibre surface and the polymeric matrix. Chemical bonding mechanisms include primary bonding forms, such as covalent bonding (e.g. esterification), strong secondary interactions, as hydrogen bonding, and mechanical adhesion, like macromolecular chain entanglement². CA can be classified into organic, inorganic and organic-inorganic types^{2,12}, as exemplified in Figure 2.1.

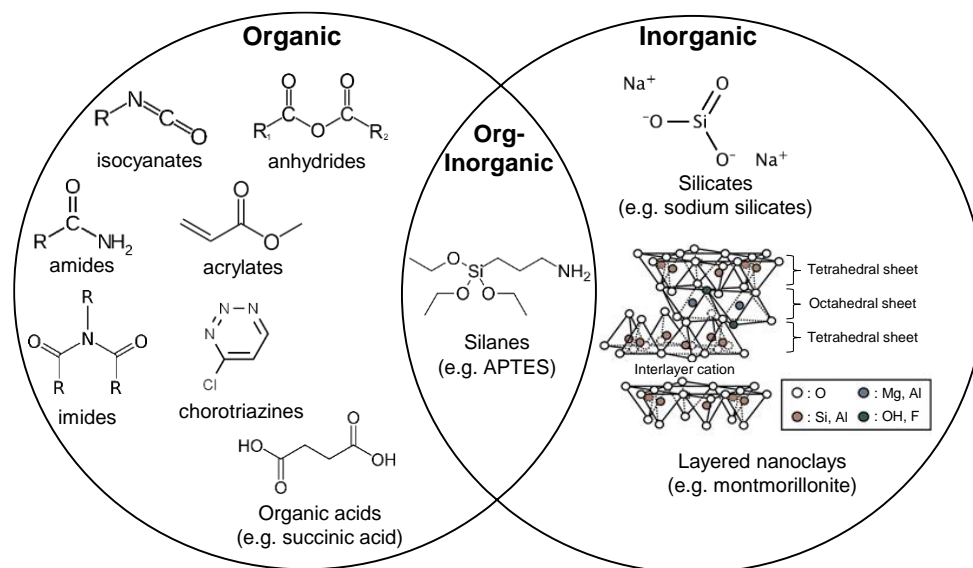


Figure 2.1 / Examples of different types of CA.

APTES, 3-Aminopropyl)triethoxysilane; image of montmorillonite adapted from Oliveira, A. *et al.*¹⁵

MA grafted polyolefins are the most widely used and popular CA due to their graft reactivity and commercial availability¹². They are composed by two functional domains: one, a polyolefin typically high-density PE (HDPE) or polypropylene (PP), which is able to form entanglements with the polymer matrix; and two, MA which is able to strongly interact with the fibre at processing temperatures¹⁶. The mechanical properties of composites are influenced by CA being relevant the following factors: (i) the amount added to the matrix/fibre, (ii) the saturation of the matrix/fibre interface, (iii) the functionalization site and (iv) its functionality¹⁷. Usually, it is used 1-5% wt of maleated polyolefins in

the composite formulation containing natural fibers^{16,18}. Looking at Table 2.1, it is visible that the addition of CA resulted on improved mechanical properties. For instance, Fernandes, E. M. *et al.*³ reported that the addition of 4 % wt of PP grafted MA (PPgMA) promoted an increase of 20% on σ_{max} and of 19% on ϵ_{max} of CPC. This enhancement on tensile properties can be attributed to the improvement of the interfacial adhesion between the polymeric matrix and cork particles as a result of the establishment of covalent and hydrogen bonds between hydroxyl and anhydride groups. Abdallah, F. B. *et al.*¹⁹ explored the development of PP-Cork composites with different chemical modifications, namely cork treatment with silane, NaOH and addition of PPgMA (5, 10 and 15 %wt). They concluded that the silanization treatment enhanced the interfacial adhesion between PP and cork, when compared to other chemical treatments. This enhancement is verified by CPC mechanical performance during tensile trials. It seems that the selected amount of PPgMA was not indicated and probably led to secondary reactions. In fact, authors report that MA concentrations of 10 and 15 %wt did not have a positive influence on the mechanical behaviour.

2.1.3 Injection Moulding

IM, a formative manufacturing technology, is one of the most used technology on the processing of thermoplastic materials, due to the high production rate of complex parts with dimensional accuracy and surface finishing. Besides machine and tooling high costs, they are usually recovered through short cycle times, automation and low labour costs²⁰. PP, acrylonitrile butadiene styrene, PE and polystyrene are the major thermoplastic materials processed by IM. Short-fibre reinforced or particulate filled composites are also injected moulded, namely using glass fibres, talc, calcium carbonate, carbon fibres, wood, etc.²⁰ Extremely varied applications of IM products can be found, from daily-basis products, such as containers, lenses, tool handlers, to automotive and healthcare solutions, such as bumpers, dashboards and syringes.

The study of polymers' physical behaviour is of paramount importance in the development of good quality products based in IM technology. Such physical properties involve thermal and rheological behaviour and, consequently, the mechanical performance of polymers under IM processing conditions. The fabrication of high-quality products with sufficient strength and stiffness is the main goal throughout this technology. Therefore, it is required that melt flows easily into the mould and be free of residual stresses.

The glass transition temperature (T_g), the melting temperature (T_m) and the crystalline structure, influence polymer's physical behaviour. The density of molecular chain branches influences the value of T_g of a specific polymer, where a high density of branches decreases chain mobility and increase the value of T_g . T_m is also a relevant parameter on material selection and it is associated with the crystalline phase of the material. In the case of polymers, T_m is dependent on thermal history and the temperature at which polymers crystallize²¹. Polymers can be semi-crystalline or amorphous.

Crystallization occurs through the nucleation and growth mechanisms of small molecules²². Crystallites usually have a chain-folded structure, but many of semi-crystalline polymers form

spherulites. The growth of spherulites can be limited from the impingement of adjacent spherulites to one another. Crystallization can affect mechanical, thermal, optical and chemical properties of the polymer. The addition of natural materials can influence the crystallization process mostly by revealing nucleation activity and/or transcrystallization^{23–25}. The processing conditions also affects the crystallization behaviour. In industrial processes, like extrusion and IM, composites experience non-isothermal crystallization rather than isothermal crystallization. In IM, processing parameters, such as melting temperatures, high pressures, and shear rates are applied during the process. These severe conditions influence polymer's crystals nucleation and growth and, therefore, the spherulites number and size.

The use of nucleating agents can contribute for a shorter IM cycle reducing the manufacturing costs. It can also improves optical and mechanical properties through the development of small spherulites^{25, 26}. Soleimani, M. *et al.*²⁵ studied the effect of flax fibre loading, chemical modification, and the use of compatibilizer PPgMA on the non-isothermal crystallization kinetics of PP. They found that the addition of flax fibres resulted in higher degree of crystallinity (X_c). This was attributed to the nucleation ability of the fibres which provides nucleation sites and facilitates crystallization of the polymer as well as transcrystallinity. Some fibres have the ability to act as heterogeneous nucleating agents promoting high density of nucleation centres. The crystals grow in a direction perpendicular to the fibres surface occurring the transcrystallinity phenomenon. At the same cooling rate, the addition of fibres increased crystallization temperature (T_c). For higher cooling rates, a lower T_c and X_c were observed, but a faster kinetic of crystallization was attained. Also, PPgMA reduced the crystallinity degree, but accelerated the crystallization rate. The same trend was observed by Grozdanov, A. *et al.*²³, who have studied the non-isothermal crystallization kinetics of kenaf fibre/polypropylene composites.

In terms of rheological behaviour, polymer melts are non-Newtonian fluids and their viscosity decreases with increasing shear rate – as known as shear thinning or pseudoplastic behaviour. Polymers molecular structure, which includes chain branching and its configuration, average molecular weight (\overline{M}_w) and molecular weight distribution (MWD) have direct impact on how the melt flows, affecting its viscosity and elasticity²⁷. More specifically, a polymer with a broad distribution tend to transit to a shear-thinning behaviour at lower shear rates than those with a narrow distribution. In polymer processing, a transition at lower shear rates is desired once the energy consumption is reduced^{27,28}. In addition, the number, the size and the flexibility of molecular chain branches also affect the polymer melt flow behaviour. A polymer with few branches with enough length to entangle have higher viscosity at lower shear rates than the same polymer with a linear configuration (with the same \overline{M}_w). This is due to the fact that branched polymers are less compact than linear polymers, which result in an increased melt viscosity. Other factors influence the rheological behaviour of polymers, namely the processing parameters, such as temperature, pressure and equipment's geometrical factor; and, the addition of fillers and other additives^{27–30}. Tazi, M. *et al.*³⁰ studied the rheological, thermal and thermo-physical properties of HDPE-wood composites as a function of temperature and filler concentration. As expected, the viscosity of these wood-plastic composites

(WPC) increases as the concentration of wood phase increases, while it decreases as temperature increases. In the presence of PE grafted MA, the viscosity of HDPE-WPC increased as well as the relaxation time and the activation energy of polymer chains. The authors suggested that this behaviour can be due to an improved interaction between wood particles and polymer matrix. A rapid alternative to rheological analysis is the determination of the melt flow index (MFI)³¹ to estimate polymer's viscosity for comparative purposes, commonly used in the industry.

There are already CPC solutions in the market for IM^{32,33}. However, the high pressure applied during the IM process compresses cork alveolar structure, as shown in Figure 1.2, and cork intrinsic properties (Table 1.2) are lost. One of the main motivations of the present thesis is to study an adapted IM technology to overcome the high pressure applied and take advantage of cork unique properties. The basic ideas will consist on two strategies: (1) to give enough time to cork alveoli return to its initial shape or (2) to apply shear stress on polymer melt during cooling to facilitate the expansion of cork alveoli. As inspiration, it will be seek an open-cell structure, similarly to that obtained during IM of polymeric foams. Generally, polymeric foams can be obtained by a chemical route that consists on the addition of foaming agents, or by a physical route, that involves the injection of blowing gases³⁴. In this particular case, it is desired that cork alveoli expansion on polymer melt will happen naturally, without the addition of any chemical or physical agent.

References

1. Gil, L. Cork Composites: A Review. *Materials (Basel)*. 2, 776–789 (2009).
2. Stokke, D. D., Wu, Q. & Han, G. *Introduction to Wood and Natural Fibers Composites*. (John Wiley & Sons, Ltd., 2014).
3. Fernandes, E. M., Correlo, V. M., Mano, J. F. & Reis, R. L. Polypropylene-based cork–polymer composites: Processing parameters and properties. *Compos. Part B Eng.* 66, 210–223 (2014).
4. Rosa, M. E. & Fortes, M. A. Thermogravimetric analysis of cork. *J. Mater. Sci. Lett.* 7, 1064–1065 (1988).
5. Pereira, H. *Cork : Biology, Production and Uses*. (Elsevier, 2007).
6. Fernandes, E. M., Correlo, V. M., Mano, J. F. & Reis, R. L. Cork–polymer biocomposites: Mechanical, structural and thermal properties. *Mater. Des.* 82, 282–289 (2015).
7. Fernandes, E. M., Correlo, V. M., Chagas, J. a. M., Mano, J. F. & Reis, R. L. Cork based composites using polyolefin's as matrix: Morphology and mechanical performance. *Compos. Sci. Technol.* 70, 2310–2318 (2010).
8. Fernandes, E. M., Correlo, V. M., Mano, J. F. & Reis, R. L. Novel cork–polymer composites reinforced with short natural coconut fibres: Effect of fibre loading and coupling agent addition. *Compos. Sci. Technol.* 78, 56–62 (2013).
9. Vilela, C., Sousa, A. F., Freire, C. S. R., Silvestre, A. J. D. & Pascoal Neto, C. Novel sustainable composites prepared from cork residues and biopolymers. *Biomass and Bioenergy* 55, 148–155 (2013).
10. Fernandes, E. M., Aroso, I. M., Mano, J. F., Covas, J. A. & Reis, R. L. Functionalized cork-polymer composites (CPC) by reactive extrusion using suberin and lignin from cork as coupling agents. *Compos. Part B Eng.* 67, 371–380 (2014).
11. Andrzejewski, J., Szostak, M., Barczewski, M. & Łuczak, P. Cork-wood hybrid filler system for polypropylene and poly(lactic acid) based injection molded composites. Structure evaluation and mechanical performance. *Compos. Part B Eng.* 163, 655–668 (2019).
12. Thakur, V. K. *Lignocellulosic Polymer Composites: Processing, Characterization and Properties*. (Scrivener Publishing, Wiley, 2015).
13. Fernandes, E. M., Mano, J. F. & Reis, R. L. Hybrid cork–polymer composites containing sisal fibre: Morphology, effect of the fibre treatment on the mechanical properties and tensile failure prediction. *Compos. Struct.* 105, 153–162 (2013).

14. Bettini, S. H. P., Biteli, A. C., Bonse, B. C. & Morandim-Giannetti, A. de A. Polypropylene composites reinforced with untreated and chemically treated coir: Effect of the presence of compatibilizer. *Polym. Eng. Sci.* 55, 2050–2057 (2015).
15. Oliveira, A. D. & Breatice, C. A. G. Polymer Nanocomposites with Different Types of Nanofiller. in *Nanocomposites - Recent Evolutions* (ed. Sivasankaran, S.) 26 (InTechOpen, 2018).
16. Sobczak, L., Brüggemann, O. & Putz, R. F. Polyolefin composites with natural fibers and wood-modification of the fiber/filler-matrix interaction. *J. Appl. Polym. Sci.* 127, 1–17 (2013).
17. González-López, M. E., Robledo-Ortíz, J. R., Manríquez-González, R., Silva-Guzmán, J. A. & Pérez-Fonseca, A. A. Polylactic acid functionalization with maleic anhydride and its use as coupling agent in natural fiber biocomposites: a review. *Compos. Interfaces* 25, 515–538 (2018).
18. Visahk, P. M. & José Martinez Morlanes, M. Polyethylene Composites with Lignocellulosic Material. in *Polyethylene-Based Blends, Composites and Nanocomposites* (Scrivener Publishing, Wiley, 2015).
19. Abdallah, F. B., Cheikh, R. B., Baklouti, M., Denchev, Z. & Cunha, A. M. Effect of surface treatment in cork reinforced composites. *J. Polym. Res.* 17, 519–528 (2009).
20. Osswald, T. A., Turng, L.-S. & Gramann, P. *Injection molding handbook*. (Hanser Publishers, 2002).
21. Callister, W. D. & Rethwisch, D. G. *Materials Science and Engineering*. (John Wiley & Sons, Inc., 2015).
22. Long, Y., Shanks, R. A. & Stachurski, Z. H. Kinetics of polymer crystallisation. *Prog. Polym. Sci.* 20, 651–701 (1995).
23. Grozdanov, A. et al. Nonisothermal crystallization kinetics of kenaf fiber/polypropylene composites. *Polym. Eng. Sci.* 47, 745–749 (2007).
24. Liu, X., Tang, Y., Zhang, B., Chen, F. & Xu, W. Nonisothermal crystallization kinetics of polypropylene composites reinforced with down feather fiber. *Polym. Compos.* 37, 1–10 (2015).
25. Soleimani, M., Tabil, L., Panigrahi, S. & Oguocha, I. Crystallization and Thermal Properties of Biofiber. in *Thermoplastic - Composite Materials* (ed. El-Sonbati, A. P.) 131–146 (InTech, 2012).
26. Mucha, M. & Królikowski, Z. Application of dsc to study crystallization kinetics of polypropylene containing fillers. *J. Therm. Anal. Calorim.* 74, 549–557 (2003).
27. Dealy, J. M. & Wissbrun, K. *Melt rheology and its role in plastics processing: theory and applications*. (Chapman & Hall, 1995).
28. Gupta, R. K. *Polymer and Composite Rheology*. (CRC Press, 2000).
29. Ariff, Z. M., Ariffin, A., Jikan, S. S., Azura, N. & Rahim, A. Rheological Behaviour of Polypropylene Through Extrusion and Capillary Rheometry.
30. Tazi, M., Erchiqui, F., Godard, F., Kaddami, H. & Ajjji, A. Characterization of rheological and thermophysical properties of HDPE-wood composite. *J. Appl. Polym. Sci.* 131, 40495–40506 (2014).
31. ISO 1133:2005 Plastic - Determination of the melt mass-flow rate (MFR) and the melt volume-flow rate (MVR) of thermoplastics. (2005).
32. ACC. Cork Solutions & Manufacturing Processes. (2017). Available at: https://amorimcorkcomposites.com/media/3948/171124_acc_book_cork_solutions_and_processes_short_digital_web.pdf.
33. Hexpol. Lifocork. Available at: <https://www.hexpol.com/tpe/product-brands/lifocork/>.
34. Altan, M. Thermoplastic Foams: Processing, Manufacturing, and Characterization. in *Recent Research in Polymerization* 117–137 (InTech, 2018)

2.2 Rheological behaviour of cork-polymer composites for injection moulding ^d

Sara P. Magalhães da Silva^{1*}, Paulo Silva Lima¹, José Martinho Oliveira^{1,2}

¹ School of Design, Management and Production Technologies, University of Aveiro, Estrada do Cercal, nº449, 3720-509 Santiago de Riba-Ul, Oliveira de Azeméis, Portugal

² Centre for Research in Ceramic and Composite Materials (CICECO), University of Aveiro, Campus Universitário de Santiago, 3810-193 Aveiro, Portugal

*corresponding author: sarapms@ua.pt

Abstract

The incorporation of cork in synthetic polymers has become an effective approach to develop new sustainable materials. Cork-polypropylene composites (CPC) filled with three different cork granulometries were studied. Rheological analyses were performed to assess the processability of these CPC and a set of experiments was conducted keeping the same matrix/cork weight ratio, varying the cork granulometric distribution. The effect of three different cork granulometries, temperature and the effect of a coupling agent, polypropylene graft maleic anhydride (PPgMA), were analysed. All composites exhibited non-Newtonian, pseudoplastic behaviour. Related to neat PP, cork incorporation led to a viscosity increase. This increase is more significant in the CPC with the lowest powder cork granulometry used. On the other side, the addition of PPgMA resulted on a decrease of CPC viscosity. The experimental results were fitted to Cross-WLF Model through a viscosity master curve obtained by the time-temperature superposition principle (TTSP). This study showed that cork can be considered on the development of sustainable materials for injection moulding technology.

Keywords: A. Polymer-matrix composites (PMCs), B. Thermoplastic resin, C. Rheological properties, D. Injection moulding

1. Introduction

The incorporation of lignocellulosic materials in synthetic polymers has become an effective approach to develop new sustainable materials. Polypropylene (PP) is a thermoplastic commonly used in industry and frequently charged with inorganic fillers to improve its mechanical properties ^{1,2}. The advantages of applying natural materials as fillers to reinforce thermoplastic composites are based on their low density, hardness and cost, good relation between strength/weight, good insulation properties and high levels of filling. Also, they are renewable and readily available materials, recyclable and non-toxic ^{1,3}.

^d Magalhães da Silva, S. P., Lima P. S., Oliveira J. M. Rheological behaviour of cork-polymer composites for injection moulding, *Compos. Part B-Eng.* 2015, **90**, 172–178.

The author had contributed to the planning and execution of all the rheological analyses and modelling calculations herein presented, as well as on the discussion, interpretation and preparation of the manuscript.

Cork is the outer bark of the cork oak *Quercus suber L.*, which is periodically harvested, usually every 9-12 years depending on the culture region. In terms of structure, cork presents tiny hollow cells of hexagonal shape in a closed-cell foam⁴. The main chemically component is suberin (33-50%), followed by lignin (20-25%); the carbohydrate fraction is composed by cellulose and hemicelluloses (12-20%); extractives represent nearly 14-18% and $\approx 1\%$ are ashes^{1,4-6}. Cork possesses a unique combination of properties, more specifically, low density, elasticity and compressibility (without lateral expansion), high recovery capacity after impact, impermeability to liquids and gases, excellent thermal and acoustic insulation and, microbial and fire resistance. It is well known that the major use for cork is the production of stoppers^{4,7}. However, during cork processing a relative high amount ($\approx 30\%$) of residues are produced⁶. Owing to the low granulometry of the residues, they aren't suitable for typical cork applications and, usually, they are burned or disposed in landfills. Hence, these residues are suitable raw materials for the development of new materials solutions tailoring the needs of different applications. Namely, in construction (thermal and acoustic solutions), decoration, design of functional objects (for instance, orthopaedic shoes) as well as the development of materials to the automobile, aeronautical and aerospace industries.

CPC are one of the most propitious applications of cork to produce new products based on sustainable development. The final properties of CPC are extremely dependent on the processing conditions. The size, shape and structure of filler particles have a pronounced effect on the mechanical and rheological properties of the neat polymers^{1,3,5,8-10}. The mechanical properties of cork composites are highly dependent on the interaction between the polymer matrix and the filler. The ability to stress transfer from the matrix to the filler depends on the interface of both materials. Coupling agents are usually applied to promote the compatibility between polymer matrices and lignocellulosic materials. PPgMA is one of the most used coupling agents. The interactions between PPgMA maleic groups and hydroxyl groups of natural fibres increase the interfacial adhesion between both materials leading to a better mechanical performance^{1,3}. Another way to improve the adhesion is the modification of cork surface through silanization, alkaline solutions, hot water and plasma treatment¹¹⁻¹³.

The understanding of polymer rheology is necessary for an accurate design, material and processing selection as well as for an efficient fabrication and service performance. Several factors influence the rheological behaviour of materials: (1) molecular structure, such as chain branching and its configuration, average molecular weight and molecular weight distribution; (2) process parameters, like temperature, pressure and equipment's geometrical factor; (3) addition of fillers and other additives^{10,14}. The study of the melt rheology is of paramount importance in the development of good quality products based in injection moulding technology. The fabrication of high-quality products with sufficient strength and stiffness is the main goal throughout this technology. Therefore, this requires that melt flow easily into the mould and free of residual stresses. The shortest injection cycle time should also be applied in order to minimize costs¹⁴. Tazi *et al.*³ studied the rheological, thermal and thermo-physical properties of high-density polyethylene (HDPE)-wood composites as a function of temperature and filler concentration. As expected, the viscosity of these wood-plastic

composites (WPC) increases as the concentration of wood phase increases, while it decreases as temperature increases. In the presence of polyethylene graft maleic anhydride (PEgMA), the viscosity of HDPE-WPC increased as well as the relaxation time and the activation energy of polymer chains. The authors suggest that this behaviour can be due to a good interaction between wood particles and polymer matrix. Also, a viscosity master curve for each HDPE-WPC based on the TTSP using temperature-dependent shift factor was presented.

This study analyses the effect of temperature, granulometry and the presence of a coupling agent (PPgMA) on the rheological behaviour of CPC for injection moulding applications. The rheological properties of CPC should be addressed.

2. Experimental

2.1 Materials

The polymeric matrix used in this work is a homopolymer PP (PPH 10060) from Total Petrochemicals, with a Melt Fluid Index (MFI) of 35 g·10min⁻¹ (230°C, 2.16 Kg) and a melting point of 165°C. Three different cork granulometries were used. The cork was supplied by a Portuguese cork producer. The samples were fractionated through sieving (Retsch, Germany) and the average particle size was determined. The characterisation of the different cork particles are presented in Table 1. PPgMA from ExxonMobil, Germany (ExxelorTM PO 1020) containing 0.5-1.0 wt% of grafted maleic anhydride, with a MFI of 430 g·10min⁻¹ (230°C, 2.16 Kg) and a melting point of 162°C, was used as coupling agent.

Table 1. Cork particles: physical characteristics.

Granulometry mesh (µm)	Sample 1 (%)	Sample 2 (%)	Sample 3 (%)
1000	2.3	0	0
800	45.8	0.1	0
400	51.4	40.9	1.1
200	0.6	54.3	2.6
100	0	4.2	48.8
80	0	0.3	4.8
63	0	0.2	9.6
20	0	0	30.2
<20	0	0	2.9
<i>sum</i>	100	100	100
Average particle size* (µm)	596	276	70
Specific weight (Kg·m⁻³)	121	115	101

* $d_p = \frac{\sum w_i d_i^4}{\sum w_i d_i^3}$, where w_i is the weight fraction in each sieve and d_i is the sieve mesh size.

2.2 Preparation of cork-polymer composites

Before compounding, the cork particles were dried at 70°C for 24h in a vacuum oven (Carbolite AX60 model) to stabilize the moisture content. It is known that the cork structure and composition do not suffer significant changes up to 250°C¹⁵. CPC were compounded in a Brabender type internal mixer. The total volume of the mixing chamber is 22 cm³. Firstly, PP pellets were charged and melted during 2 minutes at 180°C and 40 rotations per minute. Then, cork particles were added and the system was mixed for additional 8 minutes. The same matrix/cork weight ratio (85/15) was kept constant through all the experiments. For the preparation of CPC in the presence of coupling agent, PPgMA was added together with cork particles. The amount of PPgMA present was also kept constant in all formulations (4 %wt). Table 2 shows the formulations. A formulation of PP/PPgMA (PPg) was prepared to evaluate the individual effect of PPgMA in the PP matrix.

Table 2. Compositions used in the preparation of CPC.

Sample Code	Components									
	PP		Cork						PPgMA	
	% wt	% vt	596 μm		276 μm		70 μm		% wt	% vt
PPg			100	100						
CPC 1	85	43	15	57					-	
CPC 2	85	42			15	58			-	
CPC 3	85	39					15	61	-	
CPC 4	85	43	15	57					4	2
CPC 5	85	42			15	58			4	2
CPC 6	85	39					15	61	4	2

* %wt of PP.

2.3 Rheological Analyses

Prior to rheological analyses, the formulated CPC were shredded into small granules (Dynisco, 1620 model). A double capillary rheometer (LCR 7002 Dynisco) equipped with two dies with same diameter (1 mm) and different length were used. The L/D ratio was 5 and 30. The analyses were carried out at three different temperatures (180, 200 and 220°C) and an initial melting time of 5 minutes was applied. The instrument was set at constant speed/shear rate mode to a shear rate range of 10 to 6000s⁻¹. The melt viscosity was calculated according to equations Eqs. (A1-A6) presented in Appendix A.

Both Rabinowitsch-Weissenberg¹⁴ and Ryder-Bagley¹⁶ corrections as well as the melt viscosity values were calculated by the LAB KARS software (version 3), Alpha Technologies. The melt viscosity values for each experiment correspond to the average of at least 3 trials.

Cross-WLF Model¹⁷ was used to describe the composite melt viscosity dependence upon temperature and shear rate Eq. (1). This model is currently been applied in injection moulding technology, once it is able to describe both Newtonian and shear thinning regions. Herewith, a good approximation of the real processing conditions during filling and post-filling phases is accomplished.

$$\eta = \frac{\eta_0}{1 + \left(\frac{\eta_0}{\tau^*} \dot{\gamma}_w\right)^{(1-n)}} \quad (1)$$

where η_0 (Pa·s) is the zero-shear rate viscosity, $\dot{\gamma}_w$ (s⁻¹) is the wall shear rate, τ^* (Pa) is the critical stress level at the transition from the Newtonian to shear thinning and n (dimensionless) is the power law index which symbolizes the pseudoplastic behaviour. To determine the η_0 , the Williams-Landel-Ferry¹⁸ equation was applied Eq. (2):

$$\eta_0 = D_1 e^{\frac{-A_1(T-\tilde{T})}{-A_2+(T-\tilde{T})}} \quad \begin{aligned} A_2 &= \tilde{A}_2 + D_3 P \\ \tilde{T} &= D_2 + D_3 P \end{aligned} \quad (2)$$

where \tilde{T} (K) is the material transition temperature. $D_1, A_1, \tilde{A}_2, D_3$ and D_2 are data-fitted coefficients. The Cross-WLF coefficients were determined with *Solver* tool from MS Excel through the minimization of an objective function Eq. (3). This objective function consisted on the sum of the chi-square errors across i temperatures and j shear rates.

$$O = \min \sum_i \sum_j \left(\frac{\eta_{i,j}^{Obs} - \eta_{i,j}^{Pre}}{\eta_{i,j}^{Pre}} \right)^2 \quad (3)$$

where $\eta_{i,j}^{Obs}$ and $\eta_{i,j}^{Pre}$ are the observed and predicted viscosity at a given temperature (T_i) and the shear rate ($\dot{\gamma}_{wi}$). For the fitting to the Cross-WLF Model (Eqs. (1-3)), the coefficients τ^* , n , A_1 , D_1 and D_2 were allowed to vary, while A_2 and D_3 were held at 51.6K¹⁸ and 0, respectively. The pressure dependence in rheological characterisation is often assumed to be negligible. For each temperature, Cross-WLF model coefficients were determined (data not shown) and used in the construction of the master curve for each CPC.

Polymers are very sensitive to temperature and shear rate, thus a large number of experimental results are necessary to characterise their flow behaviour. Sometimes these results are time-consuming or inaccessible, due to equipment limitations (for instance, capillary rheometers are unable to measure at low shear rates). Therefore, the design of a master curve through the superposition of several curves obtained at different temperatures is required. The construction of the master curve was based on the TTSP¹⁹. The application of this principle allowed the construction of a master curve to each CPC through the employment of the horizontal shift factor (a_T). In this case, viscosity curves were shifted to a reference temperature (T_0) equal to 200°C. The superposition

was determined by Eq. (4), from which the reduced viscosity (η/a_T) and reduced shear rate ($\dot{\gamma}_w \cdot a_T$) were obtained.

$$a_T(T) = \frac{\eta_0(T)}{\eta_0(T_0)} \quad (4)$$

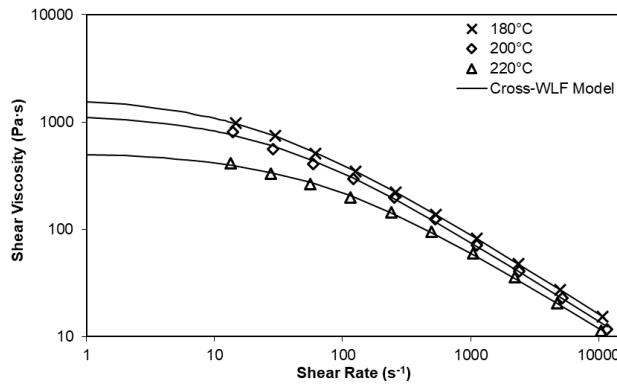
As referred above, the master curve for each CPC was then fitted to the Cross-WLF model and the master curve Cross-WLF coefficients determined.

3. Results and Discussion

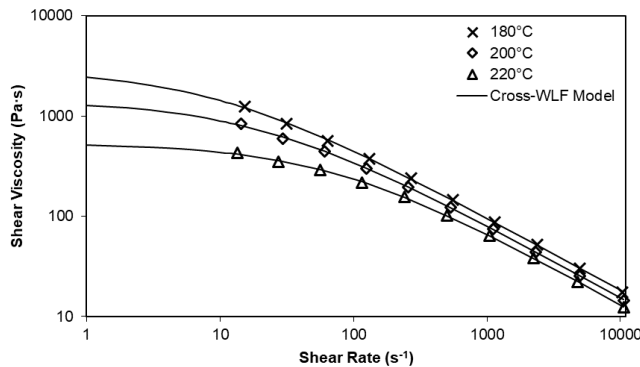
3.1 Temperature dependence of viscosity

Temperature affects significantly the rheological behaviour of the developed CPC. Dependence of viscosity with temperature is shown in Figure 1 and, as expected, for all CPC viscosity decreases as temperature increases. High temperatures lead to an increase of the free volume, allowing more space for the polymer chain motions (or reduced friction between them). More free volume means easier flow and, hence decreased viscosity. Higher temperatures also favour the disentanglements of the molecular chains enhancing the Newtonian regime. Thus, it can be assumed that the transition Newtonian to a Non-Newtonian regime is temperature dependent.

(a)



(b)



(c)

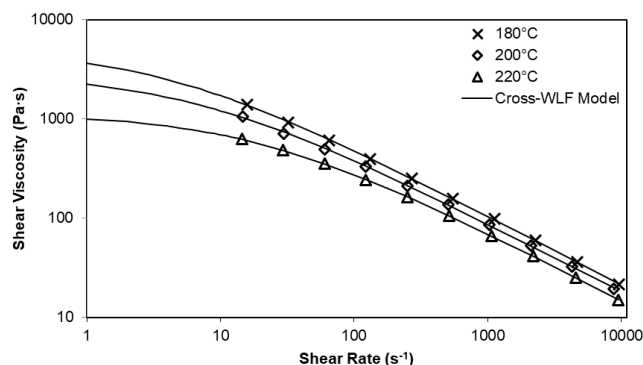


Figure 1. Viscosity curves of (a) CPC 1, (b) CPC 2 and (c) CPC 3 at various temperatures.

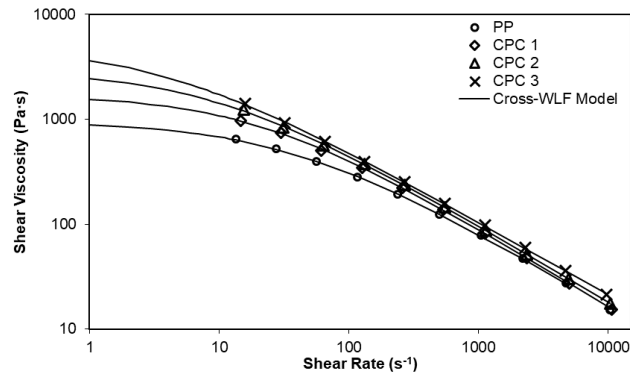
From Figure 1, it is also evident that the decrease of viscosity with temperature is shear rate dependent. A stronger temperature dependence of viscosity occurs at lower shear rates. As the shear rate increases, the entanglements of polymer chains have a more pronounced effect.

3.2 Effect of cork and particles size distribution on viscosity

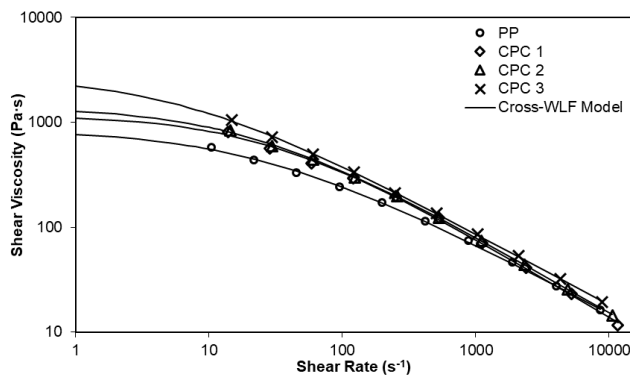
The presence of fillers affects the rheological behaviour of the polymeric system. The type, size and shape of filler as well as its size distribution and concentration are important factors to be considered for the determination of rheological properties⁸. The influence of cork presence and cork particles size distribution on the viscosity of CPC at various temperatures is shown in Figure 2. The addition of cork to neat PP results in an increase of viscosity. The incorporation of cork decreases the fluidity of PP by increasing the flow resistance, and consequently an increase of the viscosity is attained. This agrees with other rheological studies involving polymers and natural fillers^{3,9,20–22}.

It is also important to point out that the addition of cork has not changed the characteristic pseudoplastic behaviour of neat PP¹⁰ – an important factor on the development of CPC for the injection moulding process. Regarding the particles size effect on the rheological behaviour, composites with smaller cork particles (70 μm) exhibit a higher viscosity than polymers with large-sized particles (596 and 276 μm). Due to the larger specific surface area a better wetting of the smaller cork particles is obtained, resulting in an increase of viscosity. It is important to bear in mind that, in this study, the proportion of PP/Cork in all CPC is kept constant and equal to 85/15 %wt, varying only the particle size distribution. As discussed on the section 3.1, the shear rate has impact on viscosity. With increasing shear rate the effect of particles size becomes less pronounced. At high shear rates, cork particles size do not provide a significant effect on composite viscosity, because the composite structure is governed by the polymeric matrix and not by the cork particles^{2,9,23}.

(a)



(b)



(c)

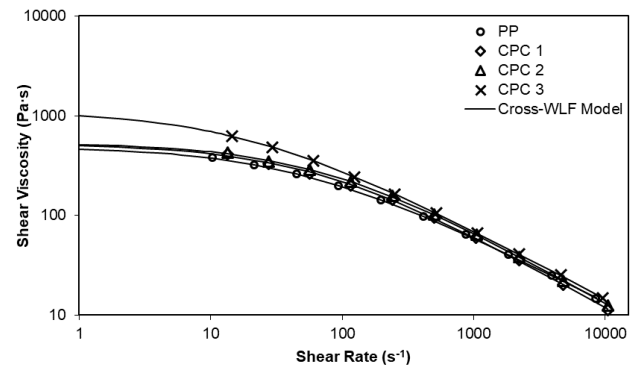


Figure 2. Viscosity curves of CPC at (a) 180°C, (b) 200°C and (c) 220°C.

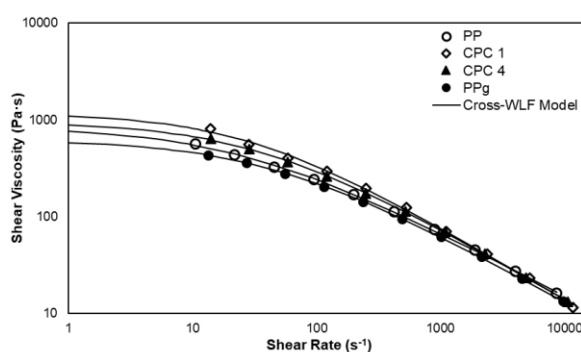
Another observed trend is that, with increasing temperature, the large-sized particles seem to have a lower effect on the viscosity. Working with wood flour with different particles sizes added to PE matrices, Hristov *et al.*²⁴ reported that smaller particles revealed to have higher storage modulus. It seems that cork particles assumed the same behaviour, and thus presented higher resistance to

deformation. Contrarily, the large-sized particles with lower storage modulus along with their higher free volume are more deformed favouring the flow.

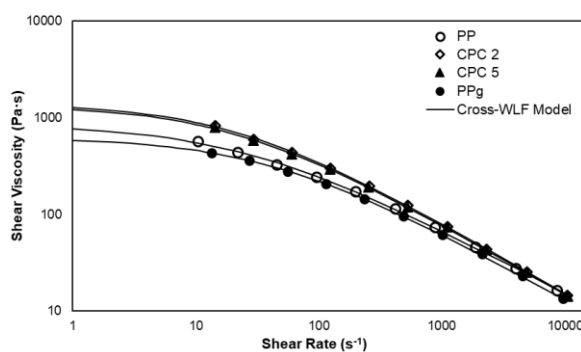
3.3 Effect of the coupling agent on viscosity

In this study, PPgMA was selected as the coupling agent. The main PPgMA chain is similar to the composite matrix which is a major advantage in terms of compatibility. Furthermore, maleic anhydride can react with the hydroxyl groups present on cork's surface promoting a better interfacial adhesion between cork and the polymer. The influence of PPgMA in the CPC viscosity is represented in Figure 3.

(a)



(b)



(c)

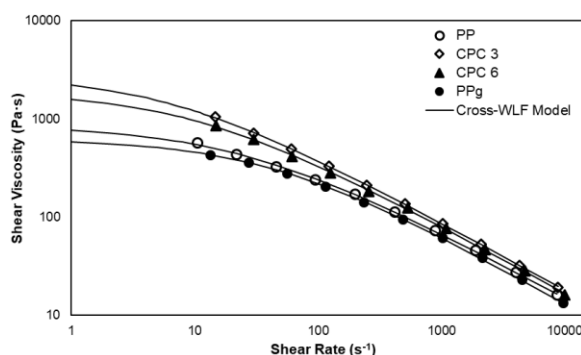


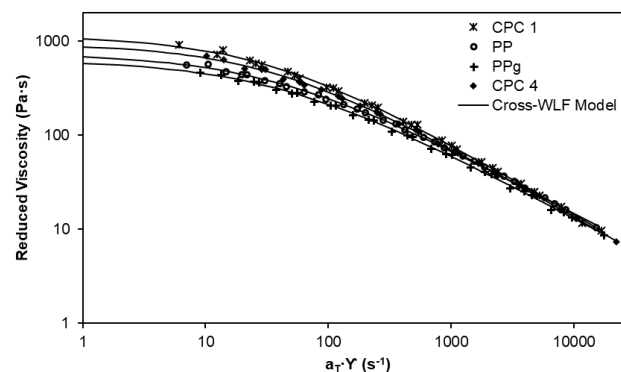
Figure 3. Effect of PPgMA on the CPC viscosity: (a) CPC 1 and CPC 4, (b) CPC 2 and CPC 5, (c) CPC 3 and CPC 6, at 200°C.

In the presence of 4% wt of PPgMA the CPC revealed lower viscosity when compared with the equivalent CPC (PPgMA free), which is an indication that PPgMA can act as a flow promoter in PP matrix. The softening effect of maleic anhydride on cork's particles surface results in a decreasing of their resistance to flow. This may be attributed to the lubricant/plasticising effect of coupling agents similar to that noted in other studies^{10,20,22,23,25}. Bettini *et al.*²², have performed rheological analyses on PP/sawdust composites. When compared with the non-compatible composite, the presence of PPgMA promotes an increase on the viscosity of the compatibilized composite. They also reported that PPgMA acted as internal lubricant and as a compatibilizer. However, in this case, PPgMA lubricant ability had a more pronounced effect on viscosity. Nevertheless, to a better evaluation of the adhesion between PP and cork particles with PPgMA, further studies are required, namely the study of CPC mechanical properties. Figure 3 also shows the isolated effect of PPgMA in a PP matrix. As referred above, PPgMA plays a role as flow promoter, once PPgMA has the ability to react with the PP matrix and to space out the PP molecules increasing their mobility, and thus reducing the viscosity.¹⁰ As the rheology behaviour is very sensitive to molecular structure, the addition of low molecular weight and short-chain branching molecules result on the decreasing of viscosity. Li *et al.*²⁵ reported that the presence of a low viscosity dispersed phase can easily become anisotropic in shape as it goes through the die, creating elongated drops, which could result in less resistance to flow. As the shear rate increases the effect of PPgMA becomes less pronounced – high shear rate deforms the continuous phase, reducing the effect of PPgMA role in the melt viscosity.

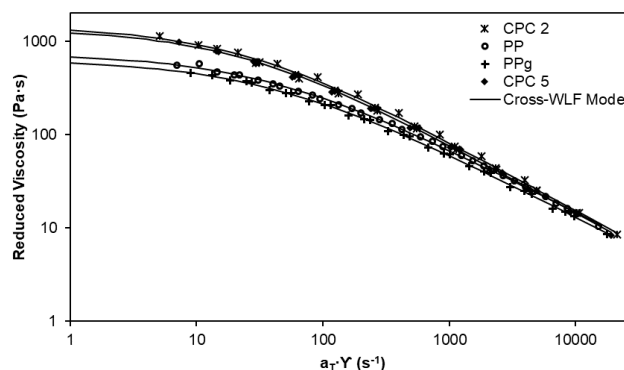
3.4 Viscosity Master Curve

Figure 4 shows the changes of reduced viscosity (η/a_T) as a function of reduced shear rate ($\dot{\gamma} \cdot a_T$). The TTSP is mainly applied to homogenous amorphous polymers, however it can also be applied if the composite materials reveal thermo-rheological behaviour simplicity. Thermo-rheological behaviour simplicity means that the viscoelastic functions measured at different temperatures can be shifted by a shift factor to a single curve (master curve) at a selected reference temperature.

(a)



(b)



(c)

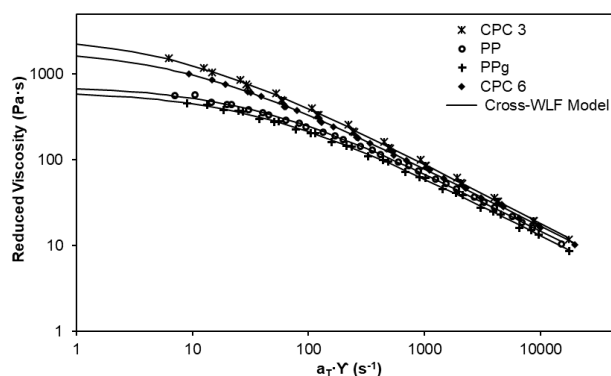


Figure 4. Master curves of (a) CPC 1 and CPC 4, (b) CPC 2 and CPC 5, (c) CPC 3 and CPC 6.

As can be seen from Figure 4, all the materials present thermo-rheological simplicity. Moreover, it can be assumed that all the relaxation times have the same temperature dependence. The master curves were fitted to Cross-WLF Model allowing the definition of a single behaviour for each CPC covering different temperatures and shear rates. Additionally, they allowed the prediction of the rheological behaviour out of the experimental shear rate range measured (determination of the zero-shear rate viscosity).

Table 3 resumes the rheological coefficients (η_0 , τ^* , n) obtained from the fitting. For all curves, a correlation factor closer to 1 was obtained revealing the accuracy of the Cross-WLF Model to describe the pseudoplastic behaviour of CPC. As discussed above, the composites with smaller cork particle granulometries (CPC 3 and CPC 6) present the higher viscosity, thus higher η_0 . On the other hand, the addition of PPgMA resulted in η_0 decrease when added to pure PP as well as in CPC. It's evident the plasticizer effect of PPgMA (already explained). Furthermore, the incorporation of cork in the PP matrix resulted in an increase of the Newtonian regime (increase of τ^*) for the CPC with large-sized particles.

Table 3. Rheological coefficients of PP, PP+PPgMA and CPC.

Materials	η_0 (Pa·s)	τ^* (Pa)	n
PP	733	27159	0.306
PP+PPgMA	629	23951	0.308
CPC 1	1131	34966	0.247
CPC 2	1439	32249	0.258
CPC 3	2817	20621	0.302
CPC 4	933	31628	0.259
CPC 5	1339	30401	0.258
CPC 6	1999	18721	0.315

However, CPC with the smallest cork particle granulometry revealed a decrease of the Newtonian regime, even when compared to neat PP. This shows that cork particles with the lowest granulometry interact more with PP increasing the non-Newtonian range and the transition occurs at lower shear rates. The addition of PPgMA affects the Newtonian behaviour due to the increase of entanglements between PP and cork reduce the Newtonian range. In the presence of higher entanglements, sooner the molecular orientation and the deviation from the Newtonian regime occur. The power law index is lower than 1 describing the pseudoplastic behaviour of all the studied materials.

4. Conclusions

The effect on the rheological properties of CPC of three different cork granulometries as well as the addition of a coupling agent, was studied. The cork presence led to a viscosity increase, related to neat PP. This viscosity increase is more evident with the presence of cork particles with smaller granulometry (70 μm). While in the presence of PPgMA it was observed a decrease on CPC viscosity, a consequence of its lubricant/plasticising effect. The Cross-WLF Model provided an accurate approximation of the experimental data obtained from the capillary rheometer. Moreover, the characteristic pseudoplastic behaviour of neat PP did not changed by the addition of cork or even PPgMA, which is an advantage regarding injection moulding applications. The design of the master curves and the determination of its rheological coefficients enable the use of numerical methods for injection moulding simulation process, previous to the industrialization step. The present work represents a viable and a possible strategy for the up-grading of industrial residues. It also contributes for the development of a new class of sustainable composites, in which environmental concern and aesthetics are reflected.

Acknowledgements

The authors are grateful to COMPETE – Programa Operacional Factores de Competitividade (POFC), project number 30176, for financial support.

Appendix A

The apparent shear rate ($\dot{\gamma}_a$) was determined according to Eq. (1).

$$\dot{\gamma}_a = \frac{4Q}{\pi R^3} \text{ (s}^{-1}\text{)} \quad (1)$$

In this equation, Q is the volumetric flow rate of the polymer melt and R (mm) is the capillary die radius. The volumetric flow rate was calculated by Eq. (2), where R_b (mm) is the radius of the barrel and S_p (mm·s⁻¹) is the speed of the plunger.

$$Q = \pi R_b^2 S_p \text{ (mm}^3 \cdot \text{s}^{-1}\text{)} \quad (2)$$

The apparent shear stress (τ_a) is calculated from Eq. (3), where ΔP (Pa) is the pressure drop measured across the L (mm) which corresponds to the capillary length.

$$\tau_a = \Delta P \frac{R}{2L} \text{ (Pa)} \quad (3)$$

From the $\dot{\gamma}_a$, the $\dot{\gamma}_w$ (s⁻¹) corresponding to the wall shear rate values were calculated through the Rabinowitsch-Weissenberg Correction¹⁴ Eq. (4):

$$\dot{\gamma}_w = \left(\frac{3+b}{4} \right) \dot{\gamma}_a, \text{ where } b \equiv \frac{d \ln \dot{\gamma}_a}{d \ln \tau_a} \quad (4)$$

To estimate the true wall shear stress (τ_w), the Ryder-Bagley Correction¹⁶ was applied Eq. (5). The end correction term (e) is the negative of the slope from P versus L/R plot over a range of shear rates.

$$\tau_w = \frac{P}{2L/R + e} \text{ (Pa)} \quad (5)$$

The melt viscosity (η) is then calculated Eq. (6) through the relation between both corrected shear rate and shear stress.

$$\eta = \frac{\tau_w}{\dot{\gamma}_w} \text{ (Pa} \cdot \text{s)} \quad (6)$$

References

1. Fernandes, E. M., Correló, V. M., Mano, J. F. & Reis, R. L. Polypropylene-based cork–polymer composites: Processing parameters and properties. *Compos. Part B Eng.* 66, 210–223 (2014).
2. Samsudin, M. S. F., Ishak, Z. A. M., Jikan, S. S., Ariff, Z. M. & Ariffin, A. Effect of filler treatments on rheological behavior of calcium carbonate and talc-filled polypropylene hybrid composites. *J. Appl. Polym. Sci.* 102, 5421–5426 (2006).
3. Tazi, M., Erchiqui, F., Godard, F., Kaddami, H. & Ajji, A. Characterization of rheological and thermophysical properties of HDPE-wood composite. *J. Appl. Polym. Sci.* 131, (2014).
4. Pereira, H. *Cork: Biology, Production and Uses*. (Elsevier, 2007).
5. Fernandes, E. M., Correló, V. M., Chagas, J. A. M., Mano, J. F. & Reis, R. L. Properties of new cork–polymer composites: Advantages and drawbacks as compared with commercially available fibreboard materials. *Compos. Struct.* 93, 3120–3129 (2011).

6. Fernandes, E. M., Aroso, I. M., Mano, J. F., Covas, J. A. & Reis, R. L. Functionalized cork-polymer composites (CPC) by reactive extrusion using suberin and lignin from cork as coupling agents. *Compos. Part B Eng.* 67, 371–380 (2014).
7. Mano, J. F. The viscoelastic properties of cork. *J. Mater. Sci.* 37, 257–263 (2002).
8. Shenoy, A. V. *Rheology of Filled Polymer Systems*. 475 (Springer, 1999).
9. Hristov, V. & Vlachopoulos, J. Effects of polymer molecular weight and filler particle size on flow behavior of wood polymer composites. *Polym. Compos.* 29, 831–839 (2008).
10. Ariff, Z. M., Ariffin, A., Rahim, N. A. A. & Jikan, S. S. Rheological Behaviour of Polypropylene Through Extrusion and Capillary Rheometry. Polypropylene, Dr. Fatih Dogan (Ed.), InTech (2012).
11. Abdallah, F. B., Cheikh, R. B., Baklouti, M., Denchev, Z. & Cunha, A. M. Effect of surface treatment in cork reinforced composites. *J. Polym. Res.* 17, 519–528 (2009).
12. Abenojar, J. et al. Effect of surface treatments on natural cork: surface energy, adhesion, and acoustic insulation. *Wood Sci. Technol.* 48, 207–224 (2013).
13. Abdallah, B. F., Cheikh, B. R., Baklouti, M., Denchev, Z. & Cunha, A. M. Characterization of composite materials based on PP-Cork blends. *J. Reinf. Plast. Compos.* 25, 1499–1506 (2006).
14. Dealy, J. M. & Wissbrun, K. M. *Melt Rheology and Its Role in Plastics Processing: Theory and Applications*. 665 (Chapman & Hall, 1995).
15. Rosa, M. E. & Fortes, M. A. Thermogravimetric analysis of cork. *J. Mater. Sci. Lett.* 7, 1064–1065 (1988).
16. Schramm, G. *A Practical Approach to Rheology and Rheometry*. 290 (Gebueder Haake GmbH, 1994).
17. Cross, M. M. Rheology of Non-newtonian fluids: a new flow equation for pseudo-plastic systems. *Colloid Sci.* 20, 417–437 (1965).
18. Williams, M. L., Landel, R. F. & Ferry, J. D. The Temperature Dependence of Relaxation Mechanisms in Amorphous Polymers and Other Glass-forming Liquids. *J. Am. Chem. Soc.* 77, 3701–3707 (1955).
19. Dealy, J. M. & Plazek, D. Time-Temperature Superposition - A users guide. *Br. Soc. Rheol.* (2009).
20. Maiti, S. N., Subbarao, R. & Ibrahim, M. N. Effect of wood fibers on the rheological properties of i-PP/wood fiber composites. *J. Appl. Polym. Sci.* 91, 644–650 (2004).
21. Godard, F., Vincent, M., Agassant, J.-F. & Vergnes, B. Rheological behavior and mechanical properties of sawdust/polyethylene composites. *J. Appl. Polym. Sci.* 112, 2559–2566 (2009).
22. Bettini, S. H. P., de Miranda Josefovich, M. P. P., Muñoz, P. A. R., Lotti, C. & Mattoso, L. H. C. Effect of lubricant on mechanical and rheological properties of compatibilized PP/sawdust composites. *Carbohydr. Polym.* 94, 800–6 (2013).
23. Maiti, S. N., Singh, G. & Ibrahim, M. N. Rheological properties of calcium silicate-filled isotactic polypropylene. *J. Appl. Polym. Sci.* 87, 1511–1518 (2003).
24. Hristov, V. & Vlachopoulos, J. Effects of polymer molecular weight and filler particle size on flow behavior of wood polymer composites. *Polym. Compos.* 29, 831–839 (2008).
25. Li, S., Järvelä, P. K. & Järvelä, P. A. Melt rheological properties of polypropylene-maleated polypropylene blends. I. Steady flow by capillary. *J. Appl. Polym. Sci.* 71, 1641–1648 (1999).

2.3 Non-isothermal crystallization kinetics of cork-polymer composites for injection moulding ^e

Sara P. Magalhães da Silva^{1*}, Paulo S. Lima¹, José M. Oliveira^{1,2}

¹ School of Design, Management and Production Technologies, University of Aveiro, Estrada do Cercal, nº449, 3720-509 Santiago de Riba-UI, Oliveira de Azeméis, Portugal

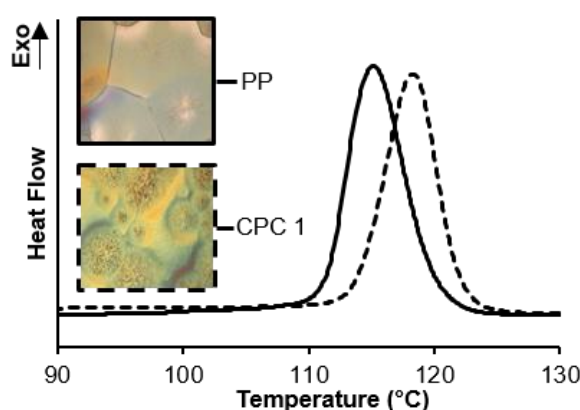
² Aveiro Institute of Materials (CICECO), University of Aveiro, Campus Universitário de Santiago, 3810-193 Aveiro, Portugal

*Correspondence to: Sara Silva (E-mail: sarapms@ua.pt)

Abstract

The non-isothermal crystallization behaviour of cork-polymer composites (CPC) based on polypropylene (PP) matrix was studied. Using differential scanning calorimetry (DSC), the crystallization behaviour of CPC with 15 %wt cork powder at different cooling rates (5, 10, 15 and 20°C/min) was studied. The effect of a coupling agent based on maleic anhydride was also analysed. A composite (PPg) containing polypropylene grafted maleic anhydride (PPgMA) and PP was prepared for comparison purposes. Crystallization kinetic behaviour was studied by Avrami, Ozawa, Liu and Kissinger methods. The Ozawa method fail to describe the behaviour of these composites. Results show that cork powder surface acts as a nucleating agent during non-isothermal crystallization, while the addition of PPgMA decrease the crystallization rate.

Graphical Abstract



^e Magalhães da Silva, S. P., Lima P. S., Oliveira J. M. Non-isothermal crystallization kinetics of cork-polymer composites for injection moulding, *J. Appl. Polym. Sci.* 2016, **133**, 44124 – 44133.

The author had contributed to the planning and execution of all the DSC analyses and modeling calculations herein presented, as well as on the discussion, interpretation and preparation of the manuscript.

Keywords: Composites, Differential Scanning Calorimetry (DSC), Crystallization, Kinetics, Compatibilization

Introduction

Given the current environmental, societal and political situation, there is a pressing and growing need for innovative, sustainable and recyclable materials. Cork is a technologically relevant material for the 21st century, competing in areas traditionally dominated by metal and oil derivatives. In a society that requires a more intelligent use of resources, cork is a reliable and sustainable raw material. Cork oak forests also contribute to the biodiversity of species and to the retention of CO₂.¹ Cork is the outer bark of the cork oak tree *Quercus suber* L. and its main chemical composition is based on suberin (33-50%), lignin (20-25%); polysaccharides (12-20%) and extractives (14-18%). In terms of structure, cork presents tiny hollow cells of hexagonal shape in a closed-cell foam.^{2,3} It is well known that the major use for cork is the production of stoppers, which generates a relative high amount (≈ 30 %wt) of residues, that are usually burned.⁴ These residues are suitable raw materials for the development of new materials solutions tailoring the needs of different applications. The combination of cork with polymeric matrices reveals to be a significant added-value to cork based materials. Low density, hardness and cost, good relation between strength/weight, good insulation properties and high levels of filling are some of the advantages of applying natural materials as fillers in thermoplastic composites. They are, also, renewable and readily available materials, recyclable and non-toxic.⁴⁻⁶

Mechanical properties of composites are highly dependent on the interaction between the polymer matrix and the filler. Coupling agents are usually applied to promote the compatibility between polymer matrices and lignocellulosic materials. PPgMA is one of the most used coupling agents in several polyolefin composites with natural fibers.⁷⁻¹² The interactions between PPgMA maleic groups and hydroxyl groups of natural fibers increase the interfacial adhesion between both materials leading to a better mechanical performance.^{5,13} Composites performance depends not only on the compatibility of the matrix and filler, but also on the morphology and crystallinity. Several studies regarding morphology, mechanical and thermal properties of PP filled with natural fibers have already been reported.¹⁴⁻²³ However, few studies analysed the effect of cork on PP degree of crystallinity^{5,24} and, so far, none of the studies are related to the matrix crystallization kinetics.

The final mechanical properties of composites reinforced with natural materials are partially dependent on the crystallization behaviour of the matrix. Crystallization occurs through the nucleation and growth mechanisms of small molecules. The addition of natural materials can influence the crystallization process mostly by revealing nucleation activity and/or transcrystallization.²⁵⁻²⁷ The processing conditions also affect the crystallization behaviour. In industrial processes, like extrusion and injection moulding, composites experience non-isothermal crystallization rather than isothermal crystallization. In injection moulding, processing parameters, such as, melting temperatures, pressures and shear rates are applied during the process. These severe conditions influence the PP

crystals nucleation and growth and, therefore, the spherulites number and size. The use of nucleating agents can contribute for a shorter injection moulding cycle reducing the manufacturing costs. It can also improve optical and mechanical properties through the development of small spherulites.^{27,28}

Soleimani *et al.*²⁷ studied the effect of flax fibre loading, chemical modification and the use of compatibilizer (PPgMA) on the non-isothermal crystallisation kinetics of PP. They found that the addition of flax fibres resulted in higher degree of crystallinity (X_c). This was attributed to the nucleation ability of the fibres which provide nucleation sites and facilitate crystallization of the polymer as well as transcrystallinity. Some fibres have the ability to act as heterogeneous nucleating agents promoting high density of nucleation centres. The crystals grow in a direction perpendicular to the fibres surface occurring the transcrystallinity phenomenon.²⁷ At the same cooling rate, the addition of fibres increased crystallization temperature (T_c). For higher cooling rates a lower T_c and X_c were observed, but a faster kinetic of crystallization was attained. In this study,²⁷ PPgMA reduced the crystallinity degree, but accelerated the crystallization rate. The same trend was observed by Grozdanov *et al.*²⁵, who have studied the non-isothermal crystallization kinetics of kenaf fibre/polypropylene composites.

The present study is part of a major project which aims to evaluate the feasibility of CPC production through a modified injection moulding technology without minimising the damage of cork structure. A rheological study of CPC with three different cork granulometries was already been analysed.²⁹ This study showed that cork can be considered on the development of sustainable materials for injection moulding technology. The main objective of this work is to study the crystallization kinetics of CPC under non-isothermal conditions using DSC. The influence of cork presence on the nucleation and crystal growth behaviour of PP was evaluated using Avrami³⁰, Ozawa³¹ and Liu³² models. Crystallization activation energy (ΔE_c) was determined through Kissinger model.³³ CPC crystallisation kinetics should be addressed to better describe the crystallization behaviour during the injection moulding process.

Experimental

Materials

Cork powder used in this work was supplied by a Portuguese cork producer. Sample was fractionated through sieving (Retsch, Germany) and the relative amount of particles according to its size was determined (Table 1). No particles were retained in sieves below 100 μm . The average particle size was calculated recurring to Eq. (1).

$$d_p = \frac{\sum w_i d_i^4}{\sum w_i d_i^3} \quad (1)$$

, where w_i is the weight fraction in each sieve and d_i is the sieve mesh size.

The polymeric matrix used in this work is a homopolymer PP (PPH 10060) from Total Petrochemicals, with a Melt Flow Index (MFI) of 35 g·10min⁻¹ (230°C, 2.16 Kg) and a melting point

of 165°C. The coupling agent applied was PPgMA from ExxonMobil, Germany (Exxelor™ PO 1020) containing 0.5-1.0 wt% of grafted maleic anhydride, with a MFI of 430 g·10min⁻¹ (230°C, 2.16 Kg) and a melting point of 162°C.

Table 1. Cork particles: physical characteristics.

Granulometry	Cork	Average particle
mesh	powder	size
(μm)	(%)	(μm)
1000	2.3±0.1	
800	45.8±0.1	596
400	51.4±0.1	
200	0.6±0.1	

The polymeric matrix used in this work is a homopolymer PP (PPH 10060) from Total Petrochemicals, with a Melt Flow Index (MFI) of 35 g·10min⁻¹ (230°C, 2.16 Kg) and a melting point of 165°C. The coupling agent applied was PPgMA from ExxonMobil, Germany (Exxelor™ PO 1020) containing 0.5-1.0 wt% of grafted maleic anhydride, with a MFI of 430 g·10min⁻¹ (230°C, 2.16 Kg) and a melting point of 162°C.

Preparation of CPC

Before compounding, the cork particles were dried at 70°C for 24h in a vacuum oven (Carbolite AX60 model) to stabilize the moisture content. It is known that the cork structure and composition do not suffer significant changes up to 250°C.³⁴ CPC were compounded in a Brabender type internal mixer. The total volume of the mixing chamber is 355 cm³. Firstly, PP pellets were charged and melted during 2 minutes at 180°C and 40 rotations per minute. Then, cork particles were added and the materials were mixed for additional 8 minutes. For the preparation of CPC in the presence of coupling agent, PPgMA was added together with cork particles. A formulation of PP/PPgMA (PPg) was prepared to evaluate the individual effect of PPgMA in the PP matrix. Compositions of all samples are shown in Table 2.

Table 2. Compositions used in the preparation of CPC.

Sample Code	PP (%wt)	Cork (%wt)	PPgMA (%wt)
PPg	100	–	5% of PP
CPC 1	85	15	–
CPC 1g	85	15	5% of PP

DSC

Crystallization behaviour of all samples were carried out in a Shimadzu DSC-60 equipment. The equipment was calibrated by using indium as the reference material. Samples weights varying between 5.0 and 6.0 mg were encapsulated in aluminium pans. Each sample was heated from 20°C to 200°C at a scan rate of 20°C/min and held for 2 min at this temperature to eliminate the thermal history and prevent self-seeding of PP.³⁵ Then, they were cooled until -80°C and heated again up to 200°C. Four different heating/cooling rates: 5, 10, 15 and 20°C/min were used. Only the second run was considered to analyse the crystallization behaviour process: crystallization temperature (T_c), endset temperature (T_e), onset temperature (T_o) and crystallization enthalpy (ΔH_c). DSC thermograms analyses were made by using TA-60WS software. The crystallinity is associated with the exothermic peaks maxima obtained by DSC.

Optical Microscopy

Observations under reflected-light microscope were carried out on a Nikon Eclipse L150. Samples were melted for 2 min in a hot plate and the crystallites morphology examined upon cooling.

Results and Discussion

Non-isothermal crystallization behaviour

Melt crystallization exotherms of the samples at different cooling rates are presented in Figure 1 and 2. The DSC curves of CPC 1 at different cooling rates (all the other samples exhibited the same behaviour – not showed) are shown in Figure 1. The DSC curves of all samples at cooling rate of 5°C/min are displayed in Figure 2. The thermal properties of all samples are listed in Table 3.

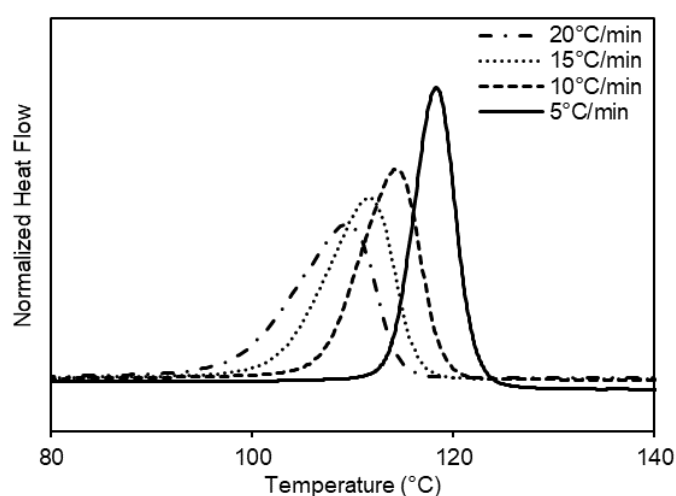


Figure 1. DSC curves of CPC 1 at different cooling rates.

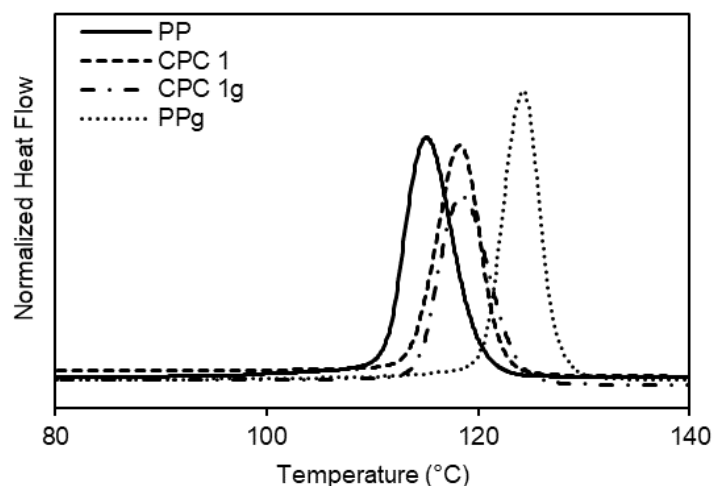


Figure 2. DSC curves of all samples at $5^{\circ}\text{C}\cdot\text{min}^{-1}$.

Table 3. Non-isothermal crystallization parameters obtained by DSC (R^2 – correlation coefficient).

Sample	ϕ ($^{\circ}\text{C}\cdot\text{min}^{-1}$)	T_0 ($^{\circ}\text{C}$)	T_c ($^{\circ}\text{C}$)	X_c (%)	$t_{1/2}$ (s)	CRP	R^2
PP	5	122.8	114.8	49.7	100	0.086	0.987
	10	114.0	106.1	41.5	54		
	15	111.5	103.6	40.1	38		
	20	109.2	99.2	39.0	32		
PPg	5	133.4	124.7	52.4	125	0.084	0.980
	10	127.6	120.0	50.7	61		
	15	125.5	118.2	48.2	41		
	20	124.6	116.9	47.5	35		
CPC 1	5	124.1	118.5	50.0	82	0.095	0.995
	10	121.5	114.6	49.8	48		
	15	120.0	111.6	50.7	34		
	20	118.5	108.8	50.6	28		
CPC 1g	5	126.1	119.0	53.0	97	0.060	0.994
	10	123.5	114.8	53.8	62		
	15	120.5	111.9	50.7	44		
	20	119.9	109.8	52.0	37		

It is visible that T_c shifted to lower values as the cooling rates increase, indicating that the crystallization process occurs sooner for lower cooling rates. The crystallization peak width became narrow as the cooling rates is decreasing. This narrowing can be associated to a lower crystallites geometry dispersion, where at lower cooling rates the formation of less perfect crystallites is attained.³⁶

At a given cooling rate, the values for the T_c of composites were higher than neat PP and the addition of the coupling agent resulted in an increase of T_c . At higher cooling rates, polymer chains were less movable and possessed shorter time to diffuse into the crystalline phase, which resulted

in a decrease of T_c . Lower cooling rates promotes conditions for better polymer crystals development due to a kinetic process. It is also known that the polymer chain length and its branches influence the crystallization process.³⁶

From Figure 2, it is seen that composites materials crystallization peaks are between PP and PPg crystallization peaks, indicating that the crystallization process is governed by the polymeric matrix.

The degree of crystallinity (X_c) was calculated according to Eq. (2), where the ΔH_c was obtained through the integration of the crystallization peak. ΔH_m^0 correspond to 100% crystalline PP being equal to 207 J·g⁻¹ and w is the weight cork fraction in the composite.³⁶

$$X_c (\%) = \frac{\Delta H_c}{\Delta H_m^0 (1 - w)} \times 100 \quad (2)$$

At the same cooling rate, crystallinity increased with the addition of cork powder to PP matrix (Table 3). This can be attributed to the nucleating effect of cork which provided nucleation sites and facilitated the crystallization of the polymer.^{5,37} Additionally, at the same cooling rate the presence of cork also increased T_c .

The use of PPgMA, not only attributes for the increasing of the degree of crystallinity of PPg and CPC 1g, but also the time needed to achieve 50% extent of crystallization (defined as half-time crystallization ($t_{1/2}$), which is obtained directly from the plot of relative degree of crystallinity (X_t) vs time). These results show that, although, the addition of PPgMA leads to higher crystallinities, it is observed that non-isothermal crystallization occurred faster in neat PP and CPC 1. This means that, however more crystals are growing, they're growing more slowly, which reduces the overall crystallization rate.

Zhang *et al.*³⁸ proposed the crystallization rate parameter (CRP), which can be used to quantitatively compare the non-isothermal crystallization rate. CRP can be determined by the slope of a linear plot of $1/t_{1/2}$ versus cooling rate. A higher slope implies a faster crystallization rate.

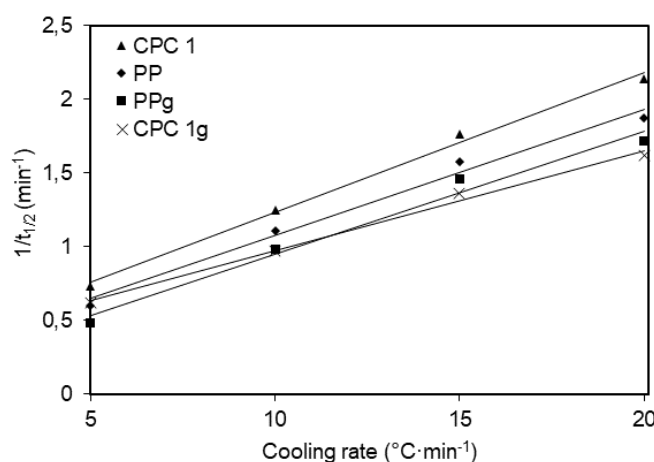


Figure 3. Plots of $1/t_{1/2}$ vs cooling rate of all samples.

Figure 3 shows the plots of $1/t_{1/2}$ vs cooling rate and CRP values are displayed in Table 3. CPC 1 presented the higher CRP value, proving the nucleating effect of cork. The presence of the coupling agent reduced the crystallization rate, probably due to the increased interactions between cork-PP in the presence of PPgMA. As the degree of grafting increases, the mobility of polymer chains segments decreases hindering the crystallization rate.²⁵

The relative degree of crystallinity (X_t), as a function of temperature, is determined applying Eq. (3), where T_0 and T_∞ are the onset and end temperatures, respectively.

$$X_t = \frac{\int_{T_0}^T \left(\frac{dH_c}{dT}\right) dT}{\int_{T_0}^{T_\infty} \left(\frac{dH_c}{dT}\right) dT} \quad (3)$$

During the non-isothermal crystallization process, the relation between crystallization time (t) and temperature is given by Eq. (4), in which ϕ is the cooling rate.

$$t = \frac{|T_0 - T|}{\phi} \quad (4)$$

Curves of relative crystallinity as function of time for all the studied samples are presented in Figure 4. At different cooling rates all curves have the same sigmoidal shape.

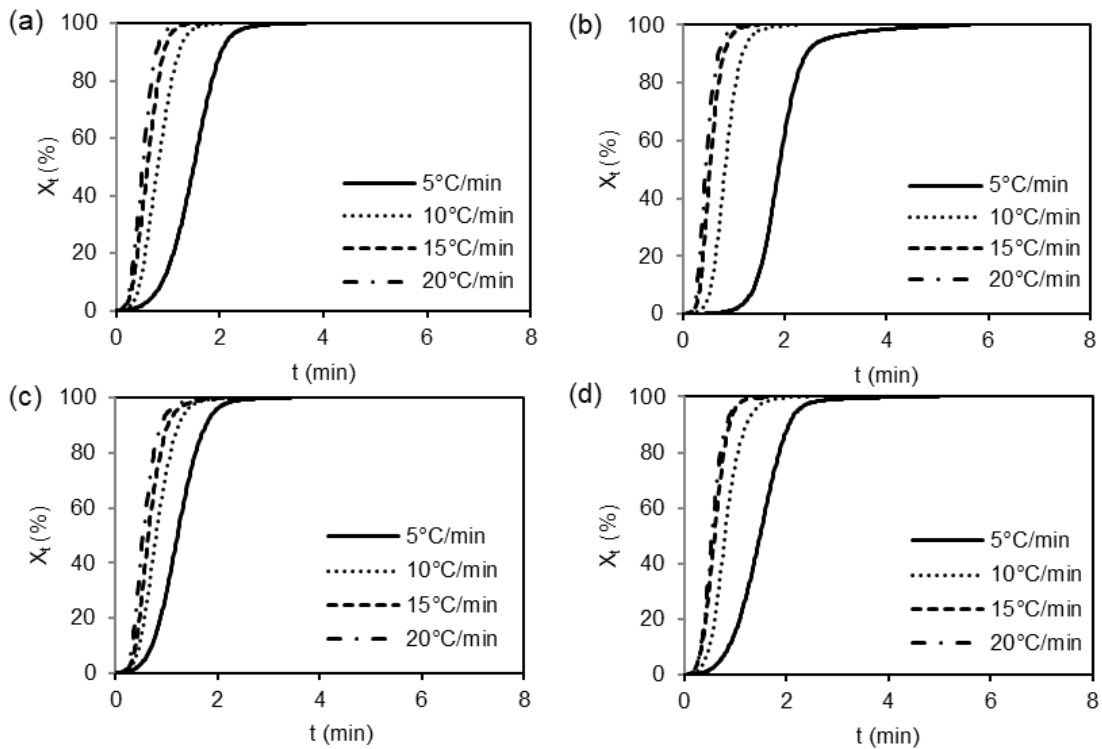


Figure 4. Relative crystallinity (X_t) vs time (t) curves of the samples: (a) PP, (b) PPg, (c) CPC 1 and (d) CPC 1g.

The first nonlinear part is usually considered the nucleation step of the crystallization process.³⁹ The longest nucleation step occurs for PPg sample (5°C/min), which indicates that more nuclei were formed. PPGMA presence seems to induce the formation of more nuclei for crystals growth. In this case, a fast primary crystallization occurred in the early stage, while a slower secondary crystallization at the latter stage is observed. The curvature of this second nonlinear part levelled off, which was probably caused by the spherulite impingement or crowding in the late stage of crystal growth.^{40,41} Higher cooling rates managed to complete the crystallization process in a shorter time. This behaviour is also observed through the $t_{1/2}$ parameter (Table 3). It is visible that, $t_{1/2}$ decreased with the increase of cooling rate, indicating that a shorter time is needed to achieve 50% extent of crystallization.

Non-isothermal crystallization kinetics

The Avrami³⁰ model is commonly used to describe the isothermal crystallization kinetic behaviour:

$$1 - X_t = \exp(-Z_t t^n) \quad (5)$$

, where Z_t is the crystallization rate constant containing the nucleation and growth rates and it is temperature dependent; n is the Avrami index which depends on the type of nucleation and growth process. The linearized form can be written as:

$$\log[-\ln(1 - X_t)] = \log(Z_t) - n \log(t) \quad (6)$$

Mandelkern⁴² considered that the primary non-isothermal crystallization stage can be described through this model, based on a constant crystallization temperature assumption. The n and Z_t parameters do not have the same physical meaning as in the isothermal crystallization processes, since the temperature changes steadily during a non-isothermal crystallization. Nucleation and crystal growth are temperature dependent, and a temperature change at a given cooling rate affects the kinetics of both processes. Jeziorny⁴³ calibrated the Z_t parameter, considering the temperature dependence of the non-isothermal crystallization:

$$\log Z_c = \frac{\log(Z_t)}{\varphi} \quad (7)$$

Avrami plots are shown in Figure 5 and the kinetic parameters are presented in Table 4. In the fitting, it was considered X_t values between 10 and 90%.

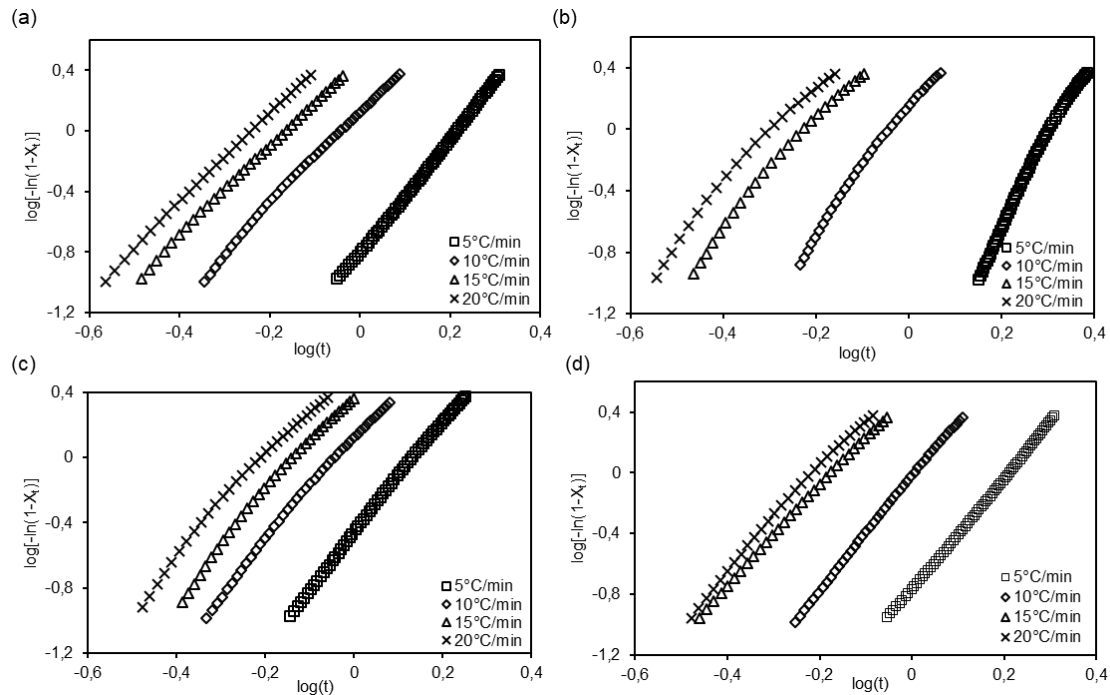


Figure 5. Avrami plots of the samples: **(a)** PP, **(b)** PPg, **(c)** CPC 1 and **(d)** CPC 1g.

Table 4. Avrami kinetic parameters.

Samples	ϕ ($^{\circ}\text{C}\cdot\text{min}^{-1}$)	n	Z_c (min^{-1})	R^2
PP	5	3.79	0.689	0.994
	10	3.09	1.030	0.997
	15	2.93	1.077	0.999
	20	2.96	1.085	0.999
PPg	5	5.89	0.434	0.993
	10	4.08	1.034	0.992
	15	3.45	1.070	0.993
	20	3.32	1.079	0.993
CPC 1	5	3.45	0.808	0.999
	10	3.18	1.029	0.996
	15	3.14	1.085	0.993
	20	2.90	1.091	0.992
CPC 1g	5	3.67	0.699	1.000
	10	3.75	0.994	1.000
	15	3.26	1.065	0.999
	20	3.39	1.070	0.996

The variation of the Avrami parameter n with cooling rate indicates the presence of a growth and nucleation mixed mechanism. According to literature, n should be an integer value varying from 1 to 4.⁴⁴ A non-integer value also designates a crystallization process in various growth forms, indicating

that the nucleation/crystallization mechanisms are difficult to be established in a single way and, additional information must be obtained. The determination of n depends upon factors, such as, volume changes due to phase transformation, incomplete crystallization, annealing, or different mechanisms involved during the process.⁴⁵

In this study, the n values variation indicates a three-dimensional (3D) growth mechanism.⁴⁶ However, non-integer values were obtained and a more detailed analysis is required to evaluate the specific nucleation mechanism.

The rate parameter Z_c increases with increasing cooling rate, meaning an increase in crystallization rate. When compared to neat PP, an increase of Z_c values are observed for CPC 1, suggesting an increase in the heterogeneous crystallite nucleation rate.⁴⁰ Contrarily, the addition of PPgMA revealed a decrease in Z_c .

Ozawa³¹ extended the Avrami model to describe the non-isothermal processes (Eq. (8)) by assuming infinitesimally small changes in the isothermal crystallization steps and obtained:

$$1 - X_t = \exp\left(-\frac{K(T)}{\varphi^m}\right) \quad (8)$$

, where m is the Ozawa exponent, which is dependent on the nucleation density. The spherulitic radial growth rate and $K(T)$ is a function of the overall crystallization rate. The linearized form of the model is shown in Eq. (9).

$$\ln[-\ln(1 - X_t)] = \ln K(T) - m \ln(\varphi) \quad (9)$$

The Ozawa model is one of the most used models for studying non-isothermal crystallization kinetics. Ozawa plots for CPC 1 at different crystallization temperatures are represented in Figure 6.

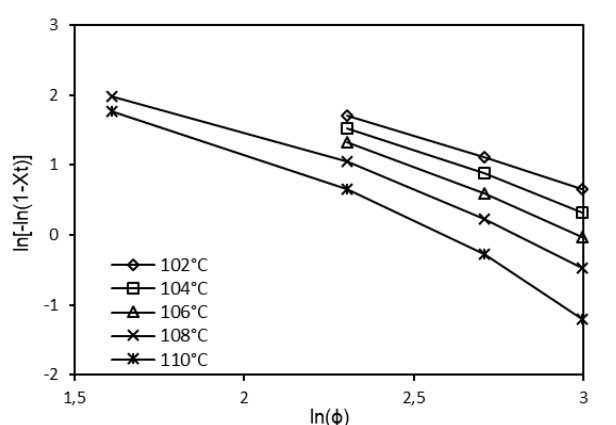


Figure 6. Ozawa plot for CPC 1 at different crystallization temperatures.

It is clearly seen that in the presence of cork, the Ozawa plots are non-linear and so, the Ozawa model could not be used to describe adequately the non-isothermal crystallization of PP/cork composites. The reason why this happened was attributed to the secondary crystallization stage that occurs during non-isothermal crystallization process of PP in the presence of cork. In a study of Grozdanov *et al.*²⁵, where they studied the non-isothermal crystallization kinetics of kenaf fiber/polypropylene composites, they found the same behaviour when fitted the data to the Ozawa model. They explain this non-linearity by the fact that for different cooling rates and at a given temperature, the crystallization processes are at different stages. More specifically, at lower cooling rates, the process is at the end of the crystallization, while at higher cooling rates, the crystallization is at an early stage. Xu and co-workers²⁶ when analysed the non-isothermal crystallization kinetics of PP composites reinforced with down feather fibres had the same Ozawa non-linearity tendency. The fact that Ozawa's model does not consider the slow secondary crystallization was appointed as the reason for this behaviour.

The description of the non-isothermal crystallization kinetics only by a single method is non-effective, once several parameters need to be considered simultaneously. Liu *et al.*³² proposed an alternative method through the combination of Avrami and Ozawa models (Eq. (10)) based on the fact the relative degree of crystallinity is correlated to the cooling rate and crystallization time.

$$\log(\varphi) = \log[F(T)] - \alpha \log(t) \quad (10)$$

, where $F(T) = [K(T)/Z_t]^{1/m}$ (Eq. (11)) refers to the cooling rate value in which the system reaches a certain degree of crystallinity in the unit of time, while α is the ratio between Avrami and Ozawa exponents ($\alpha = n/m$).

Liu's approach plots are given in Figure 7 and the corresponding parameters are presented in Table 5. A small variation of α and a R^2 closer to one reveals that Liu's method was capable to describe accurately the non-isothermal crystallization of the analysed materials.

Values of α closer to 1 were obtained for PP, PPg and CPC 1g samples, indicating that Avrami and Ozawa exponents are similar. It also discloses that the ratio of crystallization between 5°C/min and 20°C/min is constant whatever the relative crystallinity (see Figure 7). For CPC 1, α values were closer to 2, which means that Avrami exponent is superior than Ozawa exponent. As referred above, a n value between 2 and 3 can indicate a 3D crystallization growth. Furthermore, the crystallization ratio increased reinforcing the idea of cork as a nucleating agent.

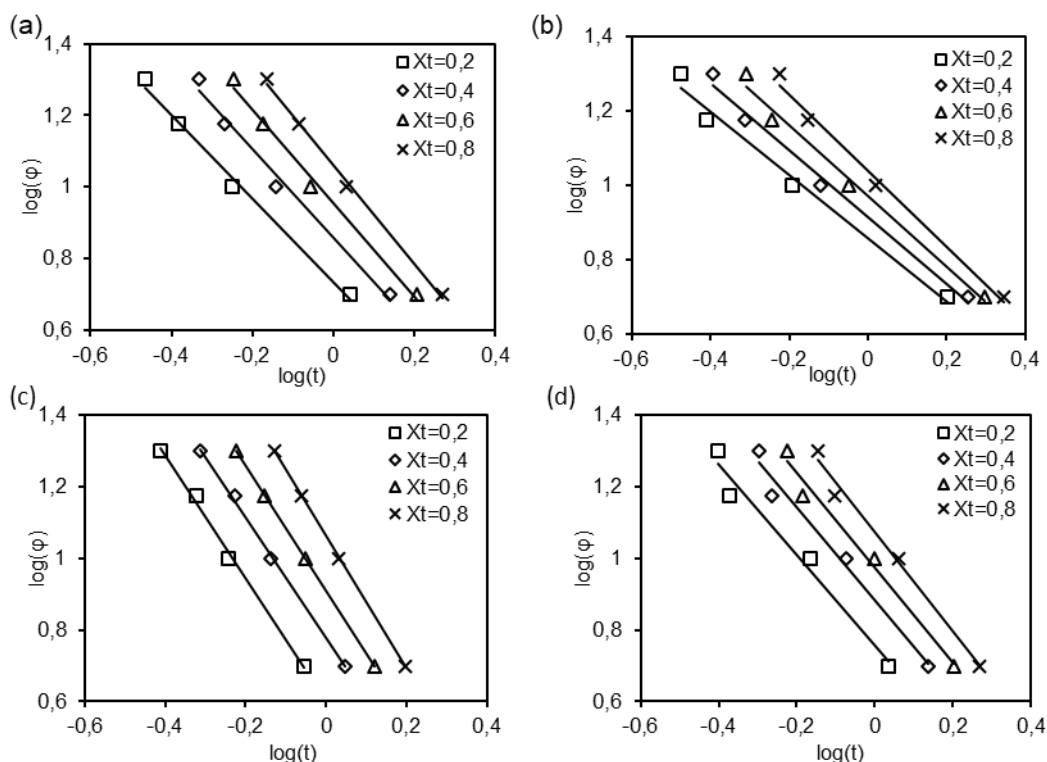


Figure 7. Liu plots of the samples: (a) PP, (b) PPg, (c) CPC 1 and (d) CPC 1g.

Table 5. Liu's kinetic parameters.

Sample	X_t	α	F(T)	R^2
PP	0.2	1.17	5.43	0.99
	0.4	1.24	7.18	0.99
	0.6	1.32	9.00	0.99
	0.8	1.39	11.50	1.00
PPg	0.2	0.85	7.21	0.99
	0.4	0.90	8.24	0.99
	0.6	0.95	9.37	0.99
	0.8	1.02	10.99	0.99
CPC 1	0.2	1.72	3.98	1.00
	0.4	1.70	5.97	1.00
	0.6	1.74	8.13	1.00
	0.8	1.86	11.53	1.00
CPC 1g	0.2	1.27	5.73	0.98
	0.4	1.29	7.63	0.98
	0.6	1.32	9.43	0.98
	0.8	1.39	11.78	0.99

F(T) value increased as the relative crystallinity increases, since the motion of molecular chains became slower as the material crystallized and the formation of new crystals is hampered.⁴⁰ Higher F(T) values imply a slower crystallization rate. CPC 1 presented the lowest F(T) values, indicating a faster crystallization rate when cork is added to the PP matrix. This result confirms, once again, the

nucleating ability of cork. On the other hand, the addition of PPgMA decreased the crystallization rate (both for PPg and CPC 1g). As discussed before, the increased interactions between cork and PP due to the presence of PPgMA, resulted in a decreased mobility of the polymer chains and, consequently, the crystallization rate is hindered. The results obtained from this model are in agreement with those obtained by the Avrami model.

According to Vyazovkin *et al.*⁴⁷, the Kissinger model³³ (Eq. (11)) seems not to be the most efficient method to evaluate crystallization activation energy (ΔE_c). Although in order to compare the activation energy with similar studies, the Kissinger method was used. ΔE_c is the activation energy required for transportation of molecular segments from melt to the crystal growth surface.

$$\frac{-\Delta E_c}{R} = \frac{d(\ln(\frac{\varphi}{T_c^2}))}{d(\frac{1}{T_c})} \quad (11)$$

, where R is the gas constant and T_c is the crystallization temperature.

Kissinger plots are visible in Figure 8 and the corresponding ΔE_c values are listed in Table 6. The ΔE_c values are negative owing to the exothermic character of the transition from melt to crystalline state.

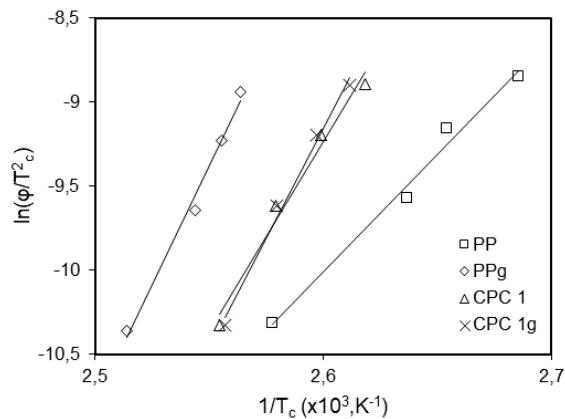


Figure 8. Kissinger plots of the samples.

Table 6. Crystallization activation energy (ΔE_c) of samples.

Sample	ΔE_c (kJ·mol ⁻¹)	R ²
PP	-115.71	0.99
PPg	-233.84	0.99
CPC 1	-187.47	0.98
CPC 1g	-217.88	0.99

From these negative values, we can also infer an increase of crystallization with decreasing temperatures, revealing a barrier-less crystallization process.⁴¹ The addition of cork resulted in a decrease of the ΔE_c compared to neat PP, indicating a faster crystallization rate in the presence of cork. Soleimani *et al.*²⁷ reported that biofibers act as high energy sites lowering the activation energy needed for nucleation. The low ΔE_c values for composites are in agreement with their higher crystallinity degree (see Table 3).

Optical microscopy analysis

Optical microscopy analysis was performed to visualize the nucleating ability of cork. Optical micrographs of pure PP and PP in the presence of cork powder at different magnifications are shown in Figure 9. The results suggest differences between the number and dimension of crystallites when PP crystallizes in the presence of cork. A higher number of crystallites with smaller dimensions is seen when PP crystallizes in the presence of cork, supporting the nucleating ability of cork already checked through the non-isothermal crystallization analyses. In semi-crystalline polymer composites reinforced with natural fibres it is usually observed a typical nucleation morphology: transcrystallinity.⁵⁰ However, in this case no transcrystalline layer on cork was found. The same observation was reported by Fernandes *et al.*²⁴

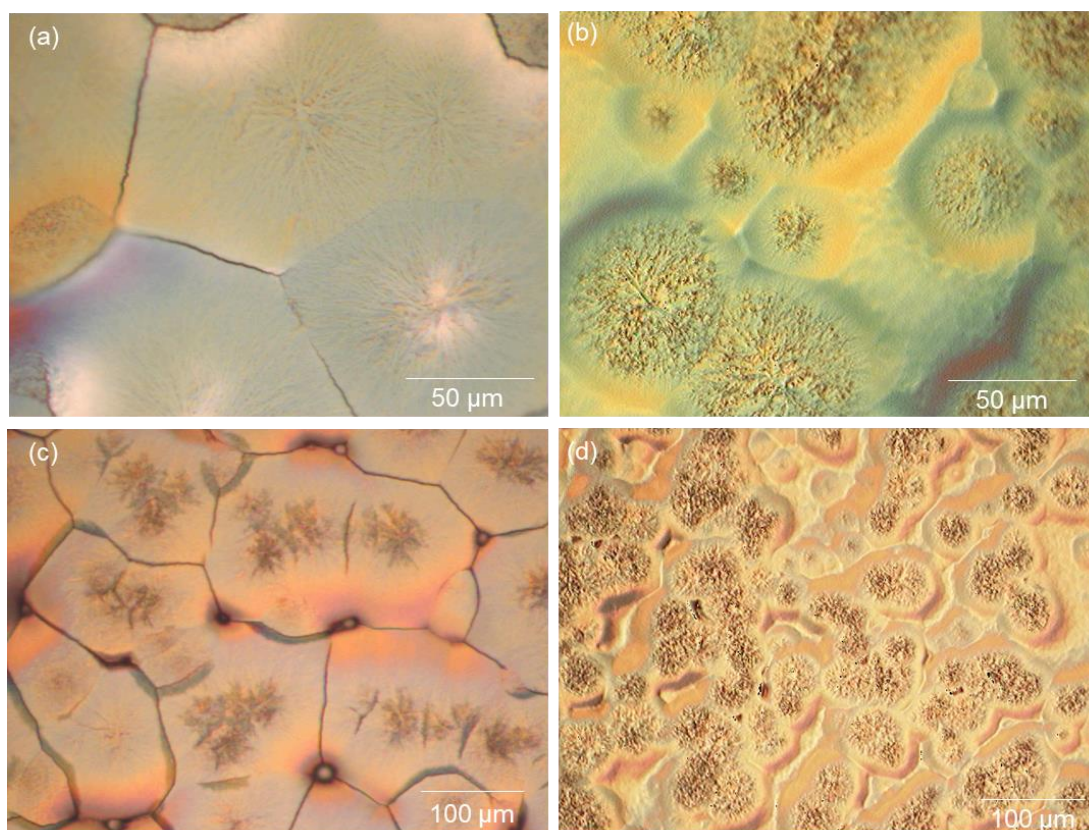


Figure 9. Optical micrographs of the samples: **(a), (c)** pure PP and **(b), (d)** PP in the presence of cork.

Conclusions

The non-isothermal crystallization behaviours of PP, PPg and CPC were investigated at different cooling rates (5, 10, 15 and 20°C/min) through DSC measurements. It was found that the crystallization behaviour was affected by the different cooling rates. At higher cooling rates, the crystallization occurred at lower temperatures. Avrami, Ozawa, Liu and Kissinger methods were applied to analyse the non-isothermal kinetics of all samples. Avrami and Liu methods successfully described the non-isothermal crystallization processes of PP and composites, while the Ozawa model failed, due to the secondary crystallization stage. The addition of cork increased the crystallization rate of PP matrix and the Avrami parameter n was between 2 and 3, indicating a 3D crystallization growth (also supported by optical microscopy). On the other hand, in the presence of PPgMA, the crystallization rate is hindered, owing to the introduction of maleic anhydride group. Even though the crystallinity degrees at all cooling rates for composites with PPgMA are higher, their $t_{1/2}$ increased, meaning that, although more crystals are growing, they're growing more slowly, which reduces the overall crystallization rate.

The present study allowed to understand the effect of different cooling rates on CPC non-isothermal crystallization process.

ACKNOWLEDGEMENTS

The authors are grateful to COMPETE – Programa Operacional Factores de Competitividade (POFC), project number 30176, for financial support.

References

1. Gil, L. *Front. Chem.* **2014**, *2*, 16.
2. Pereira, H. Cork : Biology, Production and Uses; Elsevier: Amsterdam, **2007**; pp 33-97.
3. Silva, S. P.; Sabino, M. A.; Fernandes, E. M.; Corrello, V. M.; Boesel, L. F.; Reis, R. L. *Int. Mater. Rev.* **2005**, *50*, 345–365.
4. Fernandes, E. M.; Aroso, I. M.; Mano, J. F.; Covas, J. A.; Reis, R. L. *Compos. Part B Eng.* **2014**, *67*, 371–380.
5. Fernandes, E. M.; Corrello, V. M.; Mano, J. F.; Reis, R. L. *Compos. Part B Eng.* **2014**, *66*, 210–223.
6. Pracella, M.; Haque, M.-U.; Alvarez, V. *Polymers (Basel)*. **2010**, *2*, 554–574.
7. Gassan, J.; Bledzki, A. K. *Compos. Part A Appl. Sci. Manuf.* **1997**, *28*, 1001–1005.
8. Feng, D.; Caulfield, D. F.; Sanadi, A. R. *Polym. Compos.* **2001**, *22*, 506–517.
9. Espert, A.; Camacho, W.; Karlson, S. *J. Appl. Polym. Sci.* **2003**, *89*, 2353–2360.
10. Soccalingame, L.; Bourmaud, A.; Perrin, D.; Bénézet, J.-C.; Bergeret, A. *Polym. Degrad. Stab.* **2015**, *113*, 72–85.
11. Mishra, S.; Verma, J. *J. Appl. Polym. Sci.* **2006**, *101*, 2530–2537.
12. Pal, K.; Mukherjee, M.; Frackowiak, S.; Kozłowski, M.; Das, C. K. *J. Vinyl Addit. Technol.* **2014**, *20*, 24–30.
13. Tazi, M.; Erchiqui, F.; Godard, F.; Kaddami, H.; Ajjji, A. *J. Appl. Polym. Sci.* **2014**, *131*.
14. Nekhlaoui, S.; Essabir, H.; Kunal, D.; Sonakshi, M.; Bensalah, M. O.; Bouhfid, R.; Qaiss, A. *Polym. Compos.* **2015**, *36*, 675–684.
15. Tanjung, F. A.; Husseinsyah, S.; Hussin, K. *Fibers Polym.* **2014**, *15*, 800–808.
16. Gupta, A. K.; Biswal, M.; Mohanty, S.; Nayak, S. K. *Fibers Polym.* **2014**, *15*, 994–1003.
17. Chaharmahali, M.; Hamzeh, Y.; Ebrahimi, G.; Ashori, A.; Ghasemi, I. *Polym. Bull.* **2013**, *71*, 337–349.
18. Luo, S.; Cao, J.; Peng, Y. *Polym. Compos.* **2014**, *35*, 201–207.

19. Wang, C.; Ying, S. *Fibers Polym.* **2014**, *15*, 117–125.
20. Jeencham, R.; Suppakarn, N.; Jarukumjorn, K. *Compos. Part B Eng.* **2014**, *56*, 249–253.
21. Thakur, V. K.; Nayak, S. K.; Dixit, G. In *Lignocellulosic Polymer Composites: Processing, Characterization and Properties*; Thakur, V. K., Eds.; Wiley: New Jersey; **2014**; pp 523–549.
22. Amieva, E. J.-C.; Velasco-Santos, C.; Martinez-Hernandez, A.; Rivera-Armenta, J.; Mendoza-Martinez, A.; Castano, V. *J. Compos. Mater.* **2014**, *49*, 275–283.
23. Pang, M. M.; Pun, M. Y.; Ishak, Z. A. M. *Polym. Eng. Sci.* **2014**, *54*, 1357–1365.
24. Fernandes, E. M.; Correlo, V. M.; Chagas, J. A. M.; Mano, J. F.; Reis, R. L. *Compos. Sci. Technol.* **2010**, *70*, 2310–2318.
25. Grozdanov, A.; Buzarovska, A.; Bogoeva-Gaceva, G.; Avella, M.; Errico, M. E.; Gentile, G. *Polym. Eng. Sci.* **2007**, *47*, 745–749.
26. Liu, X.; Tang, Y.; Zhang, B.; Chen, F.; Xu, W. *Polym. Compos.* **2015**, 1–10.
27. Soleimani, M.; Tabil, L.; Panigrahi, S.; Oguocha, I. In *Thermoplastic - Composite Materials*; El-Sonbati, A. P., Eds.; InTech, **2012**, pp 131–146.
28. Mucha, M.; Królikowski, Z. *J. Therm. Anal. Calorim.* **2003**, *74*, 549–557.
29. Magalhães da Silva, S. P.; Lima, P. S.; Oliveira, J. M. *Compos. Part B Eng.* **2016**, *90*, 172–178.
30. Avrami, M. *J. Chem. Phys.* **1939**, *7*, 1103.
31. Ozawa, T. *Polymer (Guildf.)* **1971**, *12*, 150–158.
32. Liu, T.; Mo, Z.; Wang, S.; Zhang, H. *Polym. Eng. Sci.* **1997**, *37*, 568–575.
33. Kissinger, H. E. *J. Res. Natl. Bur. Stand.* **1956**, *57*, 217–221.
34. Rosa, M. E.; Fortes, M. A. *J. Mater. Sci. Lett.* **1988**, *7*, 1064–1065.
35. Zheng, G.; Jia, Z.; Li, S.; Dai, K.; Liu, B.; Zhang, X.; Mi, L.; Liu, C.; Chen, J.; Shen, C.; Peng, X.; Li, Q. *Polym. Int.* **2011**, *60*, 1434–1441.
36. Ehrenstein, G. W.; Riedel, G.; Trawiel, P. *Thermal Analysis of Plastics: Theory and Practise*; Hanser Gardner Publications: Nuremberg, **2004**; pp 12–20.
37. Fernandes, E. M.; Correlo, V. M.; Mano, J. F.; Reis, R. L. *Mater. Design.* **2015**, *82*, 282–289.
38. Zhang, R.; Zheng, H.; Lou, X.; Ma, D. *J. Appl. Polym. Sci.* **1994**, *51*, 51–56.
39. Ding, W.; Chu, R. K. M.; Mark, L. H.; Park, C. B.; Sain, M. *Eur. Polym. J.* **2015**, *71*, 231–247.
40. Abdel Aziz, M. S.; Saad, G. R.; Naguib, H. F. *Thermochim. Acta* **2015**, *605*, 52–62.
41. Şanlı, S.; Durmus, A.; Ercan, N. *J. Appl. Polym. Sci.* **2012**, *125*, E268–E281.
42. Mandelkern, L. *Methods of Experimental Physics*; Academic Press: New York, **1980**, pp 81–105.
43. Jeziorny, A. *Polymer (Guildf.)* **1978**, *19*, 1142–1144.
44. Alamo, R. G.; Mandelkern, L. *Macromolecules* **1991**, *24*, 6480–6493.
45. Di Lorenzo, M. L.; Silvestre, C. *Prog. Polym. Sci.* **1999**, *24*, 917–950.
46. Huang, Y.; Liu, H.; He, P.; Yuan, L.; Xiong, H. *J. Appl. Polym. Sci.* **2010**, *116*, 2119–2125.
47. Vyazovkin, S.; Sbirrazzuoli, N. *Macromol. Rapid Commun.* **2004**, *25*, 733–738.
48. Dobrev, A. and Gutzow, I. *J. Non-Cryst. Solids.* **1993**, *162*, 1–12.
49. Dobrev, A. and Gutzow, I. *J. Non-Cryst. Solids.* **1993**, *162*, 13–25.
50. Quan, H.; Li, Z.-M.; Yang, M.-B.; Huang, R. *Compos. Sci. Technol.* **2005**, *65*, 999–1021

2.4 Nucleating ability of cork in polypropylene-based composites ^f

Magalhães da Silva, S. P.¹, Lima, P. S.² and Oliveira, J. M.³

¹Aveiro Institute of Materials (CICECO), University of Aveiro, Campus Universitário de Santiago, 3810-193, Aveiro, Portugal

Email: sarapms@ua.pt,

Web Page: <http://www.ciceco.ua.pt/index.php?tabela=peessoaldetail&menu=221&user=1331>

²School of Design, Management and Production Technologies Northern Aveiro, University of Aveiro, Estrada do Cercal, nº 449, 3720-509, Oliveira de Azeméis, Portugal

Email: plima@ua.pt,

Web Page: <http://www.ua.pt/esan/>

³Aveiro Institute of Materials (CICECO), University of Aveiro, Campus Universitário de Santiago, 3810-193, Aveiro, Portugal

Email: martinho@ua.pt,

Web Page: <http://www.ciceco.ua.pt/index.php?tabela=peessoaldetail&menu=218&user=222>

Keywords: cork-polymer composites (CPC), polypropylene (PP), nucleating activity (Φ), differential scanning calorimetry (DSC)

Abstract

The nucleating activity (Φ) of cork-polymer composites (CPC) in a polypropylene (PP) matrix was analyzed by Dobreva and Gutzow method. CPC with 15 %wt of cork powder was used in this study. The non-isothermal crystallization behaviour was studied using differential scanning calorimetry (DSC) at four different cooling rates (5, 10, 15 and 20°C/min). Results show that cork acted as an active surface by revealing Φ value lower than 1. This suggests that cork can act as a nucleating agent during non-isothermal crystallization.

1. Introduction

The demand for new materials derived from renewable resources has been increasing, mostly due to environmental concerns and waste accumulation, driven by the restrictive measures imposed by the European Commission. Nowadays, there is a need for more innovative, sustainable and recyclable materials, combined with an increase market demand for products with lower ecological footprint.

^f Magalhães da Silva, S. P., Lima P. S., Oliveira J. **2016**. Nucleating ability of cork in polypropylene-based composites. In Proceedings of the 17th European Conference on Composite Materials (ECCM), Munich, Germany.

The author had contributed to the planning and execution of all the DSC analyses and modeling calculations herein presented, as well as on the discussion, interpretation and preparation of the manuscript.

Lignocellulosic materials' incorporation in synthetic polymers has become an effective approach to develop new sustainable materials [1]. Cork is a well-recognized Portuguese raw material and product. Cork is the outer bark of oak tree *Quercus suber L.*, which regenerates in every 9-10 years. The main chemically component is suberin (33-50%), followed by lignin (20-25%); the carbohydrate fraction is composed by cellulose and hemicelluloses (12-20%); extractives represent nearly 14-18% and $\approx 1\%$ are ashes [2]. Cork possesses an unique combination of properties, more specifically, low density, elasticity and compressibility (without lateral expansion), high recovery capacity after impact, impermeability to liquids and gases, excellent thermal and acoustic insulation and, microbial and fire resistance [2]. Stoppers are the major cork product and its production generates $\approx 30\%$ wt of industrial residues. These residues are usually burned (thermal energy recovery) representing a low value disposal solution. The development of new polymeric materials based in these cork by-products is a promising strategy to upcycle these residues. Low density, hardness and cost, good relation between strength/weight, good insulation properties and high levels of filling are some of the advantages of applying natural materials as fillers in thermoplastic matrices. Natural materials are also renewable, readily available and non-toxic [3].

The present study is part of a larger project that focuses on the research of cork-polymer composites (CPC) for injection molding applications. Studies on CPC thermal behavior are essential in fields like injection molding, in order to improve thermal resistance, mechanical properties and material processing. During injection molding process, plastic matrix composites experience non-isothermal crystallization rather than isothermal crystallization. A previous work [4] regarding the CPC non-isothermal crystallization study showed that the presence of cork particles can influence the crystallization process, mostly by revealing nucleating activity. Moreover, composites mechanical properties can be partially dependent on how cork influences the crystallization behavior.

In this particular study, the evaluation of cork nucleating activity was assessed by Dobрева and Gutzow method [5, 6]. Nucleating activity is defined as a factor in which three-dimensional (3D) nucleation decreases with the addition of a foreign substrate. If the foreign substrate is active Φ approaches to 0, while for inert substrates Φ approaches to 1.

2. Experimental Procedure

2.1. Materials

The polymeric matrix used is a homopolymer PP (PPH 10060) from Total Petrochemicals, having a Melt Flow Index (MFI) of 35g/10min (230°C, 2.16 Kg) and a melting temperature (T_m) of 165°C. Cork powder was supplied by a Portuguese cork producer. It was fractionated through sieving (Retsch, Germany) and the relative amount of particles according to its size was determined (Table 1).

The average particle size, d_p , was calculated using (Eq. 1), where w_i is the weight fraction of the i th particle size and d_i is the diameter of the i th particle.

$$d_p = \frac{\sum w_i d_i^4}{\sum w_i d_i^3} \quad (1)$$

Table 1. Cork particles: physical characteristics.

Granulometry (μm)	Cork powder (%)	Average particle size (μm)
1000	2.3 \pm 0.1	596
800	45.8 \pm 0.1	
400	51.4 \pm 0.1	
200	0.6 \pm 0.1	

2.2. CPC formulation

Prior to compounding, cork particles were dried at 70°C for 24h in a vacuum oven (Carbolite AX60 model) to stabilize moisture content. It is known that cork structure and composition do not suffer significant changes up to 250°C [7]. CPC were compounded in a Brabender type internal mixer with a mixing volume chamber of 355 cm³. Firstly, PP pellets were charged and melted during 2 minutes at 180°C and 40 rotations per minute (rpm). Then, cork particles (15 %wt) were added and materials were mixed for additional 8 minutes.

2.3. DSC analyses

Crystallization behavior analysis was carried out in a Shimadzu DSC-60 apparatus. The equipment was calibrated using indium as reference material. Samples weights varying between 5.0 and 6.0 mg were encapsulated in aluminum pans. Each sample was heated from 20°C to 200°C at a scan rate of 200°C/min and held for 2 minutes at this temperature to eliminate thermal history and prevent self-seeding of PP [8]. Then, they were cooled until -80°C and heated again up to 200°C. Four different heating/cooling rates (ϕ) – 5, 10, 15 and 20 °C/min – were used. Only the second run was considered to analyze the crystallization behavior process: crystallization temperature (T_c) and melting temperature (T_m).

3. Results and Discussion

3.1. Non-isothermal behavior

Thermal parameters of PP and CPC are listed in (Table 2). Melting temperatures of PP and CPC at different cooling rates did not vary significantly. On the other hand, T_c shifted to lower values as

the cooling rates increase. This indicates a cooling rate effect on the crystallization kinetics. Polymer chains, at higher cooling rates, are less movable and have shorter time to diffuse into the crystalline phase, which results in a decrease of T_c . Contrarily, lower cooling rates promotes better conditions for the development of polymer crystals due to a kinetic process. The length and branches of the polymer chains also influence the crystallization process [9].

Table 2. Non-isothermal crystallization parameters obtained by DSC.

Samples	ϕ (°C/min)	T_m (°C)	T_c (°C)
PP	5	164.51	114.81
	10	164.39	106.13
	15	164.01	103.61
	20	164.97	99.22
CPC	5	160.13	118.32
	10	162.99	114.55
	15	162.46	111.60
	20	161.68	108.77

From (Table 2), it is also visible that, for a specific cooling rate, T_c values were higher for CPC when compared to PP. The crystallization process is governed by two major events, namely nucleation and crystal growth. In a neat polymer matrix, like PP, polymer chains have to overcome the free energy of primary nucleation and create a new surface for crystal growth [10]. While in the case of CPC, the incorporation of a foreign substrate (cork) can reduce the free energy needed for nucleation, leading to a faster crystallization process. Consequently, more crystals are formed and a higher T_c value is obtained.

From (Table 2), it is also visible that, for a specific cooling rate, T_c values were higher for CPC when compared to PP. The crystallization process is governed by two major events, namely nucleation and crystal growth. In a neat polymer matrix, like PP, polymer chains have to overcome the free energy of primary nucleation and create a new surface for crystal growth [10]. While in the case of CPC, the incorporation of a foreign substrate (cork) can reduce the free energy needed for nucleation, leading to a faster crystallization process. Consequently, more crystals are formed and a higher T_c value is obtained.

3.2. Nucleating activity

Dobrova and Gutzow developed a simple method [5, 6] to estimate the nucleating activity of a foreign substrate in a polymer melt. The nucleating activity is defined as a factor in which three-dimensional (3D) nucleation decreases with the addition of a foreign substrate. It is determined as the ratio of β parameters (Eq. 2) in heterogeneous (β^*) and homogeneous (β) medium.

$$\Phi = \frac{\beta^*}{\beta} \quad (2)$$

For homogeneous nucleation, β parameter can be calculated from (Eq. 3):

$$\ln(\varphi) = \text{const} - \frac{\beta}{\Delta T_p^2} \quad (3)$$

, where β is related to the 3D nucleation and ΔT_p^2 is the degree of supercooling (Eq. 4).

$$\Delta T_p^2 = T_m - T_c \quad (4)$$

For heterogeneous nucleation, β^* parameter can be calculated from (Eq. 5):

$$\ln(\varphi) = \text{const} - \frac{\beta^*}{\Delta T_p^2} \quad (5)$$

Both β and β^* for PP and CPC can be obtained from plotting $\ln(\varphi)$ against the reciprocal of ΔT_p^2 . These plots are presented in (Figure 1) and nucleating activity values for samples are listed in (Table 3).

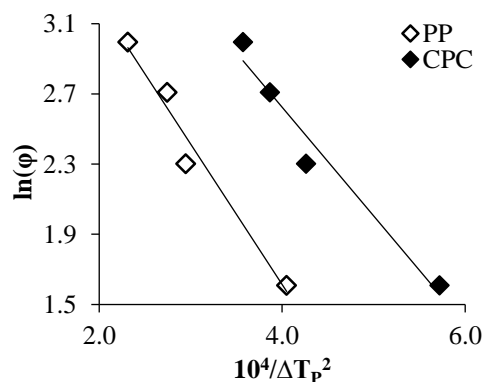


Figure 1. Plots of $\ln(\varphi)$ against reciprocal ΔT_p^2 for PP and CPC.

As referred above, for active substrates the Φ value approaches to 0, while for absolutely inert substrates Φ is 1. The obtained Φ value for CPC was lower than 1 suggesting that cork acted as an effective nucleating agent in PP matrix, creating an active surface.

Table 3. Nucleating activity.

Samples	β	β^*	Φ	R^2
PP	0.80	-	-	0.97
CPC	-	0.62	0.78	0.96

4. Conclusions

The presented work focuses on the study of cork nucleating activity on a PP matrix through non-isothermal crystallization analyses. Dobrevá and Gutzow method was used and it was possible to estimate the nucleating activity value. It was found that Φ was lower than 1 (equal to 0.78), which indicates that cork acted as an active surface promoting the crystallization process.

Acknowledgments

The authors are grateful to COMPETE – Programa Operacional Factores de Competitividade (POFC), project number 30176, for financial support.

References

- [1] N. M. Belgacem and A. Gandini. *Monomers, polymers and composites from renewable resources*. Elsevier, 2008.
- [2] H. Pereira. *Cork: biology, production and uses*. Elsevier, 2007.
- [3] V. K. Thakur. *Lignocellulosic Polymer Composites: processing, characterization and properties*. Wiley, 2015.
- [4] S. P. Magalhães da Silva, P. S. Lima and J. M. Oliveira. Non-isothermal crystallization kinetics of cork-polymer composites for injection moulding. *Journal of Applied Polymer Science*. 2016 (submitted).
- [5] A. Dobrevá and I. Gutzow. Activity of substrates in the catalysed nucleation of glass-forming melts. I. Theory. *Journal of Non-Crystalline Solids*. 162–1:12, 1993.
- [6] A. Dobrevá and I. Gutzow. Activity of substrates in the catalysed nucleation of glass-forming melts. II. Experimental evidence. *Journal of Non-Crystalline Solids*. 162–13:25, 1993.
- [7] M. E. Rosa and M. A. Fortes. Thermogravimetric analysis of cork. *Journal of Materials Science Letters*. 7–1064:1065, 1988.
- [8] G. Zheng, Z. Jia, S. Li, K. Dai, B. Liu, X. Zhang, L. Mi, C. Liu, J. Chen, C. Shen, X. Peng and Q. Li. Oriented structure in stretched isotactic polypropylene melt and its unexpected recrystallization: optical and X-ray studies. *Polymer International*. 60–1434:1441, 2011.
- [9] G. W. Ehrenstein, G. Riedel and P. Trawiel. *Thermal Analysis of Plastics: Theory and Practise*. Hanser Gardner Publications, 2004.
- [10] M. S. Abdel Aziz, G. R. Saad and H. F. Naguib. Non-isothermal crystallization kinetics of poly(3-hydroxybutyrate) in copoly(ester-urethane) nanocomposites based on poly(3-hydroxybutyrate) and cloisite 30B. *Thermochimica Acta*. 605–52:62, 2015.

2.5 Cork-Polymer Composites for Injection Moulding ⁹

S. P. Magalhães da Silva^{1,2,3*}, J. M. Oliveira^{1,2,3}

¹EMaRT Group – Emerging: Materials, Research, Technology, University of Aveiro, Portugal

²School of Design, Management and Production Technologies Northern Aveiro (ESAN), University of Aveiro, Portugal

³Aveiro Institute of Materials (CICECO), University of Aveiro, Portugal

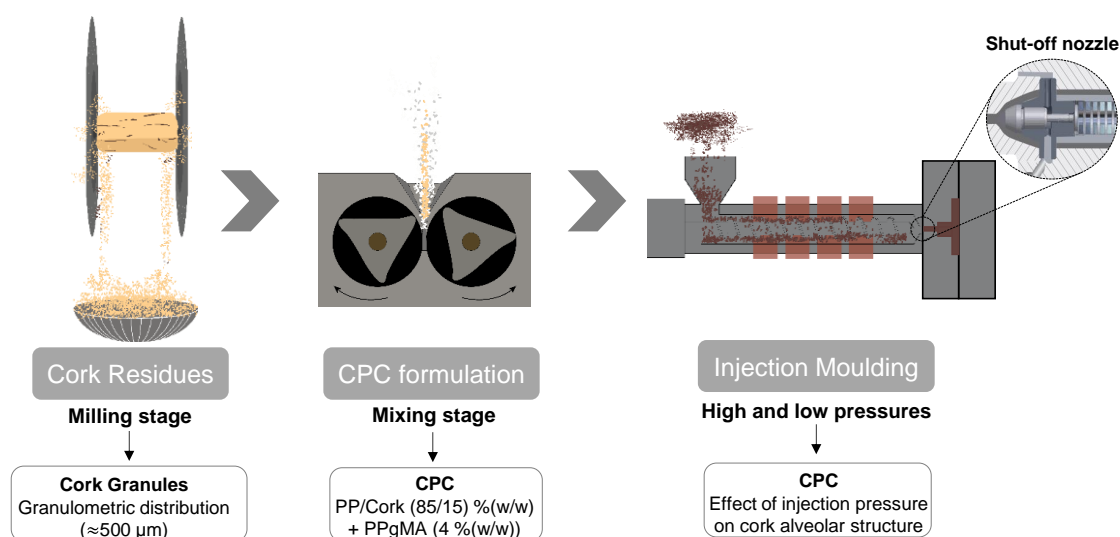
*corresponding author: sarapms@ua.pt

Abstract

A cork-polymer composite (CPC) material composed by 85% (w/w) polypropylene (PP), 4% (w/w) of polypropylene grafted maleic anhydride (PPgMA) and 15% (w/w) of cork was used to perform a case study. The selection was based on previous studies on the rheological and thermal behaviour of CPC. The case-study was conducted to evaluate the effect of the high pressure in cork applied during a standard injection moulding (IM) process. The obtained results will serve as comparison to those achieved by a modified IM process.

A modified IM process was conducted to overcome the damage on cork alveoli triggered by the standard IM. In this sense, it was studied the effect of three levels of injection pressures with holding and back pressures set to 0 bar. The modified IM process was also characterized by an injection system equipped with a shut-off nozzle. Morphological analyses were performed to evaluate cork alveoli integrity after standard and modified IM processes. The obtained results have shown that cork granules near to matrix defects (voids) were able to expand naturally and return to its initial shape and size. This indicates that cork cell walls are not irreversible damaged by the IM process itself.

Graphical Abstract



⁹ To be submitted.

The author had contributed to the planning and execution of all IM experiments and definition of the most adequate IM parameters set.

Keywords: Cork; Cork-polymer composites; Injection Moulding; Microcellular

1. Introduction

Cork is a natural foamed material. It is the outer bark of an oak tree defined as *Quercus suber* L. Cork characteristic honeycomb structure is composed by 42 million closed cells per cubic centimetre [1,2]. Chemically, cork is mainly composed by suberin and lignin [1]. The combination of cork's honeycomb structure and chemical composition resulted in a natural material with a unique combination of properties. Such properties include low density, hydrophobic character, thermal, acoustic and electrical insulation properties, among others [1].

In the literature, it can be found studies reporting the development of CPC adapted to manufacturing solutions [2–10]. However, only a few studies evaluate the effect of IM process on CPC morphology and properties [2,6,7]. The high pressure applied during the IM process compresses and can destroy cork alveolar structure and cork intrinsic properties can be lost.

The main goal and motivation of the present work is to study a modified IM solution that will overcome the high pressure applied during IM and take advantage of cork unique properties. To the best of our knowledge, studies related with modified IM solutions are non-existing.

Open-cell materials or microcellular materials can already be obtained by the IM process. These types of materials are constituted by a foamed core and by a compact outer layer. Polymeric foams can be obtained by a chemical route, that consists on the addition of chemical agents, or by a physical route, that involves the injection of blowing gases [11,12]. Both routes allow to obtain parts with lower density and to eliminate the holding pressure during the IM process. These will bring several advantages over the standard IM processes, namely faster IM cycles, lower material consumption and better dimensional stability of the injected parts.

Chemical agents consist in organic or inorganic materials that decompose thermally and release gases. Azodicarbonamide, sodium bicarbonate and zinc bicarbonate are the chemical agents mostly used [11,13]. These chemical agents can be mixed directly with the polymeric material without the need to modify the IM equipment. Chemical foaming is particularly suited for producing parts with walls thicker than 4 mm. Polyolefins and polystyrenes are usually considered due to their lower processing temperatures.

Physical route involves the use of blowing agents, usually CO₂ or N₂, that are injected under high pressure into the melted material in the plasticizing IM zone [11,13]. Contrarily to the chemical route, physical foaming is particularly suited for producing parts with walls thinner than 4 mm. The presence of by-products, resultant from unreacted substances, that can compromise the performance of the foam, are eliminated with this type of foaming strategy. However, it is necessary to modify the IM system. Recently, it has been reported studies related to the combination of the physical foaming with a mould-opening strategy [14–17]. In this particular case, the IM process is divided into three main phases: (1) the blowing agent is injected into the mould cavity; (2) the melted polymer is injected into the mould cavity filled with gas (primary foaming) and the mixture melt/gas is maintained inside

the mould with a high holding pressure; next (3), the mould is opened with a defined distance to activate the secondary foaming.

In this study, it will be expected that cork itself creates the open-cell structure. It is desired that cork alveoli expansion on the polymer melt will happen naturally, without the addition of any chemical or physical blowing agent. The use of chemical or physical blowing agents to assist cork expansion is out of this project scope.

2. Methodology

2.1 Preparation of CPC

The formulation procedure of the CPC used in the present case study is published elsewhere [8,9]. The CPC 1g formulation was selected. This selection was based on the thermal [8] and rheological [9] characterization already reported of the developed CPC (Table 1).

Table 1. Rheological and thermal parameters of CPC 1g.

CPC 1g	
η_0 (Pa·s) [9]	933
T_c (°C) [8]	114.8 ¹
T_m (°C) [18]	165.0 ²

¹ 10°C/min; ² value of the polymeric matrix

In addition, CPC 1g is composed by cork powders with large particle sizes having an average particle size equal to 596 μm . This feature will contribute to the aesthetics of the injected parts in which it is desired to observe the cork granules dispersed within the polymeric matrix.

2.2 IM processes

Standard IM process occurred in an Engel ES 700 (125 ton) machine applying the IM parameters presented in Table 2. A mould with a cavity design of a plastic tensile specimen (EN ISO 527-2:1996 standard [19]) was used for both IM processes.

Table 2. Parameters for standard IM.

Temperature profile (°C)	220/215/200/180/150/30
Injection pressure (bar)	60
Injection speed ($\text{mm}\cdot\text{s}^{-1}$)	30
Holding Pressure (bar)	30
Back pressure (bar)	15
Cooling time (s)*	40

*Mould without cooling system.

The modified IM process was conducted in a Kraus Maffei (40 ton) machine equipped with a mechanical stuff-off nozzle. During injection, the shut-off nozzle pin is forced backwards caused by the material flow and pressure. Then, the injected material flows freely into the mould cavity. When

the injection pressure is released, the shut-off nozzle pin is forced against the tip caused by the spring tension and the material flow is shut-off. It is expected that this mechanism will contribute to the expansion of cork alveoli inside the mould cavity.

Table 3 presents the IM parameters applied. The minimum injection pressure (28 bar) was defined based on the mould cavity volume and the definition of the material dosage (shot) to obtain a complete part.

Table 3. Parameters for modified IM.

Temperature profile (°C)	220/210/200/190/60		
Injection pressure (bar)	28	48	60
Injection time (s)	11.1	8.3	5.0
Injection speed (mm·s ⁻¹)	20		
Holding Pressure (bar)	0		
Back pressure (bar)	0		
Cooling time (s) (water at 20°C)	20		

2.3 Morphological analyses

Morphological analyses were conducted to characterize cork granules and to evaluate the integrity of cork structure after being processed by a standard IM and by a modified IM process. Scanning electron microscopy (SEM) analyses were conducted on a Hitachi SU-70. CPC samples were broken with liquid nitrogen and the surface fracture was analysed. Samples were mounted on aluminium stubs and, then, sputter coated (Polaron E 5000) with Au/Pd target for 2 min at 12 mA.

3. Results and Discussion

3.1 Cork and CPC morphology

In Fig. 1 is displayed SEM image of cork granules. It can be observed that some cork alveoli remain closed, while few of them are damaged as a result of the industrial grinding process.

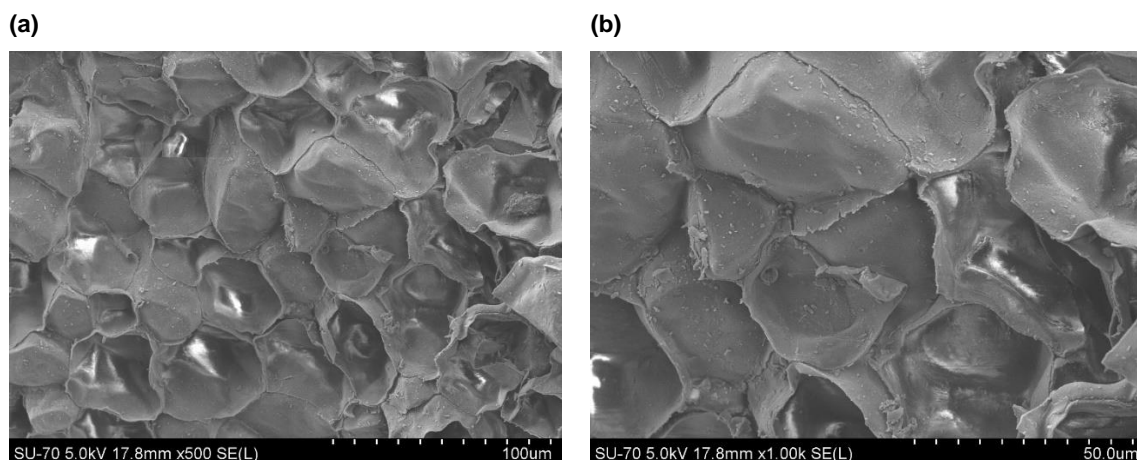


Fig. 1. SEM images of cork granules (a) x500 and (b) x1000.

The morphology of CPC, concerning the dispersion of cork granules within PP matrix as well as the adhesion of cork particles to the polymeric matrix, can be seen on Fig. 2. It is clearly visible that cork is continuously dispersed and imbibed within the PP matrix. The adhesion of PP to cork, owing to the presence of PPgMA, is also supported by the covering and fulfilling by PP of cork alveoli (Figure 2(d)).

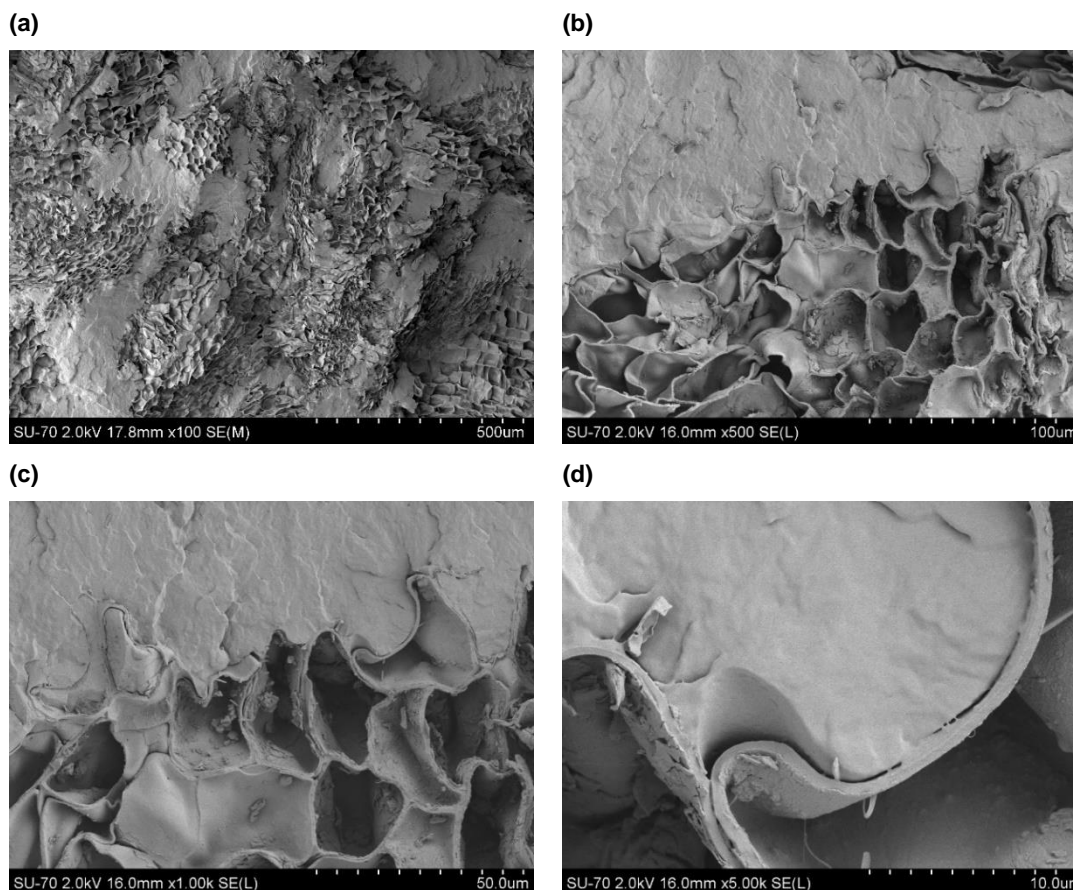


Fig. 2. SEM images of CPC (a) x100, (b) x500, (c) x1000 and (d) x5000.

3.2 Standard IM

Fig. 3 reveals the effect of the high pressure applied during the standard IM process on the integrity of cork alveoli. Cork alveolar structure is undoubtedly compressed and damaged. The intrinsic properties of cork are compromised. Andrzejewski, J. *et al.* [6] reported the same behaviour of cork-based composites. The characteristic cellular structure of cork was still visible after IM, but the majority of pores were deformed or destroyed. An interesting result was reported by Vilela, C. *et al.* [7], where cork morphology was maintained after cork-based composites processing by IM. However, in this case, a micro IM machine was used, so it can be assumed that lower injection pressures were applied (IM parameters not presented).

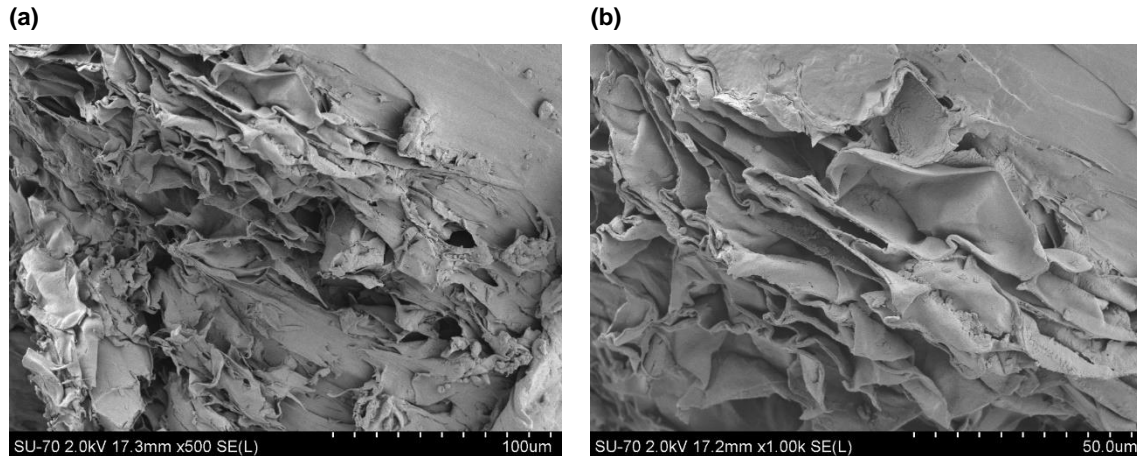


Fig. 3. SEM images of injected specimens (standard IM).

3.3 Modified IM

A modified IM process was applied to overcome the damages presented in Fig. 3. In this sense, the influence of a mechanical shut-off nozzle and different IM parameters (Table 3) was studied. Keeping all the IM parameters constant, the injection pressure was varied, and consequently the injection time. The effect of pressure onto the integrity of cork alveoli was evaluated. The holding and back pressures were set at 0 bar to avoid fluid compaction. In addition, the release of the holding pressure was ensured to assist cork granules expansion inside the polymeric fluid. Next, the mould cavity would be fulfilled completely.

It is expected that cork granules can recover from the pressure applied during the IM process and exhibit a morphology similar to that observed in Fig. 2. SEM images of the injected parts obtained by the modified IM with different injection pressures are demonstrated in Fig. 4.

From Fig. 4 (a) it is visible the expansion of cork alveoli after injection at 28 bar, when compared to Fig. 3. However, it is not attained the desired morphology exhibited in Fig. 2. As the injection pressure increases it is detected an increase on the compression of cork alveoli (Fig. 4 (a-c)). An interesting behaviour was observed in Fig. 4 (b). Cork granules were able to completely expand when they were close to defects (voids) and not completely surrounded by the polymeric matrix. This can be indicative that cork granules can naturally expand after an IM process, when they are not completely imbibed within the matrix.

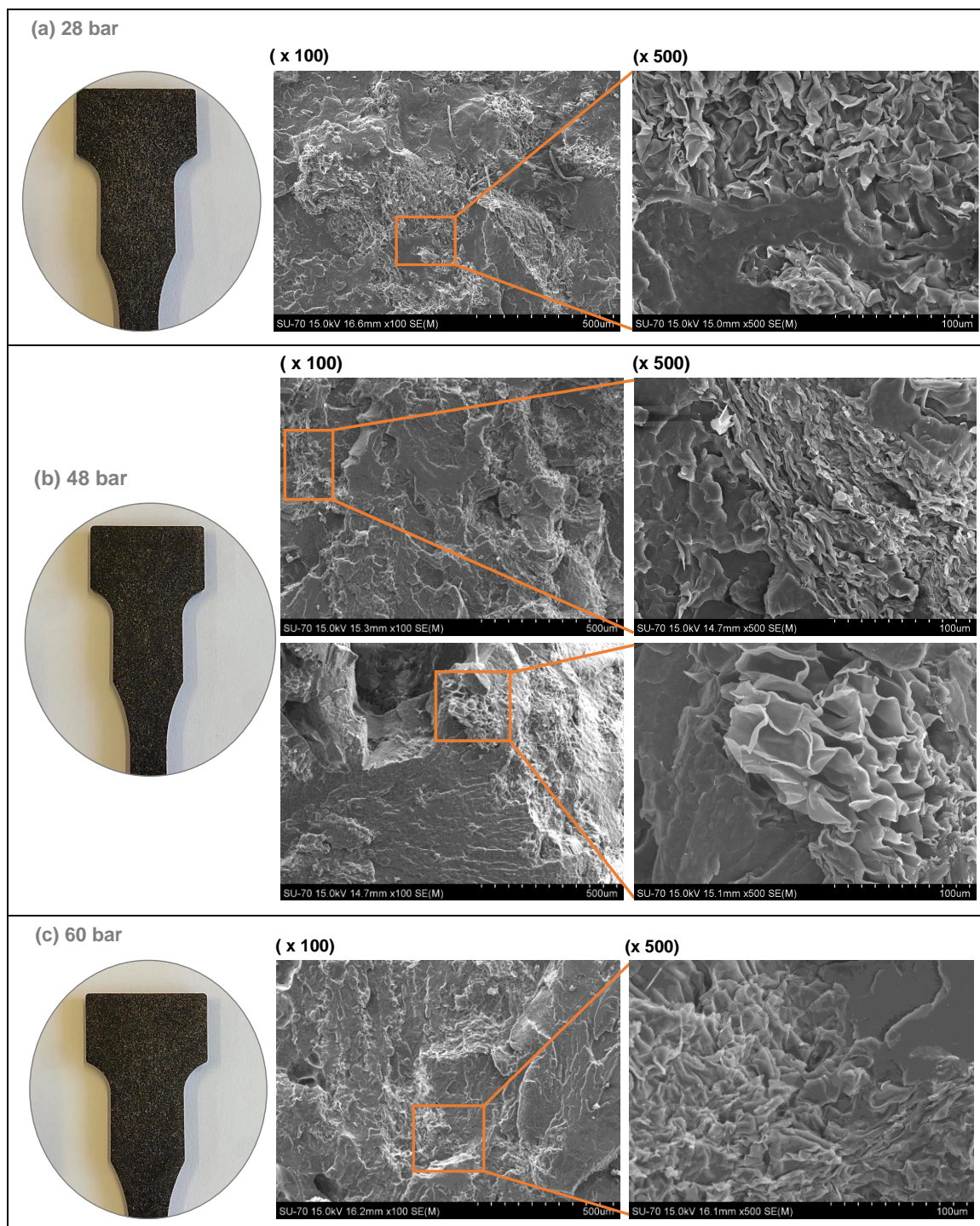


Fig 4. SEM images of surface fracture of specimens injected at (a) 28 bar (b) 48 bar and (c) 60 bar (modified IM).

Conclusions

Cork-based formulations were successfully injected. Nevertheless, owing to the high pressures applied during the standard IM process, cork structure was damaged. In this sense, the IM process

was modified to guarantee the integrity of cork structure and, consequently, to take advantage of its unique combination of properties.

A modified IM was conducted to evaluate the effect of IM parameters and the presence of a shut-off nozzle onto cork's alveoli integrity. Three levels of injection pressures were studied and holding and back pressures were annulated. Even for the lowest injection pressure, it was observed some compression of cork alveoli. However, when cork granules were close to matrix defects, they were able to expand and return to its initial shape and size. A possible strategy to take advantage of this behaviour will pass through the addition of chemical foaming agents during the plasticization phase.

The present case-study will act as a starting point and it will contribute for new industrial solutions that minimize cork alveolar structure damage instigated by the characteristic high pressure of IM process.

Acknowledgments

The authors are grateful to COMPETE – Programa Operacional Factores de Competitividade (POFC), project number 38293, for financial support. Authors are also thankful to Tiago Silva (DeMaC, UA) for SEM analyses.

References

- [1] Pereira H. *Cork : Biology, Production and Uses*. Amsterdam: Elsevier; 2007.
- [2] Fernandes EM, Correlo VM, Mano JF, Reis RL. Cork-polymer biocomposites: Mechanical, structural and thermal properties. *Mater Des* 2015;82:282–9.
- [3] Fernandes EM, Correlo VM, Mano JF, Reis RL. Polypropylene-based cork-polymer composites: Processing parameters and properties. *Compos Part B Eng* 2014;66:210–23. doi:10.1016/j.compositesb.2014.05.019.
- [4] Fernandes EM, Aroso IM, Mano JF, Covas JA, Reis RL. Functionalized cork-polymer composites (CPC) by reactive extrusion using suberin and lignin from cork as coupling agents. *Compos Part B Eng* 2014;67:371–80.
- [5] Fernandes EM, Mano JF, Reis RL. Hybrid cork-polymer composites containing sisal fibre: Morphology, effect of the fibre treatment on the mechanical properties and tensile failure prediction. *Compos Struct* 2013;105:153–62. doi:10.1016/j.compstruct.2013.05.012.
- [6] Andrzejewski J, Szostak M, Barczewski M, Łuczak P. Cork-wood hybrid filler system for polypropylene and poly(lactic acid) based injection molded composites. Structure evaluation and mechanical performance. *Compos Part B Eng* 2019;163:655–68. doi:10.1016/J.COMPOSITESB.2018.12.109.
- [7] Vilela C, Sousa AF, Freire CSR, Silvestre AJD, Pascoal Neto C. Novel sustainable composites prepared from cork residues and biopolymers. *Biomass and Bioenergy* 2013;55:148–55.
- [8] Magalhães da Silva SP, Lima PS, Oliveira JM. Non-isothermal crystallization kinetics of cork-polymer composites for injection molding. *J Appl Polym Sci* 2016;133:44124–44133. doi:10.1002/app.44124.
- [9] Magalhães da Silva SP, Lima PS, Oliveira JM. Rheological behaviour of cork-polymer composites for injection moulding. *Compos Part B Eng* 2016;90:172–8. doi:10.1016/j.compositesb.2015.12.015.
- [10] Menager C, Guigo N, Wu X, Vincent L, Sbirrazzuoli N. “Green” composites prepared from polyfurfuryl alcohol and cork residues: Thermal and mechanical properties. *Compos Part A Appl Sci Manuf* 2019;124:105473. doi:10.1016/J.COMPOSITESA.2019.105473.
- [11] Altan M. *Thermoplastic Foams: Processing, Manufacturing, and Characterization*. Recent Res. Polym., InTech; 2018, p. 117–137.
- [12] Jin F-L, Zhao M, Park M, Park S-J. Recent Trends of Foaming in Polymer Processing: A Review. *Polymers (Basel)* 2019;11:953. doi:10.3390/polym11060953.

- [13] Antonio J, Ruiz R, Vincent M, Agassant J-F, Sadik T, Pillon C. Polymer foaming with chemical blowing agents: Experiment and modeling. *Polym Eng Sci* 2015;55:2018. doi:10.1002/pen.24044i.
- [14] Wang L, Hikima Y, Ishihara S, Ohshima M. Fabrication of lightweight microcellular foams in injection-molded polypropylene using the synergy of long-chain branches and crystal nucleating agents. *Polymer (Guildf)* 2017;128:119–27. doi:10.1016/J.POLYMER.2017.09.025.
- [15] Wang G, Zhao G, Dong G, Mu Y, Park CB, Wang G. Lightweight, super-elastic, and thermal-sound insulation bio-based PEBA foams fabricated by high-pressure foam injection molding with mold-opening. *Eur Polym J* 2018;103:68–79. doi:10.1016/J.EURPOLYMJ.2018.04.002.
- [16] Wang G, Zhao G, Dong G, Song L, Park CB. Lightweight, thermally insulating, and low dielectric microcellular high-impact polystyrene (HIPS) foams fabricated by high-pressure foam injection molding with mold opening. *J Mater Chem C* 2018;6:12294–305. doi:10.1039/C8TC04248A.
- [17] Wang G, Zhao J, Wang G, Zhao H, Lin J, Zhao G, et al. Strong and super thermally insulating in-situ nanofibrillar PLA/PET composite foam fabricated by high-pressure microcellular injection molding. *Chem Eng J* 2020;390:124520. doi:10.1016/j.cej.2020.124520.
- [18] Total Petrochemicals PPH 10060 n.d.
<http://www.matweb.com/search/DataSheet.aspx?MatGUID=afac56da5d7c4845bab22f67848a6316&ckck=1> (accessed December 12, 2020).
- [19] BS EN ISO 527-2: 1996. Plastics - Determination of tensile properties - Part 2: Test conditions for moulding and extrusion plastics. 1996.

Cork-Polymer Composites and cork-based formulations for Additive Manufacturing

3.1 Introduction.....	75
3.1.1 Biopolymers.....	75
3.1.2 Additive Manufacturing.....	80
3.1.2.1 Fused Filament Fabrication.....	83
3.1.2.2 3D Printing.....	85
3.2 Non-isothermal Cold Crystallization Kinetics of Cork-Polymer Biocomposites based on Polylactic Acid for Fused Filament Fabrication.....	91
3.3 Cork-Polylactide Composites reinforced with polyhydroxyalkanoates for Additive Manufacturing.....	110
3.4 Cork-like Filaments for Additive Manufacturing.....	119
3.5 Cork powders wettability by the Washburn capillary rise method	137
3.6 Cork powder as material for 3D Printing: A case study.....	149

3.1 Introduction

3.1.1 Biopolymers

The development of fully biodegradable CPC was one of the main goals of the present thesis. In this sense, the study and development of biodegradable polymeric matrices was conducted.

PLA is a biodegradable aliphatic polyester and it is one of the most promising biopolymers. Annually, it is produced from renewable available resources and the industrial technology needed for its processing is relatively low price, when compared to petrol-based plastics^{1,2}. PLA can be manufactured from lactic acid obtained by a chemical synthesis or by a carbohydrate fermentation. Corn starch, sugarcane and tapioca are the most used agro-sources for PLA synthesis by carbohydrate fermentation. Through bacterial fermentation, these agro-sources are converted into glucose and then to lactic acid. Then, lactic acid is fermented to lactide which is further polymerized³. Different PLA polymerization routes can be applied and the most common one is the ring-opening lactide polymerization⁴. Lactic acid is chiral with two optical isomers, L- and D-isomers (Figure 3.1). The stereochemical structure of PLA can be easily changed, depending on the amount of L- and D-isomers during polymerization⁴.

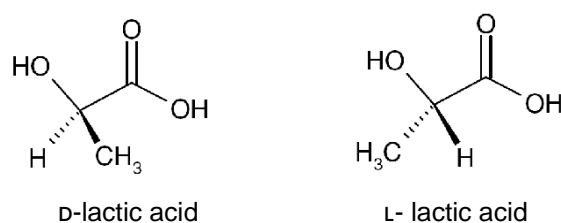


Figure 3.1| PLA stereoisomers.

This ratio of L- and D-isomers affects mechanical and thermal properties of the obtained PLA. Regarding thermal properties, PLA can be a semi-crystalline or an amorphous material depending on its stereochemical structure and thermal history. As the content of D-isomers increases, the values of T_g , T_m and the crystallization rate decreases⁵. Moreover, PLA has a particular thermal behaviour in a way that multiphase transitions, such as glass transition, chain relaxation, cold crystallization and melting are involved^{6,7}. One of the main drawbacks of using PLA in an industrial level is its low crystallization rate. Several modifications have been proposed to improve the crystallization rate, mainly by the addition of nucleating agents^{6,8-12} or by the addition of plasticizers¹³⁻¹⁵. The use of plasticizers can also be employed to overcome the intrinsic brittleness of PLA by providing an increase in its ductile behaviour. An effort of employing plasticizers without compromising PLA biodegradability has been made. The use of modified vegetable oils (MVO) can be considered as an alternative to petroleum-based plasticizers. These MVOs can be modified in some ways, such as epoxidized, maleinized, acrylated, hydroxylated, etc.) to improve adhesion to the polymeric matrix. The epoxidized MVOs form is already commercially available¹⁶. Contrarily, commercial availability of

PLA grafted MA (MAgPLA) is not existent. However, there are several ways to functionalize PLA with MA, being melt functionalization the most applied one¹⁸.

Two studies reported by Balart and co-workers showed the effect of addition 0-10 wt% content of cottonseed oil in two distinct forms – maleinized¹⁶ and epoxidized¹⁷. As can be seen from Table 3.1, an increase on PLA elongation at break values was detected. In the case of PLA formulation with 10 wt% of ECSO, it showed an increase in elongation at break of more than 1100%, while the addition of 7.5% of MCSO to PLA resulted in an increase of 292%.

Table 3.1| Elongation at break values of PLA in the absence and the presence of MVO. ECSO, Epoxidized Cottonseed Oil; MCSO, Maleinized Cottonseed Oil (Adapted from ^{16,17})

MVO structure	MVO (%wt)	Elongation at break (%)
ECSO	0	≈9
	10	≈111
MCSO	0	≈4
	7.5	≈15

Other MVOs were already investigated to optimize the ductile properties of PLA, namely linseed oil¹⁹, soybean oil²⁰ and palm oil²¹. When it comes to the use of PLA in mass production, other major drawback is its low thermal stability. For industrial processes, as injection moulding, thermoforming or extrusion, it is necessary that the material has the adequate thermal stability in order to prevent degradation. PLA thermal degradation can occur when the material is held above its melting temperature and it is associated with the decrease of molecular weight. Mechanisms of thermal degradation can be considered as intra or inter-molecular transesterification, hydrolysis, lactide reformation and oxidative main-chain scission reactions^{4,22}. From these reactions, by-products as acrylic acid, carbon oxide and acetaldehyde can be formed. This degradation affects PLA mechanical and thermal behaviour, once they are closely related to the molecular weight. In Table 3.2 is presented an overview of some PLA properties.

The biocompatibility inherent to PLA makes it attractable to biomedical (medical implants) and packaging applications allied to its mechanical performance. Other examples of applications are plastic bags, bottles, sheet/film products, homeware and clothing.

PHA is a designation of polyesters that are produced from bacterial fermentation of sugars or lipids. These polyesters act as carbon and energy storages in bacteria, where the most common bacteria are *Ralstonia Eutropha*, *Bacillus Megaterium* and *Azotobacterchroococum*²³. Over 100 monomers can be considered and the mechanical properties of PHA can be tailored according to copolymers composition.

Table 3.2| Overview of some PLA properties. (Adapted from CES Selector 2018)

General properties	
Price (€/kg)	2.51 – 3.07
Density (kg/m ³)	1.24E3 – 1.27E3
Mechanical properties	
Young's modulus (GPa)	3.3 – 3.6
Tensile strength (MPa)	47 – 70
Elongation (% strain)	2.5 – 6
Hardness – Shore D	79 – 83
Fatigue strength at 10 ⁷ cycles (MPa)	22.2 – 27.7
Fracture toughness (MPa·m ^{1/2})	3.34 – 4.79
Thermal properties	
Glass transition temperature (°C)	52 – 60
Melting temperature (°C)	145 – 175
Others	
Humidity absorption (%) (50% air humidity)	0.29 – 0.32

The most common monomers used are poly(3-hydroxyalkanoates) (P3HB), poly(4-hydroxybutyrate) (P4HB) and poly(3-hydroxybutyrate-co-3-hydroxyvalerate) (PHBV)³.

The most common commercially available PHA forms are P3HB and P4HB. The P3HB form is brittle than P4BV, and the last form improves the mechanical resistance for the copolymer PHBV. Like PLA, the biodegradability and the physical properties of PHA similar to those of synthetic plastics (Table 3.3), makes PHA an attractive alternative to petroleum-based polymers.

Table 3.3| Overview of some PHA properties. (Adapted from CES Selector 2018)

General properties	
Price (€/kg)	5.39 – 6.29
Density (kg/m ³)	1.23E3 – 1.25E3
Mechanical properties	
Young's modulus (GPa)	3.5 – 4
Tensile strength (MPa)	35 – 40
Elongation (% strain)	6 – 35
Hardness – Shore D	74 – 96
Fatigue strength at 10 ⁷ cycles (MPa)	12 – 17
Fracture toughness (MPa·m ^{1/2})	0.7 – 1.2
Thermal properties	
Glass transition temperature (°C)	12 – 15
Melting temperature (°C)	171 – 182

However, the price of PHA is the main drawback when it comes to economic performance. PHA can be blow-moulded, injection moulded or extruded, where the major applications are packaging, containers and bottles. Currently, the use of PHA is increasing in niche applications, such as medical²⁴ and agricultural²⁵ sectors.

As referred above, the PLA characteristic brittleness limits its use in an industrial scale, in particular for applications which involve extrusion processes. Two main strategies can be applied to reduce this brittleness, namely by the copolymerization of lactic acid with other monomers, such as ϵ -caprolactone or by addition of other polymers and/or fillers²⁶. Besides the addition of plasticizers to PLA, as presented earlier, other common approaches are the blending of PLA with other materials, namely rubbers²⁷, synthetic resins^{26,28}, starches²⁹, biodegradable resins³⁰ and fillers^{12,31,32}. Many of these blends with PLA are immiscible or partially miscible and need compatibilizers to improve their compatibility and dispersion within PLA matrix. Among biodegradable resins, PHA can be used as PLA modifier to improve its ductility and flexibility. In addition, PHA has a similar chemical structure to PLA and the preparation of these PLA/PHA blends can result in performance improvements without compromising biodegradability and the need of using compatibilizers³³. However, the miscibility of PLA and PHA have been further investigated and it depends on composition and blend preparation method. The molar mass (M_n) of both components affect their miscibility, in a way that PHA with low M_n ($M_n < 18000$ g/mol) is miscible with poly-L-lactic acid, while PHA with higher M_n is not³³. Loureiro, N. C. *et al.*²³ analysed the dispersion of PHA into PLA in a composition range of 0-100%. From SEM analyses, they conclude that the miscibility of PHA/PLA blends increased with the incorporation of PHA for values of PHA wt% higher than 50%. Moreover, the presence of PHA in a PLA matrix reveals an enhancement on the mechanical behaviour based on the increase on tensile and impact properties^{26,34}. On the other hand, the blend preparation method influences PLA-PHA compatibility, in which melt blended samples present higher compatibility than blends prepared by solvent casting at room temperature³³.

The development of low-cost biopolymers as alternative to cheaper petrochemical plastics has been explored. Starch is a low-cost biopolymer, wide availability and total compostability without toxic residues. Maize (corn), wheat, potato and rice are examples of starch-rich vegetables. Starch granules can be found mainly in seeds, roots and tubers. Amylose, a lightly branched carbohydrate, and amylopectin, a highly multiple-branched polymer, are the major components of starch. The ratio of each component is related to the botanical resource and can vary from 1% to 70% of amylose content³⁵. The ability to form a film, the mechanical and barrier properties, and also the conditions on how starch is converted into TPS are dependent on amylose/amylopectin ratio^{36,37}. For instance, higher amylose content results in a TPS with lower crystallinity degree and it is preferred for the preparation of TPS due to its better flow properties. Native starch can be converted into a thermoplastic-like material by conventional processing techniques, such as extrusion, through temperature and shear action, and the presence of plasticizers. Water and glycerol are the major used plasticizers, but the addition of other plasticizers can be found in literature³⁷⁻³⁹. During thermal processing of TPS, starch granules suffers several physical and chemical changes, such as water

diffusion, granules expansion, gelatinization, melting and crystallization³⁹. The plasticization with excess of water forms “gel-balls” with a Newtonian-like behaviour; while, plasticizing with excess of glycerol results in an unfolded structure, exhibiting a shear-thinning behaviour similar to a thermoplastic⁴⁰.

The processing of native starch into TPS has a limited range of applications owing to its inherent brittleness, hydrophilic and retrogradation capacity. Retrogradation occurs from cooling after cooking the starch and starch molecules realign in a crystalline structure^{38,39}. In order to overcome these unfavourable properties, starches are blended with complementary biodegradable hydrophobic polymers, such as PBS, polybutylene adipate-co-terephthalate and polybutylene succinate adipate⁴¹.

The addition of compatibilizer agents is needed to promote the linkage between the polar part of starch and the nonpolar part of hydrophobic polymers. Compatibilizer agents based on MA are the most applied by melt reactive functionalization⁴². The addition of bio-based materials to mend the processing drawbacks of TPS can also be found in literature. A study reported by Dang, K. M. *et al.*⁴³ explored the addition of chitosan to TPS. The presence of chitosan resulted in a reduction of water absorption and extensibility, and subsequent reduced surface stickiness. It increased tensile strength, melt flow ability for extrusion applications and thermal stability. Another study focused on the study of applying rosin, a solid form of resin from pines, as reinforcement agent and processing aid of TPS/Polyvinyl alcohol (PVA) blends⁴⁴. In this case, an increase on the tensile strength, as well as on the elongation at break, closer to values of synthetic polymers used in packaging applications was found. Nowadays, for the production of biodegradable packaging is common the use of TPS/PVA blends. The selection of PVA is based on its optical properties, chemical resistance and for being a non-toxic material. In Table 3.4 some properties of commercial plasticized TPS with PVA from Novamont® are listed.

Table 3.4| Overview of some TPS (Master-Bi®) properties. (Adapted from CES Selector 2018)

General properties	
Price (€/kg)	1.86 – 4.23
Density (kg/m ³)	1.26E3 – 1.28E3
Mechanical properties	
Young’s modulus (GPa)	0.2 – 1.5
Tensile strength (MPa)	16 – 22
Elongation (% strain)	10 – 80
Hardness – Shore D	58 – 64
Fatigue strength at 10 ⁷ cycles (MPa)	5.6 – 7.7
Fracture toughness (MPa·m ^{1/2})	0.8 – 1.3
Thermal properties	
Glass transition temperature (°C)	10 – 20
Melting temperature (°C)	136 – 180
Others	
Humidity absorption (%) (50% air humidity)	6 – 20

Besides packaging solutions, TPS can be processed into various products such as sheets/films, foams⁴⁵, and other specific shapes by extrusion, injection moulding, compression moulding.

3.1.2 Additive Manufacturing

AM involves a set of technologies that produce 3D parts using a layer-by-layer approach, based on computer aided design model⁴⁶. The trivialization of the expression “*3D Printing*” facilitated the dissemination of AM technologies. Looking back to early 1980s, when AM techniques started as rapid prototyping solutions, nowadays, AM has reached the landmark of actually manufacture products. In fact, according to the 3D Hubs report⁴⁷, AM is now adopted by the early majority for serial productions, in industrial sectors such as automotive, aerospace, medical, sports, and others. Further, a 24% average annual growth is forecasted for the AM market in the next 5 years. Costs are still a governing factor when comparing conventional and additive techniques. The most cost-effective solutions are conventional methods, in which as the number of parts' cost increases the cost per part decreases. Nowadays, in AM, the cost per part is independent on the number of parts printed⁴⁸. In addition, the equipment's investment for the majority of AM technologies remains a limitation for a wider usage, as well as restrictions on materials availability.

Main advantages of AM are (i) the production of highly customized and also, complex parts without tooling, (ii) faster product development and manufacturing resulting in a quicker time-to-market and (iii) on-demand manufacturing by adapting to the market needs⁴⁹. Currently, AM technologies are divided into seven categories, according to the processing principle and, consequently, the addition and adhesion mechanisms of the different layers. In Table 3.5, it is presented the most used AM technologies, at a commercial level, identifying the materials normally used, some features and main advantages and disadvantages. A detailed explanation of all AM techniques is out of the scope of the present thesis.

In 1987, Stereolithography (SLA) technique emerged, considered the pioneer technology in rapid prototyping processes. This technique is characterized by the processing of liquid-based photo-curable resins of polymeric, ceramic or composite materials^{49,50}. More recently, Digital Light Processing (DLP) technology has arose, in which the operating principle is similar to SLA, differing only in the light source used. This aspect allows for shorter manufacturing times by DLP technology compared to SLA technology, since an entire light layer is projected, each time, in contrast to the ultraviolet (UV) light beam used in SLA. SLA technology has been used in the production of prototypes for conceptual and geometric validation of products in several sectors, such as product development, dental, jewellery and entertainment, among others^{48,51}. Lately, SLA related patents expired and led to the development of new SLA-based technologies. One example is the Continuous Liquid Interface Production (CLIP) technology, developed by Carbon3D, Inc. CLIP is a similar process to the SLA, but besides using a UV beam to crosslink the resin, it also uses a controlled

oxygen flow, in order to inhibit hardening in areas where the process is unnecessary. This process achieves very short manufacturing times, around 25 to 100 times faster, compared to SLA⁵².

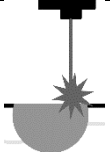
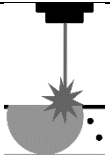
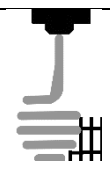

Since the development of SLA, other AM techniques have appeared on the market, expanding the range of material classes that could be processed⁵³. Selective Laser Sintering (SLS) processes a variety of powder materials and it consists on the use of a laser beam, as energy source. This laser beam (CO₂ type) focuses on the powder surface, previously spread and compacted, which partially and selectively melts powder particles, promoting the adhesion of the different powder layers that constitutes the model⁴⁹. The models obtained have some porosity, but their mechanical properties are superior to those obtained by SLA⁵³. SLS disadvantages are related to surface finish and, generally, has lower dimensional accuracy than that achieved by SLA⁵³.

SLS technology has been used in the production of injection moulds for pre-series tests, in the production of injection mould inserts with complex geometries for cooling optimization, in the production of prototypes that allow conceptual and geometric validation and in tissue engineering for the production of bone implants^{50,54,55}.

In addition, the robocasting technology, a paste extrusion-based technology, has been intensely studied in distinct areas as tissue engineering⁵⁶ and tooling⁵⁷ and, already applied in ceramic industry⁵⁸.

However, it is essential to bear in mind the technical barriers that yet need to be overcome in AM, especially related to equipment solutions available on the market. Examples of these barriers are: high acquisition and maintenance costs, low productivity, product resolutions, dimension limitations, software that does not maximize the potential of technologies and the difficulties inherent of low availability in qualified technical personnel⁵⁹. It is also important to emphasize the urgency on the development of standards to characterize all the printed products. Currently, printed products are characterized using the same standards as those applied to products obtained by conventional methods. At this moment, there is only a standard concerning the mechanical testing of metal materials obtained by AM (ASTM F3122-14).

Table 3.5| Most used AM technologies in the industry (Adapted by from ^{48,50,53}).

AM Technologies	Materials	Layer thickness (µm)	Dimensional tolerance	Build size (mm x mm x mm)	Advantages	Disadvantages
 <p>SLA</p>	<ul style="list-style-type: none"> • Polymers • Ceramics • Composites 	<ul style="list-style-type: none"> • 25 – 100 	<ul style="list-style-type: none"> • ±0.5% (lower limit: ±0.15 mm) 	<ul style="list-style-type: none"> • X < 2100 • Y < 700 • Z < 800 	<ul style="list-style-type: none"> • High resolution and accuracy • Smooth surface finish • Fine feature details 	<ul style="list-style-type: none"> • Limited to photopolymers only • Slow printing process • Brittle parts (not indicated for mechanical parts) • Precursors high cost • Support structures required • Post-processing needed
 <p>SLS</p>	<ul style="list-style-type: none"> • Metals • Ceramics • Polymers • Composites • Hybrids 	<ul style="list-style-type: none"> • 100 – 120 	<ul style="list-style-type: none"> • ±0.3% (lower limit: ±0.3 mm) 	<ul style="list-style-type: none"> • X < 200 – 300 • Y < 200 – 300 • Z < 200 - 350 	<ul style="list-style-type: none"> • Large range of material options • Powder bed acts as support material • Functional parts, good mechanical properties 	<ul style="list-style-type: none"> • Parts finish depends on particles powder size • Relatively slow printing process • High power required (laser source) • Expensive parts • Post-processing needed
 <p>FFF</p>	<ul style="list-style-type: none"> • Polymers • Composites 	<ul style="list-style-type: none"> • 50 – 400 	<ul style="list-style-type: none"> • ±0.5% (lower limit: ±0.5 mm) 	<ul style="list-style-type: none"> • X < 900 • Y < 600 • Z < 900 	<ul style="list-style-type: none"> • Widespread use • Low-cost • Scalable • Functional parts (non-commercial) 	<ul style="list-style-type: none"> • Anisotropy • Print layers visible on the surface • Unable for small details • Support structures required • May require post-processing
 <p>3DP</p>	<ul style="list-style-type: none"> • Ceramics • Polymers • Composites • Metals • Hybrids 	<ul style="list-style-type: none"> • 35 – 400 	<ul style="list-style-type: none"> • ±0.2 mm 	<ul style="list-style-type: none"> • X < 4000 • Y < 2000 • Z < 1000 	<ul style="list-style-type: none"> • Powder bed acts as support material • Large build volumes • Relatively low-cost • High print speed • Functional metal parts 	<ul style="list-style-type: none"> • Fragile parts • Post-processing needed

3.1.2.1 Fused Filament Fabrication

The designation of the FFF technology resulted, in part, from the patents expiration and from the development of alternative extrusion systems, based on the technology of Fused Deposition Modelling. FFF is the most affordable AM technology with a widespread use, fostered by the development of open-source printers. It is categorized as a material extrusion technology that consists on the extrusion of thermoplastic materials, in filament form⁴⁹ (thickness of 1.75 and 3.0 mm are most common) (Figure 3.2(a)).

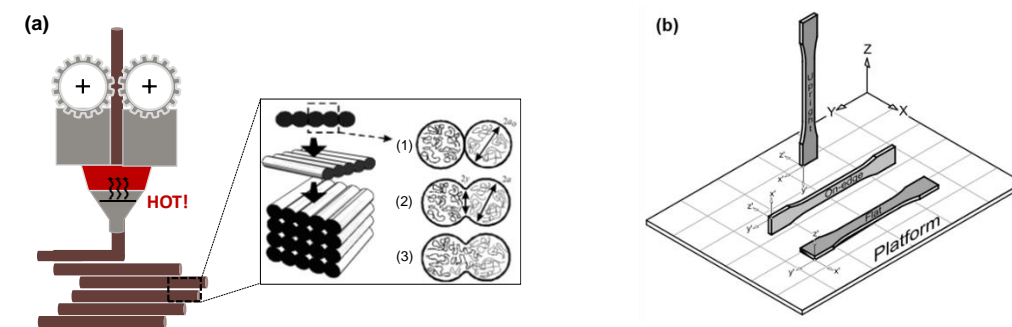


Figure 3.2| (a) FFF scheme with an illustration of bond formation mechanism: (1) surface contact; (2) neck formation and (3) diffusion (Adapted from ⁶⁰); **(b)** printing orientations⁶¹.

Thermoplastic filaments are heated to a temperature slightly higher than T_m to ensure the adhesion between the various layers⁵⁰. The extruded material is deposited on a build platform, which may or may not be heated. A heated platform will reduce the temperature gradient and, consequently, it will result in parts without or minimum warpage and with less stress concentrations^{48,49}. For parts with complex geometries it is necessary to use support structures. Printers with one extrusion head, support structures are printed with the same material as the part; while, printers with double or more extrusion heads, the support structure material is different from the printed part. In these cases, PVA or PLA are usually used as support material⁴⁸. Main disadvantages of FFF technology are: anisotropy, porosity and, layers adhesion and resolution of the printed parts^{50,62} (Table 3.5). In fact, the anisotropy acquired during printing, which is directly related to layer thickness, impacts negatively the mechanical behaviour of the printed parts. Printing parameters also influence the mechanical behaviour, such as raster angle, air gap between layers, filament orientation and build direction^{61,63}. According to Letcher, T. *et al.*⁶⁴, printed PLA exhibited higher tensile strength for a raster angle of 45°. In addition, a study reported by Chacón, J. M. *et al.*⁶¹ showed that samples produced with flat and on-edge orientations (Figure 3.2 (b)) had the highest tensile strength and stiffness values.

Significant efforts have been done to develop a wide range of filament solutions, from low-cost filaments for prototyping / general applications to high-cost filaments for high-tech applications ^{65–67}. In Figure 3.3, it is illustrated a schematic representation of the thermoplastic based materials developed for FFF systems, divided into single materials, composites and blends.

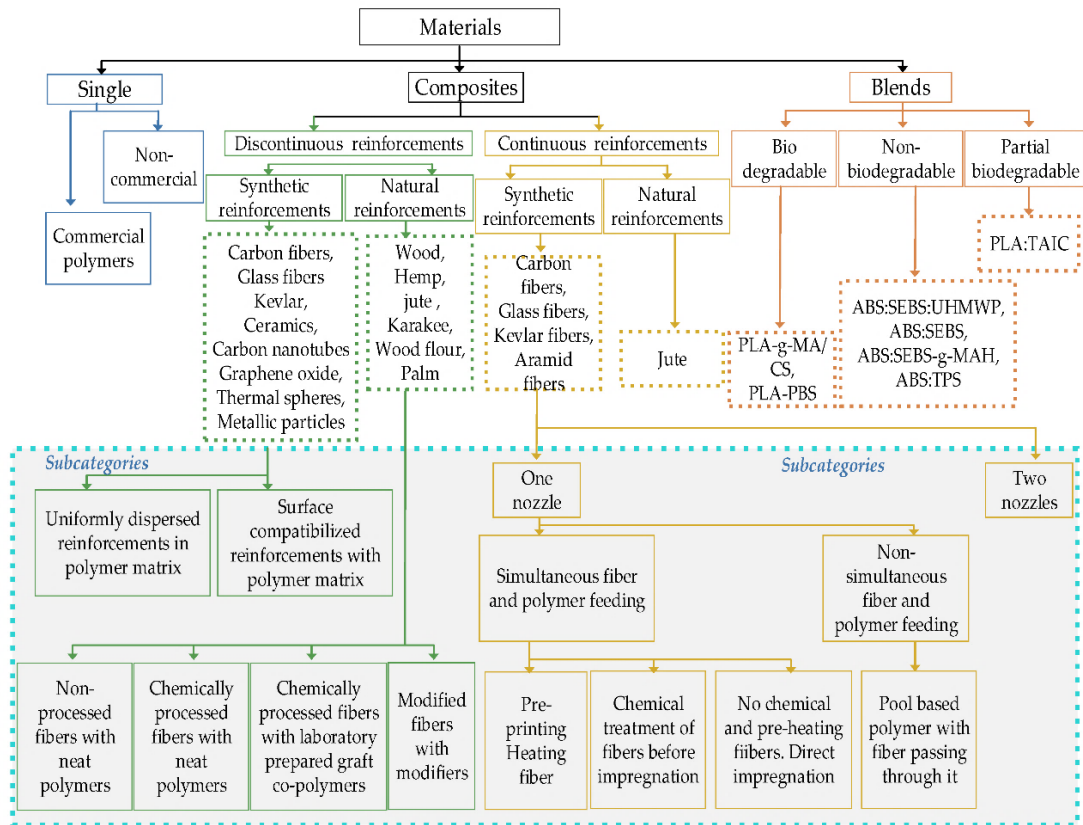


Figure 3.3/ Materials for FFF⁶².

It is important to note that materials need to possess adequate thermal and rheological properties in order to be easily processed by FFF. Most relevant properties are T_m , T_g , MFI below 6g/10 min, shear thinning behaviour induced by MWD and long-chain branching⁵⁰. Some studies exploring the development of cork or wood-based 3D printing filaments are found on the literature^{67–73}. Kariz, M. *et al.*⁶⁷ evaluated the effect of wood powder content ranging from 0% to 50% (w/w) on the properties of six filaments using PLA as matrix. They concluded that adding more than 10% (w/w) of wood resulted in a decrease of 45% on tensile strength, when compared to pure PLA filaments. Also, as the wood content increases, the surface finishing of printed parts becomes rougher, combined with the presence of voids and wood particle clusters.

Given the variety of thermoplastic materials processed by FFF systems, it can be found applications in distinct areas, such as: product development through the manufacture of prototypes; aerospace; components manufacture; electronics; conductive materials and sensors manufacture, among others^{65,66}. In addition, new developments have emerged regarding FFF technology. These developments focus on 5-axis printing, the insertion of FFF technology in hybrid manufacturing processes, polymer granulate as feeding system and, direct deposition of filaments on substrates⁷⁴.

Most scientific publications report studies of commercial filament solutions when compared to studies of the development of new filament solutions. This tendency reinforces the exigency on the processing requirements and the engineering involved on the filament manufacturing process.

3.1.2.2 3D Printing

The designation of 3DP technology comes from the similarity with the inkjet printing process applied to two-dimensional paper prints. 3DP, a binder jetting technology, is characterized by the use of powder materials where a binding agent is deposited, by a print head, on previously prepared powder layers⁴⁹ (Figure 3.4).

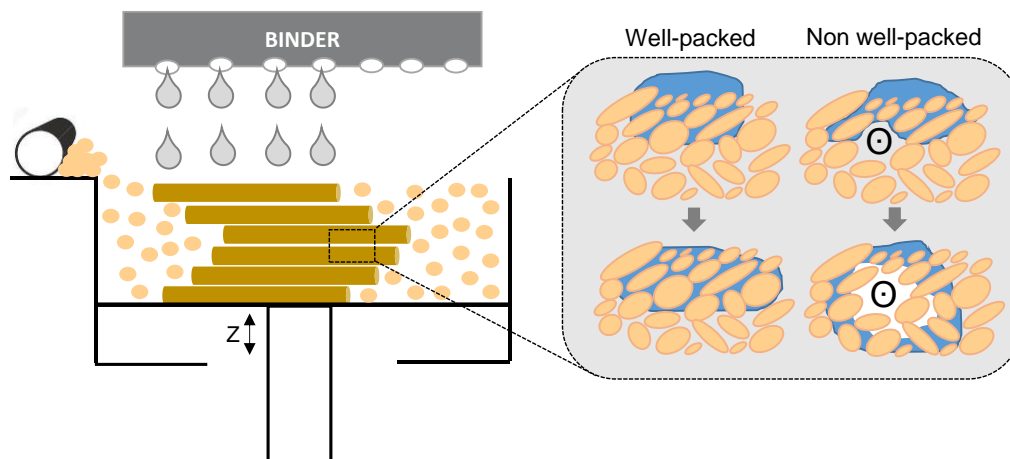


Figure 3.4| 3DP scheme with an illustration of a proposed droplet penetration behavior within well-packed and heterogeneously distributed powder beds (adapted from⁷⁵). \odot - macro-voids

Materials such as ceramics, polymers, composites, metals and hybrids can be processed by 3DP. This process does not require support structures which increases the geometric freedom of the produced parts. The resolution of 3DP parts (typically 100 μm) is dependent on binder type, on powder size and granulometric distribution, on particles geometry, on the precision of binder droplets deposition and on the interaction between binder and particles⁷⁵.

Water-based binders are normally used in ceramic materials, given their hydrophilic nature. However, for the processing of other type of materials, binders containing polyvinyl butyral, polyacrylic acid, polysiloxanes and photo-curable resins⁷⁵⁻⁷⁸ are considered. Typically, these binder solutions contain resins, which their organic components can dry and damage the print head. An alternative solution to liquid binders is the use of solid binders, or additives, which are mixed together with the powder material. Examples of these additives found in literature are maltodextrin, PVA, starch, among others^{75,79}, being PVA the most studied one.

Powders with particle sizes varying from 0.2 to 200 μm are usually used, where an ideal particle size has not been yet defined. Fine powders ($\leq 20 \mu\text{m}$) exhibit lower flowability when compared to powders with particle sizes higher than 20 μm ^{75,76}. The inter-particle forces presented in fine powders, mainly van der Waals forces, causes them to easily agglomerate. This effect will lead to the formation of a large number of macro-voids, which it will compromise the powders wettability (Figure 3.4). Contrarily, improved wettability happens when binder droplets flow throughout micro-voids by capillary forces⁷⁵. Although, fine powders exhibit lower flowability and wettability, printed

parts present improved mechanical behaviour and densification after sintering⁷⁶. In this sense, bimodal or multimodal granulometric powder distributions are usually applied to overcome these challenges. Studies have demonstrated that higher packing density is obtained with the presence of 20-30% (v/v) of fine powder^{75,76,80}. Mostafaei, A. *et al.*⁸⁰ reported that alloy 625 powders with a granulometric distribution of 16–63 μm revealed higher green density, when compared to powders with narrow distributions (16–25 μm and 53–63 μm). Ceramic commercial powders present a bimodal granulometric powder distribution varying from 20 to 100 μm , with an average powder particle size of $\approx 52 \mu\text{m}$.

Besides particle size, its geometry also plays an important role to obtain parts with full densification. Parab, N. D. *et al.*⁸¹, using X-ray imaging, reported the effect of the relationship between binder deposition and geometry of powder particles. They concluded that, particles with irregular geometry, compared to particles with spherical geometry, showed a greater interaction with binder. The higher wettability of irregular shape particles is due to the increased surface contact area of flat faces with each other and with binder, while spherical particles only have small contact points^{75,81}. A higher powder wettability will lead to the production of more cohesive parts, with greater dimensional stability.

As a consequence of the parameters presented above, 3DP presents some limitations related to parts surface finishing and porosity and, also to the fragility of green parts. It will limit the dedusting operations, which are usually hampered by the intricate shapes that these parts can present. In the majority of the cases, it is needed post-processing phases to densify green parts. Usually, it can be applied heat treatments, impregnation with resins, adhesive agents, or others^{50,76,80,82}. Very recently, some studies have appeared related to 3DP processing of organic natural materials or residues of renewable materials from biological origins^{82–84}. For example, studies for 3DP low-calorie foods using cellulose powders and xanthan gum as binder⁸³.

Given the variety of materials processed by 3DP, it can be found applications in distinct areas, such as: tissue engineering (porous/dense implants or drug release products); sand moulds for casting; product development; functional parts with complex geometries; ceramic sculptures or decorating pieces, among other^{48,50,85,86}.

References

1. Tábi, T., Sajó, I. E., Szabó, F., Luyt, A. S. & Kovács, J. G. Crystalline structure of annealed polylactic acid and its relation to processing. *eXPRESS Polym. Lett.* 4, 659–668 (2010).
2. Zhang, J. *et al.* High-pressure crystallization of poly(lactic acid) with and without N₂ atmosphere protection. *J. Mater. Sci.* 48, 7374–7383 (2013).
3. Greene, J. P. *Sustainable Plastics: Environmental Assessments of Biobased, Biodegradable, and Recycled Plastics.* (John Wiley & Sons, Inc., 2014).
4. Garlotta, D. A Literature Review of Poly(Lactic Acid). *J. Polym. Environ.* 9, 63–84 (2001).
5. Aliotta, L. *et al.* Effect of nucleating agents on crystallinity and properties of poly (lactic acid) (PLA). *Eur. Polym. J.* 93, 822–832 (2017).

6. Nofar, M., Zhu, W., Park, C. B. & Randall, J. Crystallization Kinetics of Linear and Long-Chain-Branched Polylactide. *Ind. Eng. Chem. Res.* 50, 13789–13798 (2011).
7. As'habi, L. et al. Non-isothermal crystallization behavior of PLA/LLDPE/nanoclay hybrid: Synergistic role of LLDPE and clay. *Thermochim. Acta* 565, 102–113 (2013).
8. Li, C. & Dou, Q. Non-isothermal crystallization kinetics and spherulitic morphology of nucleated poly(lactic acid): Effect of dilithium cis-4-cyclohexene-1,2-dicarboxylate as a novel and efficient nucleating agent. *Polym. Adv. Technol.* 26, 376–384 (2015).
9. Ke, T. & Sun, X. Melting behavior and crystallization kinetics of starch and poly(lactic acid) composites. *J. Appl. Polym. Sci.* 89, 1203–1210 (2003).
10. Qiu, Z. & Li, Z. Effect of Orotic Acid on the Crystallization Kinetics and Morphology of Biodegradable Poly(l-lactide) as an Efficient Nucleating Agent. *Ind. Eng. Chem. Res.* 50, 12299–12303 (2011).
11. Han, Q. et al. Nonisothermal crystallization kinetics of biodegradable poly(lactic acid)/zinc phenylphosphonate composites. *J. Compos. Mater.* 48, 2737–2746 (2014).
12. Koutsomitopoulou, A. F., Bénézet, J. C., Bergeret, A. & Papanicolaou, G. C. Preparation and characterization of olive pit powder as a filler to PLA-matrix bio-composites. *Powder Technol.* 255, 10–16 (2014).
13. Xiao, H., Yang, L., Ren, X., Jiang, T. & Yeh, J. T. Kinetics and crystal structure of poly(lactic acid) crystallized nonisothermally: Effect of plasticizer and nucleating agent. *Polym. Compos.* 31, 2057–2068 (2010).
14. Kulinski, Z. & Piorkowska, E. Crystallization, structure and properties of plasticized poly(l-lactide). *Polymer (Guildf)*. 46, 10290–10300 (2005).
15. Li, M., Hu, D., Wang, Y. & Shen, C. Nonisothermal crystallization kinetics of poly(lactic acid) formulations comprising talc with poly(ethylene glycol). *Polym. Eng. Sci.* 50, 2298–2305 (2010).
16. Carbonell-Verdu, A. et al. PLA films with improved flexibility properties by using maleinized cottonseed oil. *Eur. Polym. J.* 91, 248–259 (2017).
17. Carbonell-Verdu, A., Samper, M. D., Garcia-Garcia, D., Sanchez-Nacher, L. & Balart, R. Plasticization effect of epoxidized cottonseed oil (ECSO) on poly(lactic acid). *Ind. Crops Prod.* 104, 278–286 (2017).
18. González-López, M. E., Robledo-Ortíz, J. R., Manríquez-González, R., Silva-Guzmán, J. A. & Pérez-Fonseca, A. A. Polylactic acid functionalization with maleic anhydride and its use as coupling agent in natural fiber biocomposites: a review. *Compos. Interfaces* 25, 515–538 (2018).
19. Ferri, J. M., Garcia-Garcia, D., Sánchez-Nacher, L., Fenollar, O. & Balart, R. The effect of maleinized linseed oil (MLO) on mechanical performance of poly(lactic acid)-thermoplastic starch (PLA-TPS) blends. *Carbohydr. Polym.* 147, 60–68 (2016).
20. Quiles-Carrillo, L., Duart, S., Montanes, N., Torres-Giner, S. & Balart, R. Enhancement of the mechanical and thermal properties of injection-molded polylactide parts by the addition of acrylated epoxidized soybean oil. *Mater. Des.* 140, 54–63 (2018).
21. Chieng, B., Ibrahim, N., Then, Y. & Loo, Y. Epoxidized Vegetable Oils Plasticized Poly(lactic acid) Biocomposites: Mechanical, Thermal and Morphology Properties. *Molecules* 19, 16024–16038 (2014).
22. Berger, K. & Gregorova, A. Thermal stability of modified end-capped poly(lactic acid). *J. Appl. Polym. Sci.* 131, 41105–41114 (2014).
23. Loureiro, N. C., Ghosh, S., Viana, J. C., Esteves, J. L. & Calçada Loureiro, N. Thermal Characterization of Polyhydroxyalkanoates and Poly(lactic acid) Blends Obtained by Injection Molding. *Polym. Plast. Technol. Eng.* 544, 350–356 (2015).
24. Grigore, M. E. et al. Methods of synthesis, properties and biomedical applications of polyhydroxyalkanoates: a review. *J. Biomater. Sci. Polym. Ed.* 30, 695–712 (2019).
25. Cinelli, P. et al. Processability and Degradability of PHA-Based Composites in Terrestrial Environments. *Int. J. Mol. Sci.* 20, 284–298 (2019).
26. Mat Taib, R., Ghaleb, Z. A. & Mohd Ishak, Z. A. Thermal, Mechanical, and Morphological Properties of Polylactic Acid Toughened with an Impact Modifier. *J. Appl. Polym. Sci.* 123, 2715–2725 (2012).

27. Hao, Y. et al. Thermal and mechanical properties of polylactide toughened with a butyl acrylate-ethyl acrylate-glycidyl methacrylate copolymer. *Chinese J. Polym. Sci.* 31, 1519–1527 (2013).
28. Hong, H. et al. A Novel Composite Coupled Hardness with Flexibility—Polylactic Acid Toughen with Thermoplastic Polyurethane. *J. Appl. Polym. Sci.* 121, 855–861 (2011).
29. Müller, P. et al. Interactions, structure and properties in PLA/plasticized starch blends. *Polymer (Guildf)*. 103, 9–18 (2016).
30. Sarazin, P., Gang, L., J.Orts, W. & Favis, B. D. Binary and ternary blends of polylactide, polycaprolactone and thermoplastic starch. *Polymer (Guildf)*. 49, 599–609 (2008).
31. Wu, D. et al. Nonisothermal cold crystallization behavior and kinetics of polylactide/clay nanocomposites. *J. Polym. Sci. Part B Polym. Phys.* 45, 1100–1113 (2007).
32. Jain, S., Misra, M., Mohanty, A. K. & Ghosh, A. K. Thermal, Mechanical and Rheological Behavior of Poly(lactic acid)/Talc Composites. *J. Polym. Environ.* 20, 1027–1037 (2012).
33. Tri, P. N., Domenek, S., Guinault, A. & Sollogoub, C. Crystallization behavior of poly(lactide)/poly(β -hydroxybutyrate)/talc composites. *J. Appl. Polym. Sci.* 129, 3355–3365 (2013).
34. Zhang, M. & Thomas, N. L. Blending Polylactic Acid with Polyhydroxybutyrate: The Effect on Thermal, Mechanical, and Biodegradation Properties. *Adv. Polym. Technol.* 30, 67–79 (2011).
35. Xie, F., Halley, P. J. & Avérous, L. Rheology to understand and optimize processibility, structures and properties of starch polymeric materials. *Prog. Polym. Sci.* 37, 595–623 (2012).
36. Mendes, J. F. et al. Biodegradable polymer blends based on corn starch and thermoplastic chitosan processed by extrusion. *Carbohydr. Polym.* 137, 452–458 (2016).
37. Shanks, R. & Kong, I. Thermoplastic Starch. in *Thermoplastic Elastomers* (ed. El-Sonbati, A.) 416 (InTech, 2012).
38. Niranjana Prabhu, T. & Prashantha, K. A review on present status and future challenges of starch based polymer films and their composites in food packaging applications. *Polym. Compos.* 39, 2499–2522 (2018).
39. Khan, B., Bilal Khan Niazi, M., Samin, G. & Jahan, Z. Thermoplastic Starch: A Possible Biodegradable Food Packaging Material-A Review. *J. Food Process Eng.* 40, 1–17 (2017).
40. Tajuddin, S., Xie, F., Nicholson, T. M., Liu, P. & Halley, P. J. Rheological properties of thermoplastic starch studied by multipass rheometer. *Carbohydr. Polym.* 83, 914–919 (2011).
41. Zhang, S., He, Y., Yin, Y. & Jiang, G. Fabrication of innovative thermoplastic starch bio-elastomer to achieve high toughness poly(butylene succinate) composites. *Carbohydr. Polym.* 206, 827–836 (2019).
42. Fourati, Y., Tarrés, Q., Mutjé, P. & Boufi, S. PBAT/thermoplastic starch blends: Effect of compatibilizers on the rheological, mechanical and morphological properties. *Carbohydr. Polym.* 199, 51–57 (2018).
43. Dang, K. M. & Yoksan, R. Development of thermoplastic starch blown film by incorporating plasticized chitosan. *Carbohydr. Polym.* 115, 575–581 (2015).
44. Domene-López, D., Guillén, M. M., Martín-Gullón, I., García-Quesada, J. C. & Montalbán, M. G. Study of the behavior of biodegradable starch/polyvinyl alcohol/rosin blends. *Carbohydr. Polym.* 202, 299–305 (2018).
45. Bergel, B. F., Dias Osorio, S., da Luz, L. M. & Santana, R. M. C. Effects of hydrophobized starches on thermoplastic starch foams made from potato starch. *Carbohydr. Polym.* 200, 106–114 (2018).
46. ISO / ASTM 52900 Additive manufacturing — General principles — Terminology. (2015).
47. 3D Hubs Manufacturing LLC. 3D Printing Trends 2020. Industry highlights and market trends (2020).
48. Redwood, B., Schöffner, F. & Garret, B. *The 3D Printing Handbook - Technologies, design and applications.* (3D Hubs B.V., 2017).
49. Gibson I, Rosen D, S. B. *Additive Manufacturing Technologies: 3D Printing, Rapid Prototyping, and Direct Digital Manufacturing.* (Springer, 2015).
50. Ligon, S. C., Liska, R., Stampfl, J., Gurr, M. & Mülhaupt, R. Polymers for 3D Printing and Customized Additive Manufacturing. *Chem. Rev.* 117, 10212–10290 (2017).

51. 3D Printing for Model Making & Entertainment. Available at: <https://formlabs.com/eu/industries/model-making-entertainment/>.
52. Tumbleston, J. R. et al. Continuous liquid interface of 3D objects. *Science* (80-.). 347, 1349–1352 (2015).
53. Tofail, S. A. M. et al. Additive manufacturing: scientific and technological challenges, market uptake and opportunities. *Mater. Today* 21, 22–37 (2018).
54. Ilyas, I., Taylor, C., Dalgarno, K. & Gosden, J. Design and manufacture of injection mould tool inserts produced using indirect SLS and machining processes. *Rapid Prototyp. J.* 16, 429–440 (2010).
55. Eosoly, S., Lohfeld, S. & Brabazon, D. Effect of Hydroxyapatite on Biodegradable Scaffolds Fabricated by SLS. *Key Eng. Mater.* 396–398, 659–662 (2008).
56. Patrício, S. G. et al. Freeform 3D printing using a continuous viscoelastic supporting matrix. *Biofabrication* 12, 1–7 (2020).
57. Zhang, X., Guo, Z., Chen, C. & Yang, W. Additive manufacturing of WC-20Co components by 3D gel-printing. *Int. J. Refract. Met. Hard Mater.* 70, 215–223 (2018).
58. CTCV - RoboCer3D. Available at: https://www.ctcv.pt/projdi_robocer3d.html.
59. Sciencentris - From Knowledge to Market. Relatório 1: Tecnologias de Produção; Moldes e Materiais. (2019).
60. Brenken, B., Barocio, E., Favalaro, A., Kunc, V. & Pipes, R. B. Fused filament fabrication of fiber-reinforced polymers: A review. *Addit. Manuf.* 21, 1–16 (2018).
61. Chacón, J. M., Caminero, M. A., García-Plaza, E. & Núñez, P. J. Additive manufacturing of PLA structures using fused deposition modelling: Effect of process parameters on mechanical properties and their optimal selection. *Mater. Des.* 124, 143–157 (2017).
62. Harris, M., Potgieter, J., Archer, R. & Arif, K. M. Effect of Material and Process Specific Factors on the Strength of Printed Parts in Fused Filament Fabrication: A Review of Recent Developments. *Materials (Basel)*. 12, 1664 (2019).
63. Dizon, J. R. C., Espera, A. H., Chen, Q. & Advincula, R. C. Mechanical characterization of 3D-printed polymers. *Addit. Manuf.* 20, 44–67 (2018).
64. Letcher, T. & Waytashek, M. Material Property Testing of 3D-Printed Specimen in PLA on an Entry-Level 3D Printer. in *Proceedings of the ASME 2014 International Mechanical Engineering Congress and Exposition. Volume 2A: Advanced Manufacturing (ASME, 2014)*.
65. Ansari, M. Q., Bortner, M. J. & Baird, D. G. Generation of Polyphenylene Sulfide Reinforced with a Thermotropic Liquid Crystalline Polymer for Application in Fused Filament Fabrication. *Addit. Manuf.* 29, 100814–100823 (2019).
66. Gnanasekarana, K. et al. 3D printing of CNT- and graphene-based conductive polymer nanocomposites by fused deposition modeling. *Appl. Mater. Today* 9, 21–29 (2017).
67. Kariz, M., Sernek, M., Obućina, M. & Kuzman, M. K. Effect of wood content in FDM filament on properties of 3D printed parts. *Mater. Today Commun.* 14, 135–140 (2018).
68. Cataldi, A., Rigotti, D., Nguyen, V. D. H. & Pegoretti, A. Polyvinyl alcohol reinforced with crystalline nanocellulose for 3D printing application. *Mater. Today Commun.* 15, 236–244 (2018).
69. F.Brites, C. Malça, F.Gaspar, J.F.Horta, M.C. Franco, S. Biscaia, A. M. Cork Plastic Composite Optimization for 3D Printing Applications. *Procedia Manuf.* 12, 156–165 (2017).
70. Gama, N., Ferreira, A. & Barros-Timmons, A. 3D printed cork/polyurethane composite foams. *Mater. Des.* 179, 107905–107914 (2019).
71. Winter, A. et al. Residual wood polymers facilitate compounding of microfibrillated cellulose with poly(lactic acid) for 3D printer filaments. *Philos. Trans. R. Soc. A Math. Phys. Eng. Sci.* 376, 1–9 (2018).
72. Tanase-Opedal, M., Espinosa, E., Rodríguez, A. & Chinga-Carrasco, G. Lignin: A Biopolymer from Forestry Biomass for Biocomposites and 3D Printing. *Materials (Basel)*. 12, 3006–3021 (2019).
73. Mazzanti, V., Malagutti, L. & Mollica, F. FDM 3D Printing of Polymers Containing Natural Fillers: A Review of their Mechanical Properties. *Polymers (Basel)*. 11, 1094–1196 (2019).
74. Pierson, H. A. & Chivukula, B. Process–Property Relationships for Fused Filament Fabrication on Preexisting Polymer Substrates. *J. Manuf. Sci. Eng.* 140, 084501–084507 (2018).

75. Lv, X., Ye, F., Cheng, L., Fan, S. & Liu, Y. Binder jetting of ceramics: Powders, binders, printing parameters, equipment, and post-treatment. *Ceram. Int.* 45, 12609–12624 (2019).
76. Ziaee, M. & Crane, N. B. Binder jetting: A review of process, materials, and methods. *Addit. Manuf.* 28, 781–801 (2019).
77. Lee, K. et al. Polymeric binder based on PAA and conductive PANI for high performance silicon-based anodes. *RSC Adv.* 6, 101622–101625 (2016).
78. Lee, W. et al. Strength and Processing Properties using a Photopolymer Resin in a Powder-based 3DP Process. in *SICE-ICASE International Joint Conference* 3674–3677 (IEEE, 2006).
79. Muniz, N. O., Vechietti, F. A. & dos Santos, L. A. L. Influence of several binders on the mechanical properties of alumina parts manufactured by 3D inkjet printing. *Mater. Res. Express* 6, 115341–115349 (2019).
80. Mostafaei, A., Rodriguez De Vecchis, P., Nettleship, I. & Chmielus, M. Effect of powder size distribution on densification and microstructural evolution of binder-jet 3D-printed alloy 625. *Mater. Des.* 162, 375–383 (2019).
81. Parab, N. D. et al. Real time observation of binder jetting printing process using high-speed X-ray imaging. *Sci. Rep.* 9, 2499–2509 (2019).
82. Zeidler, H. et al. 3D printing of biodegradable parts using renewable biobased materials. *Procedia Manuf.* 21, 117–124 (2018).
83. Holland, S., Tuck, C. & Foster, T. Selective recrystallization of cellulose composite powders and microstructure creation through 3D binder jetting. *Carbohydr. Polym.* 200, 229–238 (2018).
84. Xu, W. et al. Three-Dimensional Printing of Wood-Derived Biopolymers: A Review Focused on Biomedical Applications. *ACS Sustain. Chem. Eng.* 6, 5663–5680 (2018).
85. Coniglio, N., Sivarupan, T. & El Mansori, M. Investigation of process parameter effect on anisotropic properties of 3D printed sand molds. *Int. J. Adv. Manuf. Technol.* 94, 2175–2185 (2018).
86. Choi, J. H., Kang, E. T., Lee, J. W. & Kim, U. S. Materials and process development for manufacturing porcelain figures using a binder jetting 3D printer. *J. Ceram. Process. Res.* 16, 43–49 (2018).

3.2 Non-isothermal Cold Crystallization Kinetics of Cork-Polymer Biocomposites based on Polylactic Acid for Fused Filament Fabrication ^h

S. P. Magalhães da Silva^{1,2,3}, Mónica A. Silva⁴, José. M. Oliveira^{1,2,3}

¹ EMaRT Group – Emerging: Materials, Research, Technology

² School of Design, Management and Production Technologies, University of Aveiro, Estrada do Cercal, 449, Santiago de Riba-UI, 3720-509, Oliveira de Azeméis, Portugal

³ Aveiro Institute of Materials (CICECO), University of Aveiro, Campus Universitário de Santiago, 3810-193 Aveiro, Portugal

⁴ Centro de Ciência e Tecnologia Têxtil (2C2T), University of Minho, Campus de Azurém, 4800-058 Guimarães, Portugal

Correspondence to: Sara Magalhães da Silva (E-mail: sarapms@ua.pt)

ABSTRACT

Cork-polymer composites (CPC) based on polylactic acid (PLA) matrix were prepared for the development of filaments for fused filament fabrication (FFF). The non-isothermal cold crystallization behaviors of PLA and CPC were investigated by differential scanning calorimetry (DSC). Cold crystallization kinetic behaviors of PLA and CPC with 15 mass/% of cork powder residues at different heating rates (1.25, 2.5, 5 and 7.5 K min⁻¹) were studied. Results showed that cold crystallization temperature (T_{cc}) of PLA matrix decreased with the addition of cork. Crystallization kinetic behaviour was studied by Avrami and Tobin models. It was shown that cork powder surface act as a nucleating agent during non-isothermal cold crystallization, by accelerating the crystallization rate and, therefore, by reducing the half-time crystallization ($t_{1/2}$) values. Polarized optical microscopy (POM) and X-ray diffraction (XRD) were used to evaluate the crystalline structure of PLA and CPC. Kissinger and Friedman methods were employed to determine the crystallization activation energy (E_c).

KEYWORDS

Cork

Biocomposites

Thermoplastics

Differential Scanning Calorimetry (DSC)

Crystallization Kinetics

^h Magalhães da Silva, S. P., Silva, M., Oliveira J. M. Non-isothermal Cold Crystallization Kinetics of Cork-Polymer Biocomposites based on Polylactic Acid for Fused Filament Fabrication, *J. Therm. Anal. Calorim.* **2020** (DOI: 10.1007/s10973-020-10147-6).

The author had contributed to the planning and execution of thermal, morphological and XRD analyses, as well as on the discussion, interpretation and preparation of the manuscript. Mónica A. Silva contributed to the adequacy of Tobin model.

1. INTRODUCTION

Current concerns regarding environment and increasing awareness about sustainability are pushing forward the developing of new composite materials, which incorporate renewed materials. Cork is a reliable and sustainable raw material.

Cork is the outer bark of the cork oak tree *Quercus suber* L. and presents tiny hollow cells of hexagonal shape in closed-cell foam. Its main chemical composition is 33-50 % of suberin, 20-25 % of lignin; 12-20 % of polysaccharides and 14-18 % of extractives [1]. Portugal is the world's leading cork producer and its main application is the production of stoppers. From stoppers production, a considerable amount of cork residues are generated (≈ 30 mass/%) [2]. The incorporation of these residues into polymeric matrices can be a suitable solution for the development of new materials solutions tailoring the needs of different applications.

Poly(lactic acid) (PLA) is a biodegradable thermoplastic aliphatic polyester derived from renewable resources. It is a strong candidate to be used as polymeric matrix due to its biodegradability and chemical compatibility. Different synthesis routes for PLA polymerization can be applied and the most common one is the ring-opening lactide polymerization [3]. PLA stereochemical structure can be easily changed, depending on the amount of L- and D-isomers during polymerization [3]. This ratio of L- and D-isomers affects mechanical and thermal properties of the obtained PLA. Regarding thermal properties, PLA can be a semi-crystalline or an amorphous material depending on its stereo-chemical structure and thermal history [4]. Moreover, PLA has a particular thermal behaviour in a way that multiphase transitions, such as glass transition, chain relaxation, cold crystallization and melting are involved [5,6]. The main drawback of PLA for commercial applications is its low crystallization rate. Several modifications have been proposed to improve the crystallization rate, mainly by the addition of nucleating agents [5,7–11] or by the addition of plasticizers [12–14].

Additive manufacturing (AM) offers a set of techniques that opens a possibility of creating new products with a high level of design freedom. Fused Filament Fabrication (FFF), one of the AM techniques, is an extrusion-based process, in which a plastic filament is heated and selectively extruded via a nozzle layer by layer [15]. It is a disruptive technology on a constant growing market demanding for materials innovation. The combination of biodegradable polymer matrices with natural materials could be a sustainable solution for the development of new materials for AM. More specifically, considering the actual technological demand, cork-polymer composites (CPC) should be used to open new horizons in AM.

Cork-polymer composites (CPC) are a viable and a possible strategy for up-grading cork industrial residues based on sustainable development. The incorporation of lignocellulosic materials into polymeric matrices can bring several advantages. Some examples of these advantages are: biodegradability, low density and hardness, low cost, easy availability, high levels of filling, good relation between strength/mass, good insulation/noise absorption properties and non-toxicity [16,17]. Among other factors, CPC mechanical performance is influenced by the interaction polymer-filler and by the crystallization behaviour of the matrix in the presence of the filler. Natural fibers and processing

conditions can have effect on polymer crystallization behaviour. Oliveira, J. M. *et al* [18,19] showed that cork acted as a nucleating agent in a polypropylene (PP) matrix. To the better of our knowledge, few studies analysed the effect of cork on PLA crystallinity [20–23] and, so far, none of the studies are related to the crystallization kinetics. In this work, the physical/chemical changes in PLA during its melting, the non-isothermal cold crystallization kinetics of PLA and CPC and the nucleating ability of cork in a PLA matrix will be studied. The influence of cork on the nucleation and the crystal growth behaviour of PLA will be analysed by Avrami [24,25] and Tobin [26–28] models. Crystallization activation energies (E_c) will be determined through Kissinger and Friedman methods [29,30]. In addition, the morphology and crystalline structure of PLA and CPC were evaluated recurring to Scanning Electron Microscopy (SEM), Polarized Optical Microscopy (POM) and X-Ray Diffraction (XRD) techniques.

2. EXPERIMENTAL

2.1 Materials

Cork powder from a Portuguese cork producer was used. The material was fractionated through sieving (Retsch, Germany) and the fraction retained in the sieve of 20 μm was kept. Cork powder was dried in vacuum oven (343 K) for 24 h. The average pore diameter as well as the bulk density of cork powder were measured by mercury intrusion porosimetry (MIP). The experiment was conducted in a Micromeritics Auto-pore IV 9500 apparatus with pressures ranging from 0.3 MPa to 227 MPa. The pore diameter was obtained by the Washburn equation [31], considering a surface tension of 0.485 N m^{-1} and a contact angle of 130° between cork and mercury.

The polymeric matrix used was an Ingeo™ Biopolymer PLA 4032D purchased from NatureWorks with a stereoisomer composition of 1.2-1.6 % D-isomer lactide and a melting point between 428 – 443 K.

2.2 CPC compounding

Before compounding, the cork particles and the PLA were dried at 343 K during 24 h, in a vacuum oven (Carbolite AX60 model), to stabilize the moisture content. CPC formulation was made in a Brabender type internal mixer. Initially, PLA pellets were charged and melted at 463 K, during 2 min at 40 rotations per minute (rpm), and then cork powder was added for additional 8 min. Previous studies reported that cork structure and composition do not alter at temperatures below 523 K [32,33]. After compounding, the mixture was granulated in a Dynisco granulator into granules (0.5-1.0 mm). CPC formulation contains 85 mass/% of PLA and 15 mass/% of cork powder, corresponding in terms of volume of 45 volume/% and 55 volume/%, respectively [18,34]. The selection of this mass ratio was to guarantee the highest amount of cork incorporated into PLA, in order to obtain a CPC filament with a non-plastic and natural touch, similar to cork.

2.3 Characterization by SEM

A SEM Hitachi SU-70 equipment was used to morphologically analyse cork powder particles and cork dispersion into PLA matrix after compounding. Samples were mounted on aluminium stubs and sputter coated (Polaron E 5000) with Au/Pd target for 2 min at 12 mA.

2.4 Characterization by DSC

Thermal properties and non-isothermal crystallization behaviour of PLA and CPC were studied using a Shimadzu DSC-60 equipment. All experiments were carried out in nitrogen atmosphere (50 mL/min). Samples between 9.0 to 10.0 mg were hermetically sealed in aluminium pans. Each sample was heated from 293 K to 473 K at a scan rate of 20 K min⁻¹ and held for 5 min at this temperature to eliminate the thermal history. Then, the samples were cooled at 20 K min⁻¹ to room temperature (\approx 293 K) and heated again up to 473 K. Four different heating rates were used, namely 1.25, 2.5, 5 and 7.5 K min⁻¹. The selection of the cooling rates was based on the low kinetics of PLA. A study of Miyata and Masuko [35] showed that samples cooled at rates higher than 10 K min⁻¹ did not crystallize and remained amorphous. Only the second run was considered for analysis. Glass transition temperature (T_g), cold crystallization temperature (T_{cc}), melting temperature (T_m), cold crystallization enthalpy (ΔH_{cc}) and melting crystallization enthalpy (ΔH_m) of PLA and CPC were determined from the DSC thermographs. The crystallinity degree (X_c) of samples was calculated using Eq. (1):

$$X_c = \frac{\Delta H_{cc}}{\Delta H_m^0(1-m)} \times 100 \quad (1),$$

where m is the mass percentage of the filler and ΔH_m^0 is the melting crystallization enthalpy for 100% crystalline PLA (93 J g⁻¹) [36].

2.5 Characterization by POM

POM was performed to evaluate the nucleation and spherulites growth in pure PLA and in PLA in the presence of cork powder. The observations were made on a Nikon Eclipse L150. Firstly, both samples were melted at 463 K for 5 minutes to remove thermal history. Then, samples were cooled down to 393 K. Isothermal crystallization took place at 393 K for 15 minutes.

2.6 Characterization by XRD

A Panalytical X'Pert Pro 3 equipment with a Cu K α ($\lambda = 1.5406 \text{ \AA}$) radiation source was used. Diffraction intensities were measure from 10 $^\circ$ to 40 $^\circ$ with a step size of 0.02. XRD measurements were performed at 298 K.

3. THEORETICAL PRINCIPLES

Non-isothermal kinetic parameters were determined by Avrami [24,25], Tobin [26–28], Kissinger [29] and Friedman [30] models. The relative degree of crystallinity at time ' t ' (X_t), as a function of temperature (T), was determined through Eq. (2):

$$X_t = \frac{\int_{T_0}^T \left(\frac{dH_{cc}}{dT} \right) dT}{\int_{T_0}^{T_\infty} \left(\frac{dH_{cc}}{dT} \right) dT} \quad (2),$$

where T_0 and T_∞ are the temperatures corresponding to the onset and end of the crystallization process, respectively.

In the case of the non-isothermal cold crystallization process, the relationship between the crystallization time (t) and the corresponding temperature (T) can be obtained by Eq. (3):

$$t = \frac{|T_0 - T|}{\varphi} \quad (3),$$

where φ is the heating rate.

Avrami model [24,25] is commonly used to describe the isothermal crystallization kinetic behaviour and analyse the increase of relative crystallinity with time:

$$1 - X_t = \exp(-Z_t t^n) \quad (4),$$

where Z_t is the crystallization rate constant, containing the nucleation and growth rate parameters, and it is temperature dependent, and n is the Avrami index which is dependent on the nucleation type and on the growth geometry of the crystals. The linearized form can be written as:

$$\log[-\ln(1 - X_t)] = \log(Z_t) - n \log(t) \quad (5)$$

Mandelkern [37] considered that the primary non-isothermal crystallization stage can be described through Avrami model, based on a constant crystallization temperature assumption. The n and Z_t parameters do not have the same physical meaning as in the isothermal crystallization processes, since the temperature changes constantly during non-isothermal crystallization. Jeziorny [38] calibrated the Z_t parameter, considering the temperature dependence of the non-isothermal crystallization, correcting the crystallization rate constants by introducing heating rate:

$$\log Z_c = \frac{\log(Z_t)}{\varphi} \quad (6)$$

The time required to achieve 50% of crystallization is called half-time of crystallization ($t_{1/2}$) and it is considered as a prime parameter for investigating the kinetics of crystallization process. The $t_{1/2}$ for non-isothermal crystallization can be obtained from the following expression [39]:

$$t_{1/2} = \left(\frac{\ln 2}{Z_t} \right)^{1/n} \quad (7)$$

Tobin [26–28] model was utilized to study the phase-transformation kinetics with growth site impingement on the non-isothermal crystallization kinetics of PLA and CPC (Eq. (8)):

$$X_t = \frac{K_T t^{n_T}}{1 + K_T t^{n_T}} \quad (8),$$

where K_T and n_T correspond to Tobin crystallization rate constant and Tobin exponent, respectively. The n_T parameter provides information about the type of nucleation and growth mechanism involved in the non-isothermal crystallization process. The linearized form of Eq. (9) is rewritten as:

$$\ln\left(\frac{X_t}{1 - X_t}\right) = \ln K_T + n_T \ln t \quad (9)$$

Kissinger [29] method was applied to determine the E_c for non-isothermal cold crystallization of neat PLA and CPC. E_c is the energy required for the movement of PLA molecular segments from melt to the crystal growth surface. It is determined by the variation of T_{cc} with respect to φ , as described in Eq. (10):

$$\frac{-E_c}{R} = \frac{d(\ln\left(\frac{\varphi}{T_{cc}^2}\right))}{d\left(\frac{1}{T_{cc}}\right)} \quad (10),$$

where R is the gas constant and T_{cc} is the cold crystallization temperature.

An isoconversional method developed by Friedman [30] was also used to determine the E_c . Contrarily to the Kissinger method, where a single value of E_c is determined, regardless the kinetics of the system, from the Friedman method it is evaluated the dependency of E_c with crystallinity and temperature. According to Friedman, different effective activation energies can be calculated for each X_t considering the following equation (Eq. (11)):

$$\ln\left(\frac{dX}{dt}\right)_{X,i} = \text{constant} - \frac{E_c}{RT_{X,i}} \quad (11),$$

where i represents each heating rate applied, (dX/dt) is the instantaneous crystallization rate as a function of time at a given conversion X and $T_{X,i}$ is the temperature associated to a given conversion X at different i 's. At a given X_t , E_c can be calculated from the slope (E_c/R) of the correlation between $\ln(dX/dt)$ versus $1/T_X$.

4. RESULTS AND DISCUSSION

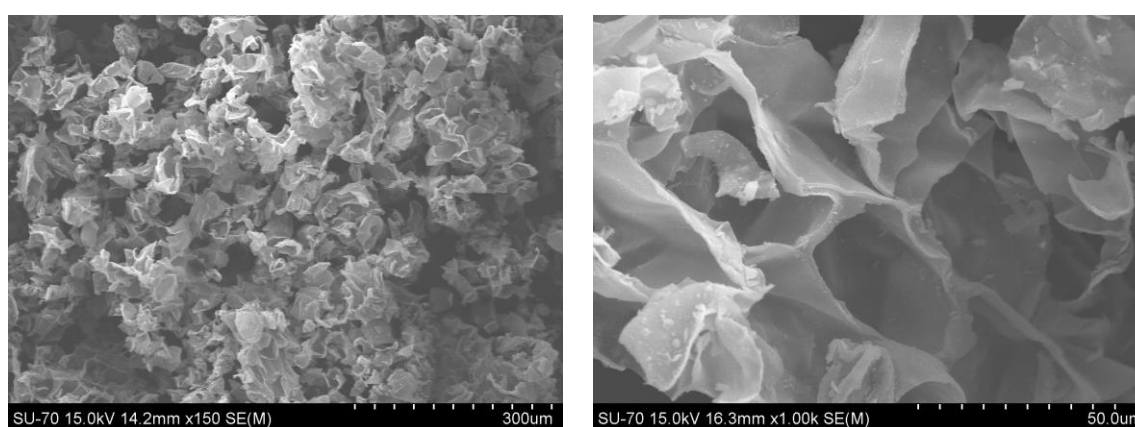
4.1. Cork powder characterization

MIP analysis was applied to characterize cork powder in terms of density and porosity. In Table 1, it is shown the average value of pore diameter, the porosity and bulk and apparent densities.

Table 1 Cork powder characterization.

Cork Powder	
Average pore diameter (μm)	16.9
Bulk density (g cm^{-3})	0.177
Apparent Density (g cm^{-3})	0.616
Porosity (%)	71.3

According to IUPAC [40], cork powder pores are classified as macropores, since they present an average diameter greater than 50nm. Cork powder presents low density and high porosity, which is mainly due to its characteristic honeycomb structure, as can be seen in Figure 1.

**Fig. 1** SEM images of cork powder.

4.2. Non-isothermal heating behaviour

Non-isothermal DSC curves of neat PLA and CPC from the second heating scan at different heating rates are presented in Figure 2. Exothermic cold crystallization peaks appear for both, pure PLA and CPC. The PLA molecular chains become mobile above T_g , allowing crystallization. Above T_g , molecular chains possess the ability to be partly ordered and the cold crystallization takes place. These crystals melt upon further heating. For PLA, cold crystallization peaks becomes smother as the heating rate increases. It suggests that lower scan rates during heating can promote PLA crystallization [6]. From Figure 2, it is also visible the T_m peaks for PLA and CPC.

There are double-melting peaks for both samples, which are usually ascribed to simultaneous occurrence of thinner lamellae melting and recrystallization. More specifically, the lower T_m peak is usually associated with the melting of some original crystals grown by primary crystallization. While, the higher T_m peak is associated to the melting of crystals formed through a melt-recrystallization process during the heating process in DSC measurement [7,41]. Other studies, involving biomaterials, allowed to visualize the presence of double T_m peaks in the crystallization behaviour of PLA [20,42].

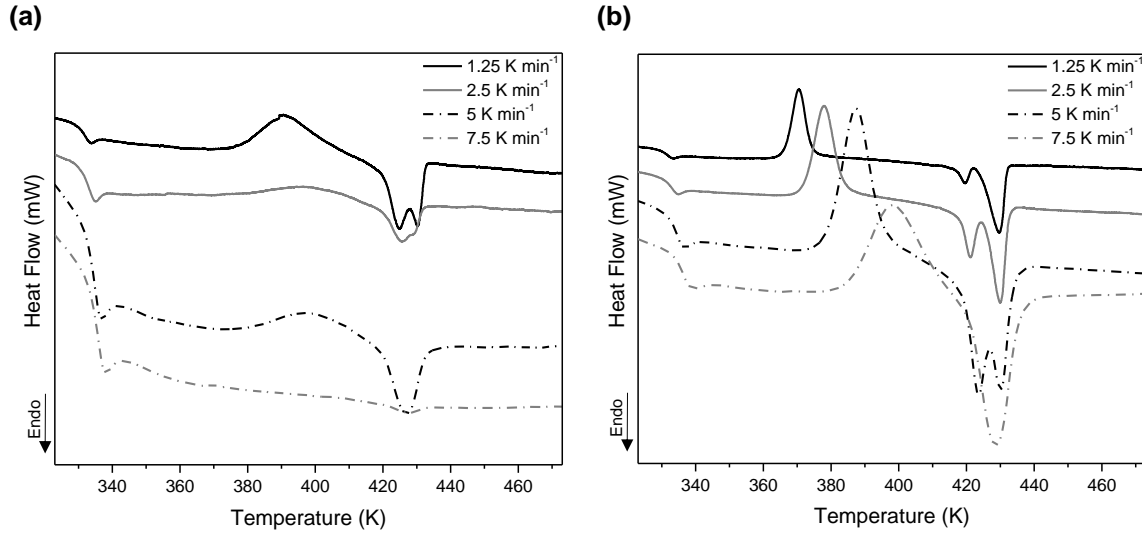


Fig. 2 DSC thermographs, in the second heating cycle, at different heating rates for **(a)** PLA and **(b)** CPC.

The presence and reorganization of different types of crystals with different stabilities was the explanation given by the authors to the appearance of these double-melting peaks. As the heating rate increases, these double-melting peaks became weakened for both samples. The same tendency was reported by Zhang and co-workers [41]. They appointed the decreasing of the rate of crystallization based in the self-adjustment of the amorphous PLA chains. The non-isothermal crystallization parameters obtained from Figure 2 and equations are listed in Table 2.

Table 2 Non-isothermal crystallization parameters of PLA and CPC materials.

Sample	ϕ (K min ⁻¹)	T_g (K)	T_{cc} (K)	ΔH_{cc} (J g ⁻¹)	X_{cc} (%)	T_m (K)	ΔH_m (J g ⁻¹)
PLA	1.25	335.2	389.6	13.6	14.7	424.4/ 430.7	11.3
	2.50	335.0	398.5	4.8	5.2	425.9/428.2*	3.9
	5.00	337.8	401.5	1.3	1.4	426.4	2.6
	7.50	337.7	405.7	0.2	0.3	426.9	0.2
CPC	1.25	334.6	370.5	21.8	27.5	419.8/ 429.9	15.8
	2.50	335.3	378.0	16.8	21.2	421.6/ 430.0	15.0
	5.00	337.4	387.8	16.4	20.7	423.9/ 429.8	15.7
	7.50	339.4	398.5	11.6	14.6	429.2	12.8

*Shoulder

The T_g values for PLA and CPC slightly increase with heating rate, which can suggest the confinement of the amorphous mobile phase [20]. In fact, for each material, the T_{cc} values also increase with heating rate, supporting the reduced ability of PLA to recrystallize on heating above T_g . In addition, as T_{cc} shifts to higher values with heating rate it implies that the crystallization process occurs earlier for lower heating rates [41]. At a given heating rate, the values for T_{cc} of CPC were lower than for neat PLA. This indicates that cork can promote the initial cold crystallization of the PLA

matrix due to the heterogeneous nucleation effect. Values of ΔH_{cc} present a downward trend as the heating rate increases. Considering that all samples were initially amorphous, as a consequence of the fast cooling rate applied, this trend indicates that, as the heating increases, polymer chains did not have sufficient time to form crystalline structures. In parallel, ΔH_m values exhibit the same trend as ΔH_{cc} . This can be an indication that PLA melting behaviour depends on the crystal structures created during cold crystallization phase. A study of Nofar, M. *et al* [5] reported the same behaviour. From the X_{cc} values, it is noticed that the amount of crystallinity developed in PLA is dependent on the heating rate. X_{cc} values increased with the addition of cork indicating that cork facilitated the crystallization of PLA during heating. Cork may act as heterogeneous nucleating agent. The ability of cork to modify the crystallization behaviour of PLA may be associated to the increased density of nucleating sites provide by cork particles. This nucleating ability of cork was also observed in other studies considering bio-based polyesters acting as matrices [20,22,43]. In Figure 3, it is represented non-isothermal DSC curves at 1.25 K min^{-1} of neat PLA and CPC.

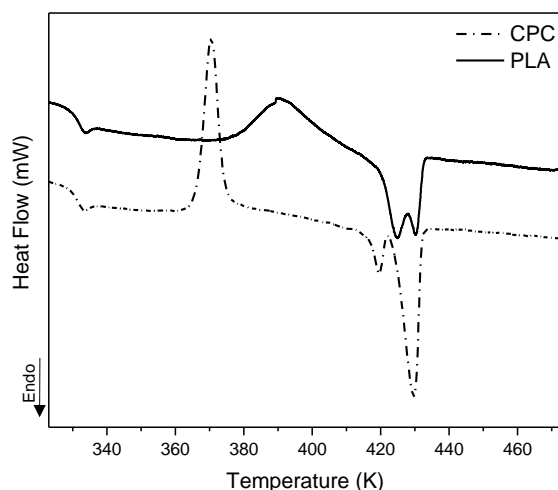


Fig. 3 DSC thermographs of PLA and CPC, at a heating rate of 1.25 K min^{-1} .

As referred above, the presence of cork shifted T_{cc} to lower values, showing the nucleating ability of cork. Its addition also led to a more well-defined and sharp cold crystallization peak, which usually corresponds to a well-defined crystal structure. This suggests that, somehow, the addition of cork resulted in a rearrangement of PLA molecules leading to a more defined crystal structure.

4.3. Non-isothermal cold crystallization kinetics

The relative crystallinity curves as function of versus crystallization time for the PLA and CPC studied samples are showed in Figure 4. At different heating rates curves exhibit the same sigmoidal shape. The first nonlinear part is usually considered the nucleation step of the crystallization process [44].

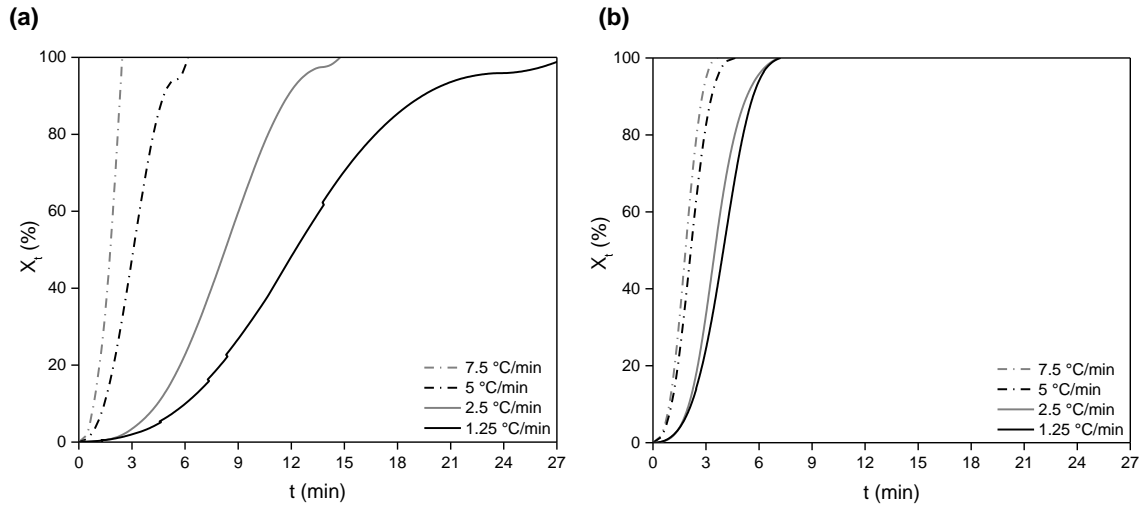


Fig. 4 Relative crystallinity (X_t) versus time (t) for **(a)** PLA and **(b)** CPC.

The longest nucleation step occurs for PLA at 1.25 K min^{-1} , meaning the formation of more nuclei. The curvature of the second nonlinear part levelled off that is attributed to the impingement or crowding of spherulites at the later stage of the crystal growth [45].

Higher heating rates have managed to complete the PLA crystallization process in a shorter time. This behaviour is also observed through $t_{1/2}$ parameter (see Table 3). A shorter $t_{1/2}$ value means a faster crystallization process, where a shorter time is needed to achieve 50 % of crystallization fraction. It is visible a decrease on $t_{1/2}$ for all heating rates when PLA crystallizes in the presence of cork when compared to neat PLA. Once again, the nucleating effect of cork is observed. The higher $t_{1/2}$ values observed for PLA and CPC at lower heating rates can be attributed to the secondary crystallization process.

4.3.1. Avrami model

Avrami plots and kinetic parameters are shown in Figure 5 and Table 3, respectively, obtained from the application of Eq. (5) and Eq. (6). It was considered X_t values ranging from 10% to 80%.

Avrami model was adequate to describe the non-isothermal cold crystallization kinetics of neat PLA and CPC (R^2 equal to 1 for almost all heating rate scans). It should be noted that Avrami model does not have the same physical meaning as in the isothermal crystallization, owing to the constantly variation of temperature in non-isothermal crystallization. This temperature dependence, will have effect on the rates of both nuclei formation and spherulite growth. Z_c values increased with heating rate, demonstrating that cold crystallization rate increases with heating rate. The n values for PLA and CPC are found in the range of ~ 2 -3. Non-integer n values reveal a combination of thermal and athermal nucleation mechanisms [7].

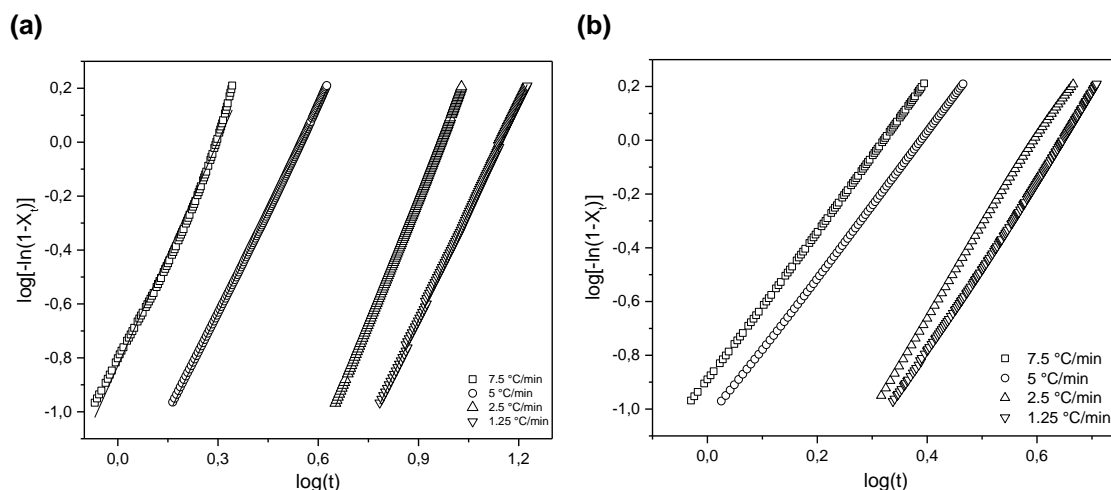


Fig. 5 Avrami plots of (a) PLA and (b) CPC.

The average n values for PLA and CPC were 2.78 and 3.02, respectively, indicating that the non-isothermal cold crystallization was initiated by an athermal nucleation and followed by a mixed two and three-dimensional spherulite growth [7,14].

Table 3 Half-time crystallization and Avrami kinetic parameters.

Sample	ϕ (K min ⁻¹)	$t_{1/2}$ (min)	n	Z_c (min ⁻ⁿ K ⁻¹)	R^2
PLA	1.25	12.2	2.7	3.46E-03	0.999
	2.50	8.20	3.1	6.28E-02	0.999
	5.00	3.10	2.5	5.26E-01	0.999
	7.50	1.70	2.8	7.75E-01	0.989
CPC	1.25	3.90	3.2	2.20E-02	0.999
	2.50	3.60	3.4	1.58E-01	0.999
	5.00	2.10	2.7	6.16E-01	0.999
	7.50	1.80	2.8	7.59E-01	0.999

4.3.2. Tobin model

Tobin model was considered to overcome the limitation of Avrami model in the study the early stage of crystallization process. More specifically, Tobin model is able to describe the phase-transformation kinetics with growth site impingement as well as secondary crystallization process [26–28]. Contrarily to Avrami exponent, Tobin exponent n_T does not need to be integer, since it is controlled directly by different types of nucleation and growth mechanisms [10]. Tobin plots for PLA and CPC obtained for different heating rates are given in Figure 6 and the related parameters are presented in Table 4. A X_t range of 10 to 80% was used for calculations.

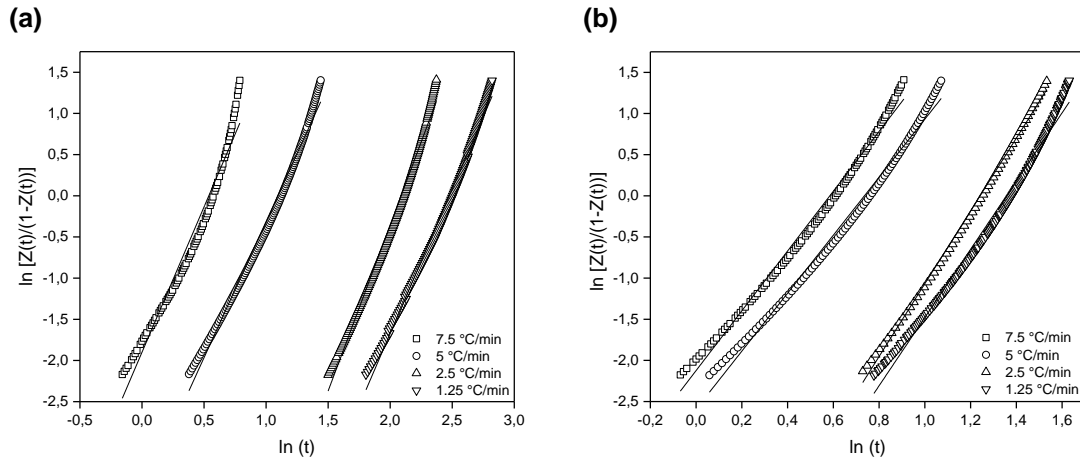


Fig. 6 Tobin plots of (a) PLA and (b) CPC.

Table 4 Tobin kinetic parameters.

Sample	ϕ (K min ⁻¹)	n_T	K_T (min ⁻ⁿ)	R ²
PLA	1.25	3.5	1.7E-04	0.99
	2.5	4.0	2.2E-04	0.99
	5	3.3	2.7E-02	0.99
	7.5	3.5	1.5E-01	0.97
CPC	1.25	4.1	3.6E-03	0.99
	2.5	4.4	4.1E-03	0.99
	5	3.5	7.5E-02	0.99
	7.5	3.6	1.2E-01	0.99

The n_T average value of PLA is 3.60 and for CPC is 3.93. For both cases, n_T values are almost independent of the heating rate. Concerning the K_T parameter, it increases as the heating rate increases. The K_T values for CPC are larger than for PLA, which indicates that the presence of cork accelerates the non-isothermal cold crystallization of PLA. Tobin parameters describe the same physical significance analogous to that of Avrami model. In this study, Tobin parameters exhibited a similar tendency to those obtained for Avrami analysis.

4.3.3. Comparison between Avrami and Tobin models

The efficiency of both models on describing the non-isothermal crystallization kinetics of PLA and CPC can be assessed from Fig. 7. For each heating rate, the curve that correlates X_t versus t (as in Figure 4) was used as a reference. Considering the kinetic parameters displayed on Tables 3 and 4, as well as the Eq. (4) and Eq. (8), the fitting accuracy of Avrami and Tobin models were determined.

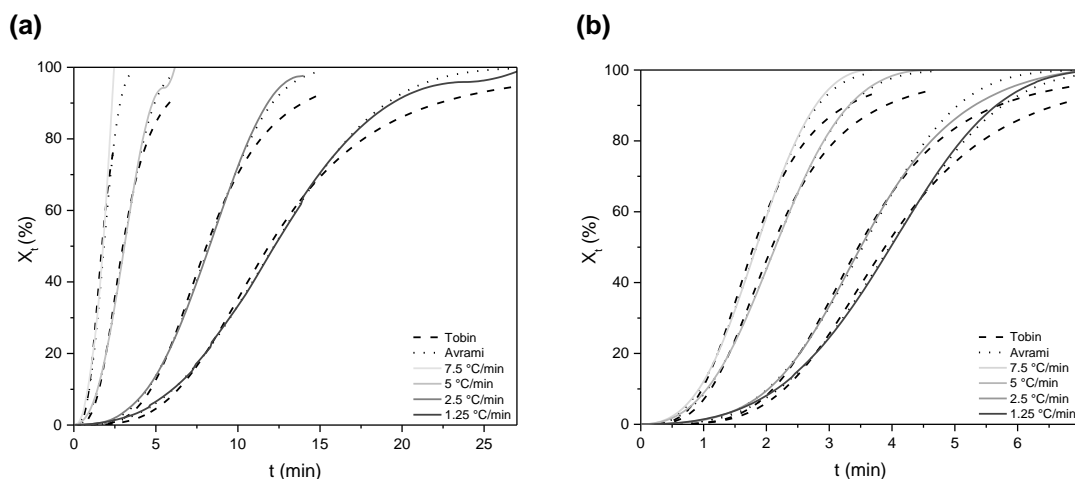


Fig. 7 Comparison between Avrami and Tobin models – Relative crystallinity (X_t) as function of time (t) for **(a)** PLA and **(b)** CPC.

According to Figure 7, similar tendency was observed for PLA and CPC samples. The accuracy of Avrami model fitting becomes higher as the heating rates increase. On the contrary, for each heating rates, Tobin model fitting under predicts the evolution of relative crystallinity. This tendency is more accentuated at higher relative crystallinity values ($X_t \geq 75\%$). Working with syndiotactic polypropylene, Supaphol, P. [46] observed a deviation of the Tobin model fitting, which was attributed to the use of a simplified form of Eq. (8) or it could be associated to the over prediction of the impingement effect.

4.3.4. Activation Energy

Kissinger plots are visible in Figure 8 and the corresponding E_c values are listed in Table 5. The plots exhibit good linearity, and regression coefficients (R^2) values are obtained with values of ~ 0.990 .

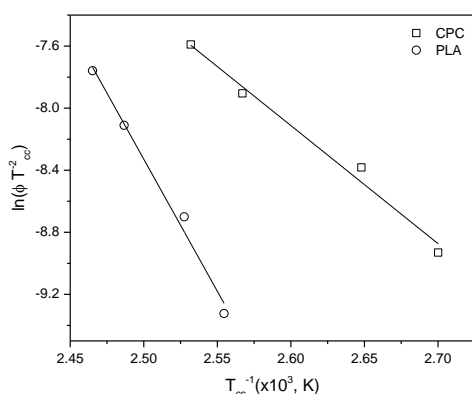


Fig. 8 Kissinger plots for PLA and CPC.

Table 5 Activation energies for PLA and CPC according to Kissinger method.

Sample	E_c (kJ mol ⁻¹)	R^2
PLA	141.5	0.990
CPC	63.3	0.986

The addition of cork resulted in a decrease of the E_c , from 141.5 to 63.3 kJ mol⁻¹, suggesting that the energy barrier of cold crystallization is lower for CPC, causing an increase of crystallization ability for CPC as compared with PLA. An expected result since cork acted as nucleating agent, as presented before. Comparable results have also been found for the cold crystallization activation energy of PLA in the presence of the multiwalled carbon nanotubes [47], clay [6] and a combination of several nucleating agents [48].

The dependency of E_c as function of X_t was evaluated according to the Friedman method. X_t values ranging from 0.1 to 0.8 were considered and it was obtained R^2 from 0.95–0.99. In Figure 9 it is illustrated E_c versus X_t for both materials and the corresponding average E_c values are listed in Table 6.

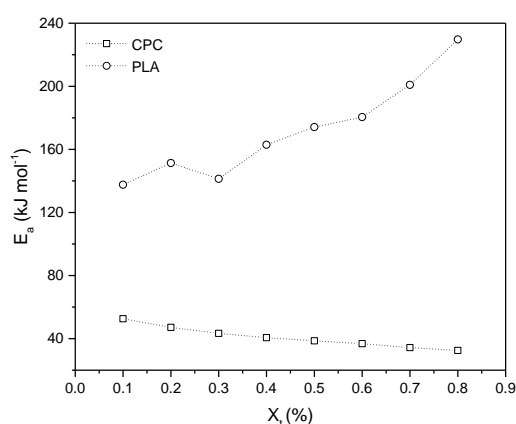


Fig. 9 Dependency of E_c as a function of X_t for PLA and CPC.

Table 6 Average activation energies ($\overline{E_c}$) for PLA and CPC according to Friedman method.

Sample	$\overline{E_c}$ (kJ mol ⁻¹)
PLA	172.3
CPC	40.8

The E_c values indicate that the energy barrier for the cold crystallization process is lower for the composite than for the unfilled PLA. The same tendency was observed in similar studies [49,50]. The results are also in agreement with those obtained in the previous kinetic analysis, reinforcing the nucleating ability of cork. In fact, for X_t equal to 0.1, the E_c values acquired from Kissinger method are similar to E_c values from Friedman method. This can be indicative that the Kissinger method can represent one E_c value obtained by Friedman, as also observed by Li, C. *et al* [7] and Ries, A. *et al* [50].

4.4. Morphology and POM observations

The morphology of CPC was evaluated by SEM and it is presented in Figure 10. It is seen that cork particles are homogeneously dispersed and imbedded within PLA matrix. Cork particles are completely covered by PLA (highlighted in orange).

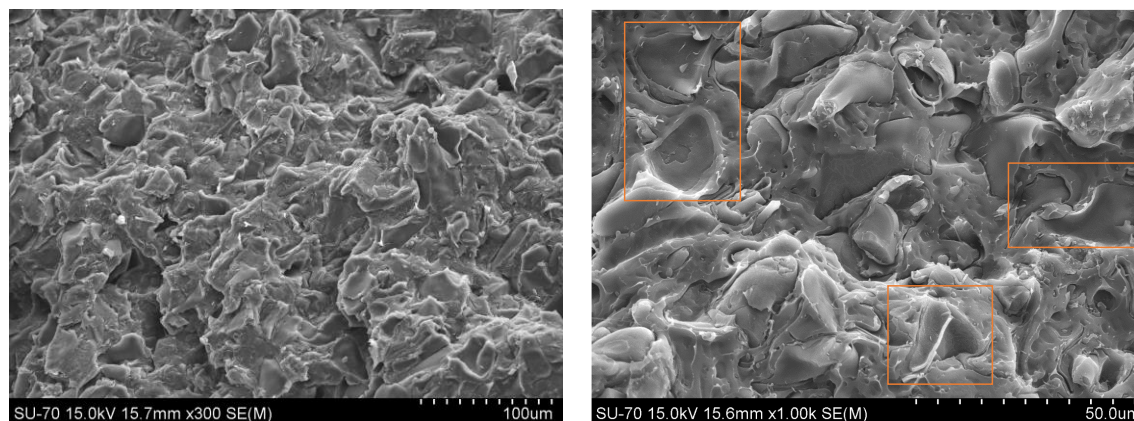


Fig. 10 SEM images of CPC after compounding.

The evaluation of cork powder as nucleating agent in PLA matrix was evaluated through POM. Optical micrographs of pure PLA and CPC after 15 minutes at 393.2 K are shown in Figure 11.

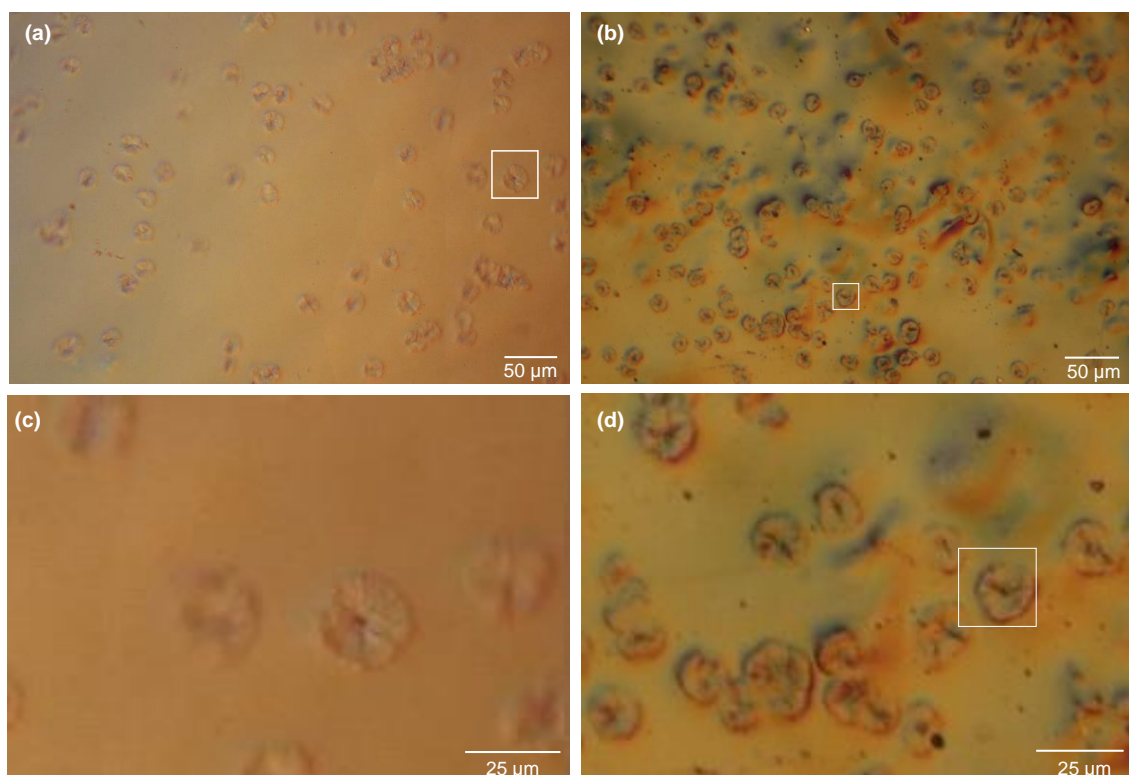


Fig. 11 Optical micrographs of **(a)-(c)** PLA and **(b)-(d)** CPC. (15min at 393.2 K)

It is revealed the nucleating ability of cork powder in PLA matrix, already determined by the non-isothermal crystallization kinetic analyses. Within 15 minutes, CPC exhibited higher nucleation density and smaller spherulite size when compared to pure PLA. The same tendency was visualized by Li, C. *et al* [51].

4.5. XRD

XRD analyses were performed to evaluate PLA and CPC crystalline structures. PLA exhibits several polymorphisms during melt or cold crystallization, such as α , β , and γ -forms [52,53]. The α -form is considered the most stable and it is produced at high crystallization temperatures (>393.2 K); while, a disordered α' -form can be developed at lower temperatures [52,54,55]. A combination of these α forms is usually made in industrial processes to decrease PLA processing temperature. In Figure 12 is displayed XRD patterns of PLA and CPC measured at 298.2 K.

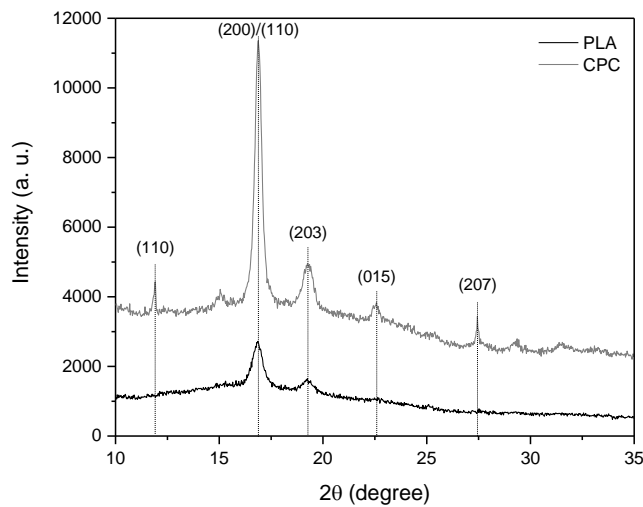


Fig.12 XRD patterns of PLA and CPC.

For PLA, two characteristic reflections planes of α -phase crystals can be identified, namely (200)/(110) and (203), with scattering angles (2θ) of 16.9° and 19.2° , respectively [52,54]. As for CPC, stronger peaks at 16.9° and 19.2° can be observed, indicating that cork can improve the crystallization of PLA. In addition, the presence of cork during the cold crystallization of PLA alter its crystalline structure, which is reflected by the appearance of α -phase characteristic peaks, namely at 11.9° (110), 22.6° (015) and 27.4° (207) [52,54,56]. These findings are in agreement with those obtained by the non-isothermal crystallization kinetic analyses.

5. CONCLUSIONS

The non-isothermal cold crystallization behaviors of PLA and CPC were investigated at different heating rates ($1.25, 2.5, 5$ and 7.5 K min^{-1}) through DSC measurements. In the presence of cork, T_{cc} shifted to lower values revealing that cork facilitates the initial cold crystallization of the PLA matrix. Additionally, an increase of $\sim 300\%$ of X_{cc} was observed when PLA cold crystallizes in the presence of cork. Avrami and Tobin models were applied to analyze the non-isothermal kinetics of the samples. Both methods successfully described the non-isothermal cold crystallization processes of PLA and

CPC. The same tendency was attained for both methods, where the addition of cork increased the crystallization rate of PLA matrix and n values indicated a mixed two and three-dimensional crystallization growth. These results were supported by POM and XRD analyses. From the Kissinger and Friedman methods, lower ΔE_c values for CPC were obtained, indicating a reduction in energy barrier for crystallization compared to neat PLA.

This study allows to understand the cold crystallization behaviour of CPC filament during FFF, which is considered a fast local cooling process. As reported above, the addition of cork to PLA considerably increased the crystallization rate and X_{cc} , revealing the ability of PLA to crystallize rapidly in the presence of cork, as experienced during FFF. This will have an impact on the mechanical behaviour of printing parts. The presence of small spherulites, will enhance ductility and impact strength. It will also help on the definition of printing settings and on the evaluation of layers adhesion and warpage.

ACKNOWLEDGMENTS

This work was supported by COMPETE 2020 – Programa Operacional Competividade e Internacionalização within TT@ESAN project (NORTE-01-0246-FEDER-000001). Authors would also want to acknowledge Maria Celeste Coimbra Azevedo for the DSC measurements and Artur Sarabando for the XRD analyses.

REFERENCES

1. Pereira H. Cork : Biology, Production and Uses. Amsterdam: Elsevier; 2007.
2. Fernandes EM, Aroso IM, Mano JF, Covas JA, Reis RL. Functionalized cork-polymer composites (CPC) by reactive extrusion using suberin and lignin from cork as coupling agents. *Compos Part B Eng.* 2014;67:371–80.
3. Garlotta D. A Literature Review of Poly(Lactic Acid). *J Polym Environ.* 2001;9:63–84.
4. Magoń A, Pyda M. Study of crystalline and amorphous phases of biodegradable poly(lactic acid) by advanced thermal analysis. *Polymer (Guildf).* 2009;50:3967–73.
5. Nofar M, Zhu W, Park CB, Randall J. Crystallization Kinetics of Linear and Long-Chain-Branched Polylactide. *Ind Eng Chem Res.* 2011;50:13789–98.
6. As'habi L, Jafari SH, Khonakdar HA, Häussler L, Wagenknecht U, Heinrich G. Non-isothermal crystallization behavior of PLA/LLDPE/nanoclay hybrid: Synergistic role of LLDPE and clay. *Thermochim Acta.* 2013;565:102–13.
7. Li C, Dou Q. Non-isothermal crystallization kinetics and spherulitic morphology of nucleated poly(lactic acid): Effect of dilithium cis-4-cyclohexene-1,2-dicarboxylate as a novel and efficient nucleating agent. *Polym Adv Technol.* 2015;26:376–84.
8. Ke T, Sun X. Melting behavior and crystallization kinetics of starch and poly(lactic acid) composites. *J Appl Polym Sci.* 2003;89:1203–10.
9. Qiu Z, Li Z. Effect of Orotic Acid on the Crystallization Kinetics and Morphology of Biodegradable Poly(l -lactide) as an Efficient Nucleating Agent. *Ind Eng Chem Res.* 2011;50:12299–303.
10. Han Q, Wang Y, Shao C, Zheng G, Li Q, Shen C. Nonisothermal crystallization kinetics of biodegradable poly(lactic acid)/zinc phenylphosphonate composites. *J Compos Mater.* 2014;48:2737–46.
11. Koutsomitopoulou AF, Bénézet JC, Bergeret A, Papanicolaou GC. Preparation and characterization of olive pit powder as a filler to PLA-matrix bio-composites. *Powder Technol.* 2014;255:10–6.
12. Li M, Hu D, Wang Y, Shen C. Nonisothermal crystallization kinetics of poly(lactic acid) formulations comprising talc with poly(ethylene glycol). *Polym Eng Sci.* 2010;50:2298–305.
13. Kulinski Z, Piorkowska E. Crystallization, structure and properties of plasticized poly(l-lactide). *Polymer (Guildf).* 2005;46:10290–300.

14. Xiao H, Yang L, Ren X, Jiang T, Yeh JT. Kinetics and crystal structure of poly(lactic acid) crystallized nonisothermally: Effect of plasticizer and nucleating agent. *Polym Compos.* 2010;31:2057–68.
15. Gibson I, Rosen D SB. *Additive Manufacturing Technologies: 3D Printing, Rapid Prototyping, and Direct Digital Manufacturing*. Second Edi. New York: Springer; 2015.
16. Fernandes EM, Correlo VM, Mano JF, Reis RL. Polypropylene-based cork–polymer composites: Processing parameters and properties. *Compos Part B Eng.* 2014;66:210–23.
17. Thakur VK. *Lignocellulosic Polymer Composites: Processing, Characterization and Properties*. Thakur VK, editor. Scrivener Publishing, Wiley; 2015.
18. Magalhães da Silva SP, Lima PS, Oliveira JM. Non-isothermal crystallization kinetics of cork-polymer composites for injection molding. *J Appl Polym Sci.* 2016;133.
19. Magalhães Da Silva SP, Lima PS, Oliveira JM. Nucleating ability of cork in polypropylene-based composites. *ECCM 2016 - Proceeding 17th Eur Conf Compos Mater.* 2016.
20. Fernandes EM, Correlo VM, Mano JF, Reis RL. Cork–polymer biocomposites: Mechanical, structural and thermal properties. *Mater Des.* 2015;82:282–9.
21. Vilela C, Sousa AF, Freire CSR, Silvestre AJD, Pascoal Neto C. Novel sustainable composites prepared from cork residues and biopolymers. *Biomass and Bioenergy.* 2013;55:148–55.
22. Daver F, Lee KPM, Brandt M, Shanks R. Cork–PLA composite filaments for fused deposition modelling. *Compos Sci Technol.* 2018;168:230–7.
23. Andrzejewski J, Szostak M, Barczewski M, Łuczak P. Cork-wood hybrid filler system for polypropylene and poly(lactic acid) based injection molded composites. Structure evaluation and mechanical performance. *Compos Part B Eng.* 2019;163:655–68.
24. Avrami M. Kinetics of Phase Change. II Transformation-Time Relations for Random Distribution of Nuclei. *J Chem Phys.* AIP Publishing; 1940;8:212.
25. Avrami M. Kinetics of Phase Change. I General Theory. *J Chem Phys.* 1939;7:1103.
26. Tobin MC. Theory of phase transition kinetics with growth site impingement. I. Homogeneous nucleation. *J Polym Sci Polym Phys Ed.* 1974;12:399–406.
27. Tobin MC. The theory of phase transition kinetics with growth site impingement. II. Heterogeneous nucleation. *J Polym Sci Polym Phys Ed.* 1976;14:2253–7.
28. Tobin MC. Theory of phase transition kinetics with growth site impingement. III. Mixed heterogeneous–homogeneous nucleation and nonintegral exponents of the time. *J Polym Sci Polym Phys Ed.* 1977;15:2269–70.
29. Kissinger HE. Variation of Peak Temperature with Heating Rate in Differential Thermal Analysis. *J Res Natl Bur Stand (1934).* 1956;57:217–21.
30. Friedman HL. Kinetics of thermal degradation of char-forming plastics from thermogravimetry. Application to a phenolic plastic. *J Polym Sci Part C Polym Symp.* 1964;6:183–95.
31. Washburn EW. The Dynamics of Capillary Flow. *Phys Rev.* 1921;17:273–83.
32. Şen A, Van den Bulcke J, Defoirdt N, Van Acker J, Pereira H. Thermal behaviour of cork and cork components. *Thermochim Acta.* 2014;582:94–100.
33. Rosa ME, Fortes MA. Thermogravimetric analysis of cork. *J Mater Sci Lett.* 1988;7:1064–5.
34. Magalhães da Silva SP, Lima PS, Oliveira JM. Rheological behaviour of cork-polymer composites for injection moulding. *Compos Part B Eng.* 2016;90.
35. Miyata T, Masuko T. Crystallization behaviour of poly(l-lactide). *Polymer (Guildf).* 1998;39:5515–21.
36. Fischer EW, Sterzel HJ, Wegner G. Investigation of the structure of solution grown crystals of lactide copolymers by means of chemical reactions. *Kolloid-Zeitschrift und Zeitschrift für Polym.* 1973;251:980–90.
37. Mandelkern L. *Methods of Experimental Physics*. New York: Academic Press; 1980.
38. Jeziorny A. Parameters characterizing the kinetics of the non-isothermal crystallization of poly(ethylene terephthalate) determined by d.s.c. *Polymer (Guildf).* 1978;19:1142–4.
39. Liu Y, Wang L, He Y, Fan Z, Li S. Non-isothermal crystallization kinetics of poly(L-lactide). *Polym Int.* 2010;59:1616–21.
40. INTERNATIONAL UNION OF PURE, AND APPLIED CHEMISTRY (IUPAC). Recommendations for the characterization of porous solids (Technical Report). *Pure Appl Chem.* 1994;66:1739–58.

41. Wu D, Wu L, Wu L, Xu B, Zhang Y, Zhang M. Nonisothermal cold crystallization behavior and kinetics of polylactide/clay nanocomposites. *J Polym Sci Part B Polym Phys*. 2007;45:1100–13.
42. Masirek R, Kulinski Z, Chionna D, Piorkowska E, Pracella M. Composites of poly(L-lactide) with hemp fibers: Morphology and thermal and mechanical properties. *J Appl Polym Sci*. 2007;105:255–68.
43. Magalhães da Silva SP, Antunes T, Costa ME V, Oliveira J. M. Cork-like Filaments for Additive Manufacturing. *Addit Manuf*. 2020;34:101229.
44. Ding W, Chu RKM, Mark LH, Park CB, Sain M. Non-isothermal crystallization behaviors of poly(lactic acid)/cellulose nanofiber composites in the presence of CO₂. *Eur Polym J*. 2015;71:231–47.
45. Abdel Aziz MS, Saad GR, Naguib HF. Non-isothermal crystallization kinetics of poly(3-hydroxybutyrate) in copoly(ester-urethane) nanocomposites based on poly(3-hydroxybutyrate) and cloisite 30B. *Thermochim Acta*. 2015;605:52–62.
46. Supaphol P. Nonisothermal bulk crystallization and subsequent melting behavior of syndiotactic polypropylenes: Crystallization from the melt state. *J Appl Polym Sci*. 2000;78:338–54.
47. Zhao Y, Qiu Z, Yan S, Yang W. Crystallization behavior of biodegradable poly(L-lactide)/multiwalled carbon nanotubes nanocomposites from the amorphous state. *Polym Eng Sci*. 2011;51:1564–73.
48. Chen L, Dou Q. Influence of the combination of nucleating agent and plasticizer on the non-isothermal crystallization kinetics and activation energies of poly(lactic acid). *J Therm Anal Calorim*. 2020;139:1069–90.
49. dos Santos Silva ID, Schäfer H, Jaques NG, Siqueira DD, Ries A, de Souza Morais DD, et al. An investigation of PLA/Babassu cold crystallization kinetics. *J Therm Anal Calorim*. 2019;1–9.
50. Ries A, Canedo EL, Souto CR, Wellen RMR. Non-isothermal cold crystallization kinetics of poly(3-hydroxybutyrate) filled with zinc oxide. *Thermochim Acta*. 2016;637:74–81.
51. Li C, Dou Q, Bai Z, Lu Q. Non-isothermal crystallization behaviors and spherulitic morphology of poly(lactic acid) nucleated by a novel nucleating agent. *J Therm Anal Calorim*. 2015;122:407–17.
52. Di Lorenzo ML, Androsch R. Influence of α' - α -crystal polymorphism on properties of poly(l-lactic acid). *Polym. Int*. 2019. p. 320–40.
53. Aliotta L, Cinelli P, Coltelli MB, Righetti MC, Gazzano M, Lazzeri A. Effect of nucleating agents on crystallinity and properties of poly (lactic acid) (PLA). *Eur Polym J*. 2017;93:822–32.
54. Chen X, Kalish J, Hsu SL. Structure evolution of α' -phase poly(lactic acid). *J Polym Sci Part B Polym Phys*. 2011;49:1446–54.
55. Běhálek L, Borůvka M, Brdlík P, Habr J, Lenfeld P, Kroisová D, et al. Thermal properties and non-isothermal crystallization kinetics of biocomposites based on poly(lactic acid), rice husks and cellulose fibres. *J Therm Anal Calorim*. 2020;
56. Katiyar V. *Bio-based Plastics for Food Packaging Applications*. Shawbury: Smithers Pira; 2017.

3.3 Cork-Polylactide Composites reinforced with polyhydroxyalkanoates for Additive Manufacturing ⁱ

Sara. P. Magalhães, da Silva^{1,2} and José M. Oliveira^{1,2}

¹Aveiro Institute of Materials (CICECO), University of Aveiro, Portugal

²School of Design, Management and Production Technologies, University of Aveiro, Portugal

e-mail: sarapms@ua.pt

e-mail: martinho@ua.pt

Keywords:

Cork; Biodegradable matrices; Cork-Polymer Composites; Mechanical properties

Abstract

Cork-polymer composites (CPC) consisting of 85% wt of polymeric matrix and 15% wt. of cork powder residues were developed. The polymeric matrix was composed by PLA, PHA and different blends of PLA/PHA. Three different blend weight ratios of PLA/PHA were studied, namely 75:25, 50:50 and 25:75. CPC were prepared by melt compounding using a Brabender type mixer. Mechanical analyses, including tensile and impact tests, as well as morphological analyses through scanning electron microscopy, were performed. When compared to composite only prepared with PLA (CPC 1), the addition of PHA to PLA promotes more ductile composites. Through impact tests, it was also observed the toughening effect of PHA when added to PLA. The CPC prepared with the blend PLA:PHA=75:25 revealed to have better mechanical performance among the ones prepared with the other blend ratios. From morphological analyses, it was perceived the miscibility of both polymeric matrices.

1. Introduction

The use of biodegradable polymers and natural fillers for the development of biocomposites have arose great interest in the composite science. Theirs biodegradation ability allows complete degradation in ambient conditions, without toxic compounds emissions. Polylactic acid (PLA) is one of the most promising biopolymers, since it is produced from annually renewable available resources and the industrial technology needed for its processing is relatively low cost, when compared to petrol-based plastics [1,2]. Similar to PLA, the use of polyhydroxyalkanoates (PHA) is an attractive alternative to petroleum-based polymers. PHA are biodegradable polyesters produced from bacterial fermentation of sugars or lipids. PHA can be used as PLA modifier to improve its ductility and flexibility. In addition, PHA has a similar chemical structure as PLA and the preparation of these

ⁱ Magalhães da Silva, S. P., Oliveira J. M. **2018**. Cork-Polylactide Composites reinforced with Polyhydroxyalkanoates for Additive Manufacturing. In Proceedings of the 18th European Conference of Composites Materials (ECCM), Athens, Greece.

The author had contributed to the planning and execution of all experiments presented herein, as well as on the discussion, interpretation and preparation of the manuscript.

PLA/PHA blends can result in performance improvements without compromising biodegradability and the need of using compatibilizers [3].

Cork is a natural, versatile and sustainable material, being an emblematic material in Portugal. It is the outer bark of the oak tree *Quercus suber* L. and its main chemical composition is based on suberin (33-50%), lignin (20-25%), polysaccharides (12-20%) and extractives (14-18%). It presents tiny hollow cells of hexagonal shape in closed-cell foam [4].

Cork-polymer composites (CPC) formulation is a viable solution for the utilization of cork powder industrial residues on the development of new materials based on biodegradable thermoplastic matrices. From cork stoppers industrial processing is generated about 30 % wt. of low granulometric cork powder residues [5]. The development of CPC filaments for Fused Filament Fabrication (FFF) can potentiate new design freedom solutions and products through the combination of cork unique properties and aesthetics. FFF is an additive manufacturing (AM) technique based on an extrusion process, in which a thermoplastic filament is melted and selectively extruded via nozzle, deposited layer by layer [6].

2. Materials and Methods

2.1. Materials

Cork powder from a Portuguese cork producer was used. The material was fractionated through sieving (Retsch, Germany) and it was kept the fraction retained in the sieve of 20 μm . The polymeric matrices used were an IngeoTM Biopolymer PLA 4032D purchased from NatureWorks with a stereoisomer composition of 1.2-1.6 % D-isomer lactide and PHA from Goodfellow (PH326302). All materials were dried in vacuum oven at 70 °C for 24 h before using to stabilize the moisture content.

2.2. Blends and CPC preparation

CPC formulation was made in a Brabender type internal mixer. Initially, PLA pellets were charged and melted at 190 °C, during 2 min at 40 rotations per minute (rpm), and then cork powder was added for additional 8 min. In the case of formulations prepared with PLA and PHA, both polymers were added together at the beginning. After compounding, the mixture was granulated in a Dynisco granulator into small granules. CPC formulations containing 85 %wt. of polymeric matrix and 15 %wt. of cork powder were developed, corresponding in terms of volume percentage of 45 and 55. The chemical compositions of the different blends of PLA/PHA are described in Table 1.

Table 1. Chemical composition of the developed CPC.

Samples	Cork Powder (wt. %)	PLA (wt. %)	PHA (wt. %)
CPC 1	15.0	85.0	-
CPC 2	15.0	63.8	21.2
CPC 3	15.0	42.5	42.5
CPC 4	15.0	21.2	63.8
CPC 5	15.0	-	85.0

2.3. Mechanical analyses

Samples tensile properties were measured on a universal testing machine Autograph AG-IS (Shimadzu) with a 10kN load cell. Tests were performed at a constant crosshead speed of 1 mm/min. All measurements were done at ambient temperature and the reported results are averaged values of at least six samples. Specimens were injected using a Babyplast 610P with the conditions presented in Table 2.

Table 2. Injection moulding conditions.

Conditions	
Temperature profile (°C)	160-170-180
Injection pressure (bar)	150
Second pressure (bar)	130

The mould cavity was designed considering the standard ISO 527-2:1996 for the preparation of specimens type IV. Charpy impact tests were performed in a Ray Ran system. The impact velocity of testing of machine hammer was 2.9 m/s and the biggest impact energy of the striker was set as 0.5 J. Un-notched specimens with a dimension of 20 mm × 5 mm × 2 mm (L×W×T) were used.

2.4. Morphological analyses

Morphological studies of samples were carried out using a SEM Hitachi S4100. Fracture surface after tensile tests were analysed. Then, they were assembled on aluminium stubs and subsequently fixed in a sputter coater chamber (Polaron E 5000). Samples were sputtered with Au/Pd target for 2 minutes at 12 mA in order to avoid electrostatic charging during SEM analyses.

3. Results and discussion

3.1 Mechanical behaviour

3.1.1 Tensile tests

Figure 1 illustrates the granulated CPC 5 and the composite after injection molding along with the pure PHA biopolymer. The remaining CPC specimens presented a similar aspect.

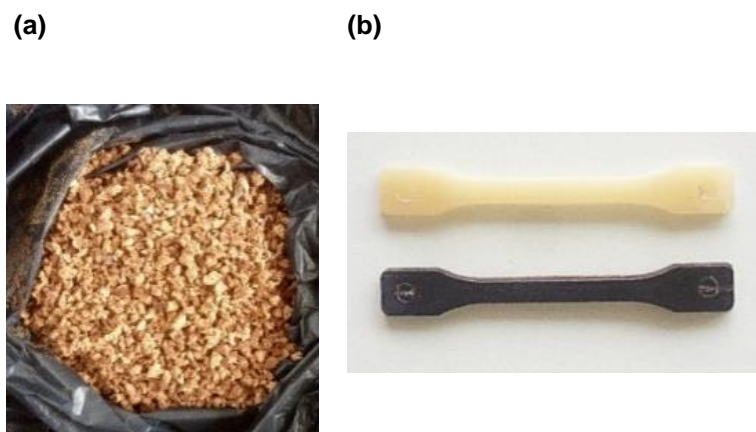


Figure 1. (a) CPC 5 granules; (b) Injected specimens for tensile tests: pure PHA and CPC 5.

The stress-strain curves of pure matrices and the corresponding CPC (CPC 1 and CPC 5) are presented in Figure 2. The tensile properties of these materials and its standard deviations, including tensile strength, maximum strain and Young modulus are given in Table 2.

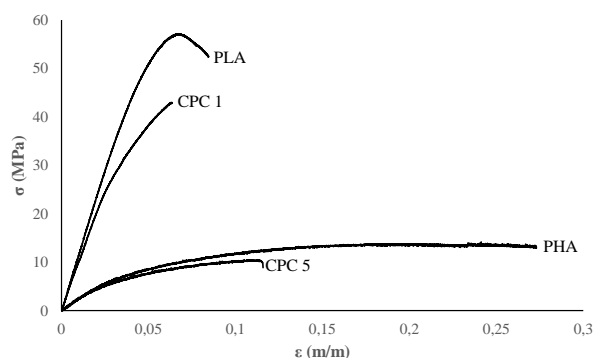


Figure 2. Tensile stress-strain curves of pure PLA, PHA, CPC 1 and CPC 5.

Table 2. Tensile properties of pure PLA, PHA, CPC 1 and CPC 5.

Samples	$\sigma_{\text{m}\acute{\text{a}}\text{x}}$ (MPa)	$\epsilon_{\text{m}\acute{\text{a}}\text{x}}$ (%)	E (MPa)
PLA	55.4 (2.2)	8.8 (1.2)	1110.9 (40.3)
PHA	14.1 (1.6)	27.3 (3.7)	227.4 (2.9)
CPC 1	41.3 (2.2)	5.8 (1.0)	1024.1 (18.9)
CPC 5	10.4 (0.9)	11.5 (1.8)	210.2 (2.9)

Pure PLA exhibited higher tensile strength when compared to pure PHA, but also showed a brittle behaviour, i.e. a lower maximum strain at break. PHA revealed an elastomeric behaviour given by a lower Young modulus and a higher strain at break.

The addition of cork led to the reduction of tensile strength for both matrices. CPC 1 presented a 25% reduction of tensile strength against the 26% shown by CPC 5. This reduction can be explained by the lower mechanical properties of cork as compared with the pure matrices. Other mechanisms can also influence the mechanical behaviour of CPC, namely (1) the type of matrix; (2) the compatibility between polymeric matrix and cork and (3) cork content [7]. A compatible polymeric matrix and filler is crucial to obtain a composite with sufficient interfacial adhesion between both materials. The maximum strain also decreased when cork was added. In this case, the elasticity of cork was not observed in both biocomposites (CPC 1 and CPC 5). It was observed a decrease in Young modulus when cork was present. This can be attributed to the lower stiffness and to the foamed cork structure, which exhibits a lower Young modulus when compared to neat biopolymers.

Three different polymeric blends and correspondent CPC were prepared based on PLA and PHA (CPC2, CPC3 and CPC 4) in order to overcome the brittleness of PLA and CPC 1 and to take advantage of cork elasticity. Tensile tests were also applied to these composites to evaluate dispersion and adhesion of PHA into PLA and the adhesion between cork particles and the polymeric blends (Figure 3).

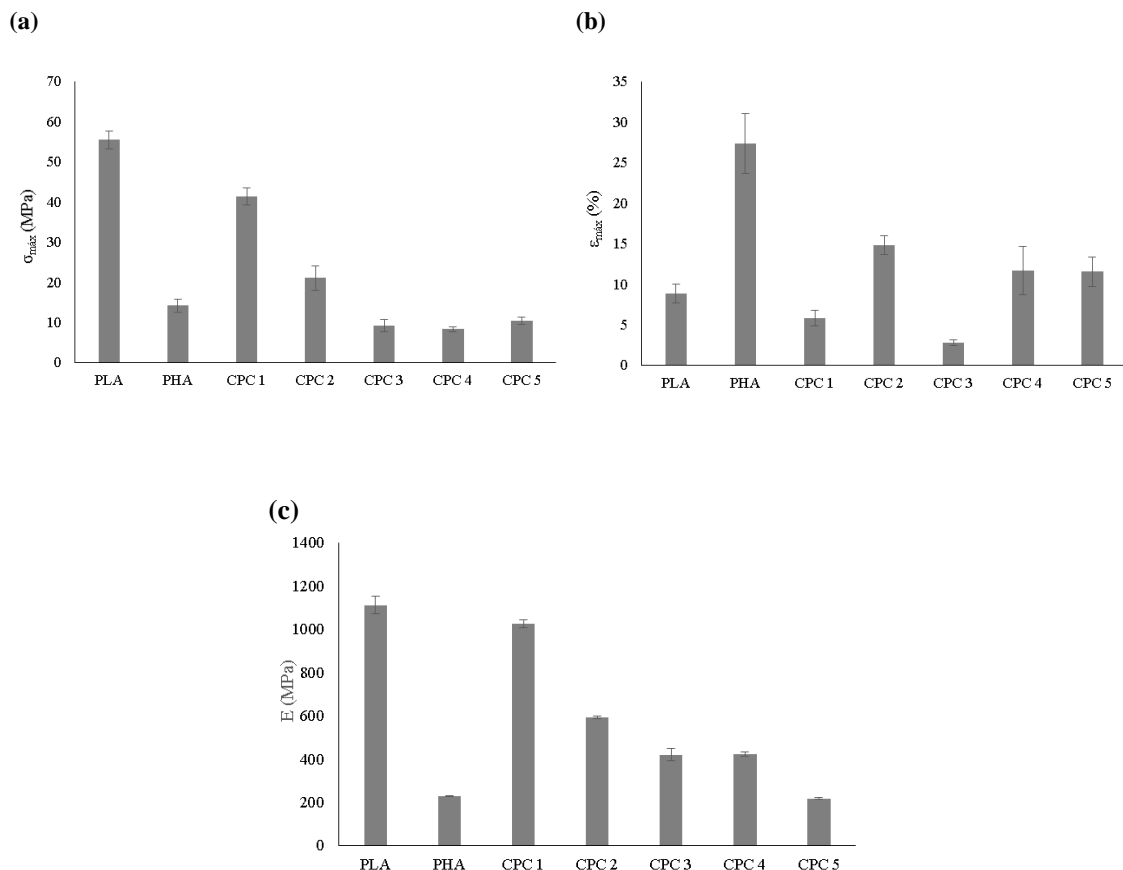


Figure 3. Tensile properties of all samples: **(a)** tensile strength, **(b)** maximum strain and **(c)** Young modulus.

From Figure 3(b), it can be seen that the addition of PHA to PLA resulted in the increase of maximum strain for CPC 2 and CPC 4 when compared to CPC 1. It can be assumed a reduction of the inherent PLA brittleness. At this point, it is important to remember that CPC 2 presents a ratio of PLA to PHA equal to 75%/25%, while CPC 4 has the opposite ratio of 25%/75%. CPC 3 has the half amount of both polymers. However, on the other hand, tensile strength and Young modulus decreased when PHA was added to the matrix. This can be associated with the lower tensile strength and Young modulus of the neat PHA, as displayed in Table 2.

3.1.2 Impact tests

Impact tests were performed and the impact strength results are presented in Figure 4. It is visible that when PHA is present in the matrix, the composites (CPC 2, CPC 3 and CPC 4) possess a higher impact strength when compared to CPC 1.

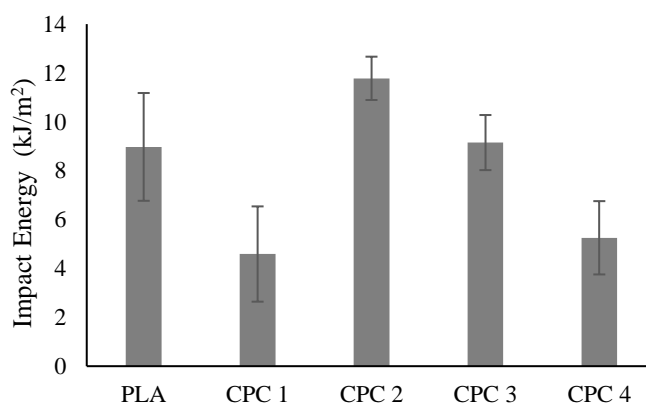


Figure 4. Impact strength of PLA, CPC 1 and composites with PLA/PHA blends.

These results can indicate a toughening effect of PHA to the PLA matrix. It is also visible that, as the amount of PHA present in the matrix increases, the mechanical behaviour became closer to CPC 1. The blend with higher impact resistance is equal to 75%/25% wt.% (PLA/PHA). This blend also exhibited higher tensile strength, maximum strain and Young modulus when compared to CPC 3 and CPC 4.

3.2 Morphological behaviour

PLA/PHA blends morphology and cork powder distribution in those blends were analysed by SEM. In Figure 5 it is represented the morphology of the blend with 50% of PLA and PHA along with the correspondent composite (CPC 3).

From Figure 5(a), it is visible a good dispersion of both polymers and the elastic behaviour of PHA. As seen in the areas surrounded by the red circles, the PHA particles presented plastic deformation (ductile behaviour) as a result of the tensile trial. In Figure 5(b) it can be seen that the polymeric matrix recovered totally the cork powder particles.

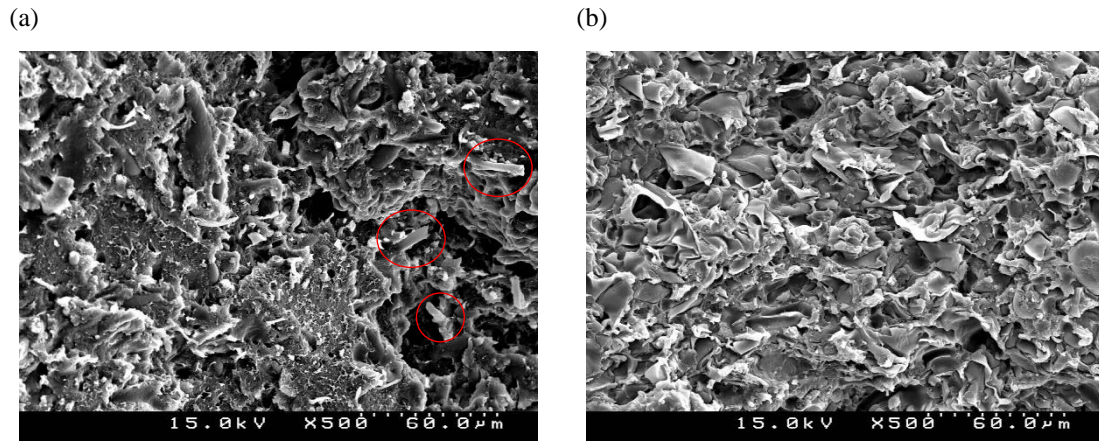


Figure 5. SEM images of: (a) PLA/PHA (50%) blend and CPC 3.

4. Conclusions

This work showed that a more elastic behaviour was obtained when PHA was added to PLA. The composites prepared with PLA/PHA blends exhibit a more ductile behaviour when compared to CPC 1. In addition, the impact strength was also improved when PHA was added to the matrix, revealing the toughening effect of PHA. Morphological analyses revealed a good dispersion of PHA into PLA and a good dispersion of cork powder particles into the polymeric matrices.

The combination of cork powder residues into polymeric matrices can lead to the development of sustainable composites. The use of such composites on the development of filaments for FFF technology can bring new design solutions and products.

Acknowledgments

This work was supported by COMPETE 2020 – Programa Operacional Competividade e Internacionalização within TT@ESAN project (NORTE-01-0246-FEDER-000001).

References

- [1] V.K. Thakur, *Lignocellulosic Polymer Composites: Processing, Characterization and Properties*, Scrivener Publishing, Wiley, 2015.
- [2] J.P. Greene, *Sustainable Plastics: Environmental Assessments of Biobased, Biodegradable, and Recycled Plastics*, John Wiley & Sons, Inc., New Jersey, 2014.
- [3] P.N. Tri, S. Domenek, A. Guinault, C. Sollogoub, Crystallization behavior of poly(lactide)/poly(β -hydroxybutyrate)/talc composites, *J. Appl. Polym. Sci.* 129 (2013) 3355–3365.
- [4] H. Pereira, *Cork: Biology, Production and Uses*, Elsevier, Amsterdam, 2007.

- [5] E.M. Fernandes, I.M. Aroso, J.F. Mano, J.A. Covas, R.L. Reis, Functionalized cork-polymer composites (CPC) by reactive extrusion using suberin and lignin from cork as coupling agents, *Compos. Part B Eng.* 67 (2014) 371–380.
- [6] S.B. Gibson I, Rosen D, *Additive Manufacturing Technologies: 3D Printing, Rapid Prototyping, and Direct Digital Manufacturing*, Second Edi, Springer, New York, 2015.
- [7] E.M. Fernandes, V.M. Correlo, J.F. Mano, R.L. Reis, Cork–polymer biocomposites: Mechanical, structural and thermal properties, *Mater. Des.* 82 (2015) 282–289.

3.4 Cork-like Filaments for Additive Manufacturing^j

S. P. Magalhães da Silva ^{a,b,c*}, T. Antunes ^c, M. E. V. Costa ^c, J. M. Oliveira ^{a,b,c}

^a EMaRTGroup – Emerging: Materials, Research, Technology

^b School of Design, Management and Production Technologies, University of Aveiro, Estrada do Cercal, 449, Santiago de Riba-Ul 3720-509, Oliveira de Azeméis, Portugal

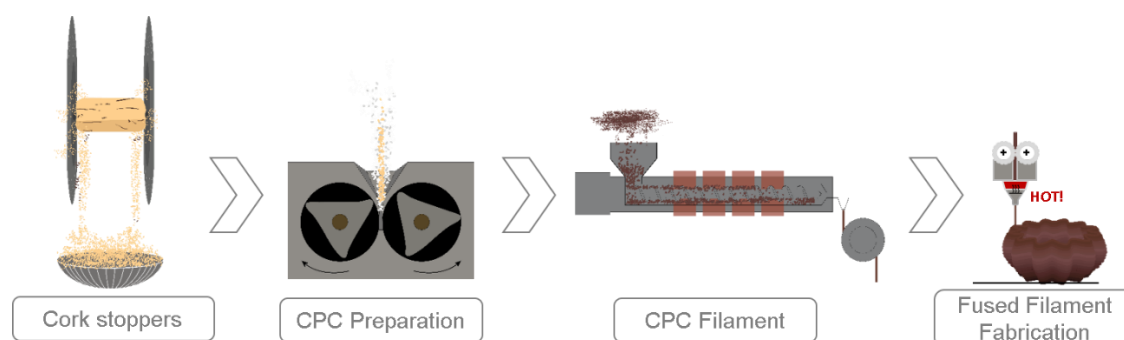
^c Aveiro Institute of Materials (CICECO), University of Aveiro, Campus Universitário de Santiago, 3810-193 Aveiro, Portugal

*corresponding author: sarapms@ua.pt

Abstract

A cork-like filament fully biodegradable and filled with low granulometry cork powder residues was developed. Cork-polymer composites (CPC) were prepared using a Brabender type mixer incorporating 15% (w/w) of cork powder (corresponding to 55% (v/v)) and having polylactic acid (PLA) as matrix. In order to promote a chemical adhesion between cork particles and PLA, the effect of maleic anhydride grafted PLA (MAGPLA) was studied. Fourier Transform Infrared – Attenuated Total Reflection (FTIR-ATR) analysis was used to evaluate the functionalization of MAGPLA onto the polymeric chain. The addition of MAGPLA enhanced the mechanical behaviour by increasing tensile properties while improving the dispersion of cork particles within PLA matrix. In addition, cork particles and MAGPLA acted as nucleating agents during PLA melting process. To evaluate the printability of the developed CPC filament, specimens were printed by Fused Filament Fabrication (FFF) and compared to those obtained by injection molding (IM). FFF allowed to preserve the cork alveolar structure in the specimens, benefiting CPC mechanical behaviour. 3D parts could be printed with the CPC filament thereby demonstrating the usefulness of the fully biodegradable cork-based filament here developed. 3D printed parts exhibit unique characteristics, such as a non-plastic and warm touch, a natural colour and the release of a pleasant odour during the printing process.

Graphical Abstract



^j Magalhães da Silva, S. P., Antunes, T., Costa, M. E. V., Oliveira, J. M. Cork-like Filaments for Additive Manufacturing, *Addit. Manuf.* 2020, **34**, 101229-101238.

The author had contributed to the planning and execution of all experiments presented herein, as well as on the discussion, interpretation and preparation of the manuscript. Tatiana Antunes contributed to the experimental procedure related to the preparation of MAGPLA and composites formulations.

Keywords: Cork; Composites; Material Extrusion; Additive Manufacturing; Coupling agent

1. Introduction

Additive manufacturing (AM) processes involve a set of technologies that produce parts using a layer-by-layer approach. A wide range of materials can be considered for AM, from polymers, metals, ceramics to composite materials. Main advantages of AM are (i) the production of highly customized and also, complex parts without tooling, (ii) a faster product development and manufacturing resulting in a quicker time to market and (iii) on-demand manufacturing by adapting to the market needs [1]. Efforts are being made to change the stigma of AM association to prototyping, with attempts to connect AM to production. Fused Filament Fabrication (FFF) is one of the AM techniques, which builds parts through the extrusion of fused thermoplastic materials. FFF is the most affordable technology with a widespread use, fostered by the development of open-source FFF printers. A lot of effort has been put on the development of a wide range of filament solutions, from low-cost filaments for prototyping/general applications to high-end filaments for technological applications [2–5]. Anisotropy, porosity, layer adhesion and resolution are the main disadvantages when it comes to FFF [6].

Cork is a natural product and Portugal is its main producer in the World. Cork is the outer bark of the *Quercus suber* L. oak tree, which is harvested every 9 years. Owing to its chemical composition, mainly suberin and lignin, and its honeycomb structure composed by closed cells filled with gas, cork has a unique set of properties. Such properties include low density, hydrophobic behaviour, high elastic behaviour and thermal, acoustic and electrical insulation properties [7]. Wine stoppers continue to be the major industrial application of cork. The rectification phase of the cork stoppers production, which involves top- and bottom polishing of stoppers, generates cork powder residues with low granulometries ($< 500 \mu\text{m}$) [8]. These small cork particles are not used in the development of cork-based products, being usually burned or disposed in landfills. Other well-known cork-based products are insulation boards, wall and floor covering, impact absorption artefacts and aeronautical applications [9–12]. The development of bio-based cork composites for FFF was triggered by the search of new applications for cork and, also by the need to add value to the low granulometry cork powder residues.

Poly(lactic acid) (PLA) is the most abundant biopolymer with properties similar to those of synthetic polymers. It can be found in the market as a biodegradable filament solution. PLA is an aliphatic polyester obtained from ring-opening polymerization of lactide, used as monomer. Lactide results from the depolymerisation of lactic acid obtained by fermentation of sugar from plant-based materials. PLA can be processed by the technologies commonly applied to commercial polymers, such as extrusion, injection moulding, thermoforming and injection blow moulding [13]. However, PLA brittleness, slow crystallization rate, hydrophobicity and high cost limit its extended commercialization [14,15]. Within this context, several strategies are being undertaken to overcome these drawbacks, namely the addition of plasticizers [16,17], blending PLA with other synthetic or biodegradable polymers [18,19], addition of reinforcement fillers [20–22] and grafting with

compatibilizers [23,24]. The development of sustainable composites with improved thermal and mechanical properties imply the addition of a compatibilizer to improve the interfacial adhesion between the hydrophobic polymeric matrix and the hydrophilic lignocellulosic fibers. Maleic anhydride (MA) is the most used compatibilizer due to its reactivity and biodegradability [25]. There are several ways to functionalize PLA with MA, being melt functionalization the most applied one [21]. MA grafted PLA (MAgPLA) reacts with hydroxyl groups existing on the surface of natural fibers, creating chemical bonds that bridge polymer and fibers, resulting in composite materials not only with mechanical adhesion but also with improved chemical adhesion between its constituents [21,26]. Numerous studies exploring the development of cork or wood-based 3D printing filaments are found on the literature [4,27–32] and some filaments are already available in the market [33,34]. Kariz *et al.* [4] evaluated the effect of wood content ranging from 0% to 50% (w/w) on the properties of six filaments using PLA as matrix. They concluded that adding more than 10% (w/w) of wood resulted in a decrease of 45% on tensile strength, when compared to pure PLA filaments. Also, as the wood content increases, the surface finishing of printed parts becomes rougher, combined with the presence of voids and wood particle clusters.

The aim of this work was to develop a cork-based and fully biodegradable filament for FFF. Obtaining a filament that exhibits a non-plastic appearance while offering a warm touch after printing was also a goal of this project. This work is part of a continuous research presented elsewhere [35–38]. Thermal, chemical and morphological characterization of the developed cork-polymer composites (CPC) is here assessed. In addition, mechanical and morphological analyses were carried out on injected and printed CPC specimens. The effect of MAgPLA on CPC behaviour was also studied.

2. Methodology

2.1 Cork

Cork powder residues from a Portuguese cork company were used. The as-received material was fractionated through sieving (Retsch, Germany) using a vibrational sieve shaker. The amplitude used on sieve shaker was 70. Sieves with sizes varying from 200 to 20 μm were used [38]. Particle size distribution (PSD) was determined by measuring the powder mass retained in each sieve and by the design of the cumulative curve, as seen in Fig. 1. The presented values correspond to the average of 3 trials. Through Fig. 1, it is visible that the as-received cork powder presents a bimodal volume distribution over the 40-63 μm and 100-200 range.

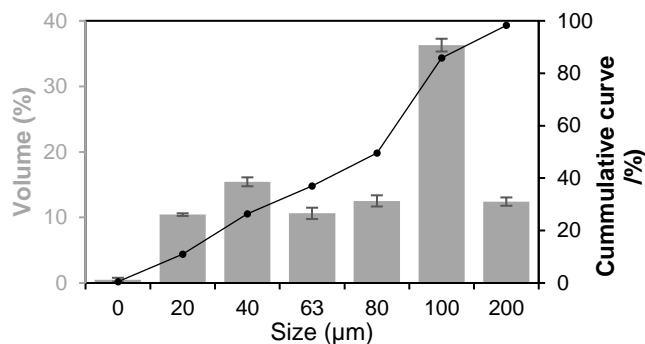


Fig. 1. Particle size distribution of as-received cork powder.

For composites preparation, it was retrieved the cork powder retained in the 40 µm sieve. The average pore diameter as well as the bulk density of this cork powder were determined by mercury intrusion porosimetry (MIP). For that, cork powder was previously dried in a vacuum oven (70 °C) for 24 h. The experiment was conducted in a Micromeritics Auto-pore IV 9500 apparatus. Mercury was then forced to enter into the pores under a pressure ranging from 0.3 MPa to 227 MPa. MIP characterization results of cork powder are presented in Table 1. The reason for the selection of this particle size was related to the typical nozzle size of FFF extrusion system.

Table 1. Cork powder characterization by MIP.

Average pore diameter (µm)	23.3
Bulk density (g/cm ³)	0.156
Apparent Density (g/cm ³)	0.694
Porosity (%)	77.6

2.2 Composites formulation

A PLA with reference 4032D (Ingeo™) from NatureWorks was used and presents a stereoisomer composition of 1.2-1.6 % D-isomer lactide [37,38]. It presents a melting point lying between 155 and 170 °C and a melt flow index (MFI) of 4.60 g/10 min (190°C, 2.16 Kg). The method used for composites formulation is published elsewhere [37,38]. To remove the moisture content, cork powder and PLA were dried at 70 °C during 24h in a vacuum oven (Carbolite AX60 model). In Table 2 are displayed the compositions of the developed CPC. A Brabender type internal mixer was used to prepare the composite materials. The formulation of MAgPLA was also performed by melt functionalization.

Table 2. CPC formulation compositions.

Samples	PLA (w/w %)	Cork (w/w %)	MAgPLA (w/w %)
CPC 1	85	15	-
CPC 2	81	15	4

Firstly, PLA was charged and melted at 190 °C, during 2 min at 40 rpm, and then cork powder was added and mixed for an additional 8 min. Then, composite materials were granulated into granules (0.5–1.0 mm) using a granulator (Dynisco). The volumetric composition of the final mixture is 45 vol. % of polymeric matrix and 55 vol. % of cork powder, respectively. For CPC 2 preparation, MAgPLA was added together with PLA.

2.3 Thermal analyses

Differential scanning calorimetry (DSC) analysis was employed to evaluate samples thermal behaviour using a Shimadzu DSC-60 equipment. Samples weighing from 8.0 to 10.0 mg were conditioned in aluminium pans and the experiments were carried out in air atmosphere. The temperature profile employed was of 20 to 200°C with a heating rate of 2.5°C/min. The second run was the one considered to determine thermal properties, such as glass transition temperature (T_g), cold crystallization temperature (T_{cc}), melting temperature (T_m), cold crystallization enthalpy (ΔH_{cc}). Melting (ΔH_m) and cold crystallization (ΔH_{cc}) enthalpies were also calculated and the crystallinity degree (X_c) was determined by Eq. 1.

$$X_c = \frac{\Delta H_m - \Delta H_{cc}}{\Delta H_m^0 (1 - w)} \times 100 \quad (1),$$

where w is the percentage weight of cork and ΔH_m^0 is the melting enthalpy for 100% crystalline PLA ($\Delta H_m^0 = 93.0$ J/g) [39].

2.4 Chemical analyses

Fourier Transform Infrared – Attenuated Total Reflection (FTIR-ATR) measurements were performed in Bruker Tensor apparatus equipped with an ATR golden gate (diamond) from Specac®. Each spectrum was obtained from 256 scans with a 4 cm⁻¹ resolution in absorbance mode in the range of 4000-400 cm⁻¹. An average of 3 trails for each sample was considered.

2.5 Mechanical analyses

Mechanical tests were performed using the procedure published elsewhere [37,38]. A universal testing machine Autograph AG-IS (Shimadzu) with a 10kN load cell applying a constant crosshead speed of 1 mm/min was used. Tests were performed at ambient temperature and at least six measurements were made for each sample. The tensile strength (σ_{max}) and elongation at break (ϵ_{max}) were taken as the maximum values from the stress-strain curve. Only for comparison purposes, the Young modulus (E) was estimated from the initial slope by linear regression. A micro-injection moulding machine (Babyplas® 610P) was used to prepare the specimens using the conditions presented in Table 3.

Table 3. Injection moulding conditions.

Temperature profile (°C)	180-185-190
Injection pressure (MPa)	13
Second pressure (MPa)	10

Mould cavity was machined considering the preparation of specimens type IV, according to ISO 527-2:1996 standard [40].

2.6 Density

The density (ρ) of samples was determined using an analytic balance (Explorer Pro 210, Ohaus) equipped with a density determination kit (Ohaus, 80253384 model). Distilled water at 25°C was used as immersion medium. For each sample, six measurements were performed being the average value presented here.

2.7 Filament extrusion

CPC 2 filament was prepared using a 3Devo NEXT 1.0 extruder with temperatures ranging from 170 to 190°C [37]. A filament thickness of 1.75 mm was obtained with a tolerance deviation of 5 μm .

2.8 FFF printing conditions

Filaments of PLA and CPC filament were printed into specimens according the standard ISO 527-2:1996 (specimens type IV) [40]. In Fig. 2 is presented a scheme with the performed steps from the filament until the printed parts. A Delta WASP 3D printer was used with a 0.4 mm diameter stainless steel nozzle.

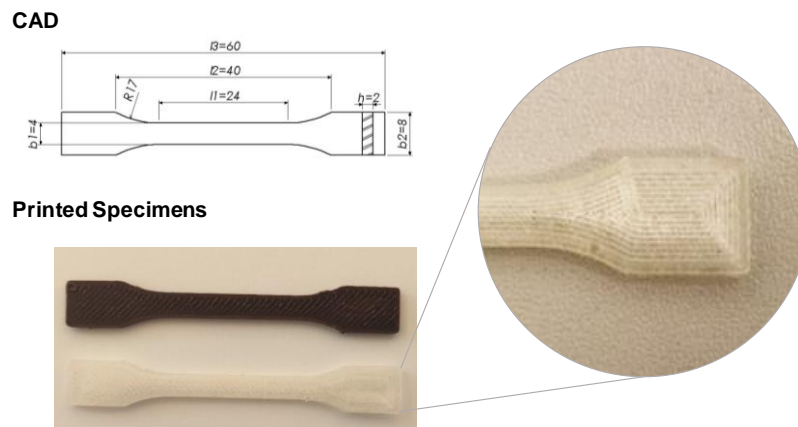


Fig. 2. Scheme representing the steps from the filament to the printed parts. The last image focuses the concentric infill pattern used.

The printing head was set to 40 mm/s, the nozzle temperature to 190°C and the printing bed temperature to 40°C, for preventing the printed material from warping. It was applied a concentric

infill pattern with a layer height of 0.06 mm and an infill percentage of 100%, as published elsewhere [38]. Cura software was used to generate the G-code.

2.9 Morphological analyses

Scanning electron microscopy (SEM) analyses were performed using a SEM Hitachi S4100 equipment. Fracture surfaces obtained after tensile tests of both injected and printed specimens were analysed. The samples were prepared using the methodology published elsewhere [38]. Samples were assembled on aluminium stubs and, then, fixed in a sputter coater chamber (Polaron E 5000). Consequently, to avoid electrostatic charging, samples were sputtered with an Au/Pd target for 2 minutes at 12 mA.

3. Results and Discussion

3.1 Thermal and chemical characterization

DSC melting thermograms of all samples are presented in Fig. 3 and the correspondent thermal parameters are listed in Table 4. PLA exhibited a double melting peaks, while MAgPLA and composites showed a single peak, with T_m values ranging from 150 to 169°C. The lower T_m of PLA in comparison to other materials can be attributed to a more cohesive polymeric structure. In addition, the presence of a double-melting peak can be attributed to the occurrence of melting of thinner lamellae followed by the melting of crystals derived from melt-recrystallization [41].

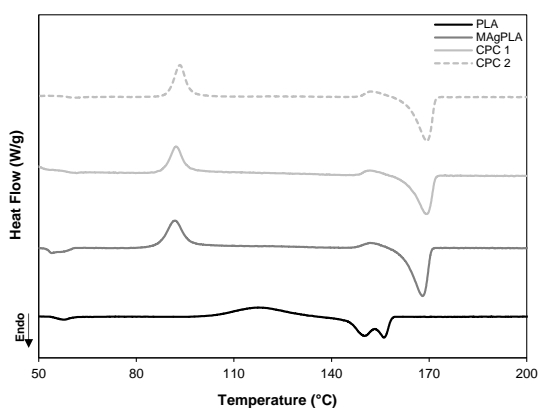


Fig. 3. DSC thermograms of all studied samples.

A shift to lower T_{cc} values occurred when cork was added to the PLA matrix. This is an indication that cork promotes the initial cold crystallization of the PLA matrix due to the heterogeneous nucleation effect. An increase of the crystallinity degree was observed reinforcing the nucleating ability of cork. Also, the presence of MA contributed to the increase of the crystallinity degree of the

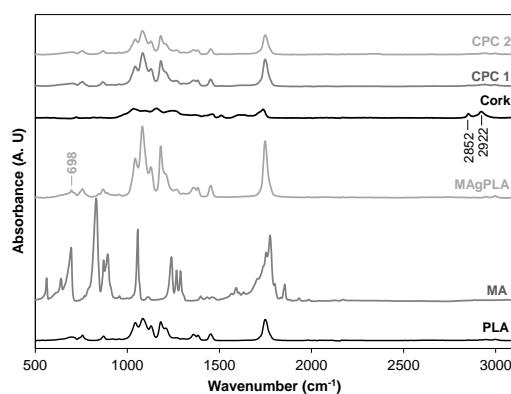
polymeric matrix. The same tendency was visualized in a previous work performed by Oliveira and co-workers [42].

Table 4. Samples thermal parameters obtained from DSC thermograms.

Samples	T_{cc} (°C)	ΔH_{cc} (J/g)	T_m (°C)	ΔH_m (J/g)	X_c (%)
PLA	118.3	29.3	150.1; 156.2	-35.9	7.2
MAGPLA	91.9	33.7	168.0	-47.2	14.6
CPC 1	92.7	25.6	169.6	-37.5	15.1
CPC 2	93.4	28.0	169.2	-43.0	19.0

Fig. 4 presents the FTIR-ATR spectra of all the studied samples. These analyses were made in order to firstly evaluate the grafting of MA onto PLA chain and then to access the interaction of MAGPLA with cork (CPC 2).

(a)



(b)

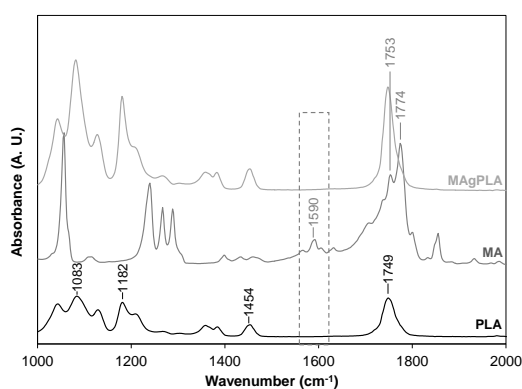


Fig. 4. FTIR-ATR spectra of (a) all studied samples and (b) zoom-out of PLA, MA and MAGPLA spectra to evidence MA functionalization onto PLA molecular chain.

The characteristic peaks of PLA can be well identified, namely the peak at 1749 cm^{-1} , which is attributed to C=O stretching of PLA ester group. Also the peaks at 1182 cm^{-1} and 1083 cm^{-1} , both related to the C–O bond, are detected [20,43]. For MA, it is also visible its distinguishing peaks, such as the peak at 1590 cm^{-1} , which corresponds to the cyclic C=C stretching of anhydride, and the peaks at 1753 and 1774 cm^{-1} associated with the asymmetric stretching of the carbonyl group (C=O) of the cyclic anhydride [21,44]. For MAgPLA spectrum, the absence of the peak at 1590 cm^{-1} is noticed (box delimited area in Fig. 4 (b)) thereby suggesting that MA was grafted onto the PLA chain. The same tendency was observed by Raghu *et al.* [44]. In addition, the presence of the peak at 698 cm^{-1} also indicates that MA was grafted onto the PLA by the bending of the CH group of the anhydride ring [23]. The FTIR-ATR spectrum of cork exhibited the characteristic peaks assigned to suberin, namely the absorption peaks at 2922 cm^{-1} and 2852 cm^{-1} corresponding to asymmetric and symmetric vibrations of C-H, respectively [7]. Vibrations at 1738 cm^{-1} (C=O in suberin), 1159 cm^{-1} (C-O-C ester group in suberin) and 1242 cm^{-1} (C-O stretch in suberin) can also be found. The presence of lignin (guaiacyl) was detected by the vibration peaks at 1510 cm^{-1} and 1463 cm^{-1} [7]. Concerning the composite materials, the addition of cork to PLA (CPC 1) resulted in a spectrum similar to that of pure PLA (vibration peaks at 1083 , 1182 and 1749 cm^{-1}). This can be attributed to the poor interaction between the filler and the polymeric matrix. In the case of CPC 2, those characteristic vibration peaks of PLA shifted to 1081 , 1180 and 1747 cm^{-1} , respectively, suggesting that interactions between cork and PLA were improved.

In order to perform an accurate analysis without the influence of experimental procedure, these characteristic peaks were normalized by the absorbance peak of PLA at 1454 cm^{-1} . The peak at 1454 cm^{-1} is associated with CH_3 bending vibration, being an internal characteristic peak of PLA [43,45]. In Fig. 5 are displayed the absorbance ratios of pure PLA, MAgPLA, CPC 1 and CPC 2. It is observed that the grafted PLA exhibits a higher intensity of vibration peaks of carbonyl and ether groups due to the presence of MA.

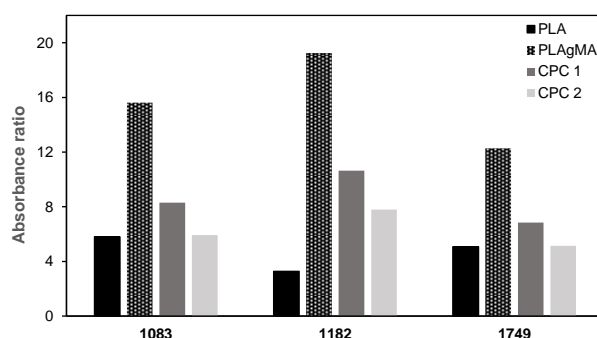


Fig. 5. Absorbance ratio of peaks at 1083 , 1182 and 1749 cm^{-1} for pure PLA, MAgPLA, CPC 1 and CPC 2.

Comparing the vibration peak intensities of both composites, the reduced intensity values for CPC 2 can be an indication of an esterification reaction between the hydroxyl groups of cork and MA [21].

3.2 Effect of MAgPLA on CPC mechanical behaviour

The effect of the addition of MAgPLA on the mechanical behaviour of CPC was evaluated. Tensile properties of the developed materials, namely σ_{\max} , ϵ_{\max} and Young modulus (E) are presented in Fig. 6.

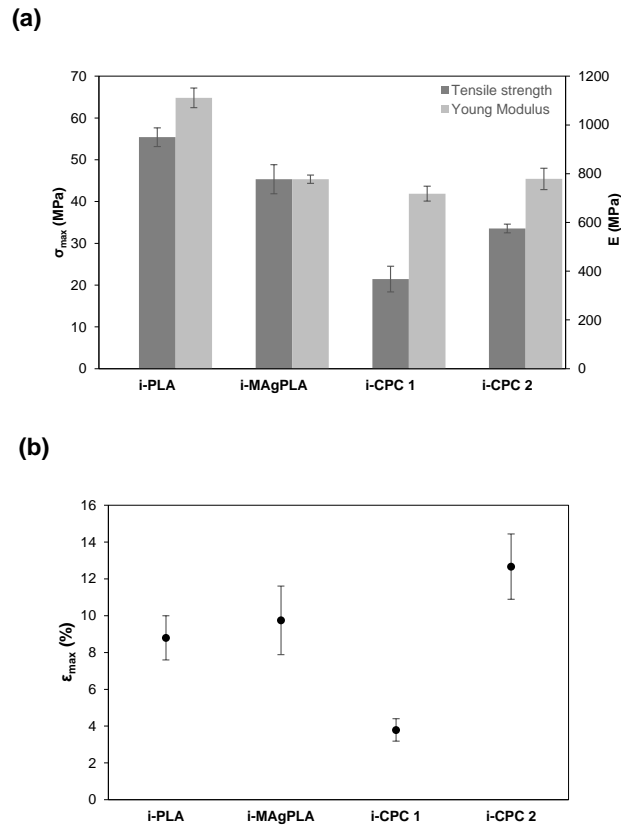


Fig. 6. Mechanical properties of the injected PLA, MAgPLA, CPC 1 and CPC 2: **(a)** tensile strength (σ_{\max}) and Young modulus (E); **(b)** elongation at break (ϵ_{\max}). Note: *i*- stands for the injected specimens.

When compared to composites, pure i-PLA exhibits higher tensile strength and modulus. The incorporation of cork into the PLA matrix led to a decrease of $\approx 61\%$ on the σ_{\max} and $\approx 35\%$ on the Young modulus (i-CPC 1). The decrease on Young modulus can be attributed to the characteristic lower stiffness and foamed structure of cork. Neat PLA is a brittle material and when cork is added to the matrix (i-CPC 1) a decrease of $\approx 59\%$ on the ϵ_{\max} is noticed. The effect of the high pressure applied during IM process may have an impact on the mechanical properties of composites. Since cork is a cellular material, the high pressure applied will compress the honeycomb structure and the intrinsic cork properties will be damaged. It is known that other mechanisms can also influence the mechanical behaviour of CPC, namely (1) the type of matrix; (2) the compatibility between cork and polymeric matrix; (3) the cork content; and, (4) the dispersion within the matrix and homogenization [37,46]. In order to improve the mechanical behaviour of CPC 1, the effect of a coupling agent to

promote the adhesion of cork to PLA was evaluated. To the PLA-Cork system, it was added 4% (w/w) of MAgPLA. The selected amount of MAgPLA was based on previous studies [42,47].

As a result of the addition of MAgPLA to PLA-Cork system, an increase of $\approx 56\%$ on σ_{\max} , of $\approx 8\%$ on Young modulus and of $\approx 234\%$ on the ϵ_{\max} were attained. This enhancement of tensile properties can be attributed to the improvement of the interfacial adhesion between the polymeric matrix and cork particles resulted by the formation of covalent and hydrogen bonds between the hydroxyl and anhydride groups. The presence of a coupling agent, such as MA, improves the stress transfer between polymer and filler resulting on the enhancement of composites mechanical behavior. Fig. 6 also shows that MA can act as a plasticizer by reducing σ_{\max} and tensile modulus, and by increasing the ϵ_{\max} (i-MAgPLA) [17]. On the other hand, Fourati *et al.* [48] reported an increase of 21% on σ_{\max} , of 314% on Young modulus and of 105% on ϵ_{\max} when 2% of MA-based coupling agent was added to a Thermoplastic Starch/Polybutylene Adipate Terephthalate blend.

Several studies on the use of coupling agents in lignocellulosic composites and consequent improvement of mechanical properties are found on the literature. A study from Raghu *et al.* [44] on the development of thermoplastic starch/PLA blends showed that the presence of 10% of MAgPLA and 20% of wood fiber induced a 86% improvement on σ_{\max} and a 106% raise on flexural strength. Fernandes *et al.* [26] reported that the addition of 4 wt.% of polypropylene grafted maleic anhydride promoted an increase of 20% on σ_{\max} and of 19% on ϵ_{\max} of CPC. The effect of the same amount of coupling agent showed an increase of 19% on σ_{\max} and of 21% on ϵ_{\max} for PLA/Soy protein composites [49]. The mechanical properties of composites are influenced by coupling agents being relevant the following factors: (i) the amount added to the matrix/fiber, (ii) the saturation of the matrix/fiber interface, (iii) the functionalization site and (iv) its functionality [21].

In Fig. 7 are shown SEM micrographs of pure PLA, cork particles and composite materials. PLA exhibited a brittle behaviour reflected on a smooth surface fracture (Fig. 7 (a)). [50]

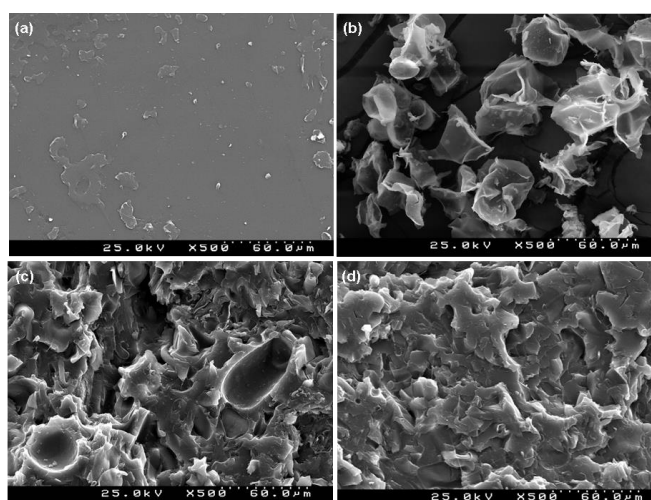


Fig. 7. SEM images of (a) pure PLA; (b) cork powder; (c) i-CPC 1; (d) i-CPC 2.

Cork powder residues used in this work came from an industrial polishing process of cork stoppers. In Fig. 7. (b), it is possible to observe that some cork alveolus remain closed, while few of them are damaged as a result of the grinding process. According to Flores *et al.* [51], cork elastic properties are more affected by the content of damaged cells than by their size. This effect on elastic properties is more pronounced for particles smaller than 200 μm . The addition of MAgPLA results on the disappearance of voids and an undetectable interface between cork particles and polymer matrix, as observed when comparing CPC 1 and CPC 2 (Fig. 7 (c)-(d)). SEM micrographs thus reveal that MA acts as a compatibilizing agent by improving the interfacial adhesion between matrix and filler. These results support those obtained from mechanical analysis.

3.3 Effect of printing conditions on CPC mechanical behaviour

The mechanical behaviour of 3D printed parts should present a behaviour similar to that of parts obtained by conventional methods [52]. Besides manufacturing technologies, the mechanical behaviour of parts is also dependent on the properties of the material itself. For parts printed by FFF the anisotropy acquired during printing is the major problem that is related mainly to the layer size and its consequent thickness. In Fig. 8 is displayed SEM micrographs of a CPC specimen to emphasize the homogeneity and adhesion of printed layers and the average layer height of 60 μm . Printing parameters also influence the mechanical behaviour, such as raster angle, air gap between layers, filament orientation and build direction [52–56]. According to Letcher *et al.* [55], printed PLA exhibited higher tensile strength for a raster angle of 45°. In addition, a study reported by Chacón *et al.* [53] showed that samples produced with flat and on-edge orientations had the highest tensile strength and stiffness values. It is important to point out that these were the printing conditions applied in this study.

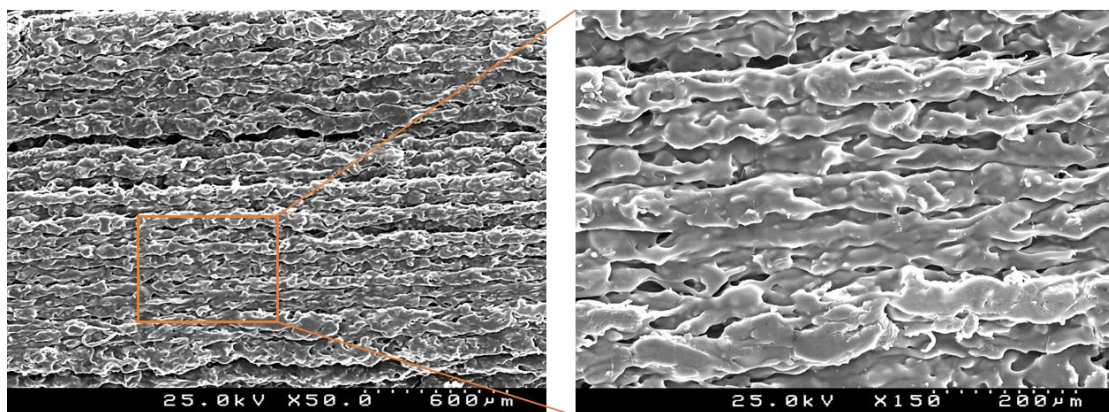


Fig. 8. SEM images of printed CPC specimen.

The mechanical behaviour of printed and injected specimens of PLA and CPC 2 are presented and compared in Fig. 9. As observed, p-PLA sample shows a $\approx 12\%$ reduction of tensile strength as

compared to i-PLA. This reduction can be due to the porosity associated with the FFF process, as can be seen in Fig. 10 (b). In the case of CPC 2, both injected and printed specimens display similar σ_{\max} and E values. The higher ϵ_{\max} value observed for the injected part can be attributed to the rapid cooling down of the molten CPC 2 after the injection process. Contrarily, in the FFF process, CPC 2 is subjected to a longer thermal treatment resulting in a lower cooling rate and, consequently, a higher crystallinity degree.

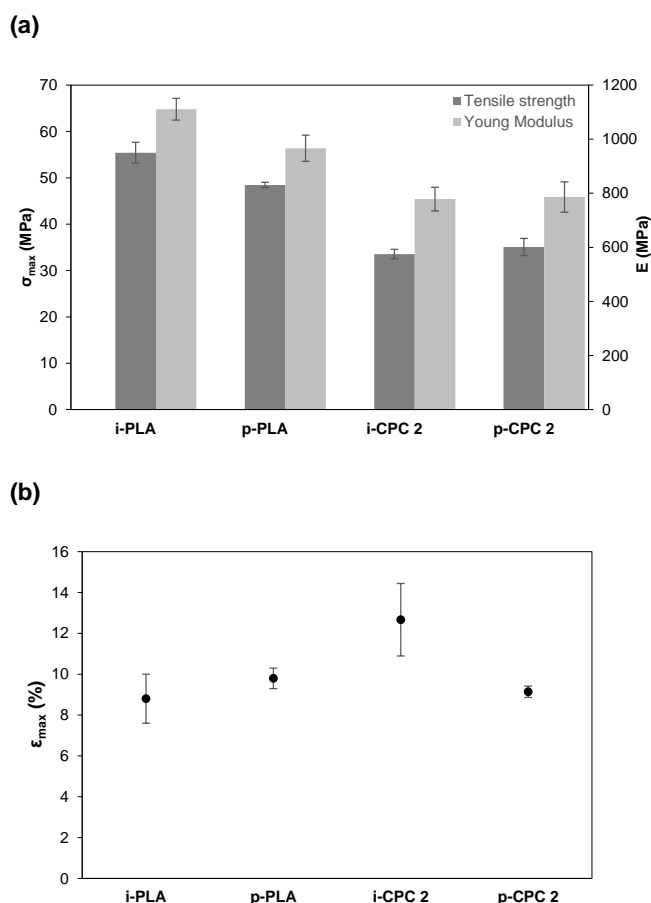


Fig. 9. Mechanical properties of the injected and printed specimens of PLA and CPC 2: **(a)** tensile strength (σ_{\max}) and Young modulus (E); **(b)** elongation at break (ϵ_{\max}).

The same tendency was observed by Zhu *et al.* [57], where these differences on the crystallization behaviour resulted in higher σ_{\max} and E values and lower ϵ_{\max} values for printed parts, when compared to the IM parts.

SEM micrographs of the injected and printed specimens are presented in Fig. 10. It can be seen that i-CPC 2 and p-CPC 2 specimens exhibit different fracture mechanisms. i-CPC 2 exhibits a fracture mechanism governed by the matrix while p-CPC 2 shows an intergranular fracture mechanism. A hypothesis for these distinct fracture mechanisms is being currently studied and it can be related to the different magnitude of pressures applied during IM and FFF processes, which can be classified as high- and low-pressure processes, respectively.

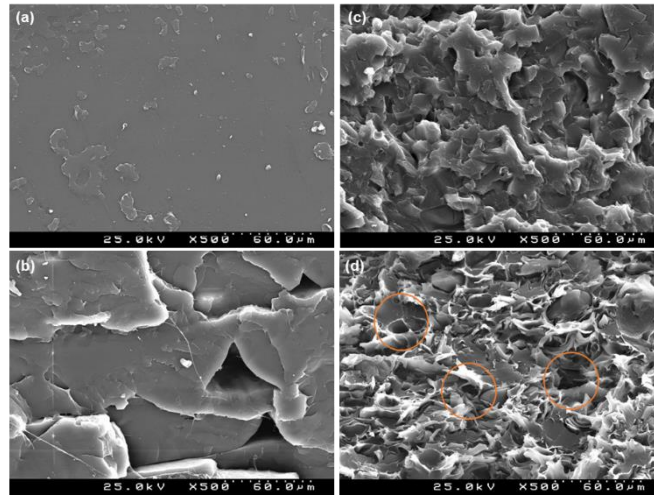


Fig. 10. SEM images of injected and printed specimens: **(a)** i-PLA, **(b)** p-PLA, **(c)** i-CPC 2 and **(d)** p-CPC 2.

3.4 Density of injected and printed specimens

In Table 5 the density values for injected and printed specimens are listed. The processing technology and the presence of cork particles affected the density values. As expected, the injected specimens present higher density values than the printed ones. This is due to the higher pressures applied during the injection moulding process as compared to the lower pressures associated to the filament extrusion printing process. The addition of cork did not induce a significant reduction of specimens' density.

Table 5. Density values for injected and printed specimens –
 $\rho(\text{PLA})$ equal to 1.24 g/cm^3 [58].

Specimens	ρ (g/cm^3)
i-PLA	1.26 ± 0.01
i-MAgPLA	1.26 ± 0.02
i-CPC 1	1.22 ± 0.01
i-CPC 2	1.24 ± 0.08
p-PLA	1.11 ± 0.05
p-CPC 2	1.19 ± 0.02

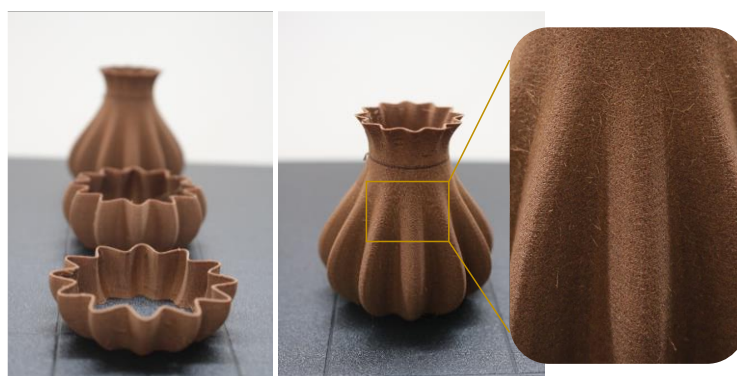
This tendency could be associated with the densification of cork particles caused by the pressures applied in both processing methods, also reported by Fernandes *et al.* [46,59]. As it is already known, cork low density is related to its honeycomb structure composed by cells filled with gas. However, in this study, cork powder results from the polishing stage of cork stoppers production, in which the honeycomb cork structure is damaged to some extent. It can be assumed that the contribution of

cork particles to the density measurements of composites is associated to the density of cork cell wall, which is estimated to be 1.25 g/cm^3 , and also, to the incorporation of PLA into that same damaged cork cells [51].

3.5 Case-study | Printed parts

Fig. 11 shows examples of printed parts using CPC 2 filament. Parts exhibited a non-plastic appearance and a warm touch, similar to that of cork, as well as a smooth surface finishing. An interesting characteristic when using CPC 2 filament is the pleasant smell that is released during the printing process. This is an important feature for desktop printers.

(1)



(2)



Fig. 11. Examples of printed parts using CPC 2 filament.

The obtained dark-brownish colour is related to the natural colour of cork. The development of CPC filaments presenting new colours solutions is now being conducted.

4. Conclusions

A filament composed by industrial low granulometry cork residues and a biodegradable matrix was developed. The use of these residues on the development of filaments provides a new material solution for AM world with unique characteristics, namely a non-plastic and warm touch, a natural colour and the release of an agreeable odour during the printing process.

PLA was functionalized with MA by a melt functionalization process and the extent of MA grafting was evaluated through FTIR-ATR analyses. The addition of MAgPLA during composite preparation promoted the adhesion and dispersion of cork particles into the polymeric matrix, resulting in an increase of the tensile properties. Both cork and MAgPLA materials acted as nucleating agents during PLA melting process. The specimens prepared by FFF allowed the cork to preserve its alveolar structure, which benefits CPC mechanical behaviour in opposition to those obtained by IM.

It is here envisaged that the characteristics and properties of this cork-like filament will foster the development of new design solutions and products.

Acknowledgements

This work was supported by COMPETE 2020 – Programa Operacional Competividade e Internacionalização within TT@ESAN project (NORTE-01-0246-FEDER-000001). This work was also developed within the scope of the project CICECO-Aveiro Institute of Materials, FCT Ref. UID/CTM/50011/2019, financed by national funds through the FCT/MCTES. Authors would also want to acknowledge Maria Celeste Azevedo for the FTIR-ATR measurements and Marta Ferro for the support during SEM analyses.

References

- [1] S.A.M. Tofail, E.P. Koumoulos, A. Bandyopadhyay, S. Bose, L. O'Donoghue, C. Charitidis, Additive manufacturing: scientific and technological challenges, market uptake and opportunities, *Mater. Today*. 21 (2018) 22–37. doi:10.1016/J.MATTOD.2017.07.001.
- [2] M.Q. Ansari, M.J. Bortner, D.G. Baird, Generation of Polyphenylene Sulfide Reinforced with a Thermotropic Liquid Crystalline Polymer for Application in Fused Filament Fabrication, *Addit. Manuf.* 29 (2019) 100814. doi:10.1016/j.addma.2019.100814.
- [3] K. Gnanasekarana, T. Heijmans, S. van Bennekomb, H. Woldhuis, S. Wijnia, G. de Witha, et al., 3D printing of CNT- and graphene-based conductive polymer nanocomposites by fused deposition modeling, *Appl. Mater. Today*. 9 (2017) 21–29.
- [4] M. Kariz, M. Sernek, M. Obućina, M.K. Kuzman, Effect of wood content in FDM filament on properties of 3D printed parts, *Mater. Today Commun.* 14 (2018) 135–140. doi:10.1016/J.MTCOMM.2017.12.016.
- [5] B. Brenken, E. Barocio, A. Favalaro, V. Kunc, R.B. Pipes, Fused filament fabrication of fiber-reinforced polymers: A review, *Addit. Manuf.* (2018). doi:10.1016/j.addma.2018.01.002.
- [6] S.C. Ligon, R. Liska, J. Stampfl, M. Gurr, R. Mülhaupt, Polymers for 3D Printing and Customized Additive Manufacturing, *Chem. Rev.* 117 (2017) 10212–10290. doi:10.1021/acs.chemrev.7b00074.
- [7] H. Pereira, *Cork: Biology, Production and Uses*, Elsevier, Amsterdam, 2007.
- [8] L. Gil, Cork powder waste: An overview, *Biomass and Bioenergy*. 13 (1997) 59–61. doi:10.1016/S0961-9534(97)00033-0.
- [9] J.M. Silva, C.Z. Nunes, N. Franco, P. V. Gamboa, Damage tolerant cork based composites for aerospace applications, *Aeronaut. J.* 115 (2011) 567–575. doi:10.1017/S0001924000006205.
- [10] S.P. Silva, M.A. Sabino, E.M. Fernandes, V.M. Correlo, L.F. Boesel, R.L. Reis, Cork: properties, capabilities and applications, *Int. Mater. Rev.* 50 (2005) 345–365.
- [11] F.A.O. Fernandes, R.T. Jardim, A.B. Pereira, R.J. Alves de Sousa, Comparing the mechanical performance of synthetic and natural cellular materials, *Mater. Des.* 82 (2015) 335–341. doi:10.1016/J.MATDES.2015.06.004.
- [12] A.P. Duarte, J.C. Bordado, Cork - A Renewable Raw Material: Forecast of Industrial Potential and Development Priorities, *Front. Mater.* 2 (2015). doi:10.3389/fmats.2015.00002.
- [13] E. Castro-Aguirre, F. Iñiguez-Franco, H. Samsudin, X. Fang, R. Auras, Poly(lactic acid)—Mass production, processing, industrial applications, and end of life, *Adv. Drug Deliv. Rev.* 107 (2016) 333–366. doi:10.1016/j.addr.2016.03.010.

- [14] K. Kamau-Devers, Z. Kortum, S.A. Miller, Hydrothermal aging of bio-based poly(lactic acid) (PLA) wood polymer composites: Studies on sorption behavior, morphology, and heat conductance, *Constr. Build. Mater.* 214 (2019) 290–302. doi:10.1016/J.CONBUILDMAT.2019.04.098.
- [15] E. Vatanserver, D. Arslan, M. Nofar, Polylactide cellulose-based nanocomposites, *Int. J. Biol. Macromol.* 137 (2019) 912–938. doi:10.1016/J.IJBIOMAC.2019.06.205.
- [16] A. Carbonell-Verdu, M.D. Samper, D. Garcia-Garcia, L. Sanchez-Nacher, R. Balart, Plasticization effect of epoxidized cottonseed oil (ECSO) on poly(lactic acid), *Ind. Crops Prod.* 104 (2017) 278–286. doi:10.1016/J.INDCROP.2017.04.050.
- [17] S.H. Clasen, C.M.O. Müller, A.T.N. Pires, S.H. Clasen, C.M.O. Müller, A.T.N. Pires, Maleic Anhydride as a Compatibilizer and Plasticizer in TPS/PLA Blends, *J. Braz. Chem. Soc.* 26 (2015) 1583–1590. doi:10.5935/0103-5053.20150126.
- [18] R. Guo, Z. Ren, H. Bi, Y. Song, M. Xu, Effect of toughening agents on the properties of poplar wood flour/poly (lactic acid) composites fabricated with Fused Deposition Modeling, *Eur. Polym. J.* 107 (2018) 34–45. doi:10.1016/J.EURPOLYMJ.2018.07.035.
- [19] M. Wang, Y. Wu, Y.-D. Li, J.-B. Zeng, Progress in Toughening Poly(Lactic Acid) with Renewable Polymers, *Polym. Rev.* 57 (2017) 557–593. doi:10.1080/15583724.2017.1287726.
- [20] R. Revati, M.S. Abdul Majid, M.J.M. Ridzuan, M. Normahira, N.F. Mohd Nasir, M.N. Rahman Y., et al., Mechanical, thermal and morphological characterisation of 3D porous Pennisetum purpureum/PLA biocomposites scaffold, *Mater. Sci. Eng. C* 75 (2017) 752–759. doi:10.1016/j.msec.2017.02.127.
- [21] M.E. González-López, J.R. Robledo-Ortíz, R. Manríquez-González, J.A. Silva-Guzmán, A.A. Pérez-Fonseca, Polylactic acid functionalization with maleic anhydride and its use as coupling agent in natural fiber biocomposites: a review, *Compos. Interfaces.* (2018) 1–24. doi:10.1080/09276440.2018.1439622.
- [22] T. Mukherjee, N. Kao, PLA Based Biopolymer Reinforced with Natural Fibre: A Review, *J. Polym. Environ.* 19 (2011) 714–725. doi:10.1007/s10924-011-0320-6.
- [23] S. Detyothin, S.E.M. Selke, R. Narayan, M. Rubino, R. Auras, Reactive functionalization of poly(lactic acid), PLA: Effects of the reactive modifier, initiator and processing conditions on the final grafted maleic anhydride content and molecular weight of PLA, *Polym. Degrad. Stab.* 98 (2013) 2697–2708. doi:10.1016/J.POLYMDEGRADSTAB.2013.10.001.
- [24] S.W. Hwang, S.B. Lee, C.K. Lee, J.Y. Lee, J.K. Shim, S.E.M. Selke, et al., Grafting of maleic anhydride on poly(L-lactic acid). Effects on physical and mechanical properties, *Polym. Test.* 31 (2012) 333–344. doi:10.1016/J.POLYMERTESTING.2011.12.005.
- [25] J.J. Koh, X. Zhang, C. He, Fully biodegradable Poly(lactic acid)/Starch blends: A review of toughening strategies, *Int. J. Biol. Macromol.* 109 (2018) 99–113. doi:10.1016/J.IJBIOMAC.2017.12.048.
- [26] E.M. Fernandes, V.M. Correlo, J.F. Mano, R.L. Reis, Polypropylene-based cork–polymer composites: Processing parameters and properties, *Compos. Part B Eng.* 66 (2014) 210–223. doi:10.1016/j.compositesb.2014.05.019.
- [27] A. Cataldi, D. Rigotti, V.D.H. Nguyen, A. Pegoretti, Polyvinyl alcohol reinforced with crystalline nanocellulose for 3D printing application, *Mater. Today Commun.* 15 (2018) 236–244. doi:10.1016/j.mtcomm.2018.02.007.
- [28] A.M. F.Brites, C. Malça, F.Gaspar, J.F.Horta, M.C. Franco, S. Biscaia, Cork Plastic Composite Optimization for 3D Printing Applications, *Procedia Manuf.* 12 (2017) 156–165. doi:10.1016/J.PROMFG.2017.08.020.
- [29] N. Gama, A. Ferreira, A. Barros-Timmons, 3D printed cork/polyurethane composite foams, *Mater. Des.* 179 (2019) 107905. doi:10.1016/J.MATDES.2019.107905.
- [30] A. Winter, N. Mundigler, J. Holzweber, S. Veigel, U. Müller, A. Kovalcik, et al., Residual wood polymers facilitate compounding of microfibrillated cellulose with poly(lactic acid) for 3D printer filaments, *Philos. Trans. R. Soc. A Math. Phys. Eng. Sci.* 376 (2018). doi:10.1098/rsta.2017.0046.
- [31] M. Tanase-Opedal, E. Espinosa, A. Rodríguez, G. Chinga-Carrasco, Lignin: A Biopolymer from Forestry Biomass for Biocomposites and 3D Printing, *Materials (Basel)*. 12 (2019) 3006. doi:10.3390/ma12183006.
- [32] V. Mazzanti, L. Malagutti, F. Mollica, FDM 3D Printing of Polymers Containing Natural Fillers: A Review of their Mechanical Properties, *Polymers (Basel)*. 11 (2019) 1094. doi:10.3390/polym11071094.
- [33] ColorFabb, WoodFill, (n.d.). <https://colorfabb.com/woodfill> (accessed October 29, 2019).
- [34] ColorFabb, CorkFill, (n.d.). <https://colorfabb.com/corkfill> (accessed October 29, 2019).
- [35] S.P. Magalhães da Silva, J.M. Oliveira, Cork-Polymer Composites based on Polylactic Acid for Fused Filament Fabrication, in: *Mater. 2017, Aveiro, Portugal, 2017*.
- [36] S.P. Magalhães da Silva, J.M. Oliveira, Green Composites based on Cork Residues for Additive Manufacturing, in: *3rd Int. Conf. Polym. Sci. Eng., Chicago, USA, 2017*.
- [37] S.P. Magalhães da Silva, J.M. Oliveira, Cork-Polylactide Composites reinforced with Polyhydroxyalkanoates for Additive

Manufacturing, in: 18th Eur. Conf. Compos. Mater., Athens, Greece, 2018.

- [38] T. Antunes, S.P. Magalhães da Silva, M.E. V Costa, J.M. Oliveira, Cork-based filaments for Additive Manufacturing – The use of cork powder residues from stoppers industry, in: Int. Conf. Addit. Manuf., Maribor, Slovenia, 2018.
- [39] E.W. Fischer, H.J. Sterzel, G. Wegner, Investigation of the structure of solution grown crystals of lactide copolymers by means of chemical reactions, *Kolloid-Zeitschrift Und Zeitschrift Für Polym.* 251 (1973) 980–990.
- [40] BS EN ISO 527-2: 1996. Plastics - Determination of tensile properties - Part 2: Test conditions for moulding and extrusion plastics, 1996.
- [41] C. Li, Q. Dou, Non-isothermal crystallization kinetics and spherulitic morphology of nucleated poly(lactic acid): Effect of dilithium cis-4-cyclohexene-1,2-dicarboxylate as a novel and efficient nucleating agent, *Polym. Adv. Technol.* 26 (2015) 376–384. doi:10.1002/pat.3463.
- [42] S.P. Magalhães da Silva, P.S. Lima, J.M. Oliveira, Non-isothermal crystallization kinetics of cork-polymer composites for injection molding, *J. Appl. Polym. Sci.* 133 (2016).
- [43] A.A. Cuadri, J.E. Martín-Alfonso, Thermal, thermo-oxidative and thermomechanical degradation of PLA: A comparative study based on rheological, chemical and thermal properties, *Polym. Degrad. Stab.* 150 (2018) 37–45. doi:10.1016/J.POLYMDEGRADSTAB.2018.02.011.
- [44] N. Raghu, A. Kale, A. Raj, P. Aggarwal, S. Chauhan, Mechanical and thermal properties of wood fibers reinforced poly(lactic acid)/thermoplasticized starch composites, *J. Appl. Polym. Sci.* 135 (2018) 1–10. doi:10.1002/app.46118.
- [45] D. Garlotta, A Literature Review of Poly(Lactic Acid), *J. Polym. Environ.* 9 (2001) 63–84.
- [46] E.M. Fernandes, V.M. Correlo, J.F. Mano, R.L. Reis, Cork–polymer biocomposites: Mechanical, structural and thermal properties, *Mater. Des.* 82 (2015) 282–289.
- [47] S.P. Magalhães da Silva, P.S. Lima, J.M. Oliveira, Rheological behaviour of cork-polymer composites for injection moulding, *Compos. Part B Eng.* 90 (2016). doi:10.1016/j.compositesb.2015.12.015.
- [48] Y. Fourati, Q. Tarrés, P. Mutjé, S. Boufi, PBAT/thermoplastic starch blends: Effect of compatibilizers on the rheological, mechanical and morphological properties, *Carbohydr. Polym.* 199 (2018) 51–57. doi:10.1016/J.CARBPOL.2018.07.008.
- [49] R. Zhu, H. Liu, J. Zhang, Compatibilizing effects of maleated poly(lactic acid) (PLA) on properties of PLA/soy protein composites, *Ind. Eng. Chem. Res.* 51 (2012) 7786–7792. doi:10.1021/ie300118x.
- [50] E.M. Fernandes, V.M. Correlo, J.F. Mano, R.L. Reis, Novel cork–polymer composites reinforced with short natural coconut fibres: Effect of fibre loading and coupling agent addition, *Compos. Sci. Technol.* 78 (2013) 56–62. doi:10.1016/j.compscitech.2013.01.021.
- [51] M. Flores, M.E. Rosa, C.Y. Barlow, M.A. Fortes, M.F. Ashby, Properties and uses of consolidated cork dust, *J. Mater. Sci.* 27 (1992) 5629–5634. doi:10.1007/BF00541634.
- [52] J.R.C. Dizon, A.H. Espera, Q. Chen, R.C. Advincula, Mechanical characterization of 3D-printed polymers, *Addit. Manuf.* 20 (2018) 44–67. doi:10.1016/J.ADDMA.2017.12.002.
- [53] J.M. Chacón, M.A. Caminero, E. García-Plaza, P.J. Núñez, Additive manufacturing of PLA structures using fused deposition modelling: Effect of process parameters on mechanical properties and their optimal selection, *Mater. Des.* 124 (2017) 143–157. doi:10.1016/J.MATDES.2017.03.065.
- [54] N. Mohan, P. Senthil, S. Vinodh, N. Jayanth, A review on composite materials and process parameters optimisation for the fused deposition modelling process, *Virtual Phys. Prototyp.* 12 (2017) 47–59. doi:10.1080/17452759.2016.1274490.
- [55] T. Letcher, M. Waytashek, Material Property Testing of 3D-Printed Specimen in PLA on an Entry-Level 3D Printer, in: Vol. 2A Adv. Manuf., ASME, 2014. doi:10.1115/IMECE2014-39379.
- [56] I. Durgun, R. Ertan, Experimental investigation of FDM process for improvement of mechanical properties and production cost, *Rapid Prototyp. J.* 20 (2014) 228–235. doi:10.1108/RPJ-10-2012-0091.
- [57] W. Zhu, C. Yan, Y. Shi, S. Wen, J. Liu, Y. Shi, Investigation into mechanical and microstructural properties of polypropylene manufactured by selective laser sintering in comparison with injection molding counterparts, *Mater. Des.* 82 (2015) 37–45. doi:10.1016/J.MATDES.2015.05.043.
- [58] NatureWorks, Ingeo Biopolymer 4032D Technical Data Sheet, n.d. https://www.natureworkslc.com/~media/Technical_Resources/Technical_Data_Sheets/TechnicalDataSheet_4032D_films_.pdf (accessed March 25, 2019).
- [59] E.M. Fernandes, V.M. Correlo, J.F. Mano, R.L. Reis, Polypropylene-based cork–polymer composites: Processing parameters and properties, *Compos. Part B Eng.* 66 (2014) 210–223. doi:doi.org/10.1016/j.compositesb.2014.05.019.

3.5 Cork powders wettability by the Washburn capillary rise method ^k

S. P. Magalhães da Silva^{1,2,3*}, J. M. Oliveira^{1,2,3}

¹EMaRT Group – Emerging: Materials, Research, Technology, University of Aveiro, Portugal

²School of Design, Management and Production Technologies Northern Aveiro (ESAN), University of Aveiro, Portugal

³Aveiro Institute of Materials (CICECO), University of Aveiro, Portugal

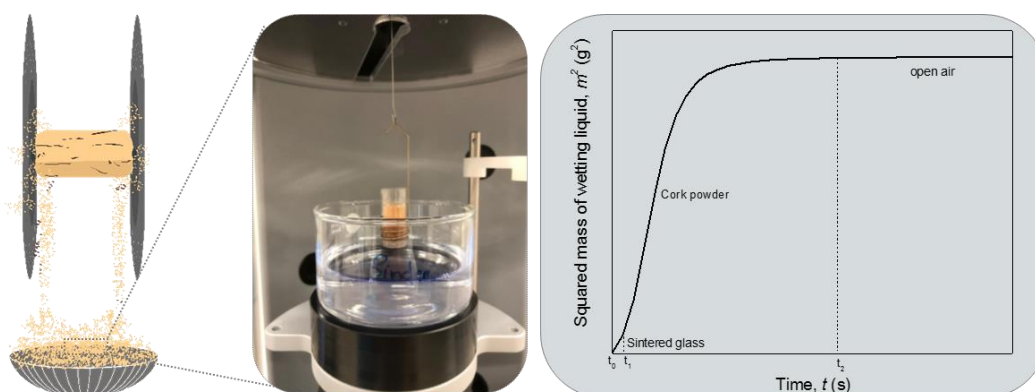
*corresponding author: sarapms@ua.pt

Abstract

The applicability of Washburn capillary rise (WCR) method on cork powders wettability was investigated. An adapted sample preparation method was also developed to guarantee measurements accuracy and reproducibility. The processing of cork powders by 3D Printing (3DP) presents a clear challenge related to cork wettability. The common liquid binders used in 3DP printers are composed mainly by water (95% w/w).

Two sets of cork powders with different particle size distributions (PSD) were prepared and studied, namely Full Range powder with a wider distribution (20–100 μm) and Coarse powder with a narrow distribution (63–80 μm). Among the studied wetting liquids, hexane revealed to be the wetting liquid with higher ability to completely wet cork powders in a short period of time (14 – 18s). Coarse powder exhibited higher packing ability based on the calculated parameter C values. Contact angles between a commercial binder and Full Range and Coarse powders were estimated as $86.1 \pm 2.1^\circ$ and $87.3 \pm 1.5^\circ$, respectively. The obtained results showed that WCR method can successfully describe the wettability behaviour of cork powders.

Graphical Abstract



Keywords

Cork; Powders; Liquid binder; Washburn Capillary Rise (WCR); Contact Angle; 3D Printing (3DP)

^k Submitted to Powder Technology Journal.

The author had contributed to the planning and execution of all experiments presented herein, as well as on the discussion, interpretation and preparation of the manuscript.

1. Introduction

Cork is the bark of the cork oak (*Quercus suber L.*) and its extraction, every 9 years, does not compromise the tree. It is a 100% natural material, reusable, recyclable and with a Portuguese nationality. Owing to its chemical composition, mainly composed by suberin and lignin, and its honeycomb structure composed by closed cells filled with gas, makes cork a versatile material with a unique set of properties. Such properties include low density, hydrophobic behaviour, high elastic behaviour and thermal, acoustic and electrical insulation properties [1]. Cork major industrial application is the production of wine stoppers. The rectification phase of the cork stoppers production, which involves top- and bottom polishing of stoppers, generates approximately 50000 tons/year of cork residues with low granulometries ($< 500 \mu\text{m}$) [2]. These cork particles are not used in the development of cork-based products, being usually burned or disposed in landfills.

In the incessant search for new cork applications, the possibility to use directly these low granulometry residues as building material in 3D Printing (3DP) processes is of major interest. It will lead, by one hand, to the valorisation of these residues under the circular economy principles and, by the other hand, to the development of innovative and eco-sustainable cork products. 3DP, an additive manufacturing technology, is characterized by the use of powder materials and, a binding agent is deposited, through a print head, on previously prepared powder layers [3]. The processing of cork powders by 3DP presents a clear challenge related to the wettability of cork, once the liquid binders used in 3DP printers are composed mainly by water (95% w/w). The resolution of 3DP parts (typically $100 \mu\text{m}$) is dependent on binder type, on powder granulometric distribution, on particles geometry, on the precision of binder droplets deposition and the interaction between binder and particles [4–6].

The wettability of a solid by a specific liquid is dependent on the chemical affinity of liquid-solid interface and on the surface tension at the liquid-solid-air interfaces [1]. Sessile drop, Wilhelmy plate, dynamic contact angle and Washburn capillary rise (WCR) are examples of applied methods to determine a material's wettability [7]. WCR method is recommended to characterize the wettability of powders and/or porous materials [8–13]. Main concerns regarding measurements with WCR method are the dependency on particle size distribution (PSD), on pore sizes and on particles morphology [10,14,15]. These parameters will influence powder packing and, therefore, the ability of the liquid to penetrate into those powders.

To the best of our knowledge studies related to cork wettability by WCR are non-existing. However, a few studies are found in literature concerning the wettability behaviour of cork plates or its main components by the sessile drop method [16–19]. The present study is part of a major project which aims the processing of cork powders by 3DP through the development of adapted cork-based formulations. This paper proposes to validate the applicability of WCR method on cork powders wettability. The development of an adapted sample preparation method is also presented.

2. Methodology

2.1 Cork

Cork powder residues were kindly supplied by a Portuguese cork company. The sieving method applied to fractionate the as-received material is already published elsewhere [20,21]. An average of three trials were considered to determine PSD. Two cork powder sets were prepared exhibiting different PSD, namely a wider distribution (20–100 μm) defined as Full Range and a narrow distribution (63–80 μm) defined as Coarse. The Full Range powder was obtained by the sieving of the as-received powder using 20, 40, 63, 80, 100 and 200 μm sieves. Full Range distribution represents the cork powders retained in sieves from 20 to 100 μm . The Coarse powder was acquired by the sieving of as-received powder using 20, 40, 63, 80 μm sieves. Coarse distribution represents the cork powder that was retained in 63 μm sieve. The selection of such powder sets was based on the PSD presented by the commercial powder (Zp[®]140), as reported by Oliveira, J. M and co-workers [22].

Mercury intrusion porosimetry (MIP) technique was employed to determine the average pore diameter, the bulk density as well as the porosity of these sets of cork powders. The adopted MIP procedure has been published elsewhere [20,23].

Scanning electron microscopy (SEM) was performed to morphologically analyse both cork powder sets. A Hitachi SU-70 equipment was used and samples were sputter-coated (Polaron E5000) with Au/Pd target for 2 min at 12 mA.

2.2 Adapted WCR method

Cork powders wettability measurements were performed using a Sigma 701 tensiometer from Biolin Scientific. A glass tube (reference T112) with sintered glass (pore size of 1 μm) on the bottom and a diameter of 10 mm was used. The same amount (approx. 70 mg) of cork powder was filled and packed in inside the tube. It was designed and tested three sample methods preparation, in order to guarantee accurate and reproducible measurements of cork wettability by WRC method. Only the selected method based on higher reproducibility will be herein presented. Prior the wettability trials, cork powders were kept in the oven (FD 56, Binder GmbH) at 50°C to avoid static electricity caused by adsorption of air humidity (> 25%). Powders presenting static electricity are unable to settle and to be packed uniformly inside the glass tube [10]. The selected method consisted on: (1) filling the glass tube with half of the amount of cork powder (\approx 35 mg) and tapping 10 times at a constant tapping height of 20 mm; (2) filling again the same amount of powder and apply the same procedure as (1); and, (3) placing the packed tube on ultrasons (J. P. Selecta[®]) during 1 minute. Powder compaction is mandatory for better reproducibility. For each measurement the glass tube was cleaned sequentially with pure acetone (99%, Enzymatic) and distilled water (Micra, ELGA LabWater) and then dried in the oven (AX60, Carbolite) at 100°C to eliminate moisture.

Washburn [24] proposed the capillary rise method based on the assumption that powders or porous materials can be described as bundles of capillary tubes of constant radius [8,10,13]. It is

derived from Poiseuille's Law principle and it is defined assuming a linear relationship between the squared mass (m^2) of wetting liquid versus measurement time (t) (Eq. (1) and (2)).

$$m^2 = \frac{C\rho^2\sigma\cos(\theta)}{2\eta} \times t \quad (1)$$

$$C = rA^2\varepsilon^2 \quad (2)$$

where C is the material constant, θ is the contact angle and ρ , σ and η are the density, surface tension and viscosity of the wetting liquid, respectively. C is a geometric factor that is related to the geometry of the pores, where r is the effective pores radius, A is the cross-section area of the tube and ε is the porosity of the powder material. C is determined by using a reference liquid with low σ for which is assumed that completely wets the powder material ($\theta = 0^\circ$). Once C is defined it is possible to calculate θ between the studied powders and liquids of interest.

In Table 1 the organic solvents used are displayed, along with its physical-chemical properties, to evaluate cork powder wettability and to determine C parameter. The θ value was calculated using a commercial 3DP binder as wetting liquid (Table 1).

Table 1. Physical-chemical properties of the used wetting liquids.

Wetting liquids	Commercial grade	ρ (g/cm ³)	σ (mN/m) (at 20°C)	η (mPa·s) (at 20°C)	Vapour Pressure (Pa) (at 20-25°C) [25]
Chloroform	200-663-8, JMGS	1.49	27.15	0.56	32E03
Dichloromethane	32222, Honeywell	1.33	26.50	0.43	0.6E03
Xylene	CL00.2402.2500, Chem-Lab	0.86	28.90	0.81	0.9E03
Toluene	CL00.2010.1000, Chem-Lab	0.87	28.52	0.59	3.7E03
Hexane	CL00.0822.2500, Chem-Lab	0.66	18.40	2.94	16E03
Binder	VisiJet® PXL™ Clear, 3D Systems	1.00	33.15 ^a	1.00	NA

^a Determined by Du Nouy Ring using Sigma 701 tensiometer (± 0.01)

NA – Not applicable

The measurement automatically started when the wetting liquid touched the surface of the sample with an immersion depth of 0.5 mm. Data related to the mass loss of the wetting liquid into the packed tube was acquired at room temperature (20°C) during 120 seconds for each measurement. To guarantee the reproducibility of our data, each measurement was repeated at least three times. The average values of the penetrating rate (g^2/s), parameter C (cm^5) and θ ($^\circ$) will be presented.

3. Results and Discussion

3.1. Cork Powders

The granulometric distribution and morphology of Full Range and Coarse powders are shown in Fig. 1. It is visible that Full Range powder presents a bimodal volume distribution over the 40–63 μm and 100–200 μm ranges. For Coarse powder, more than 80% in volume are particles with sizes equal or superior to 80 μm .

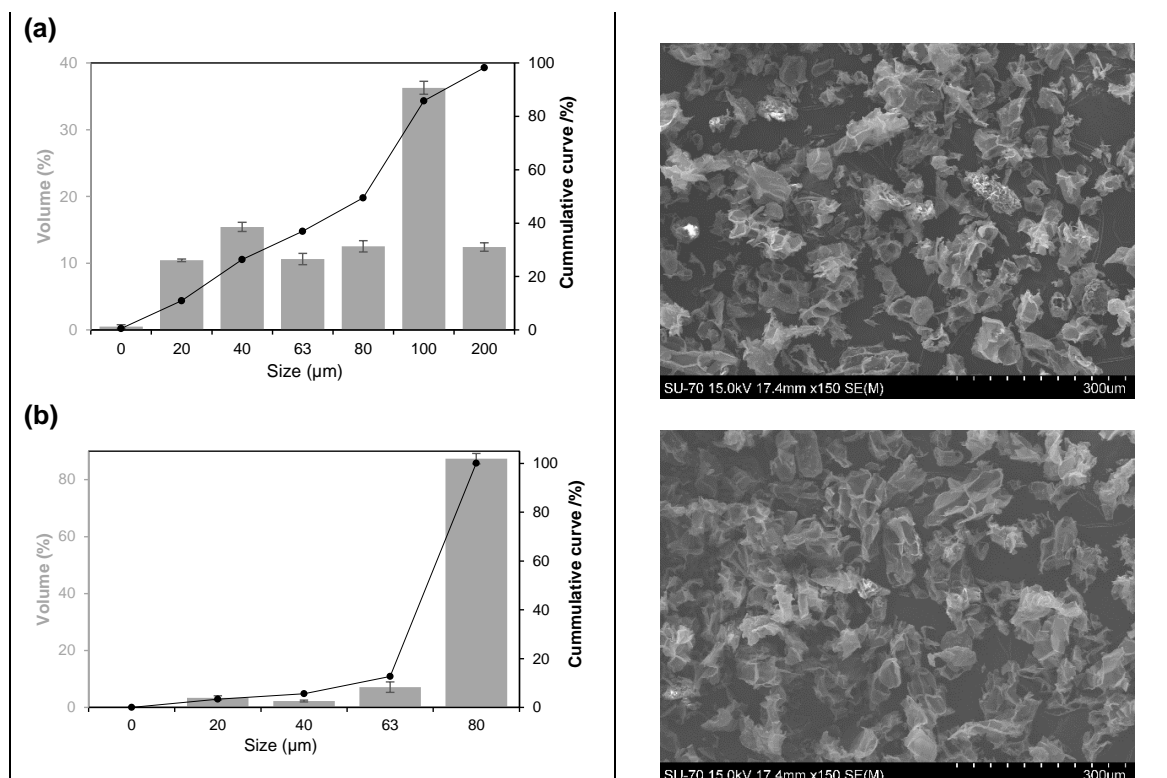


Fig. 1. Granulometric distribution and SEM images of (a) Full Range and (b) Coarse powders.

SEM images reveal the heterogeneity in size, mainly in Full Range, and irregular shape of cork particles. It is also seen that for both powders some of cork alveoli remained closed and others were open as a consequence of the industrial polishing process.

Density and porosity values of cork powders obtained by MIP are presented in Table 2.

Table 2. MIP characterization of cork powders.

Cork Powders	Full Range	Coarse
Average pore diameter (μm)	36.6	23.3
Bulk density (g/cm^3)	0.083	0.156
Apparent density (g/cm^3)	0.449	0.694
Porosity (%)	81.6	77.6

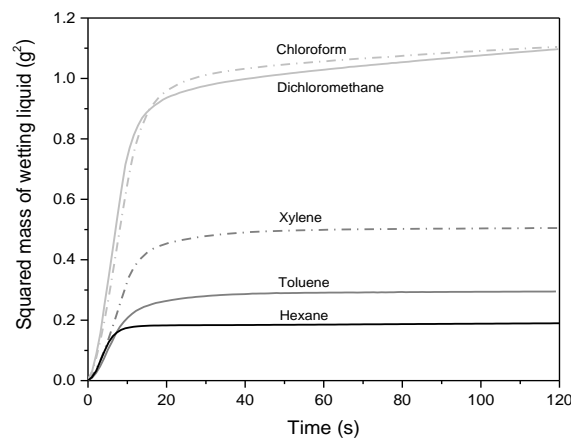
As expected, both powders present low density and high porosity due to the characteristic honeycomb structure of cork, as also visible in Fig. 1.

3.2. Wettability of cork powders by WRC

A typical penetrating rate curve is divided into three main stages. These stages are defined by the difference on how liquid flows through the packed tube which will result in different slopes. In this particular work, the first stage is governed by inertia forces and it is related to the wetting liquid penetrating the pores of sintered glass on the bottom of the glass tube. Then, the second stage is characterized by capillary forces and it is associated to the wetting liquid penetrating the cork powders. Finally, the third stage is determined by the equilibrium of these forces and it is related to the wetting liquid reaching open air, which it is evidenced by a plateau and it is assumed that penetration is over [8,10]. Equations (1) and (2) were applied to the second stage.

The penetrating profiles of different wetting liquids for both cork powders are presented in Fig. 2.

(a)



(b)

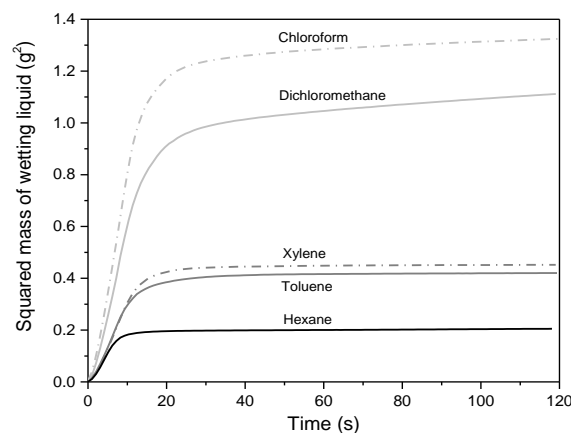


Fig. 2. Penetrating profiles of different wetting liquids into tubes packed with (a) Full Range and (b) Coarse cork powders.

It is clearly seen that a typical penetrating profile was attained for all wetting liquids. The selection of several organic solvents as wetting liquids with different physical-chemical properties (Table 1) was (1) to evaluate the wettability of each liquid and (2) to determine which wetting liquid exhibited a complete wetting of cork powders ($\theta \approx 0^\circ$). The same tendency was observed for both cork powders. Hexane exhibited a superior penetrating rate while chloroform presented the lowest. For the tube packed with Full Range powder the penetration of hexane ended at ≈ 18 s and for Coarse powder finished ≈ 4 s sooner (Fig. 2 (b)). This trend can be an indication of an improved packing ability for Coarse cork powders. In addition, it is noticed a distinct behaviour of cork wettability for liquids in the presence or absence of chlorine. The chlorine-based solvents took longer to reach the equilibrium. Kirdponpattara, S. *et al.* [10] reported that the presence of chemical interactions between the wetting liquid and the powder can lead to a deviation of reaching the equilibrium. In fact, dichloromethane and chloroform are used to solubilize extractives-fraction and to precipitate suberin fraction from a methanol solution in acidic media [1,18,26]. The affinity of these solvents with cork can be an explication of this particular behaviour. From the obtained results it can be assumed that hexane is the best choice as wetting liquid for cork powders. Besides presenting the higher viscosity among the studied liquids (Table 1), its lower surface tension and higher vapour pressure have contributed positively to the achieved results.

Parameter C was calculated considering the second stage, where the penetrating profile was found to be linear ($R^2 \approx 0.98$ – 0.99). In Fig. 3 is exposed the obtained parameter C values.

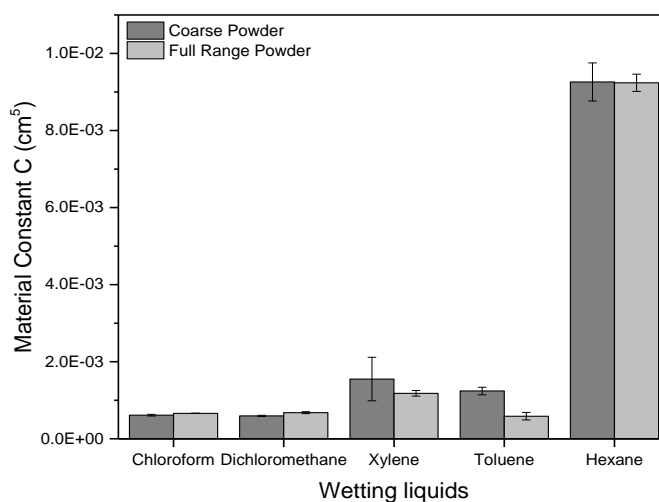


Fig. 3. Parameter C values for the studied powders and wetting liquids.

The values of parameter C are affected by the geometrical factor associated with packing of powder materials. As a consequence, the estimation of penetrating rate and θ are affected by PSD and by pore sizes of powder materials packed along the tube. It is assumed that a higher parameter C value implies a higher penetrating rate and, consequently, a higher θ . A wetting liquid rising up within a compact powder structure without voids will reflect in a higher parameter C value. It is also important to note that the estimated values of parameter C are dependent on the physical-chemical properties

of the wetting liquids. From Fig. 3, it is evidenced that wetting both cork powders with hexane presented the higher parameter C values. An expected value due to the increased penetrating rates already shown in Fig. 2. However, in this particular study, it is not detected significant changes when wetting cork with Full Range or Coarse powder distributions. A possible explanation is related to the selection of smaller particles ($< 200 \mu\text{m}$) for both powders. Studies reporting the dependence of penetrating kinetics into PSD and pore size can be found [9,10,12]. A study from Dang-Vu, T. *et al* [12] reported the effect of packing glass beads with different pore sizes ($60 - 110 \mu\text{m}$, $150 - 250 \mu\text{m}$ and $60 - 250 \mu\text{m}$). Smaller pores and narrow PSD ($60 - 110 \mu\text{m}$) exhibited a uniform advancing front due to the similarity of pore sizes distribution and, consequently, the existence of the same capillary forces. It was found that a wider PSD ($60 - 250 \mu\text{m}$) with larger particles also present a homogenous and faster advancing front. The smaller fraction was able to fill the voids created by the larger fraction ($150 - 250 \mu\text{m}$). The same tendency was observed by [10], where nylon 6/6 powders with PSD of $0 - 250 \mu\text{m}$ and $0 - 2000 \mu\text{m}$ exhibited higher penetrating rates than powders with PSD of $500 - 2000 \mu\text{m}$.

3.3 Contact angle of binder on cork powders

The processing of cork powders by 3DP using a commercial binder, which is composed mainly by water (95% w/w), presents a clear challenge related to the low water affinity of cork. The main purpose of the present study is to validate the applicability and reproducibility of WCR method for cork powders and to evaluate the wettability of cork by a commercial binder for 3DP processing. The precision of binder droplets deposition and the interaction between binder and particles are among the factors that interfere on the resolution of 3DP parts [4–6]. The penetrating profiles of binder wetting both cork powders are represented in Fig. 4. As it can be seen, penetrating curves presented an abnormal profile, where binder was not able to reach open-air and completely wet both cork powders.

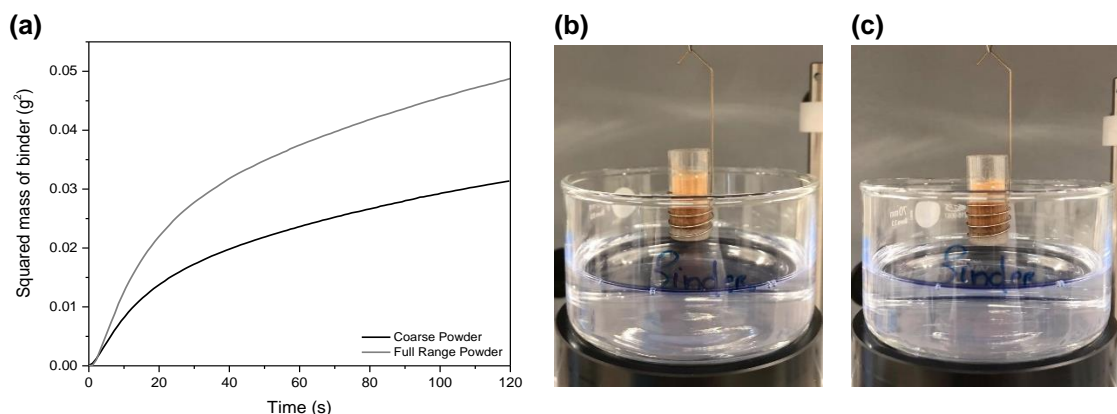


Fig. 4. (a) Penetrating profiles of binder into tubes packed with Full Range and Coarse cork powders. Photographs of (b) Coarse and (c) Full Range powders after measurements with binder.

This abnormal wetting profile for both cork powders can be an indication of the lower affinity of cork with water or water-based liquids. It was also performed measurements with superior duration (1000 s) to eliminate the possibility that a longer time was needed for binder to achieve open-air. Nevertheless, the same profile was attained (Supplementary Data - Fig. S1).

The estimated θ values between binder and cork powders are displayed in Table 3.

Table 3. Estimated binder θ values for tubes packed with Full Range and Coarse cork powders. θ values reported on the literature (adapted from [16–19]).

Cork-based material	Method	θ (°)
Coarse powder (This work)	WCR	87.3 ± 1.5^a
Full Range powder (This work)	WCR	86.1 ± 2.1^a
Cork plate [16]	Sessile drop	84^b
Cork plate [17]	Sessile drop	$90 - 100^c$
Suberin film [18]	Sessile drop	75^b
Cork black condensate [19]	Sessile drop	$99.3 - 111.7^b$

^a Independently of the wetting solvent used; ^b Values obtained by extrapolation to $t=0$; ^c Values obtained after 1 min of liquid drop is released on the surface.

For comparison purposes, it is also presented estimated θ values obtained by sessile drop method for cork or its main components with water [16–19]. To the best of our knowledge, studies regarding the wettability of cork powders by WCR method are non-existent. The estimated θ values presented in Table 3 for cork powders are the average values of the calculated θ for binder considering all wetting solvents used. The θ values are relatively close to 90° , however it can be assumed that cork powders are wetted by binder ($\theta < 90^\circ$), even though in a small extent. No differences are detected between Full Range and Coarse powders. The lower deviation values acquired can be an indication of the accuracy and reproducibility of WCR method with cork powders. In addition, the calculated θ values by WCR are in agreement with those reported in literature by sessile drop (Table 3).

An interesting feature regarding cork and suberin wettability behaviour with time was reported elsewhere [1,16,18]. Gomes, C. *et al* [16] observed a decrease in water θ from 84° to 40° after 1h. They appointed the characteristic cork cellular structure and, consequently, the water diffusion through these channels as a possible explanation of this phenomena. Cordeiro, N. *et al* [18] observed the same tendency with θ of water with suberin, where a reduction of 25° was perceived after 100 s. Authors discussed the deformation of the contact line between suberin and water as the reason for θ decrease. Cork wettability is also affected by its surface roughness, where usually the surface direction with lower roughness is selected for θ measurements [16,17]. In the present work, owing to the origin of cork powder residues, it cannot be assumed any specific direction and evaluate its contribution for the estimated θ values. It is also important to bear in mind the variability in composition and structure of natural materials. The determination of θ will be therefore directly impacted by this particularity.

4. Conclusions

The applicability of WCR method for determining cork powders wettability was validated. Hexane revealed to be the wetting liquid with higher ability to completely wet cork powders in a short period of time (14 – 18s). Based on parameter C values, cork powders with Coarse distribution seems to have a higher packing ability. However, the different PSD studied had no effect on the estimated θ with binder. The θ between binder and Full Range powders was found to be $86.1 \pm 2.1^\circ$, while for Coarse powders was equal to $87.3 \pm 1.5^\circ$. The small deviation values achieved support the accuracy and reproducibility of the WCR method using cork powders. Values of θ determined by WCR are in agreement with those reported in literature by sessile drop method.

Powders with θ values close to 90° are not suitable for 3DP applications. In this sense, as future work, it is needed to prepared cork-based powder formulations with hydrophilic additives to increase cork wettability by water-based binders. As a reference, commercial 3DP powders are composed by ceramic materials with known affinity with water. The present work provides helpful information regarding the processing of cork powders by 3DP, namely (i) the selection of hexane as wetting liquid to evaluate the presence of additives to mask the 'hydrophobic' behaviour ($\theta \approx 90^\circ$) of cork and (ii) the selection of Coarse powder as the reference granulometric distribution.

Acknowledgements

This work was developed within the scope of the project CICECO-Aveiro Institute of Materials, UIDB/50011/2020 & UIDP/50011/2020, financed by national funds through the Portuguese Foundation for Science and Technology/MCTES. Authors would also want to acknowledge Tiago Silva for the availability and support for SEM analyses.

Supplementary Data

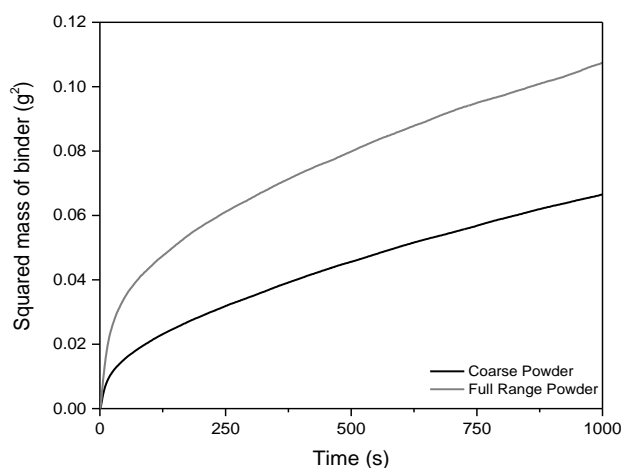


Fig. S1. Penetrating profiles of binder, during 1000 s, into tubes packed with Full Range and Coarse cork powders.

References

- [1] H. Pereira, *Cork: Biology, Production and Uses*, Elsevier B.V., Amsterdam, 2007.
- [2] L. Gil, *Cork powder waste: An overview*, *Biomass and Bioenergy*. 13 (1997) 59–61.
- [3] S.B. Gibson I, Rosen D, *Additive Manufacturing Technologies: 3D Printing, Rapid Prototyping, and Direct Digital Manufacturing*, Second Edi, Springer, New York, 2015.
- [4] X. Lv, F. Ye, L. Cheng, S. Fan, Y. Liu, *Binder jetting of ceramics: Powders, binders, printing parameters, equipment, and post-treatment*, *Ceram. Int.* 45 (2019) 12609–12624. doi:10.1016/J.CERAMINT.2019.04.012.
- [5] F. Dini, S.A. Ghaffari, J. Jafar, R. Hamidreza, S. Marjan, *A review of binder jet process parameters; powder, binder, printing and sintering condition*, *Met. Powder Rep.* 75 (2020) 95–100. doi:10.1016/J.MPRP.2019.05.001.
- [6] S.-Y. Chun, T. Kim, B. Ye, B. Jeong, M. Lee, D.H. Lee, et al., *Capillary pressure and saturation of pore-controlled granules for powder bed binder jetting*, *Appl. Surf. Sci.* 515 (2020) 145979. doi:10.1016/J.APSUSC.2020.145979.
- [7] A. Alghunaim, S. Kirdponpattara, B.M.Z. Newby, *Techniques for determining contact angle and wettability of powders*, *Powder Technol.* 287 (2016) 201–215. doi:10.1016/j.powtec.2015.10.002.
- [8] B. Jóźwiak, M. Dziubiński, M. Orczykowska, *Wettability of commercial starches and galactomannans*, *J. Dispers. Sci. Technol.* 39 (2018) 1085–1092. doi:10.1080/01932691.2017.1382374.
- [9] G.A. Valencia, R.G. Pileggi, *Applicability of the modified Washburn method to contact angle measurements of calcium carbonate*, *Cerâmica*. 64 (2018) 197–206. doi:10.1590/0366-69132018643702232.
- [10] S. Kirdponpattara, M. Phisalaphong, B.Z. Newby, *Applicability of Washburn capillary rise for determining contact angles of powders/porous materials*, *J. Colloid Interface Sci.* 397 (2013) 169–176. doi:10.1016/j.jcis.2013.01.033.
- [11] L. Galet, S. Patry, J.A. Dodds., *Determination of the wettability of powders by the Washburn capillary rise method with bed preparation by a centrifugal packing technique*, *J. Colloid Interface Sci.* 346 (2010) 470–475. doi:10.1016/j.jcis.2010.02.051.
- [12] T. Dang-Vu, J. Hupka, *Characterization of porous materials by capillary rise method*, *Physicochem. Probl. Miner. Process.* 39 (2005) 47–65.
- [13] B. Neirinck, J. Van Deursen, O. Van Der Biest, J. Vleugels, *Wettability assessment of submicrometer alumina powder using a modified Washburn method*, *J. Am. Ceram. Soc.* 93 (2010) 2515–2518. doi:10.1111/j.1551-2916.2010.03854.x.
- [14] T.T. Chau, W.J. Bruckard, P.T.L. Koh, A. V Nguyen, *A review of factors that affect contact angle and implications for flotation practice*, *Adv. Colloid Interface Sci.* 150 (2009) 106–115. doi:https://doi.org/10.1016/j.cis.2009.07.003.
- [15] J. Kammerhofer, L. Fries, J. Dupas, L. Forny, S. Heinrich, S. Palzer, *Impact of hydrophobic surfaces on capillary wetting*, *Powder Technol.* 328 (2018) 367–374. doi:10.1016/j.powtec.2018.01.033.
- [16] C.M.C.P.S. Gomes, A.C. Fernandes, B. de J.V.S. de Almeida, *The Surface Tension of Cork from Contact Angle Measurements*, *J. Colloid Interface Sci.* 156 (1993) 195–201. doi:10.1006/JCIS.1993.1099.
- [17] J. Abenojar, A.Q. Barbosa, Y. Ballesteros, J.C. del Real, L.F.M. da Silva, M.A. Martínez, *Effect of surface treatments on natural cork: surface energy, adhesion, and acoustic insulation*, *Wood Sci. Technol.* 48 (2014) 207–224. doi:10.1007/s00226-013-0599-7.
- [18] N. Cordeiro, P. Aurenty, M.N. Belgacem, A. Gandini, C. Pascoal Neto, *Surface properties of suberin*, *J. Colloid Interface Sci.* 187 (1997) 498–508. doi:10.1006/jcis.1996.4735.
- [19] R.A. Pires, J.F. Mano, R.L. Reis, *Surface properties of extracts from cork black condensate*, *Holzforschung*. 64 (2010) 217–222. doi:10.1515/HF.2010.032.
- [20] S.P. Magalhães da Silva, T. Antunes, M.E. V Costa, Oliveira J. M., *Cork-like Filaments for Additive Manufacturing*, *Addit. Manuf.* 34 (2020) 101229. doi:https://doi.org/10.1016/j.addma.2020.101229.
- [21] T. Antunes, S.P. Magalhães da Silva, M.E. V Costa, J.M. Oliveira, *Cork-based filaments for Additive Manufacturing – The use of cork powder residues from stoppers industry*, in: *Int. Conf. Addit. Manuf.*, Maribor, Slovenia, 2018.
- [22] L.S.O. Pires, M.H.F.V. Fernandes, J.M.M. de Oliveira, *Biofabrication of glass scaffolds by 3D printing for tissue engineering*, *Int. J. Adv. Manuf. Technol.* 98 (2018) 2665–2676. doi:10.1007/s00170-018-2369-z.
- [23] S. P. Magalhães da Silva, Mónica A. Silva, José M. Oliveira, *Non-isothermal cold crystallization kinetics of cork–polymer biocomposites based on polylactic acid for fused filament fabrication*, *J. Therm. Anal. Calorim.* (2020) 1–12. doi:10.1007/s10973-020-10147-6.

- [24] E.W. Washburn, The Dynamics of Capillary Flow, *Phys. Rev.* 17 (1921) 273–283.
- [25] H.F. Hemond, E.J. Fechner, Chapter 1 - Basic Concepts, in: H.F. Hemond, E.J. Fechner (Eds.), *Chem. Fate Transp. Environ.* (Third Ed., Third Edit, Academic Press, Boston, 2015: pp. 1–73. doi:<https://doi.org/10.1016/B978-0-12-398256-8.00001-3>.
- [26] A. Şen, J. Van den Bulcke, N. Defoirdt, J. Van Acker, H. Pereira, Thermal behaviour of cork and cork components, *Thermochim. Acta.* 582 (2014) 94–100. doi:<https://doi.org/10.1016/j.tca.2014.03.007>.

3.6 Cork powders as material for 3D Printing: A case-study ¹

S. P. Magalhães da Silva^{1,2,3*}, J. M. Oliveira^{1,2,3}

¹EMaRT Group – Emerging: Materials, Research, Technology, University of Aveiro, Portugal

²School of Design, Management and Production Technologies Northern Aveiro (ESAN), University of Aveiro, Portugal

³Aveiro Institute of Materials (CICECO), University of Aveiro, Portugal

*corresponding author: sarapms@ua.pt

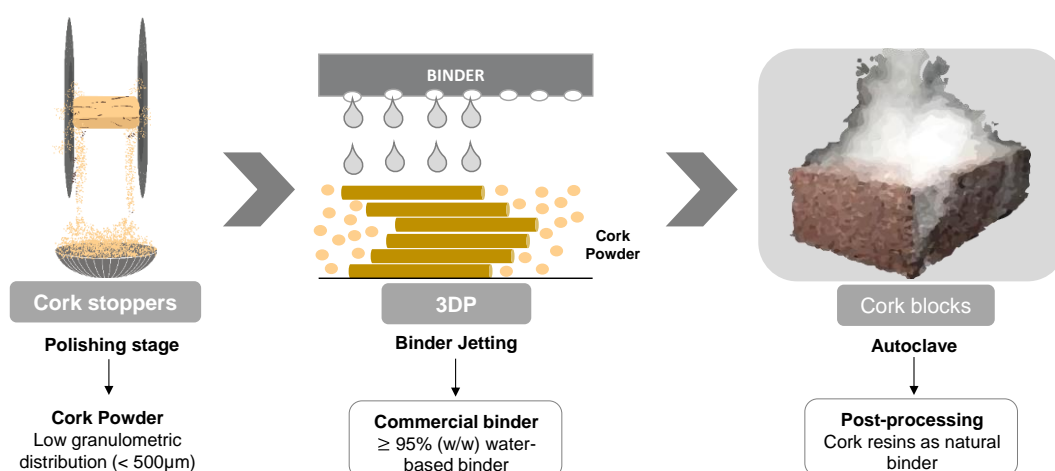
Abstract

The development of cork-based formulations adapted to 3D Printing (3DP) processes was herein investigated. Two cork powder sets with different particle size distributions (PSD) were studied in order to evaluate cork particles ability to pack. Cork powders exhibiting a Coarse distribution revealed a higher packing ability. In addition, two hydrophilic additives to mask cork lower affinity to water-based binders were also explored.

3DP cork parts with a simple geometry were firstly printed. An innovative technique was evaluated as post-processing phase to improve cork particles adhesion after printing. Inspired by the production of expanded cork agglomerates, it is proposed to use the autoclave technique as post-processing phase for cork parts. After autoclave, cork parts exhibited a more cohesive structure. FTIR analyses demonstrated that the polysaccharide and suberinic fractions decreased after autoclave. The thermochemical degradation can be an indication of the improved adhesion of cork particles after autoclave.

3DP cork parts with a complex design solution were successfully printed. The present work contributes to new and complex design solutions of cork-based products maintaining cork's natural lightweight, warmth and softness to the touch.

Graphical abstract



¹ To be submitted.

The author had contributed to the planning and execution of all experiments and printing procedures presented herein, as well as on the discussion, interpretation and preparation of the manuscript.

Keywords

Cork; Powders; Additive Manufacturing; Binder Jetting; 3D Printing; Natural materials

1. Introduction

“*One of Nature's most extraordinary materials*” [1]. Cork is the bark of the cork oak tree (*Quercus suber* L.) and it is mainly composed by suberin (33–50 % wt), lignin (20–25 % wt), polysaccharides (12–20 % wt) and extractives (14–18 % wt) [2]. Structurally, cork presents a honeycomb structure composed by closed cells filled with gas. The combination of cork chemical composition and porous structure makes cork a versatile material with a unique set of properties [2]. From the production of cork wine stoppers it is generated a high amount of cork powder residues, approximately 50000 tons/year, with low granulometries ($< 500 \mu\text{m}$) [3]. These cork residues are not used in the development of cork-based products, being usually burned or disposed in landfills. However, studies related to the valorisation of these residues and, consequently, to the development of cork-based solutions can already be found in literature. Some examples can be found elsewhere [4–10].

The 3DP technology, an additive manufacturing technique, is characterized by the use of powder materials and, by a binding agent, which is deposited through a print head, on previously prepared powder layers [11]. The resolution of 3DP parts ($\approx 100 \mu\text{m}$) is dependent on several factors, namely (i) binder type, (ii) powder PSD, (iii) particles geometry, (iv) binder droplets deposition precision and (v) binder and powder particles interaction [12–15]. Liquid or solid binders can be used in 3DP process. For processing ceramic materials water-based binders are normally used. Commercial liquid binders are composed mainly by water ($\geq 95\%$ (w/w)). In addition, liquid binders containing polyvinyl butyral, polyacrylic acid, photo-curable resins and others can be found [12,15–17]. On the other hand, solid binders reported in literature are maltodextrin, polyvinyl alcohol (PVA), starch, among others, being PVA the most studied one [12,18]. Surface finishing, porosity and fragility of the green parts are some of the limitations concerning 3DP process. As a consequence, the dedusting operations will be limited, which are usually hampered by the intricate shapes that these 3DP parts can present. A post-processing phase is required to surpass the fragility of the green parts. Heat treatments, impregnation with resins or other adhesive agents are some of the examples of post-processing techniques that are usually applied [15,19–21].

To the best of our knowledge studies reporting the processing of cork powder by 3DP are non-existing. However, recently, some studies related to the processing of natural materials by 3DP have been published [21–23]. The present work proposes to develop cork-based formulations adapted to 3DP process. It will be given priority to the use of commercial water-based binders to avoid the damage of printing heads. Some challenges can already be anticipated, namely the lower affinity of cork powders with a commercial binder [24] and the lower density of cork powders. In addition, it will also be studied and validated an innovative application of autoclave technique as a post-processing phase of 3DP cork parts. The inspiration was raised by the commercial production of expanded cork agglomerates through the autoclave technique [25,26]. The superheated steam generated inside the

autoclaves will induce the expansion of cork granules and the thermochemical degradation of cork cell wall. These degradation products act as natural adhesives and it will bond cork granules [27–30]. Consequently, it is expected that the same phenomena will occur for 3DP cork parts and the adhesion of cork particles will be improved after autoclave.

2. Methodology

2.1 Cork and cork-based formulations

Powder residues from cork stoppers' polishing stage were kindly provided by a Portuguese cork company. Cork powders with two different PSD were fractionated and used to prepare the cork-based formulations adapted for 3DP. The sieving method applied to fractionate the as-received material is already published elsewhere [7,31]. It was defined a wider distribution (20–100 μm) named as Full Range and a narrow distribution (63–80 μm) named as Coarse. The methodology followed to prepare both powder sets was reported by Oliveira, J. M and co-worker [24]. Also, the bulk density and porosity determined by mercury intrusion porosimetry (MIP) technique of both powder sets, as well as the morphology of cork particles can be found here [24].

Cork-based formulations were prepared in the presence of two hydrophilic additives, in order to improve cork powders wettability. PVA (Mowiol 4-88, Sigma Aldrich) and carboxymethylcellulose (CMC) sodium salt (PanReac AppliChem) were selected as additives. Compositions of the developed cork-based formulations are displayed in Table 1. The amount of cork powders and additives was kept constant being 75 % (w/w) and 25% (w/w), respectively. Cork powders and additives were mechanically mixed using a Ferneto BTF020 mixer for 10 minutes.

Table 1. Composition of the developed cork-based formulations.

Formulation #	Cork Powder	Additives	Bulk density * (g/cm ³)
Form 1	Full Range	PVA	0.083
Form 2	Coarse	PVA	0.156
Form 3	Full Range	CMC	0.083
Form 4	Coarse	CMC	0.156

* Values considered for cork powders.

2.2 3DP

The 3DP tests were executed in two phases: (1) by printing a part with a simple geometry (rectangular parallelepiped – 25 x 25 x 14 mm³) to validate cork-based formulations and (2) by printing a part with a complex geometry (model from Thingiverse) using the cork-based formulation selected in (1). The selection of the cork-based formulation adapted for 3DP was based on the accuracy of the printed parts.

Parts were printed using a ZPrinter®310 (3D Systems) equipment and a commercial binder (zb®60, 3D Systems). For all printed parts, the printing parameters were kept constant: (i) a layer

thickness of 101 μm and (ii) a binder saturation level of 50%. The 3D printed parts were left to dry overnight in the printer. Then, dedusting took place by using brushes and by applying air to remove the excess of powder.

Autoclave (ST Dry PV 12, Selecta) tests were evaluated as a post-processing procedure for 3DP cork parts. Two autoclave cycles of twelve minutes each were applied with a temperature of 134 $^{\circ}\text{C}$ and pressure of 2.1 bar. Autoclave conditions were defined based on preliminary studies (not shown).

To better understand which process phase samples are referred to, it was created the following nomenclature: 3DP parts before autoclave: *Form #_Green* and 3DP parts after autoclave: *Form #_Autoclave*.

2.3 Morphological analyses

A Hitachi SU-70 equipment was used to morphologically analyse all samples. Scanning Electron Microscopy (SEM) was applied to (i) the dispersion of additives within the developed cork-based formulations, (2) the adhesion of cork particles after 3DP process and before autoclave tests (3) the expansion of cork alveoli and cork particles adhesion after autoclave tests. All samples were sputter-coated (Polaron E5000) with Au/Pd target for 2 min at 12 mA.

2.4 Chemical analyses

Fourier Transform Infrared-Attenuated Total Reflection (FTIR) measurements were performed in Shimadzu equipment (IRPrestige-21 model) using KBr pellets. Sixty-four scans were taken for each sample with a resolution of 4 cm^{-1} in absorbance mode in the range of 4000–400 cm^{-1} . For each spectrum the air background spectrum was subtracted. FTIR analysis was applied to evaluate the chemical structure of 3DP cork parts before and after autoclave.

3. Results and discussion

3.1 Cork-based formulations adapted for 3DP

3DP parts obtained with cork-based formulation prepared with PVA (Form 1) can be seen in Fig. 1. It is visible that the presence of PVA causes a heterogeneously distribution within cork powder bed. In addition, Form 1 and Form 2 tend to agglomerate, which resulted in 3DP cork parts with lack of adhesion between cork particles and, consequently, with difficulty to maintain its shape. Parts printed with Form 2 also exhibited the same behaviour (data not shown). Based on these results it can be assumed that PVA is not adequate to obtain a well-packed cork powder bed with a uniform binder penetration.

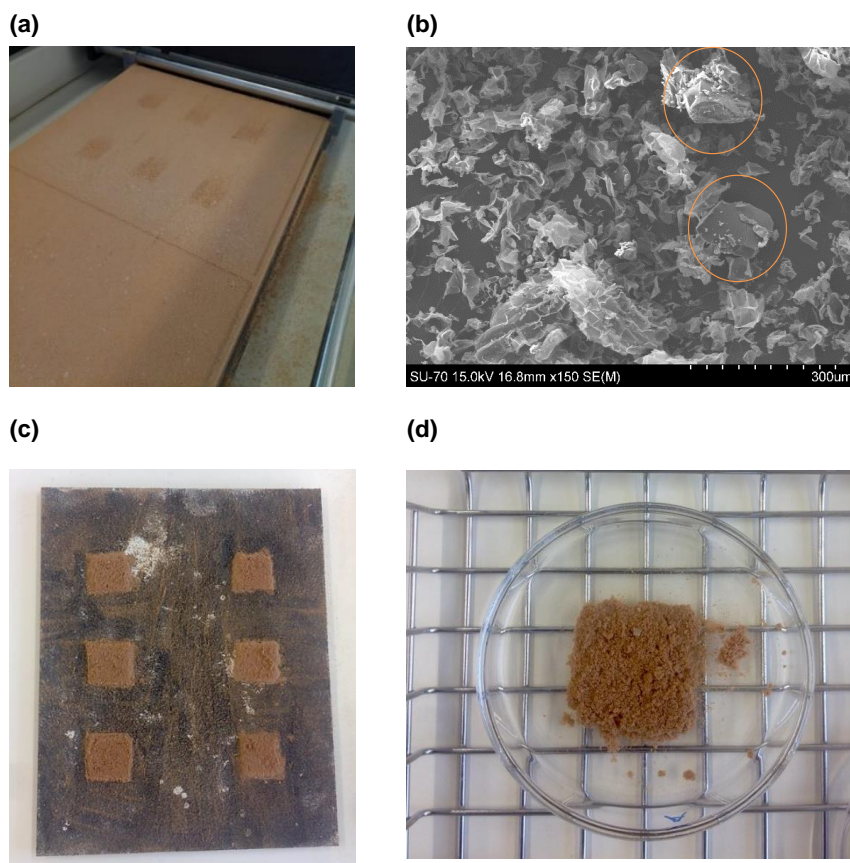


Fig. 1. 3DP parts using Form 1: **(a)** during 3DP process after binder deposition: heterogeneous dispersion of PVA within powder bed; **(b)** SEM image of Form 1 (PVA highlighted); **(c)** Form 1_Green parts after dedusting; and, **(d)** Form 1_Green part before entering in autoclave.

Cork-based formulations prepared with CMC presented an opposite behaviour. In Fig. 2 and Fig. 3 are displayed Form 3_Green and Form 4_Green parts, respectively.

From Fig. 2 (a, c) it is observed a homogeneous dispersion of CMC within cork powder bed and a packed powder bed. Form 3_Green parts were easily removed from powder bed (Fig. 2 (d, e)). After dedusting, parts presented cohesiveness and they were able to maintain its shape. However, dimensional accuracy was not attained for the first printed layers (Fig. 2 (f, g)). A possible explanation can be an unfavourable compaction of powder bed at the beginning of the printing process. As a consequence, this will affect the wettability of the first layers composed by Form 3.

In Fig. 3 it is detected that printing with Form 4 presented a different and improved outcome when compared to Form 3. Printing with Form 4, composed by cork particles with a narrow PSD, resulted in a well-packed powder bed (Fig. 3 (a, c), which is demonstrated in Fig. 3 (e)). In fact, a previous study [24] reporting the wettability behaviour of cork powders have demonstrated that Coarse powder distribution exhibited higher packing ability when compared to Full Range powder distribution.

An opposite trend is detected when compared to commercial ceramic powders and to published studies found in literature. Commercial ceramic powders have a bimodal granulometric PSD varying from 20 to 100 μm , having an average particle size equal to $\approx 52 \mu\text{m}$ [32]. Also, reported studies

have demonstrated that a higher packing density can be accomplished with bimodal or multimodal powder distributions in the presence of 20 – 30% (v/v) of fine powders ($\leq 20 \mu\text{m}$) [12,15,20].

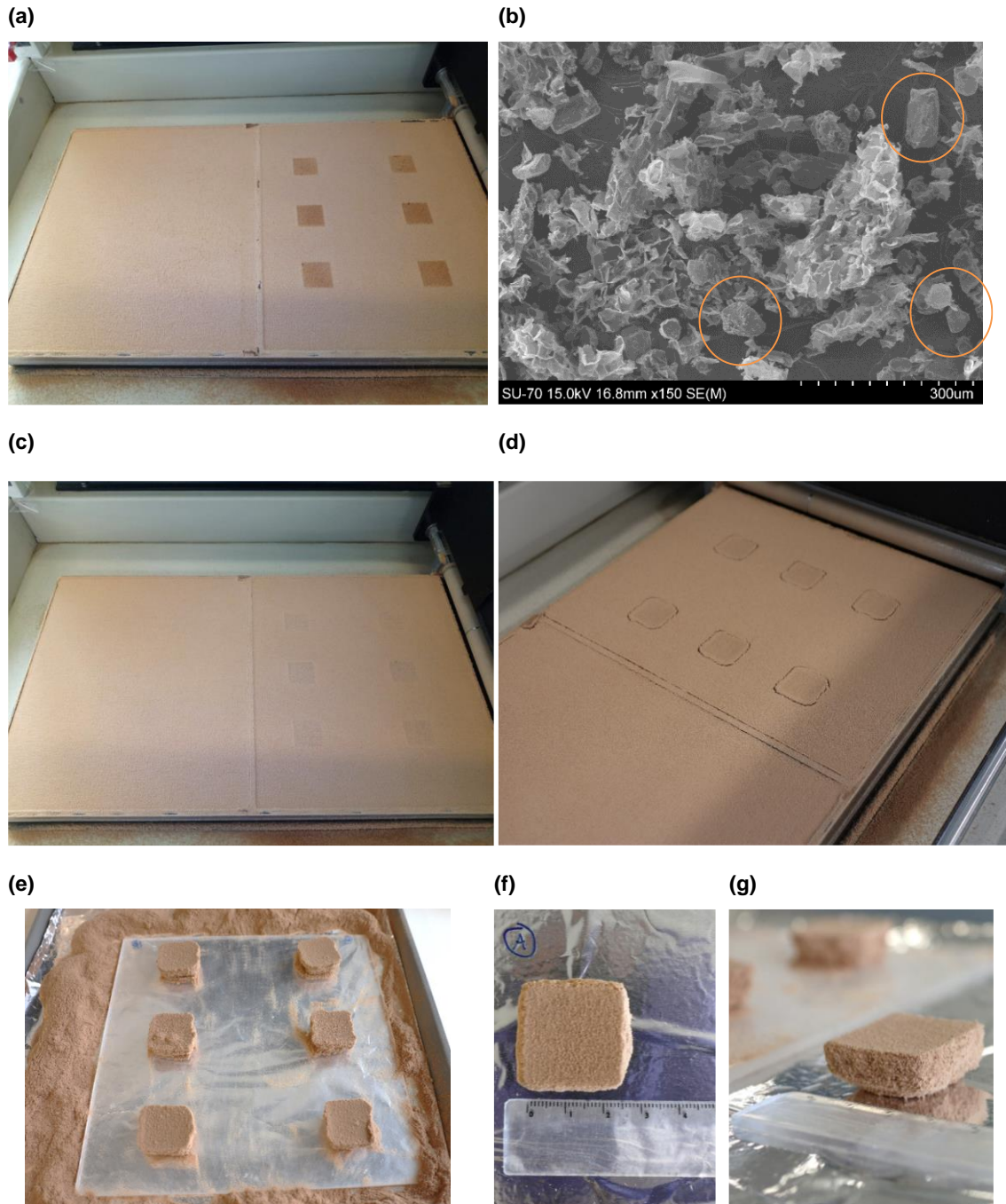


Fig. 2. 3DP parts using Form 3: **(a)** during 3DP process after binder deposition: homogenous dispersion of CMC within powder bed; **(b)** SEM image of Form 3 (CMC highlighted); **(c)** during 3DP process after the deposition of a new layer of Form 3; **(d)** Form 3_Green parts were left to dry during overnight: parts gave in with their own weight; **(e)** Form 3_Green parts during dedusting; **(f)** and **(g)** final Form 3_Green parts.

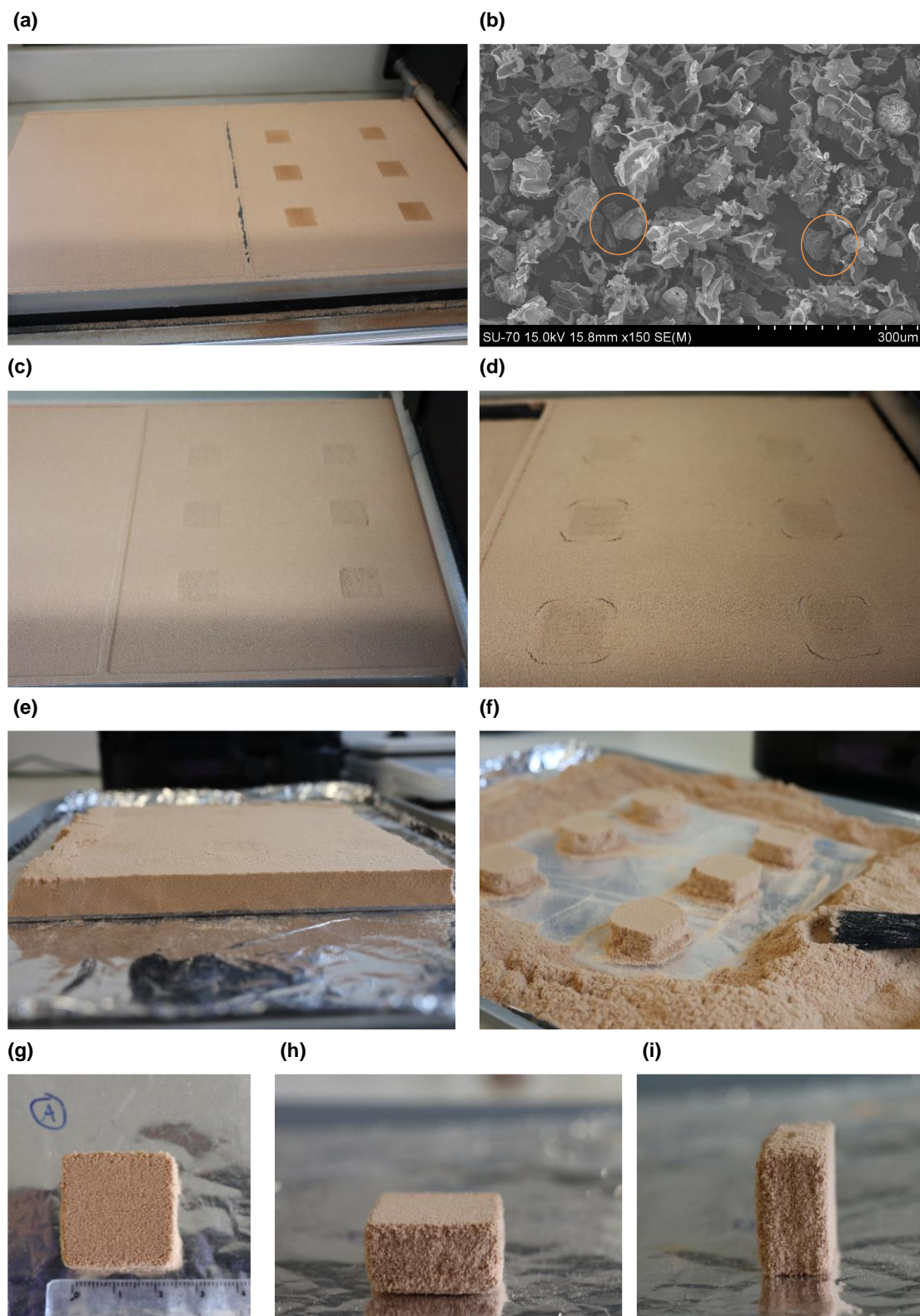


Fig. 3. 3DP parts using Form 4: **(a)** during 3DP process after binder deposition: homogenous dispersion of CMC within powder bed; **(b)** SEM image of Form 4 (CMChighlighted); **(c)** during 3DP process after the deposition of a new layer of Form 4; **(d)** Form 4_Green parts were left to dry during overnight: parts gave in with their own weight; **(e)** evidence of well-packed cork powder bed **(f)** Form 4_Green parts during dedusting; **(g)**, **(h)** and **(i)** final Form 4_Green parts.

A study reported by Chmielus, M. and co-workers [20] achieved green parts with higher density when printing powders with a PSD of 16 – 63 μm , comparatively to that obtained for powders with PSD of 16 – 25 μm and 53 – 63 μm . The irregular shape of cork particles (Fig. 1 (b), Fig. 2 (b), Fig. 3 (b)), as a consequence of the polishing stage, presents a positive contribute to particles wettability. Particles with irregular shape have higher surface contact areas, when compared to spherical particles, which will lead to a higher particles wettability by the binder and it will produce parts more cohesive and with greater dimensional stability [14].

Form 4_Green parts were easily removed from powder bed and dusted (Fig. 3 (f)). As a final result, it was achieved cohesive Form 4_Green parts with greater dimensional accuracy (Fig. 3 (g-i)).

3.2 Autoclave technique as post-processing step

The final step of a 3DP process is the so-called post-processing stage which is necessary to improve cork particles adhesion and to increase 3DP cork parts stability. Similarly to the production of expanded cork agglomerates, it is expected that after autoclave tests, the densification of 3DP cork parts will occur through the exudation of cork natural resins from cell wall and the expansion of cork alveoli [26–28].

Fig. 4 exposes the images of cork parts printed with Form 3 and Form 4, before and after autoclave tests. It is observed that, after autoclave, parts became brownish and more cohesive (Fig. 4 (b, d)).

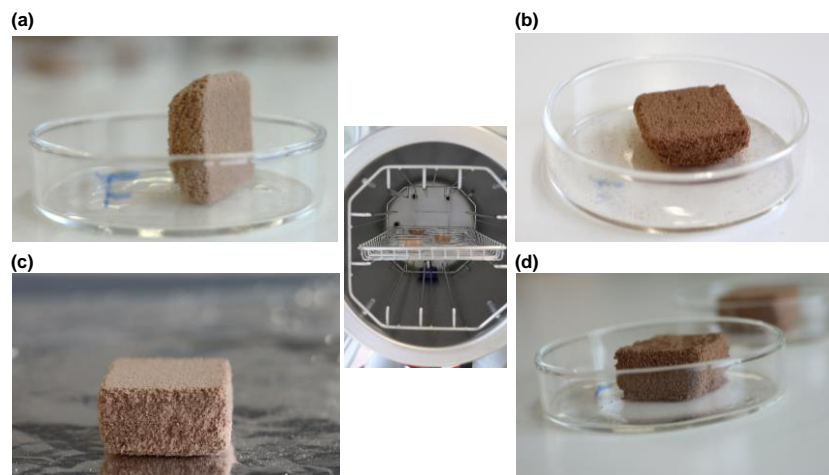


Fig. 4. Images of (a) Form 3_Green, (b) Form 3_Autoclave, (c) Form 4_Green and (d) Form 4_Autoclave.

This intensification on cork's colour can be related to the degradation of polysaccharides. Studies have reported that cork chemical degradation starts around 200 $^{\circ}\text{C}$, where the hemicellulose fraction disappears and cellulose fraction degrades considerably [27,28,33]. In addition, from Fig. 4 (b, d) it is also seen darker points dispersed on the printed parts. It is assumed that these points correspond

to CMC. In fact, the applied autoclave conditions can degrade $\approx 10\%$ of the initial mass (Supplementary data – Fig. S1). After autoclave tests, it was attained more cohesive parts without the release of loosen cork particles with handling. A simple way to observe this behaviour was conducted by releasing Form 4_Green and Form 4_Autoclave parts from a 20 cm height (Supplementary data – Fig. S2).

The effect of autoclave tests on cork alveoli structure was evaluated by SEM and it can be seen in Fig. 5 and Fig. 6.

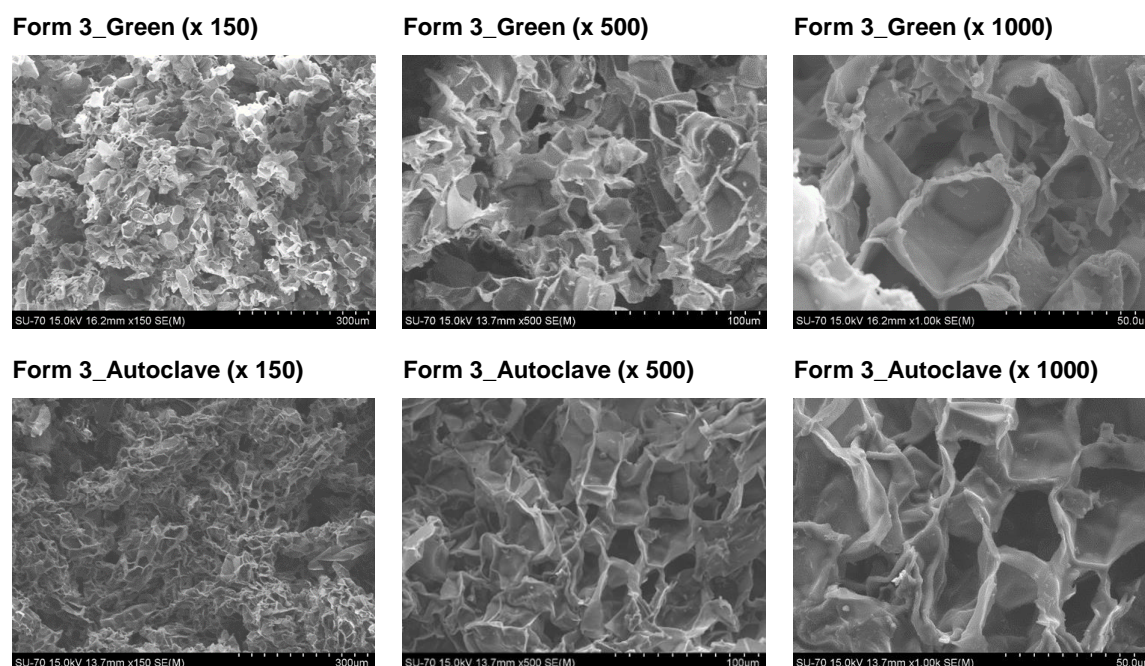


Fig. 5. SEM images of 3DP parts composed by Form 3 before and after autoclave.

The accurate quantification of cork cells expansion and cork wall thickness is not possible from Figures 5 and 6 due to the variability of cork alveoli dimensions dependent on cork's origin and age. The presence of damaged cork cells, as a consequence of the polishing stage, also affects such measurements.

Previous studies [27,29,30,34] have reported that heating above 250 °C is a requirement to prepare cork agglomerates by using autoclave equipment. Above this temperature, they observed the unfolding and stretching of cork cell walls accompanied with the expansion of cork cells. Consequently, cork granules will be compressed against each other and bond. The industrial process autoclave conditions to prepare black/expanded cork agglomerates are defined as 300 °C and 0.4 bar for cork with densities varying from 120 – 200 Kg/m³ [27,29,30,34].

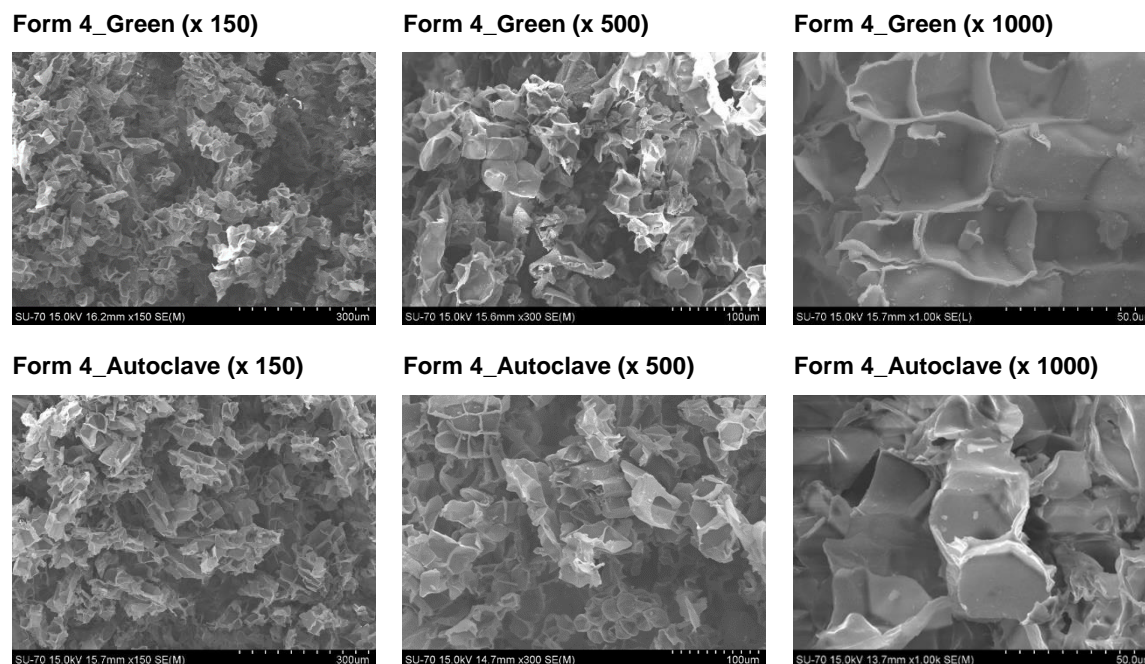


Fig. 6. SEM images of 3DP parts composed by Form 4 before and after autoclave.

In the present work, autoclave tests revealed to have positive effect on cork particles adhesion and cork parts stability (Fig. S2). These results suggest that the distinct applied autoclave conditions (135 °C, 2.1 bar), comparatively to that used in industrial processes, influence cork particles adhesion.

3.2.1 Chemical analyses

Besides the structural changes on cork cell walls instigated by autoclave conditions, the consequent thermochemical degradation of cork components also plays an important role. FTIR measurements were conducted to evaluate chemical changes in 3DP cork parts before and after autoclave. The main purpose was to assess which cork components have contributed to the self-bonding of cork particles. Former studies from Rosa, M. E *et al.* [34] and Pereira, H. *et al.* [27,30] reported that cork degradation by-products have a gluing ability. In Fig. 7 is presented the FTIR spectra of 3DP parts prepared from Form 3. Parts printed with Form 4 presented the same chemical behaviour. The detailed chemical composition of cork is known [2,35].

The 1035 cm^{-1} , which is attributed to C-O bond in polysaccharides, decreased after autoclave, indicating a partial loss of these fraction. The same tendency was reported by [27]. Suberin characteristic peaks are also perceived in Fig. 7 (a, b). The absorption peaks at 2924 cm^{-1} and 2852 cm^{-1} are detected, which correspond to asymmetric and symmetric vibrations of C-H, respectively [2,7]. Also, the following vibrations for suberin can be found: 1161 cm^{-1} (C-O-C ester group), 1261 cm^{-1} (C-O stretch) and 1740 cm^{-1} (C=O of aliphatic acids and esters) [2,7].

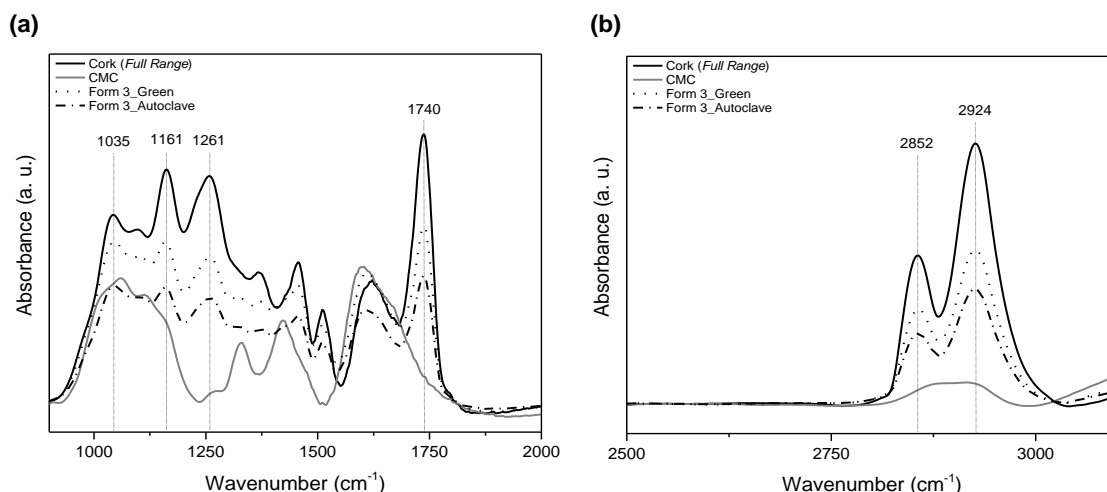


Fig. 7. FTIR spectra focusing in different wavenumber ranges **(a)** 900 – 2000 cm^{-1} and **(b)** 2500 – 3500 cm^{-1} .

A decrease in the intensity of suberin peaks is detected after autoclave tests. In order to estimate this reduction, the suberin peaks were normalized by the absorbance peak of suberin at 1161 cm^{-1} . In Fig. 8 is displayed the obtained absorption ratios.

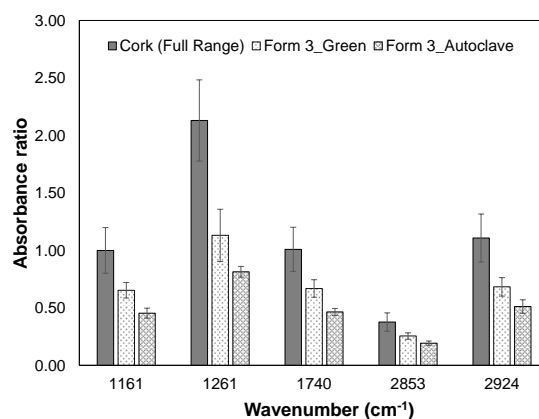


Fig. 8. Absorption ratios of suberin peaks by 1161 cm^{-1} of cork powder, Form 3_Green and Form 3_Autoclave samples.

As it can be seen from Fig. 8, a reduction for all suberin peaks is detected after autoclave tests. It can be assumed that the suberin fraction was degraded in some extent by the applied autoclave conditions. An opposite trend was observed by [27], where Pereira, H. observed an increase on the absorption of carbonyl from aliphatic acids and esters after heating cork at 250 $^{\circ}\text{C}$ (in air atmosphere).

FTIR measurements are in accordance to those presented earlier (Fig. S1). A mass loss of $\approx 10\%$ is obtained between 100 – 200 $^{\circ}\text{C}$. FTIR results can be indicative that probably not only the polysaccharide fraction contributes to the mass loss, but also the suberin fraction. Nevertheless, further studies are needed to fully characterize and understand the by-products resulted from autoclave tests. In addition, an accurate measurement is difficult when using cork powders residues from different sources due to the variability of cork chemical composition with the location of cork tree growth. The polysaccharides and extractives fractions are the most affected ones [35].

3.3 3DP with cork – A case study

A 3DP case study was conducted to evaluate the usefulness of the developed cork-based formulations. Form 4 was selected for the case study, based on the results presented in section 3.1. In Fig. 9 is illustrates the 3DP process from the 3D model until the final 3DP cork part. Parts with complex geometries can be successfully printed using adapted cork-based formulations. Binder was selectively deposited on powder bed and 3DP cork parts with dimensional accuracy were acquired (Fig. 9(f)).

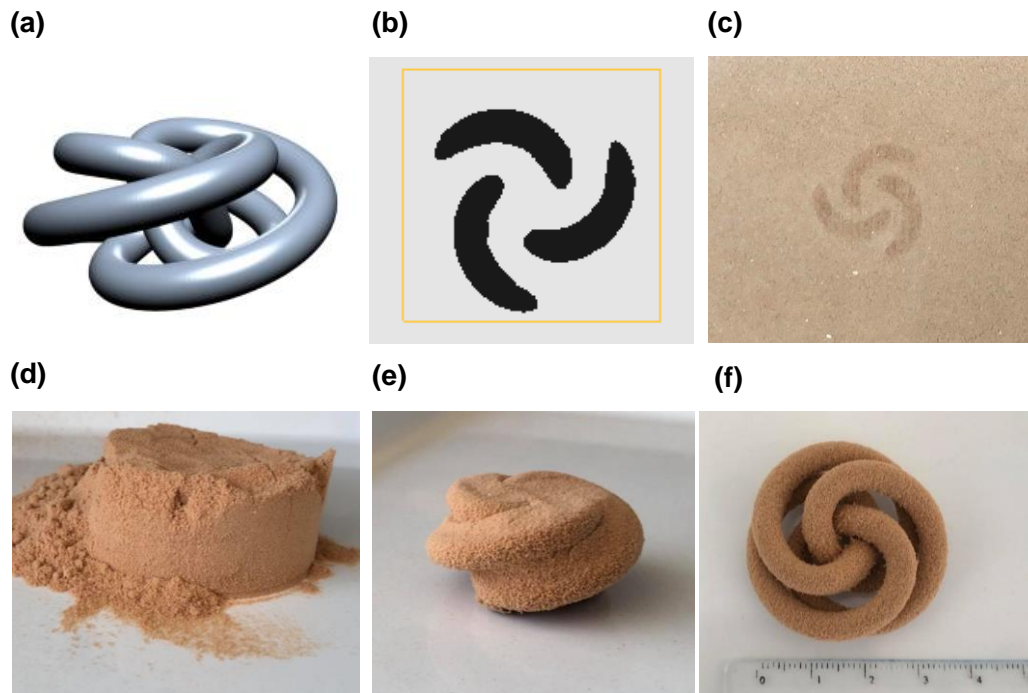


Fig. 9. Images of the 3DP process from (a) 3D model; (b) example of a layer; (c) example of a layer during printing; (d) part removed to powder bed; (e) during dedusting; to a (f) final 3DP cork part.

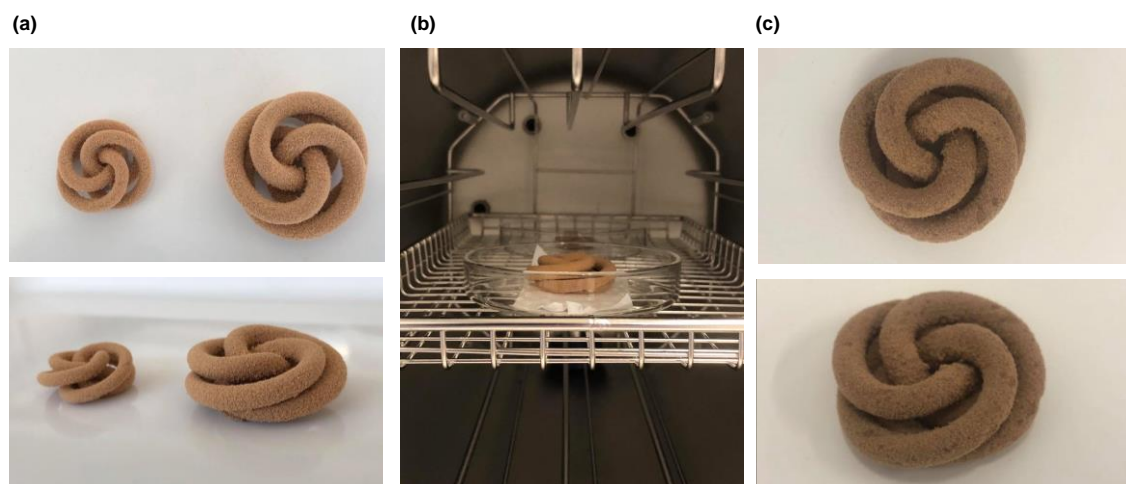


Fig. 10. Example of 3DP cork parts with a complex geometry: (a) Form 4_Green parts; (b) cork parts in autoclave and (c) Form 4_Autoclave parts.

3DP cork parts are super light, exhibiting a warm touch similar to cork and an appearance similar to that of a sponge (Fig. 10).

4. Conclusions

Cork-based formulations adapted for 3DP processes were developed. The printability of such formulations was firstly validated by printing a part with a simple geometry. From this study, cohesive parts with dimensional accuracy were achieved when printing with Form 4.

Autoclave technique have demonstrated to have a positive impact on cork particles adhesion. After autoclave, cork parts became more cohesive, without the release of loosen cork particles with handling. From SEM analyses, it was not possible to evaluate the expansion of cork alveoli. However, FTIR analyses indicated that the polysaccharide and suberinic fractions were affected and degraded in some extent after autoclave tests.

The conducted case study have shown that 3DP cork parts with intricate geometries can be successfully printed. The combination of a natural and traditional product, such as cork, with high-tech technologies, can lead to the development of cork products never processed before, or even to new applications of cork products never thought before.

Acknowledgements

This work was developed within the scope of the project CICECO-Aveiro Institute of Materials, UIDB/50011/2020 & UIDP/50011/2020, financed by national funds through the Portuguese Foundation for Science and Technology/MCTES. Authors would also like to present a special thanks to Porcelanas Costa Verde SA for theirs availability to use the company's printer.

Supplementary Data

Thermal Analyses

Thermogravimetric analysis (TGA) was conducted to evaluate the thermochemical degradation of cork and additives during autoclave tests. A NEXTA STA300 equipment from Hitachi was used. Samples were placed into alumina pans and they were heated from 25 °C to 1000 °C at 10 °C/min under air flow (50 mL/min). In Fig. S1 is shown the TGA results for cork powder and CMC.

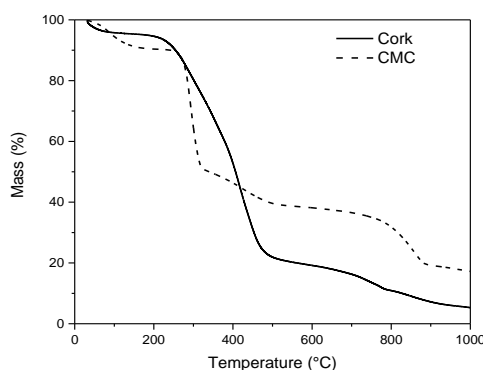


Fig. S1. TGA curves of cork and CMC.

Evaluation of particles adhesion after autoclave

A simple way to evaluate cork particles adhesion after autoclave is represented in Fig. S2. Looking at Fig. S2 (a), it is visible that cork particles were released as a consequence of falling from 20 cm height. Contrarily, after autoclave, cork part did not release particles when falling from the same height (Fig. S2 (b)).

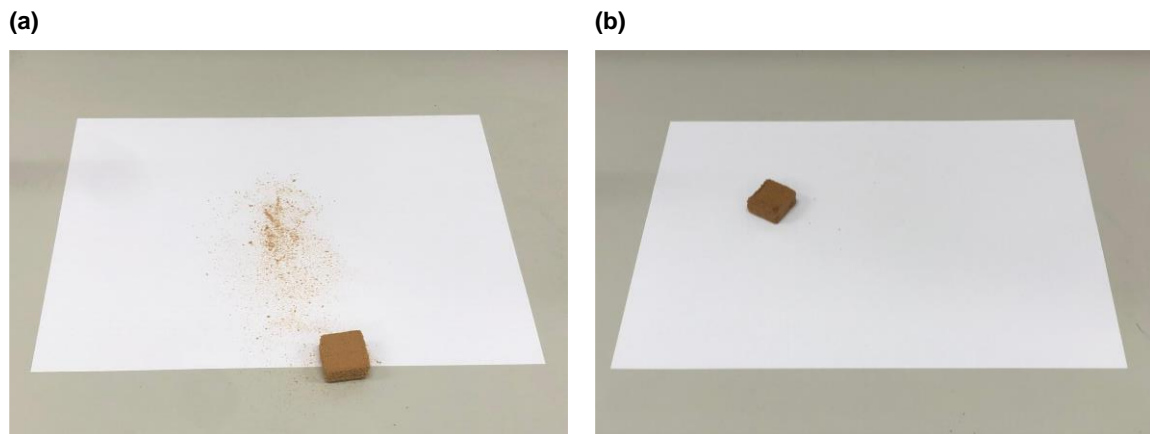


Fig. S2. (a) Form 4_Green and (b) Form 4_Autoclave parts released from a 20 cm height.

References

- [1] ACC, Why Cork?, (n.d.). <https://amorimcorkcomposites.com/en/why-cork/what-is-cork/> (accessed December 10, 2020).
- [2] H. Pereira, *Cork : Biology, Production and Uses*, Elsevier, Amsterdam, 2007.
- [3] L. Gil, Cork powder waste: An overview, *Biomass and Bioenergy*. 13 (1997) 59–61.
- [4] S.P. Magalhães da Silva, P.S. Lima, J.M. Oliveira, Rheological behaviour of cork-polymer composites for injection moulding, *Compos. Part B Eng.* 90 (2016) 172–178. doi:10.1016/j.compositesb.2015.12.015.
- [5] S.P. Magalhães da Silva, P.S. Lima, J.M. Oliveira, Non-isothermal crystallization kinetics of cork-polymer composites for injection molding, *J. Appl. Polym. Sci.* 133 (2016) 44124–44133. doi:10.1002/app.44124.
- [6] S. P. Magalhães da Silva, Mónica A. Silva, José M. Oliveira, Non-isothermal cold crystallization kinetics of cork–polymer biocomposites based on polylactic acid for fused filament fabrication, *J. Therm. Anal. Calorim.* (2020) 1–12. doi:10.1007/s10973-020-10147-6.
- [7] S.P. Magalhães da Silva, T. Antunes, M.E. V Costa, Oliveira J. M., Cork-like Filaments for Additive Manufacturing, *Addit. Manuf.* 34 (2020) 101229. doi:https://doi.org/10.1016/j.addma.2020.101229.
- [8] M. Ptak, P. Kaczyński, J. Wilhelm, J.M.T. Margarido, P.A.A.P. Marques, S.C. Pinto, et al., Graphene-Enriched Agglomerated Cork Material and Its Behaviour under Quasi-Static and Dynamic Loading., *Mater.* (Basel, Switzerland). 12 (2019). doi:10.3390/ma12010151.
- [9] P. Kaczynski, M. Ptak, J. Wilhelm, F.A.O. Fernandes, R.J.A. de Sousa, High-energy impact testing of agglomerated cork at extremely low and high temperatures, *Int. J. Impact Eng.* 126 (2019) 109–116. doi:10.1016/J.IJIMPENG.2018.12.001.
- [10] E.M. Fernandes, V.M. Correlo, J.F. Mano, R.L. Reis, Cork–polymer biocomposites: Mechanical, structural and thermal properties, *Mater. Des.* 82 (2015) 282–289.
- [11] S.B. Gibson I, Rosen D, *Additive Manufacturing Technologies: 3D Printing, Rapid Prototyping, and Direct Digital Manufacturing*, Second Ed, Springer, New York, 2015.

- [12] X. Lv, F. Ye, L. Cheng, S. Fan, Y. Liu, Binder jetting of ceramics: Powders, binders, printing parameters, equipment, and post-treatment, *Ceram. Int.* 45 (2019) 12609–12624. doi:10.1016/J.CERAMINT.2019.04.012.
- [13] F. Dini, S.A. Ghaffari, J. Jafar, R. Hamidreza, S. Marjan, A review of binder jet process parameters; powder, binder, printing and sintering condition, *Met. Powder Rep.* 75 (2020) 95–100. doi:10.1016/J.MPRP.2019.05.001.
- [14] N.D. Parab, J.E. Barnes, C. Zhao, R.W. Cunningham, K. Fezzaa, A.D. Rollett, Real time observation of binder jetting printing process using high-speed X-ray imaging, *Sci. Rep.* 9 (2019) 2499–2509. doi:10.1038/s41598-019-38862-7.
- [15] M. Ziaee, N.B. Crane, Binder jetting: A review of process, materials, and methods, *Addit. Manuf.* 28 (2019) 781–801. doi:10.1016/J.ADDMA.2019.05.031.
- [16] K. Lee, S. Lim, A. Tron, J. Mun, Y.-J. Kim, T. Yim, et al., Polymeric binder based on PAA and conductive PANI for high performance silicon-based anodes, *RSC Adv.* 6 (2016) 101622–101625. doi:10.1039/C6RA23805J.
- [17] W. Lee, D. Kim, J. Kim, T. Lee, D. Shin, M. Lee, Strength and Processing Properties using a Photopolymer Resin in a Powder-based 3DP Process, in: *SICE-ICASE Int. Jt. Conf.*, IEEE, Bexco, Korea, 2006: pp. 3674–3677. <http://ieeexplore.ieee.org/document/4108401/> (accessed January 24, 2020).
- [18] N.O. Muniz, F.A. Vechietti, L.A.L. dos Santos, Influence of several binders on the mechanical properties of alumina parts manufactured by 3D inkjet printing, *Mater. Res. Express.* 6 (2019) 115341–115349. doi:10.1088/2053-1591/ab4e3a.
- [19] S.C. Ligon, R. Liska, J. Stampfl, M. Gurr, R. Mülhaupt, Polymers for 3D Printing and Customized Additive Manufacturing, *Chem. Rev.* 117 (2017) 10212–10290. doi:10.1021/acs.chemrev.7b00074.
- [20] A. Mostafaei, P. Rodriguez De Vecchis, I. Nettleship, M. Chmielus, Effect of powder size distribution on densification and microstructural evolution of binder-jet 3D-printed alloy 625, *Mater. Des.* 162 (2019) 375–383. doi:10.1016/J.MATDES.2018.11.051.
- [21] H. Zeidler, D. Klemm, F. Böttger-Hiller, S. Fritsch, M.J. Le Guen, S. Singamneni, 3D printing of biodegradable parts using renewable biobased materials, *Procedia Manuf.* 21 (2018) 117–124. doi:10.1016/j.promfg.2018.02.101.
- [22] W. Xu, X. Wang, N. Sandler, S. Willfö, C. Xu, J. Gadolin, Three-Dimensional Printing of Wood-Derived Biopolymers: A Review Focused on Biomedical Applications, *ACS Sustain. Chem. Eng.* 6 (2018) 5663–5680. doi:10.1021/acssuschemeng.7b03924.
- [23] S. Holland, C. Tuck, T. Foster, Selective recrystallization of cellulose composite powders and microstructure creation through 3D binder jetting, *Carbohydr. Polym.* 200 (2018) 229–238. doi:10.1016/J.CARBPOL.2018.07.064.
- [24] S. P. Magalhães da Silva, J.M. Oliveira, Cork powders wettability by the Washburn capillary rise method (*Submitted*).
- [25] S.P. Silva, M.A. Sabino, E.M. Fernandes, V.M. Correló, L.F. Boesel, R.L. Reis, Cork: properties, capabilities and applications, *Int. Mater. Rev.* 50 (2005) 345–365.
- [26] A. Mestre, L. Gil, Cork for Sustainable Product design, *Ciência Tecnol. Dos Mater.* 234 (2011) 52–63. doi:[https://doi.org/10.1016/S0961-9534\(97\)00033-0](https://doi.org/10.1016/S0961-9534(97)00033-0).
- [27] H. Pereira, The thermochemical degradation of cork, *Wood Sci. Technol.* 269 (1992) 259–269. doi:<https://doi.org/10.1007/BF00200161>.
- [28] M.E. Rosa, M.A. Fortes, Thermogravimetric analysis of cork, *J. Mater. Sci. Lett.* 7 (1988) 1064–1065. doi:10.1007/BF00720828.
- [29] M.E. Rosa, M.A. Fortes, Effects of water vapour heating on structure and properties of cork, *Wood Sci. Technol.* 23 (1989) 27–34. doi:10.1007/BF00350604.
- [30] H. Pereira, E. Ferreira, Scanning electron microscopy observations of insulation cork agglomerates, *Mater. Sci. Eng. A.* 111 (1989) 217–225. doi:10.1016/0921-5093(89)90215-3.
- [31] T. Antunes, S.P. Magalhães da Silva, M.E. V Costa, J.M. Oliveira, Cork-based filaments for Additive Manufacturing – The use of cork powder residues from stoppers industry, in: *Int. Conf. Addit. Manuf.*, Maribor, Slovenia, 2018.
- [32] L.S.O. Pires, M.H.F.V. Fernandes, J.M.M. de Oliveira, Biofabrication of glass scaffolds by 3D printing for tissue engineering, *Int. J. Adv. Manuf. Technol.* 98 (2018) 2665–2676. doi:10.1007/s00170-018-2369-z.
- [33] A. Şen, J. Van den Bulcke, N. Defoirdt, J. Van Acker, H. Pereira, Thermal behaviour of cork and cork components, *Thermochim. Acta.* 582 (2014) 94–100.
- [34] M.E. Rosa, M.A. Fortes, Temperature-induced alterations of the structure and mechanical properties of cork, *Mater. Sci. Eng.* 100 (1988) 69–78. doi:10.1016/0025-5416(88)90240-6.

- [35] H. Pereira, Chemical composition and variability of cork from *Quercus suber* L., *Wood Sci. Technol.* 22 (1988) 211–218. doi:10.1007/BF00386015.

Concluding remarks & Future perspectives

4. Concluding remarks and future perspectives.....	167
4.1 IM.....	167
4.2 AM.....	167
4.3 Future work perspectives.....	168

4. Concluding remarks and future perspectives

The present work successfully demonstrated the valorisation of cork powder residues through the development of cork-based solutions for IM and AM applications. Cork industry is already known by its sustainability. From *Montados* impact on the prevention of global warming to the use of non-suitable cork for stoppers production on the development of cork-based composites. So far, cork residues with granulometric distributions lower than 500 µm are still used as heat source for boilers. The work herein presented have demonstrated new applications and strategies for these cork residues, rather than being burned.

It is important to note that the majority of conclusions have been already presented along the manuscript. Such conclusions are included in the published or submitted papers that constitute this thesis. Next, it will be presented the results that were considered to be more impactful and innovative. For better understanding, the presentation of these results will be divided into two parts: IM and AM.

4.1 IM

CPC with adequate rheological, thermal, chemical and mechanical properties were developed for IM applications. The rheological and non-isothermal crystallization behaviour of CPC were studied for the first time. Cork nucleating ability was determined and observed by POM images. Coupling agents based on MA have demonstrated (1) to act as lubricant and to improve CPC flowability; (2) to act as nucleating agents and to increase the crystallinity degree, although it reduces the overall crystallization rate; and, (3) to create “*chemical bridges*” between cork particles and the polymeric matrix and, to improve the performance of the developed CPC.

A case study was conducted to evaluate the damage caused on cork alveoli after a standard IM process. The applied case-study revealed that new strategies on the adaptation of IM technology are needed, in order to maintain intact cork’s alveolar structure and to take advantage of cork unique properties. An adapted IM was carried out and the effect of low pressures, the removal of holding and back pressures and the use of shut-off nozzles were evaluated. Preliminary results have shown that the presence of cork granules near to matrix defects (voids) led to a natural expansion of cork alveoli. This can be indicative that the IM process alone do not destroy cork cell walls and cork alveoli can recover its shape and size after being subjected to this manufacturing technology.

The mass production of CPC products by IM is of major interest. However, the processing of CPC by this conventional technology remains a challenge.

4.2 AM

CPC for FFF

The alliance between cork unicity and AM universe will raise, even more, the potential of AM disruptive technologies. It will open new horizons allying technology with tradition. CPC filaments

based on physical, thermal, chemical, mechanical and morphological analyses were successfully developed for application in FFF process. A systematic study based on the Taguchi approach was conducted for the development of a coupling agent based on MA (MAgPLA). The effect of this coupling agent led to the same features presented above.

A case study was conducted to evaluate the usefulness and printability of the developed CPC filaments. It was observed that the FFF process allowed to preserve cork alveolar structure, benefiting CPC mechanical behaviour. The printed parts exhibited unique characteristics, such as a non-plastic and warm touch, a natural colour and the release of a pleasant odour during the printing process. Such characteristics and properties of the new cork-like filament will foster the development of new design solutions and products.

Cork for 3DP

The use of cork residues as powder bed material for 3DP process was successfully demonstrated for the first time. A unique and innovative application of cork powder residues. Cork is well known by its hydrophobic character. The applicability of the WCR method to evaluate cork powders wettability by a commercial binder ($\geq 95\%$ (w/w)) was validated for the first time. Cork powders are slightly wetted by the commercial binder ($\theta \approx 86 - 87^\circ$). For application in 3DP process it is therefore necessary to prepare adapted cork-based formulations. These formulations were prepared with hydrophilic additives to mask the hydrophobic character of cork.

A case study was conducted to evaluate the printability of the developed cork-based formulations. 3DP cork parts with complex shapes were herein presented for the first time. Parts are extremely light and exhibited warmth and softness to the touch. The use of autoclave technique as the post-processing phase was used and studied for the first time. Results have shown that 3DP cork parts exhibited a more cohesive structure after the autoclave tests. The thermochemical degradation instigated by the water vapour led to partial degradation of the polysaccharide and suberinic fractions, as indicated by FTIR measurements. The uniqueness and promising results obtained so far will lead (i) to the valorisation of cork residues under the circular economy principles and (ii) to the development of innovative and eco-sustainable cork products.

4.3 Future work perspectives

From the conclusions presented above emerged several future work perspectives for each processing technology. The identification of possible future works that will have a positive impact on the work herein present will follow the same structure as presented above.

CPC for IM

In this particular case, two major studies were identified to improve the sustainability and performance of the developed CPC. Firstly, the development of biodegradable CPC solutions adapted to IM. This will pass by the preparation of completely biodegradable polymeric matrices and

the formulation of CPC with these matrices. Secondly, the study of two new strategies to overcome the high pressure applied during a standard IM process and, consequently, maintaining intact the cork alveolar structure should be considered. The basic ideas will consist on (1) the addition of chemical agents that possibly will assist the expansion of cork and (2) the application of shear stress, through an adapted IM process, during cooling of polymer melt to facilitate the expansion of cork alveoli.

CPC for FFF

The main drawback of the developed CPC filaments was its fragility. PLA is a polymorphic material when it comes to its crystalline structure. In this sense, a complete XRD study should be conducted to evaluate the changes on PLA crystalline structure when it crystallizes in the presence of cork and MAgPLA. This study will allow to understand the effect of cold crystallization behaviour on the mechanical performance of the developed filaments and, consequently, to enhance its ductility. In addition, the development of flexible CPC filaments through the development and incorporation of flexible TPS solutions are of major interest. Also, the possibility to develop coloured filaments can offer new cork-like filament solutions and compete directly with natural-based solutions presented on the market.

Cork for 3DP

The main challenge related to the processing of cork powders by 3DP concerns the post-processing phase. A detailed study related to the thermochemical degradation mechanisms of cork components after autoclave should be performed. A lot of effort had already been done, however it is not fully understood which chemical compounds contribute to the self-bonding of cork particles. In addition, the study and selection of additives that degrade completely under autoclave tests' conditions is relevant for the integrity of 3DP cork parts.

In the future, new applications should be sought for cork parts processed by 3DP. These parts ally the unique combination of cork properties with the design freedom of 3DP technology.

